Faculty of Engineering and Science

Reservoir Characterization for CO_2 Injectivity and Flooding in Petroleum Reservoirs, offshore Malaysia

Arshad Raza

This thesis is presented for the Degree of
Doctor of Philosophy
of
Curtin University

August 2017

Declaration

To the best of my knowledge and belief this thesis contains no material previously published by any other person except where due acknowledgment has been made.

This thesis contains no material which has been accepted for the award of any other degree or diploma in any university.

Signature:  (Arshad Raza)

Date: 01/08/2017

Copyright

I warrant that I have obtained, where necessary, permission from the copyright owners to use any third-party copyright material reproduced in the thesis (e.g. questionnaires, artwork, unpublished letters), or to use any of my own published work (e.g. journal articles) in which the copyright is held by another party (e.g. publisher, co-author).

Signature:  (Arshad Raza)

Date: 01/08/2017

Publications by the Author

(Following are the journal papers that have been published/in-process from current work)

1. **Raza, A**., Rezaee, R., Gholami, R., Bing, C.H., Nagarajan, R. and Hamid, M.A., 2016. A screening criterion for selection of suitable CO_2 storage sites. *Journal of Natural Gas Science and Engineering*, Elsevier, 28: 317-327.

2. **Raza, A**., Gholami, R., Rezaee, R., Bing, C.H., Nagarajan, R. and Hamid, M.A., 2017. Preliminary assessments for CO_2 storage in carbonate formations: a case study from Malaysia. *Journal of Geophysics and Engineering*, IOP, 14: 535–556 (22pp).

3. **Raza, A**., Gholami, R., Rezaee, R., Bing, C.H., Nagarajan, R. and Hamid, M.A., 2017. Well selection in depleted oil and gas fields for a safe CO_2 storage practice: a case study from Malaysia. *Petroleum, KeAi*, 3/1: 167-177.

4. **Raza, A**., Gholami, R., Rezaee, R., Bing, C.H., Nagarajan, R. and Hamid, M.A., 2017. Preliminary assessment of CO_2 injectivity potential in carbonate storage sites. *Petroleum, KeAi*, 3/1: 144-154.

5. **Raza, A**., Gholami, R., Rezaee, R., Bing, C.H., Nagarajan, R. and Hamid, M.A., 2017. Assessment of CO_2 residual trapping in depleted reservoirs used for geosequestration. *Journal of Natural Gas Science and Engineering*, Elsevier, 43C: 137-155.

6. **Raza, A**., Gholami, R., Sarmadivaleh, M., Tarom, N., Rezaee, R., Bing, C.H., Nagarajan, R., Hamid, M.A. and Elochukwu, H., 2016. Integrity analysis of CO_2 storage sites concerning geochemical-geomechanical interactions in saline aquifers. *Journal of Natural Gas Science and Engineering, Elsevier*, 36PA: pp. 224-240.

7. **Raza et al. 2017,** Numerical modeling to assess CO_2 storage in depleted gas reservoir: A case study from Malaysia. (submitted)

(Publications relevant to thesis but not forming part of it)

8. **Raza, A**., Rezaee, R., Gholami, R., Rasouli, V., Bing, C. H., Nagarajan, R. and Hamid, M.A., 2015. Injectivity and quantification of capillary trapping for CO_2 storage: A review of influencing parameters. *Journal of Natural Gas Science and Engineering*, 26, 510-517.

9. **Raza, A**., Rezaee, R., Bing, C. H., Gholami, R., Hamid, M.A., & Nagarajan, R. 2016. Carbon dioxide storage in subsurface geologic medium: A review on capillary trapping mechanism. *Egyptian Journal of Petroleum*, 25**,** 367-373.

10. **Raza, A**., Rezaee, R., Gholami, R., Bing, C. H., Nagarajan, R. and Hamid, M.A., 2016. CO_2 storage in heterogeneous aquifer: A study on the effect of injection rate and $CaCO_3$ concentration. *In IOP Conference Series: Materials Science and Engineering, IOP Publishing*, 121(1): 012023.

11. **Raza, A**., Gholami, R., Rezaee, R., Bing, C. H., Nagarajan, R. and Hamid, M.A., 2017. CO_2 storage in heterogeneous aquifer: A study on the effect of temperature and mineral precipitation. *In IOP Conference Series: Materials Science and Engineering, IOP Publishing*, 206 (1) 012002.

12. **Raza, A**., Gholami, R., Rezaee, R., Bing, C. H., Nagarajan, R. and Hamid, M.A., 2017. CO_2 storage in depleted gas reservoirs: A study on the effect of residual gas saturation. *Petroleum, KeAi*.

Acknowledgements

First and foremost, I would like to express my sincere gratitude and appreciation to my advisors for their continuous guidance, advice, support, innovation, enthusiasm, and encouragement throughout my study at Curtin University. I express my sincere appreciation to my supervisor A/Prof. Chua Han Bing for his efforts to acquire the reservoir data from PETRONAS and firm contribution towards the accomplishment of my dissertation. I am grateful to Dr. Raoof Gholami and Prof. Reza Rezaee for helping me to think critically enhancing considering their knowledge in the field of reservoir characterization. I would like to extend my deepest gratitude to A/Prof. Ramasamy Nagarajan and Dr. Mohamed Ali Hamid for their interesting technical discussion which was useful to explore the injectivity aspect of CO_2 storage.

My gratitude also goes to Curtin University, Malaysia for sponsoring my PhD study through the Curtin Sarawak Research Institute (CSRI) Flagship scheme. I sincere appreciate my fellow PhD students and faculty members at the Department of Petroleum Engineering at Curtin University, Malaysia for their great support. I acknowledge Senergy Limited and Schlumberger for providing the license of Interactive Petrophysics, Petrel and Eclipse compositional simulator software.

Last, but not least, I would like to thank my parents for allowing me to realize my potentials. The support that they have provided me over the years is the greatest gift anyone has ever given me. I deeply thank my brothers and sisters for their endless patience which helped me to go through this agonizing period of my life.

Abstract

Greenhouse gases, CO_2 in particular, are being emitted into the atmosphere due to burning of fossil fuels, and are causing adverse effects on the environment. The carbon capture and storage (CCS) technology has been recognized as the best approach of permanently storing CO_2 in suitable subsurface geologic sites, such as depleted petroleum reservoirs and deep aquifers. The reservoir characterization of the depleted petroleum reservoirs prior to injection of CO_2 is an essential step to ensure the safety and success of CO_2 storage projects. This provides the ultimate input data for reservoir modeling and for all the predictions concerning the storage complex and its surroundings. Many studies have been done so far, emphasizing on different aspects of CO_2 storage, where many questions have remained unanswered.

Identifications of suitable sites to store a large quantity of CO_2 for a long period of time is not an easy and straightforward task. Several general screening criteria have already been presented for selection of an appropriate subsurface geologic media based on local-scale projects for depleted reservoirs. Depth, permeability, porosity, CO_2 density and containment factors were among those general criteria. There are also many other preliminary factors linked to the key storage aspects, which should not be neglected during a storage site evaluation. Slight attentions have been given to the criteria proposed for the preliminary evaluation of the injection well and zones. In the context of CO_2 residual trapping, although there had been many studies utilizing experimental and numerical approaches to evaluate trapping potentials prior to injection, few studies were conducted to determine the reservoir scale CO_2 residual trapping at the depletion stage of petroleum reservoirs. In the context of injectivity, the chemical interactions induced by supercritical CO_2 on reservoir rocks have been poorly understood. Finally, the selection of injection rate in depleted petroleum reservoirs, where remaining hydrocarbons are left at the depletion stage, have not been fully addressed in the past studies.

The primary purpose of this thesis is to characterize a carbonate gas reservoir located in Malaysia for CO_2 storage, by addressing the above issues and research gaps. This

would provide insights into the key CO_2 storage aspects (i.e., storage capacity, injectivity, trapping mechanisms, and containment). A storage screening criteria was developed proposing a framework for the preliminary evaluation of depleted storage sites, suitable injection well, and injection zone. A new reservoir level approach was also presented to estimate the residual trapping ability (i.e., residual CO_2 saturation) of petroleum reservoirs at the depleted stage by utilizing wireline log data and reservoir conditions. The validated approach was applied to the gas reservoir for prediction of CO_2 residual trapping in the reservoir scale. Considering the compaction and geochemical issue in the storage sites, a series of experiments were conducted to evaluate the injectivity and changes of geomechanical parameters against different stresses applied during and after the injection of CO_2 in a short period of time. Numerical modeling of the carbonate gas reservoir was also carried out based on the proposed optimum injection rate scheme.

The results obtained through preliminary assessment suggested that the reservoir has a good potential storage site for a CO_2 storage practice, but some difficulties might arise due to the high heterogeneity level, compaction behavior and aquifer supports of the reservoir. The study on the well from depleted reservoir based on the proposed methodology indicated that a depleted well in the field may have the potential of being a suitable conduit for CO_2 injection. For injection zone selection in depleted storage sites, the methodology presented in this study can be used for preliminary evaluation of injectivity which indicated that Zones No. 2 and 3 are rational choices for injection because of their favourable characteristics. The validated CO_2 residual trapping approach was applied on the carbonate gas reservoir and it was found that the maximum volume of CO_2 residual trapped could be approximately 0.965 Tscf of the effective pore volume (excluding 30% Sgr). The results of the study for compaction and geochemical effects revealed that there are geomechanical changes under different stress states and there were signs of dissolution, kaolinite break-down and even corrosion of quartz, which indicates the fact that geomechanical parameters of reservoirs can be affected even in a short-term exposure to $scCO_2$. The numerical modeling results obtained indicated that the optimum injection rate selected based on reservoir information via steady state

analytical solution is a good strategy to evaluate the injectivity of reservoir's zones and effective storage potential. It was revealed that the maximum cumulative CO_2 injected through Zones 1 to 4 are around 2.416 Tscf, 2.78 Tscf, 2.88 Tscf, and 2.419 Tscf, respectively at the end of 20 years at 500 Mscf/D injection rate. It was also observed that injectivity is reasonable in Zones 2 and 3 where the maximum volume of CO_2 can be stored. Extended simulations also revealed that the anticline structure of the reservoir provides a reasonable structural trap for CO_2 in a short-term scale. In long-term, free CO_2 (mobile saturation) may damage the containment of storage site, due to caprock over-pressurization and geochemical activity.

Contents

List of Figures

List of Tables

Nomenclature

CO_2	Carbon dioxide
CCS	Carbon capture and storage
ppm	Parts per million
CH_4	Methane
N_2O	Nitrous oxide
km	Kilometer
EOR	Enhanced oil recovery
^oC	Degree Celsius
Mt	Million-tonnes
Atm	Atmosphere
P_c	Capillary pressure, (psi)
θ	Contact angle, (degree)
σ	Interfacial tension, (gf/cm)
gf/cm	Gram-force per centimeter
r	Pore throat radius, (cm)
$\sigma_{brine\text{-}CO2}$	Interfacial tension between brine and CO_2
P_{CO2}	CO_2 phase capillary pressure, (psi)
P_{Brine}	Brine phase capillary pressure, (psi)
mD	Milli-darcy
MPa	Mega pascal
N_2	Nitrogen
O_2	Oxygen
Ar	Argon
g/L	Gram per liter
kg/m^3	Kilogram per cubic meter
Δρ	Differential density
T_R	Reservoir temperature
M_{CO2}	Storage capacity
OGIP	Volume of original gas in place
R_f	Recovery factor
FIG	Fraction of injected gas
C_{eff}	Effective storage coefficient
C_{aq}	Reduction in the storage capacity
M_{CO2t}	Mass theoretical storage capacity
R_f	Recovery factor
P_{CO2r}	Density of CO_2 at reservoir condition
A	Reservoir area
h	Thickness
Ø	Porosity
S_w	Water saturation
k_h	Horizontal permeability
k_s	Spherical permeability
k_v	Vertical permeability
S_w	Water saturation
R_o	Resistivity of pore volumes filled with water
n	Saturation exponent
Sh	Hydrocarbon saturation
Sg	Gas saturation
So	Oil saturation
P_{ct}	Capillary rise
Mt/yr	Million tons per year
ft	Feet
MWL	Moveable water level

Tscf	Trillion standard cubic feet
g/cc	Gram per cubic centimeter
Ca	Calcium
Mg	Magnesium
Fe	Iron
Ω-m	Ohm-meter
CBL	Cement bond log
g/m^3	Gram per cubic meter
Tcm	Trillion cubic meter
Tscm	Trillion standard cubic meter
Pa/m	Pascal per meter
psi	Pounds per square inch
GWC	Gas water contact
TVD	True vertical depth
IFT	Interfacial tension
m_c	Cementation factor
^oF	Fahrenheit
Pa	Pascal
KPa	Kilo pascal
SSTVD	Subsea true vertical depth
MSL	Mean sea level
MHL	Moveable hydrocarbon level
DST	Drill stem testing
STB	Stock tank barrel
B_{gCO2}	CO_2 gas formation volume factor, (bbl/Mscf)
Sgr	Residual gas saturation, (fraction)
Kr	Krypton
Xe	Xenon
psi/m	Pounds per square inch per meter
σ_{Hmax}	Maximum horizontal stress, (MPa)
σ_{hmin}	Minimum horizontal stress, (MPa)
σ_v	Vertical stress, (MPa)
GPa	Gigapascal
P_{nw}	Non-wetting phase pressure, (psia)
P_w	Wetting phase pressure, (psia)
$Pc_{hyd\text{-}brine}$	Capillary pressure between hydrocarbon and brine, (psia)
$\sigma_{hyd\text{-}brine}$	Hydrocarbon-brine interfacial tension, (gf/cm)
$\theta_{hyd\text{-}brine\text{-}rock}$	Rock-fluids contact angle, (degree)
$Pc_{CO2\text{-}brine}$	CO_2-brine capillary pressure, (psia)
$\sigma_{CO2\text{-}brine}$	CO_2-brine interfacial tension, (gf/cm)
$\theta_{CO2\text{-}brine\text{-}rock}$	Rock-fluids (CO_2-brine) contact angle, (degree)
$SgrCO_2$	Residual CO_2 saturation, (fraction)
M	Molality
m	Meter
P	Pressure, (psia)
V_M	Molar volume, (cubic feet/lb mole)
R	Gas constant, (psia.cu.ft/lb mole)
A, B	Mixture-specific functions of T and composition with the mixing rules
T_r	Reduced temperature
c_s	Salinity, (ppm or mol/kg)
bq_i	Soreide and Whitson consant
k^a_{jw}	Aqueous phase binary interaction coefficients
J_i	Flux of component i per unit area, (mol m^2 s^{-1})
D_i	Diffusion coefficient of component i, (m^2 s^{-1})

$\partial y_i/\partial_d$	Molar concentration gradient of a component in the direction of flow, (mole fraction)
F_{ig}	Interblock diffusive flow, (mol/hour)
T_D	Diffusivity, the anaologue of transmissibility for diffusive flow, ($m^2\ s^{-1}$)
x	Total molar concentration, (mol m^{-3})
y_i	Vapor mole fractions
F^c_{pni}	Flow rate component in a phase (p=o, w, g), (mol/hour)
y^c_p	Concentration of component, c, in phase, p, (mole fraction)
k_{rp}	Relative permeability of phase, p
S_p	Saturation of phase, p, (fraction)
b^m_p	Molar density of phase , p, (mol/m^3)
b^m_g	Molar density of gas, (mol/m^3)
μ_p	Viscosity of phase, p, (cp)
T_{ni}	Transmissibility between cells, n, and i, (cP-rb/day/psi)
dP_{pni}	Potential difference of phase, p, between cells, n, and i, (psia)
scf	Standard cubic feet per day
σ_{gw}	Gas-pure water surface tensions, (gf/cm)
$\rho_{wg/cc}$	Water density, (g/cm^3)
$\rho_{hg/cc}$	Gas density, (g/cm^3)
σ_{cor}	Correct surface tensions, (gf/cm)
σ_{gw}	Gas-pure water surface tensions, (gf/cm)
σ_{hb}	Hydrocarbon-brine surface tensions, (gf/cm)
Sgi	Initial gas saturation, (fraction)
R_t	Resistivity of un-invaded zone, (ohm·meter)
R_i	Resistivity in the invaded zone, (ohm·meter)
R_{xo}	Resistivity of the flushed zone, (ohm·meter)
R_{mf}	Resistivity of salt water mud filtrate, (ohm·meter)
R_h	Residual hydrocarbon saturation, (fraction)
R_{xo}	Resistivity in the flushed zone, (ohm·meter)
R_w	Water resistivity, (ohm·meter)
µm	Micrometer
g/cm^3	Gram per cubic centimeter
MHz	Mega-hertz
$Qinj_{CO2}$	CO_2 injection flow rate
k	Permeability
μ_{CO2}	CO_2 viscosity
$P_{w,\ max}$	Maximum wellbore injection pressure
P_e	Initial reservoir pressure
K_{rCO2}	CO_2 gas relative permeability
r_e	External radius, (ft)
r_w	Internal wellbore radius, (ft)
km^2	Square kilometer
MSTB	Million stock tank barrel
Kg/m^3	Kilogram per cubic meter
Kr_{ow}	Relative permeability (condensate-brine)
S_{wc}	Connate water saturation, (fraction)
S_{gc}	Critical gas saturation, (fraction)
Kr_w	Relative permeability of brine
Kr_{lg}	Relative permeability of gas (CH_4)-liquid (CO_2)
Kr_{lw}	Relative permeability of liquid (CO_2)-brine (H_2O)
$(K_{ro})_{Swc}$	Relative permeability of oil at connate water saturation
$(K_{ro})_{Sgc}$	Relative permeability of oil at critical gas saturation
$(K_{rg})_{Swc}$	Relative permeability of gas at connate water saturation
STB/D/psia	Stock tank barrel per day per pound per square inch
Mscf	Million standard cubic feet
Bscf	Billion standard cubic feet

Mscf/D	Million standard cubic feet per day
z	Gas compressiblity factor
F	Formation factor

CHAPTER 1

INTRODUCTION

1.1 Background

Greenhouse gases play a vital role in changing the Earth's climate system. Increasing the amount of greenhouse gases in the atmosphere, carbon dioxide (CO_2) in particular, is, thus, considered as the main reason behind global warming and climate change (Herzog et al., 1997). Widespread melting of snow, ice, and rising of global average sea level indicates the fact the atmosphere is heating up. In spite of ongoing researches and continuing debates, there is a broad scientific agreement that CO_2 production due to burning of fossil fuels and human activities is major source of CO_2 emission into the atmosphere (Bryant, 1997). Carbon dioxide is essentially known as a gas with a significant potential to develop the greenhouse effect (Herzog et al., 1997), which has resulted in an increase of average global temperature by 0.8 ^{o}C over the past century (NOAA 2013). Figure 1.1 shows the increase of atmospheric CO_2 as measured at the meteorological station at Mauna Loa, Hawaii, including the superimposed seasonal fluctuations. The red line represents the monthly mean values, centered on the middle of each month. The black line represents seasonally corrected data (https://www.esrl.noaa.gov).

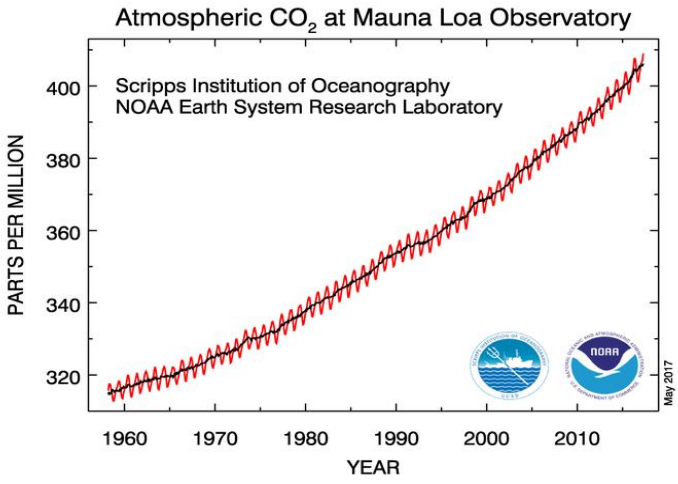

Fig. 1.1 Atmospheric CO_2 concentrations as measured at Mauna Loa, Hawaii (NOAA, 2017)

There is a broad consensus that anthropogenic interferences with the climate system should be prevented by stabilizing the concentrations of CO_2 in the atmosphere. To do this, there have been many approaches suggested such as the reducing energy consumption, swapping to fuels having less carbons, and capturing and storage of CO_2 (CCS), among which the carbon capture and storage in subsurface geologic storage sites would provide the best option (Bachu, 2001).

1.2 Principle of CO_2 capture and storage (CCS)

A CCS practice involves capturing of carbon dioxide from the stationary source, transporting it through pipelines to a site and injecting it into a suitable geologic site (Herzog et al., 1997), as illustrated in Figure 1.2. CO_2 capture is taken from large point sources: fossil fuel power plants, fuel processing plants and other industrial plants, particularly for the manufacture of iron, steel, cement and bulk chemicals (IPCC, 2005-pp80). This is the strategy taken in recent years to reduce the quantity of CO_2 released into the atmosphere (Solomon, 2007; Wright, 2007). Recognized subsurface geologic sites are depleted/active petroleum reservoirs, deep saline aquifers, deep coal beds, and salt domes (Cook, 1999). The general concern associated with the storage options is to ensure that the injected CO_2 resides in the storage site for a long period of time without any potential leakages to the atmosphere. Table 1.1 compares different subsurface geologic storage sites based on their capacity, cost, integrity, and technical feasibility. Depleted or almost depleted gas/oil reservoirs would be important targets for storage due to their proven storage integrities, relatively well-understood behaviors through exploration and production, availability of infrastructures and high effective stress levels due to hydrocarbon production (reducing the risk of leakage). Comparatively, depleted condensate gas reservoirs are more favourable than dry and wet gas reservoirs because of their higher gas compressibility and storage capacity (Sobers et al., 2004). Due to widespread existence, deep brine aquifers could hold a large amount of CO_2 than petroleum reservoirs, but their relative cost, storage integrity and technical feasibility have not been very well understood (Herzog et al., 1997). Salt domes and coal beds are also

not very attractive option due to their high exploitation cost and unknown storage space, respectively (Herzog et al., 1997; Saeedi and Rezaee, 2012).

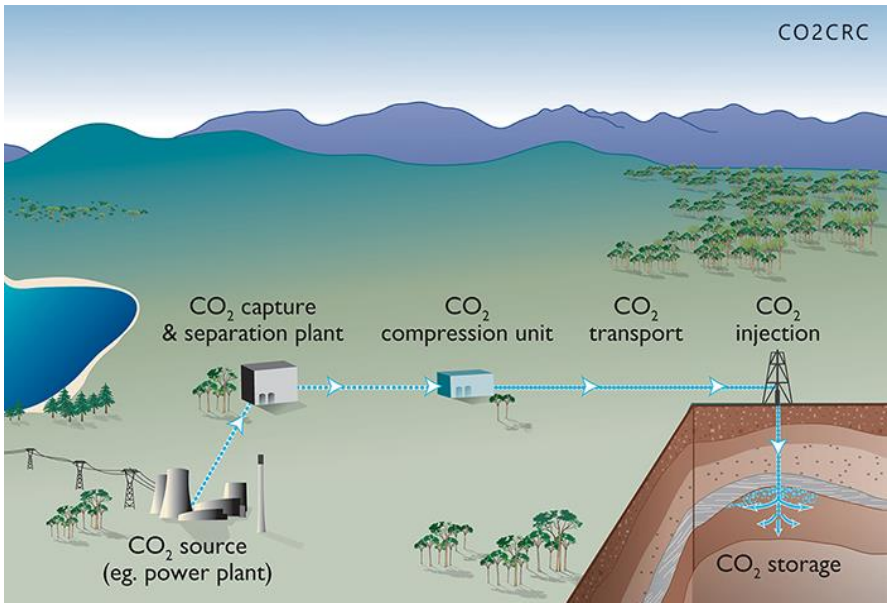

Fig. 1.2 CCS process demonstrating the capture, transportation and injection for storage (Source: Cooperative Research Centre for Greenhouse Gas Technologies, CO2CRC 2015)

Table 1.1 Comparison of different geologic storage sites (Herzog et al., 1997)

Storage Option	Relative Capacity	Relative Cost	Storage Integrity	Technical Feasibility
Active Oil Reservoirs	Small	Very Low	Good	High
Coal Beds	Unknown	Low	Unknown	Unknown
Depleted Oil/Gas Reservoirs	Moderate	Low	Good	High
Deep Aquifers	Large	Unknown	Unknown	Unknown
Mined Caverns/ Salt Domes	Large	Very High	Good	High

Prior to a storage site selection, a preliminary assessment should be done to evaluate the storage site at the basin and reservoir scales for key CO_2 storage aspects (Bachu 2001; Bachu 2003). Thereafter, a comprehensive characterization of the petroleum reservoir before the injection needs to be carried out by experimental or numerical methods to ensure the suitability of the chosen reservoir for a safe storage, in which storage capacity, injectivity, trapping mechanisms (structural, capillary (residual), solubility, and mineral) and containment are to be evaluated in details (IPCC, 2005-pp208).

1.3 Differents aspects of CO_2 storage sites

In this section, different fundamental aspects of CO_2 storages are discussed and major parameters required for a suitable storage site selection are emphasized. All the topics being presented in this section serve as a comprehensive knowledge to aid in the understanding of the fundamental of this research.

1.3.1 Storage capacity

Storage capacity is defined as the total volume of a geologic storage site that can possibly be used for storage purposes. Estimation of storage capacity in reservoirs is conventionally done by excluding the formation water during or after the production stage. However, such estimation might be too conservative when the dissolution of CO_2 in water is neglected (Van der Meer, 2005; Bachu et al., 2007; Goodman et al., 2011). Storage capacity depends mainly on subsurface pressure and temperature conditions at which CO_2 appears at supercritical state (Qi et al., 2010). This is linked to the fact that reaching the supercritical condition is essential for CO_2 to approach a high density and gas-like viscosity, resulting in a complete pore volume (PV) utilization and mobility within a reservoir (Ketzer et al., 2012). Figure 1.3 displays the phase diagram of pure CO_2 indicating the pressure and temperature at which phase changes may take place in subsurface geologic storage sites (Mazzoldi et al., 2011).

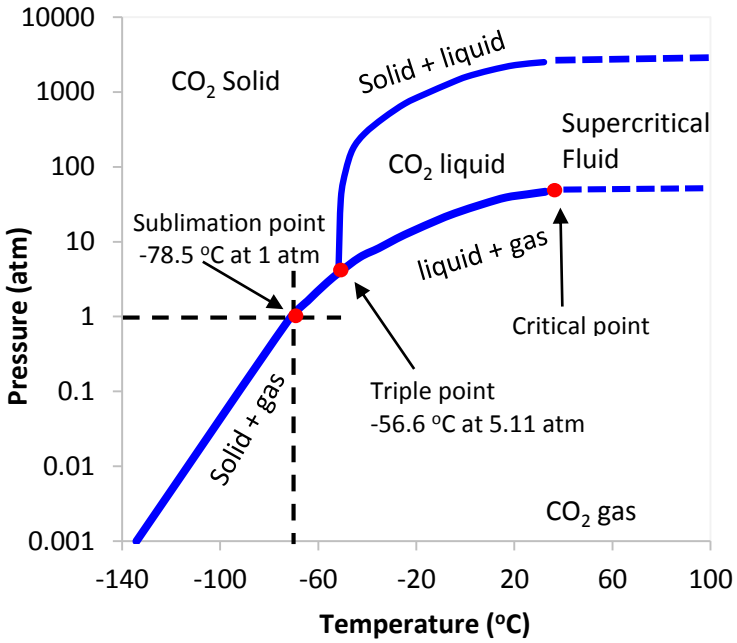

Fig. 1.3 Carbon dioxide: temperature – pressure diagram (after Mazzoldi et al., 2011)

There have been many studies where an efficient storage is reported to be the one that has taken place in the reservoirs located at the depth of more than 800 m (Qi et al., 2010; Pentland et al., 2011; Ketzer et al., 2012; Black et al., 2015; Kimbrel et al., 2015). Pressure, temperature and CO_2 density variations are playing important roles in these cases. For instance, the density of CO_2 increases with depth and this enhances the storage capacity (Bachu, 2001; Bachu, 2003; Solomon, 2007) considering the fact that a dense CO_2 occupies smaller pore volumes (Lu et al., 2009, Saeedi, 2012). This density can also be achieved in a low temperature gradient site where the pressure would be a crucial player to reach the supercritical condition (Bachu, 2003; Qi et al., 2010). Fortunately, up to 80% of hydrocarbon reservoir in the world, regardless of ages and locations, is located at depths larger than 1500 m (Van der Meer, 2005). Therefore, dense supercritical CO_2 ($scCO_2$) can be achieved and may not be a concern.

Porosity is another parameter which should be high enough for having a good storage capacity, even though it decreases with depth due to compaction and cementation phenomena (Solomon, 2007). Stratigraphic heterogeneity, referred to as the geometry of depositional facies, is also controlling the efficiency of the storage capacity. Hovorka et al. (2004) suggested that a buoyant $scCO_2$ flow avoids a significant portion of the rock volume in a homogeneous rock, resulting in having a low storage capacity. In contrast, a large volume of heterogeneous rocks accepts the injected CO_2 due to disperse flow paths (Hovorka et al., 2004; Ambrose et al., 2008).

Other parameters such as the mobility and buoyancy of CO_2, and irreducible water saturations can also reduce the capacity of a storage site. For instance, Pentland et al. (2011) performed a series of experiments considering a two-phase system by saturating Berea sandstones with $scCO_2$ (90%) and water (10%). They reported that up to 37% of CO_2 was trapped in the pore spaces due to the irreducible water saturation, which was about 10% higher than what was experienced by Suekane et al. (2008).

1.3.2 Injectivity

Injectivity is the ease with which fluids can flow through stratigraphic intervals (Ambrose et al., 2008). Permeability and thickness of storage sites along with optimum injection rate are directly related to the injectivity (Ambrose et al., 2008; Ghaderi et al., 2009; Qi et al., 2010; Raza et al., 2016). For instance, low permeability thin reservoir intervals and complex structures within an injection zone diminish the injectivity. In general, permeability near the wellbore must be greater than >100 mD for a favorable injectivity (Watson and Gibson-Poole, 2005). However, the permeability of a site should be low to ensure that a permanent storage can take place (Shi and Durucan, 2009; Qi et al., 2010). Cinar et al. (2008) stated that a high permeable site is less expensive for CO_2 storage due to lesser number of wells required for the favorable injection. The CO_2 storage modeling of Nisku aquifer in Alberta revealed that a large volume of CO_2 could be injected to avail more storage capacity by controlling the pressure build-up through hydraulic fractures of horizontal wells (Ghaderi et al., 2009). In fact, it would be more economical to consider hydraulic fractured horizontal wells rather than vertical ones in low permeable geological media, due to lesser number of injection wells required (Cinar et al., 2008).

The reservoir pressure increases during the CO_2 injection and eventually reduces the injectivity to compensate the excessive pressure build-up (Ghaderi et al., 2009; Jalil et al., 2012). This might be a problem for storage exercises in an aquifer as the significant pressure build-up may not be released due to the resistance of brine in pore spaces (Cinar et al., 2008). It is also reported that the reservoir pressure should not exceed the seal (caprock) fracture pressure in order to mitigate the escape of CO_2 to the atmosphere. Therefore, a comprehensive evaluation of seal integrity is required during the depletion or injection to ensure that fractures will not be initiated within a seal (Burke, 2011).

It seems that there is an inevitable link between the injectivity and drive systems of gas storage reservoirs. Such link has also been observed in abandoned water flooded (externally supported) reservoirs and natural water drive (internally support)

reservoirs, but the remarkable pressure increase, due to external water support, makes it hard to have an efficient injectivity and storage capacity in these kinds of reservoirs (Bachu, 2004; Van der Meer, 2005). It is, therefore, assumed that the theoretical CO_2 storage capacity in petroleum reservoirs with a weak natural water drive support is decreased by 3% (Bachu, 2004). Compacted reservoirs may not also be a very wise choice for the CO_2 storage due to pore volume collapses under a significant reduction of initial pressure (Van der Meer, 2005).

There have been many studies attempting to estimate the injectivity either in labs (Saeedi and Rezaee, 2012; Peysson et al., 2014; Ott et al., 2015a) or through numerical simulations (Giorgis et al., 2007; Oruganti and Bryant, 2009; Oldenburg and Doughty, 2011; Jalil et al., 2012; Ganesh et al., 2014). According to these studies, mineral dissolutions/precipitations near a wellbore have a significant impact on rock properties and the injectivity. Geochemical reactions, resulting in the dissolution and precipitation of minerals, depend mainly on subsurface thermodynamic conditions, fluid and rock compositions in a $scCO_2$-brine system. These interactions often occur in a shorter period of time in carbonates compared to siliciclastic rocks (Bacci et al., 2011). In fact, sandstone as a siliciclastic rock does not show any significant geochemical reactions (De Silva et al., 2015). The mobilization of detrital or diagenetic clays can also clog pore throats, and decrease the injection rates (Ambrose et al., 2008). The $scCO_2$-brine-rock chemical reactions based study carried out on the Goldeneye depleted gas reservoir located at offshore of North Sea indicated that the mechanical parameters (i.e., Young's modulus, Poisson's ratio) of sandstone reservoirs, consisting mainly of quartz (~80%) and feldspars (~10%) with small amounts of authigenic clays and intergranular cements, had not yet gone through any significant changes during the injection (Hangx et al., 2013).

Residual trapping is probably one of the trapping mechanisms with known impacts on the injectivity (Kimbrel et al., 2015). The entrapment of injected $scCO_2$ in the pore space of rocks surrounded by water develops what is known as the residual CO_2 saturation during the residual trapping (Lamy et al., 2010; Iglauer et al., 2011a). This residual saturation is impacted by rock properties and can be measured

experimentally in a lab (Suzanne et al., 2001; Suzanne et al., 2003). Previous studies investigating depleted natural gas reservoirs stated that the success of an enhanced gas recovery (EGR) practice and CO_2 storage is linked to the injection strategy, reservoir characteristics and operational parameters (Oldenburg and Benson, 2001a; Jikich et al., 2003; Feather and Archer, 2010). The residual gas in depleted reservoirs may significantly increase or decrease the storage capacity (Saeedi, 2012). It also reduces the brine mobility and decreases the density and viscosity of gas mixtures when it dissolves into the supercritical CO_2 (Oldenburg and Doughty, 2011). Saeedi and Rezaee (2012) experimental investigation showed that the saturation of residual gas in sandstone decreases the CO_2 injectivity at early stages but this injectivity improves as the injection progresses. This would be mainly due to the permeability dependent rate of replacing CO_2 with residual gases.

1.3.3 Trapping mechanisms

As the pressure builds up due to the injections, the trapping of $scCO_2$ in a geological site is known to take place. The efficiency of the trapping mechanism, however, depends mainly on reservoir characteristics and in-situ parameters (Bachu, 2001). For instance, a structural/stratigraphic trapping of free $scCO_2$ occurs due to high capillary entry pressure in the overlying seal. Solubility trapping, on the other hand, is a long-term process taken place when $scCO_2$ dissolves into subsurface fluids and the dissolved CO_2 reacts with rocks in a long term, leading to mineral trapping (Iglauer et al., 2011a; Zhang and Song, 2014). Figure 1.4 is displaying the four trapping mechanisms during CO_2 storage. Generally speaking, site selections based on dominant trapping mechanisms are essential to prevent any leakage to surface or subsurface resources.

In the context of a structural trapping, CO_2 flows vertically upon the injection in the absence of prominent barriers and accumulates below any seals due to the gravity force. Although, this accumulation is immobilized by residual or solubility trappings (Riaz and Cinar, 2014), depending on the degree of seal integrity, reactivated faults or poorly completed wells can potentially result in leakage of CO_2 into other permeable formations (Saeedi, 2012).

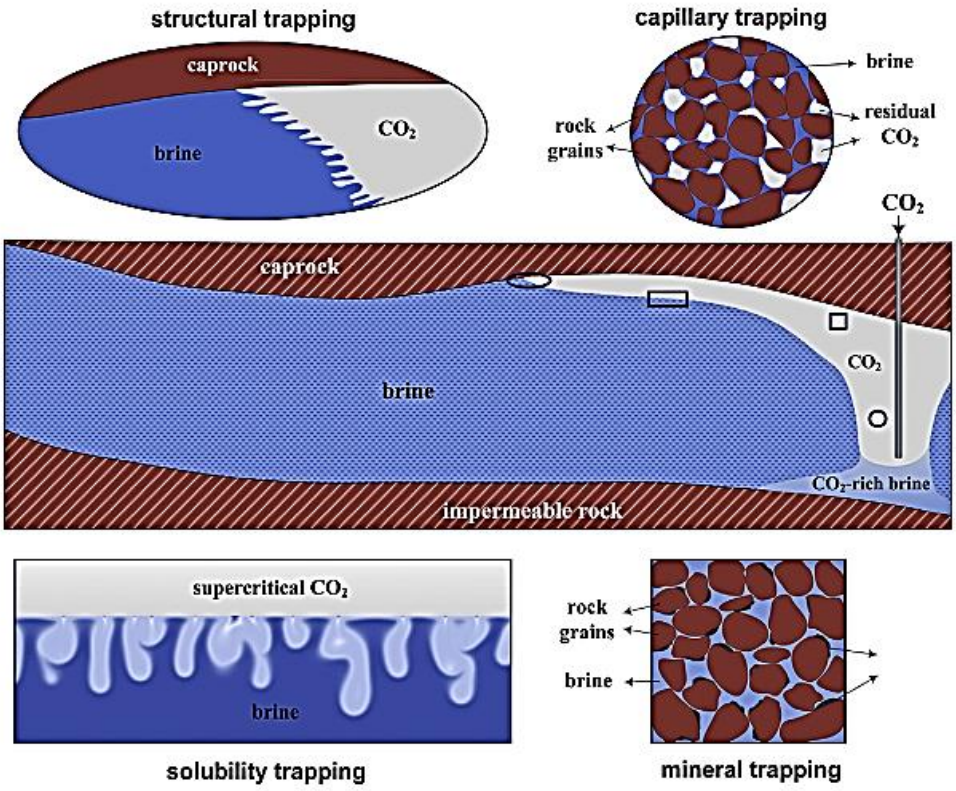

Fig. 1.4 Demonstration of CO_2 storage trapping mechanisms (Emami-Meybodi et al., 2015)

The geometry of pore spaces, rock–fluid interactions and fluid–fluid interactions play vital roles when it comes to the CO_2 storage in a geological site (Chalbaud et al., 2010). The Laplace model represents these interactions (Eq. (1.1)), which affect the flow process and in the long-term, control the capillary-sealing efficiency (Chalbaud et al., 2010):

$$P_c = P_{CO_2} - P_{Brine} = \frac{2.\sigma_{brine\text{-}CO_2}.\cos\theta}{r} \quad (1.1)$$

In Eq. (1.1), P_c is the capillary pressure, $\sigma_{brine\text{-}CO2}$ is the interfacial tension between brine and CO_2, r is the largest connected pore throat and θ is the contact angle representing the rock wettability.

There are numerous parameters which can control the residual trapping, including vertical permeability, thermodynamic properties of a CO_2 - H_2O phase, heterogeneity, etc. For instance, brine viscosity reduces the chance of having a good residual trapping mechanism (Taku Ide et al., 2007; Bandara et al., 2011). Interfacial tension

is another parameter which is linked to the residual CO_2 saturation (Wildenschild et al., 2011), particularly in consolidated sandstone reservoirs (Raza et al., 2016). However, the CO_2–brine interfacial tension is less than that of a hydrocarbon–brine and thus, a lower residual gas saturation is usually observed in a CO_2-brine system (Saeedi and Rezaee, 2012). The interfacial tension decreases with increasing the pressure and is impacted by the temperature to a great extent (Sarmadivaleh et al., 2015).

There have been many studies indicating the importance of wettability during the CO_2 storage practice. Contact angle is the parameter quantifying the wettability in a CO_2-brine system and is sensitive to the variation of pressure and temperature (Iglauer et al., 2015; Sarmadivaleh et al., 2015). According to the recent studies, this contact angle has a great impact on the injectivity, containment security, structural, residual, solubility and mineral trapping capacities (Iglauer et al., 2015). According to Iglauer et al. (2011a), the contact angle has a great impact on the residual trapping in a water-wet system because $scCO_2$ appears occasionally in a non-wetting phase. In a non-water-wet system, therefore, the pressure on the seal is increased by the $scCO_2$ plume resulting in fracture initiations and leakages through the site. Sandstone and limestone plus pure minerals such as quartz, calcite, feldspars, and mica are strongly water-wet in a CO_2-water system (Iglauer et al., 2015). Pentland et al. (2011) highlighted that the residual CO_2 saturation may not be high if CO_2 acts as a wetting phase.

The pore throat size and its distribution are important in the fluid transportation processes due to their effects on reservoir properties (i.e., fluid saturation, porosity, permeability and, to some extent, wettability) (Lake et al., 1986). In the context of CO_2 storages, having a narrow pore throat size is more beneficial than a wider pore one because the high aspect ratio (i.e., pore-body radius to pore throat radius) affects the fluid interface and causes the flow of the wetting phase to go into the pore throats offering a high non-wetting phase saturation (Grobe et al., 2009; Pentland et al., 2012). Although, a large volume of heterogeneous rocks accepts the injected CO_2 due to disperse flow paths (Ambrose et al., 2008), high heterogeneity in the pore-

throat size distribution affects the CO_2 distribution and flooding processes (Wei et al., 2014). Therefore, slow and lateral movements of $scCO_2$ in the storage site is crucial to enhance the chance of immobilization in a low permeability medium (Shi and Durucan, 2009; Teletzke and Lu, 2013). On the other hand, a fast movement of $scCO_2$ plume in the absence of any barriers in the storage site can alter the wettability due to the pressure build-up, and reduces the breakthrough capillary efficiency of the seal during a long-term contact (Chalbaud et al., 2010).

A favorable residual trapping is often achieved in quartz-rich sandstones and carbonates which are strongly water-wet (Iglauer et al., 2011a). Carbonates are mostly composed of calcite and dolomite while sandstone comprises of quartz and feldspar. The solubility rate (solubility trapping) in the pore water is linked to the composition of reservoir fluids and rocks. For instance, if a rock is composed mainly of carbonates, the chemical reactions of brine with the rock increase the solubility (De Silva et al., 2015). However, carbonates are more stress sensitive than sandstones and this may cause complexities during the storage (Lamy et al., 2010). When it comes to the solubility trapping, the temperature, the pressure, salinity ranges, and type/composition of rocks play crucial roles (De Silva et al., 2015). For instance, high temperature and low pressure conditions result in having a low-density CO_2, which in turn causes the $scCO_2$ plume to flow at a higher rate and makes the monitoring far more complicated (Lu et al., 2009). The increase of CO_2 pressure, on the other hand, increases the CO_2 dissolution and the brine density (De Silva et al., 2015). This increase in the density may result in gravitational instabilities in which denser brine moves downward away from the flowing $scCO_2$ plume, promoting the solubility trapping (Elenius et al., 2015; Iglauer et al., 2015). According to Chevalier et al. (2010), the CO_2 solubility is favorable in the low temperature and low saline areas.

Mineral trapping is the final phase of trapping occurs from the fact that when $scCO_2$ dissolves in water and it forms a weak carbonic acid (Ketzer et al., 2012). Over a long time, however, this weak carbonic acid can react with the minerals in the surrounding rock to form solid carbonate minerals (Zhang and Song, 2014).

Depending on the chemistry of the rock and brine in subsurface geologic media, this trapping can be very slow or rapid but mineral trapping binds CO_2 to the rock and $scCO_2$ becomes more securely trapped with time (De Silva et al., 2015).

1.3.4 Containment

Containments of a storage site depend mainly on the characteristics of caprocks, faults and fracture surrounding a reservoir. Caprock is not usually a concern when the integrity of a storage site is evaluated, but the sealing ability of faults has often raised an alarm. A fault must have a permeability of less than 0.1mD (Ketzer et al., 2012) and should be surrounded by clays and evaporites or other impervious rocks in order to be counted as a reliable seal (Van der Meer, 2005). Seals capacity, their geometry and integrity are the most important aspects of containment when it comes to the storage site reliability analysis (Ambrose et al., 2008).

The sealing capacity of a fault, however, is affected by the pore-throat size, contact angle (wettability) and interfacial tension of rock forming minerals (Daniel and Kaldi, 2008). These minerals, including mica, muscovite and phlogopite, are strongly water-wet and favor the sealing ability of caprocks or faults against the leakage of the $scCO_2$ plume (Iglauer et al., 2015). The upper limit of the breakthrough pressure of a seal, on the other hand, is linked to the interfacial tension of the CO_2-water system and is often less than that of the oil-water system. Thus, detailed analysis of the pressure sustained by seals is crucial before and during the injection (Li et al., 2006). For example, a study on the faults surrounding the Gippsland Basin in Australia indicated that the sealing capacity would not be the same at different locations, depending on the interfacial tension of CO_2-water systems (Divko et al., 2010).

Thickness of a seal is another aspect of integrity analysis which should not be neglected (Kaldi et al., 2013). According to Chadwick et al. (2008), Chevalier et al. (2010) and Ramirez et al. (2010), a seal must have a thickness of at least 10 m to provide resistance against the CO_2 plume pressure.

A seal integrity changes by the increase of the pore pressure and stress variations induced due to the injection (Ouellet et al., 2011; Kaldi et al., 2013). A significant

increase of the pressure during the injection decreases the normal stress on a fault surface and causes the mechanical break-down (reactivation) (Olden et al., 2012). Therefore, hydraulic integrity analysis of storage sites is essential before starting or even during the storage.

Compressibility of geologic sites is another vital piece of information which should be a part of the analysis. If a reservoir is highly compressible, changes of pore pressure reactivate the faults during the compaction, causing a significant leakage to surrounding formations. Geomechanical evaluation has then become inevitable for those hydrocarbon reservoirs suffering from a severe compaction effect, such as the Wilmington oil reservoir in California and Ekofisk reservoir in the North Sea (Olden et al., 2012).

Last, but not least is the wellbore condition which is linked to the cement placement and near-reservoir stress conditions before the injection (Hawkes et al., 2004). Analysis of seismic and well data, especially Cement Bond Logs (CBL) during the production stage, would be required to ensure that the wellbore condition may not become a serious issue during the injection.

1.3.5 Cost

There are many economic aspects included in the site selection which should not be neglected. Transportation of large quantities of CO_2 from a source to storage sites can be done through pipelines in a cost-effective way. The cost of this transportation, however, depends mainly on locations (e.g. onshore or offshore), the size and composition of pipelines and operating conditions (Bennaceur et al., 2008). According to IPCC (2005), transportation cost from a source to a site is estimated to be around 1-8 USD/tCO_2 per 250 km pipeline. The report released in the recent years indicated that as long as the distance between major sources and prospective sedimentary basins is less than 300 km, transportation may not induce excessive costs on storage projects (IPCC, 2005-Table SPM.4). Non-condensable impurities such as N_2, O_2 and Ar which are often mixed with CO_2 during the capturing practice may also pose extra costs on storage projects. These impurities are required to be

separated before the injection as they may reduce the storage capacity of a site (Wang et al., 2011). Furthermore, moisture of CO_2 needs to be removed to avoid corrosions and hydration, which can induce extra costs (Ghg, 2004). Thus, careful considerations of costs included in a storage project is an essential step at the early stages before the injection begins.

1.4 CCS practices worldwide

There have been a number of large scale projects across the world with significant milestones in the past year, where the CCS technology has been employed, as shown in Figure 1.5 (Institute, 2016).

The Sleipner CO_2 storage project, located off the Norwegian coast, with more than 16 million tones (Mt) of CO_2 injected since the commencement of the project in 1996, is great example of success in the CCS projects. The Snøhvit CO_2 storage project, which is also located offshore of Norway has started the operation since 2008 with more than three million tons of CO_2 injected. In Brazil, Petrobras announced that, as of December 2015, the Santos Basin Pre-Salt Oil Reservoir based CCS project located approximately 300 km off the coast of Rio de Janeiro in ultra-deep water had injected three million tons of CO_2 into the producing reservoirs. The Air Products Steam Methane Reformer EOR project in Texas had captured three million tons of CO_2 from the hydrogen production facilities as of June 2016. The Boundary Dam Carbon Capture and Storage Project had captured one million tons of CO_2 from its Unit 3 power generation facility as of July 2016. The Quest project in Alberta, Canada, had successfully captured and stored more than one million tons of CO_2 into a deep saline formation as of September 2016. In October 2016, the US DOE Office of Fossil Energy website highlighted that over 13 Mt of CO_2 has been injected in the US as part of the DOE's Clean Coal Research, Development, and Demonstration Programs. The Jilin Oil Reservoir EOR demonstration project in China began CO_2 injection ten years ago, and reached one million tons of CO_2 injected in 2016.

Fig. 1.5 An overview of key CCS projects and milestones around the globe (Institute, 2016)

1.5 CCS scope in Malaysia

Malaysia is on the verge of becoming an industrialized nation and soon the country would have a greater role in the fight against climate change (Lai et al., 2011). Power generations by the fossil fuel consumption, in Malaysia, is significantly contributing to the increase of the CO_2 level (IEA, 2014). This high emission is released into the atmosphere due to stationary sources along the coast of the West Malaysia. This situation may become far worse when coal reserves of the East Malaysia are utilized for the power generation after the depletion of hydrocarbon reserves (ICTPL, 2005). Given the domination of fossil fuels in Malaysia's energy sectors, CO_2 emissions would increase from 211 Mt in 2013 to almost 430 Mt by 2040 (Figure 1.6).

Coal used in the power sector is responsible for two-thirds of the increase in emissions over this period. The carbon intensity of Malaysia's economy is one-and-a-half times greater than the average in Southeast Asia. Malaysia's carbon intensity declines by 33% over this 27 years due to structural changes in its economy and the implementation of measures and policies, such as the Renewable Energy Act. The

power sector's share of CO_2 emissions would increase by 14 percentage in 2040 (IEA, 2015). Thus, there is a great need to cut down CO_2 emission in Malaysia.

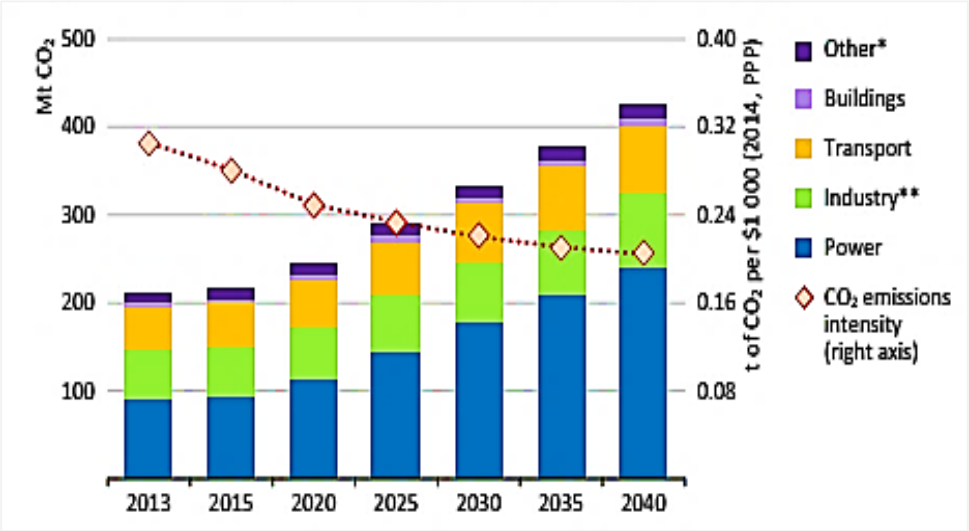

Fig. 1.6 Energy-related CO_2 emissions by sector in Malaysia (IEA, 2015)

Considering the risk of CO_2 emission in Malaysia, there have been a limited number of reviews on the potential and technical feasibility of CCS in Malaysia (e.g. see (Othman et al., 2009; Oh, 2010). There have also been very limited number of studies (Masoudi et al., 2011; Jalil et al., 2012; Masoudi et al., 2013) carried out so far to evaluate the petroleum reservoirs located in Malaysia for a storage practice. Figure 1.7 shows that a large number of offshore reservoirs in South China Sea that can potentially be used for CO_2 storage in Malaysia. For example, the Alpha carbonate gas field located approximately 250 km offshore, Sarawak, East Malaysia contained approximately 70% CO_2 and good gas reserves. As part of CO_2 mitigation plan during Alpha field development, CO_2 will be transported, injected and sequestrated into depleted nearby gas fields (Jalil et al., 2012).

When examining this Figure 1.7, it seems that Malaysia has a great potential to implement CCS, but the technical reliability, safety, implementation cost and availability of quality storage capacity of petroleum reservoirs must be properly addressed first before making any final decisions. This study would be one of the pioneering work to address the current shortcomings in the field of CO_2 storage

reservoir characterization and to conduct the reservoir characterization of carbonate gas reservoir of Malaysia for their potential as a CO_2 storage site.

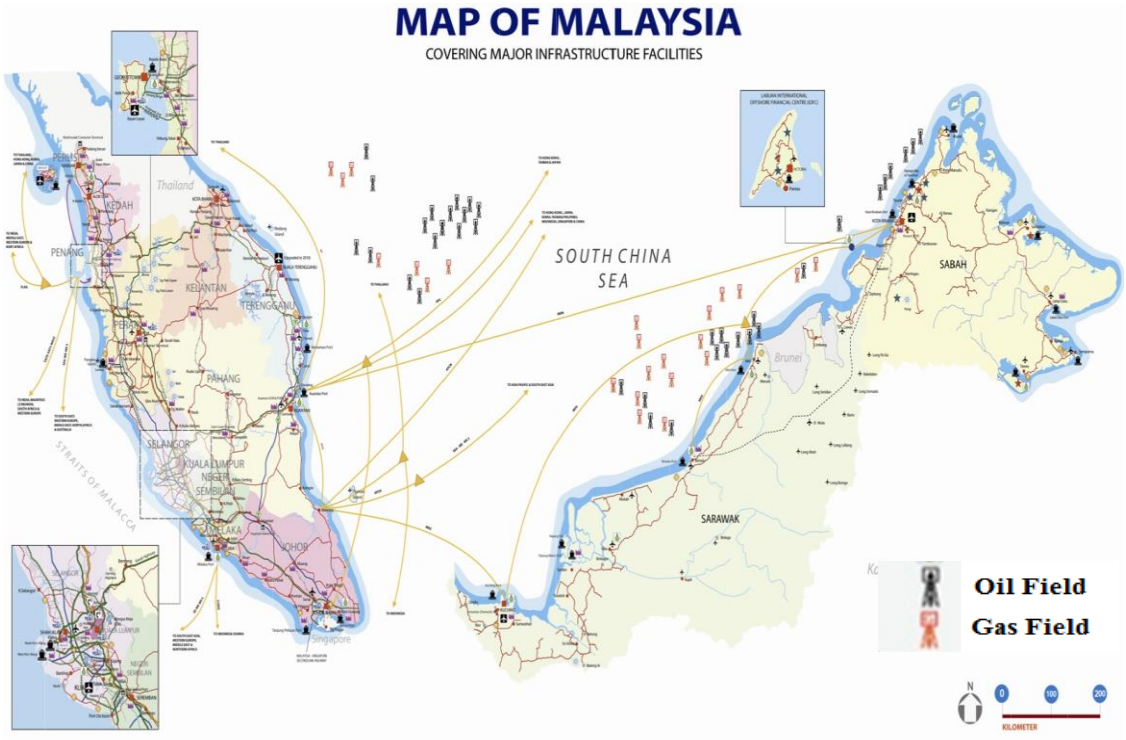

Fig. 1.7 Petroleum reservoirs in the Malaysia (modified after http://www.mida.gov.my)

1.6 Research objectives

The aim of this thesis is to characterize a carbonate gas reservoir of Malaysia for their potential as suitable CO_2 storage sites by addressing the issues related to field of CO_2 storage reservoir characterization. This would be accomplished by achieving the following objectives:

1) Reservoir characterization to evaluate the petrophysical, lithological and geomechanical aspects of the reservoir through the reservoir data.

2) Proposing an approach to assess the residual CO_2 saturation and its validation based on experimental data and numerical modeling.

3) Utilization of the proposed approach to determine the residual saturation of CO_2 by the help of the reservoir data.

4) Performing an injectivity assessment using experimental approaches at certain CO_2 injection rates on available core samples to evaluate the pressure drop, rock strength and the rock dissolution.
5) Numerical modeling based on reservoir data to examine the CO_2 injectivity in different aspects at optimum CO_2 injection rate.

1.7 Research significance

A comprehensive assessment of key storage aspects (i.e., storage capacity, injectivity, trapping mechanisms, and containment) of subsurface geologic site for CO_2 storage is crucial for the success of CCS projects. Over the last decades, a significant level of knowledge has been gained as to how to the subsurface geological media can be evaluated for their storage potentials, but there are still many remaining issues which have not been addressed yet. This study attempts to tackle few of these issues by:

1) Presenting a new CO_2 storage site, injection well and injection zone evaluation screening criteria for depleted reservoirs.

2) Proposing a method to estimate the residual saturation of CO_2 which can make the selection of depleted petroleum reservoirs easier.

3) Assessing injectivity properties of the reservoir on the core scale to provide a better insight into the reservoir capacity when it comes to the injection.

4) Developing a new scheme to determine the optimum injection rate and/or the injection scheme for storage purpose.

1.8 Research design

By addressing the issues related to CO_2 storage, reservoir characterization might be brought to the next level that will be answered in this thesis. In research design, screening tools for reservoir, injection well and injection zone have been proposed based on critical literature review. These screening tools have been applied on carbonate gas reservoir as per availability of the reservoir data (i.e., reservoir

information, petrographic analysis, well logging and coring data) for preliminary assessment of CO_2 storage aspects. For this evaluation, analytical correlations (given in Appendix) and Interactive Petrophysics Tool were used. In addition, a few well logs were calibrated with the available core data. A new CO_2 residual trapping evaluation analytical approach has been established based on Laplace method with its validation via core flooding experimental data and numerical modeling. By using the well logging data and other information, the approach has been applied on gas reservoir for CO_2 residual trapping potential. Moreover, the significance of compaction and geochemical effects in CO_2 storage sites has been explored via ultrasonic pulse measurements and SEM analysis during evaluation of injectivity. Finally, the role of optimum injection rate on injectivity evaluation has been shown by carrying out the numerical modeling of carbonate gas reservoir with Eclipse simulator (Schlumberger 2014a, 2014b).

1.9 Outline of this thesis

The thesis is organized into seven chapters. Chapter 1 in an introduction to the research subject, Chapter 2 presents a detailed literature survey highlighting significant research gaps in the field of CO_2 storage characterization. Chapter 3 brings a new screening criteria for storage site selection. A systematic guideline is also proposed for injection well evaluation in depleted reservoirs which can be followed for injection and monitoring purposes. Some indicators are proposed to justify the good zones for favorable CO_2 storage. Based on the proposed screening criteria, the preliminary assessment of the depleted gas reservoir, injection well and injection zone is also carried out by utilizing the available reservoir information. The positive and negative storage indicators associated with gas reservoir are also highlighted during the evaluation. In chapter 4, a new approach to estimate the residual trapping ability is presented by considering the interfacial tension, wettability, residual gas saturation. This approach is validated by experimental and numerical approaches. The implementation of the developed approach at the field level is also shown. In this chapter, an investigation is also done on the variation of trapping mechanisms against pressure, temperature and salinity level. Chapter 5 discusses the injectivity

(pressure drop), reservoir strength and the rock dissolution considering the geochemical and compaction effects. It is also shown that how injection of different fluids type may change the rock structure under different in-situ stresses. In chapter 6, a numerical modeling is conducted to evaluate the injectivity and effective storage potential at the optimum injection rate considering the carbonate gas reservoir. Finally, chapter 7 summarizes the research findings, provides an overview of the general conclusions of this thesis and recommendations on possible new research directions to be further evaluated.

CHAPTER 2

LITERATURE REVIEW

2.1 Introduction

This chapter presents an overview on the existing research studies on different areas related to CO_2 storage reservoir characterization of subsurface geologic sites. This includes preliminary assessment of storage site, injection well and injection zone, CO_2 residual trapping assessment method, geomechanical and geochemical interactions impact on reservoir integrity, and selection of optimum CO_2 injection rate for CO_2 storage in petroleum reservoirs. The purpose to focus on these areas is to address the current shortcomings that can influence the overall comprehensive reservoir characterization and identification of petroleum reservoirs for CO_2 storage purposes. The review is done so that the research gaps can be addressed based on the current research objectives.

2.2 Preliminary assessment of CO_2 storage site

The preliminary assessment of subsurface geologic media has been a topic of interest in recent years and carried out based on screening criteria by using field data and analytical methods. This preliminary assessment of key CO_2 storage aspects is essential to mark the most suitable storage site for comprehensive CO_2 storage reservoir characterization. For instance, Koukouzas et al. (2009) evaluated the sedimentary basins of Greece for effective CO_2 storage. This evaluation was carried out based on the criteria developed by Bachu (2003) and modified by Gibson-Poole et al. (2006). However, there were no studies on the storage capacity and structural integrity of the reservoir. Likewise, the study performed by Mao et al. (2014) as a preliminary assessment of a geological CO_2 storage site in Cambodian sedimentary basins followed the screening criteria proposed by Bachu (2003). In another study, Ramirez et al. (2010) focused on aquifers and depleted reservoirs for CO_2 storage and selected a few of them based on their own screening criteria, which were limited to

the storage capacity, depth, thickness, porosity, permeability, seal/reservoir composition, and initial pressure. Bedard et al. (2010) made a preliminary assessment of the theoretical and effective capacities of reservoirs located at the basin of the Potsdam, Beekmantown and Trenton in St Lawrence. They developed basin-level practical criteria that only considered the depth, size, and tectonic setting of the basin, fault occurrences, the presence of an extensive vertical and horizontal seal (caprock), accessibility, infrastructure and the proximity of large CO_2 sources. Fang and Li (2011) considered annual emissions of large-scale CO_2 point emission sources instead of making a thorough evaluation of geologic media in Chongqing, China for the purpose of CO_2, and estimated the theoretical CO_2 storage capacities of depleted gas reservoirs, unmineable coalbeds, and saline aquifers for site-source matching. Carneiro and Alberto (2014) assessed the Rovuma basin for CO_2 storage, and only the lithology, geologic structure, and storage capacities were taken into consideration. Solomon et al. (2014) quantified the storage potential of the Mozambique Basin to identify the best area for CO_2 storage based on a capacity assessment of deep saline aquifers using a geographic information system (GIS). In a nutshell, none of the studies carried out in recent years provided a detailed preliminary assessment of depleted reservoirs by considering all of the parameters that affect the safety and success of a storage site.

Screening criteria is used to initially mark the suitable storage site by carrying out the preliminary assessment of available subsurface geological mediums. A general CO_2 storage criteria has already been presented based on local-scale projects in which depth, permeability, porosity, CO_2 density and containment factors were considered for selection of an appropriate storage site, there are few other aspects which are yet to be considered. There are few studies presenting a screening criteria for depleted reservoirs by referring to different aspects of a storage site. For instance, Kovscek (2002) presented a screening criteria for the CO_2 storage in depleted oil reservoirs. Key parameters such as reservoir depth, storage capacity, water and oil volumes in place, formation thickness, and permeability were considered in his criteria. He indicated the density of $scCO_2$ as one of the important parameters which should be included as a part of site selection. There was also an emphasis on the

relationship between the production and fault and fractures reactivations (Kovscek, 2002). Solomon (2006) proposed a criteria in which the depth of injection, the density of CO_2 and brine, reservoir properties, impurities and durations of storages for an EOR practice were taken into consideration. Chadwick et al. (2008) presented a local scale criteria based on the integrated experiences of five CO_2 injection projects in Europe (See Table 2.1). Ramirez et al. (2010) used a Multi-Criteria Analysis (MCA) method to develop a screening criteria which could be used to rank the suitability of Netherlands reservoirs (e.g., aquifer, gas and oil) for a long-term CO_2 storage. They considered three parameters: 1) storage capacity, 2) storage costs and 3) locations as the threshold screening factors. Table 2.2 gives the threshold of screen parameters used by Ramirez et al. (2010).

Table 2.1 The screening criteria proposed for the CO_2 storage by Chadwick et al. (2008)

Parameters	Positive Indicators	Cautionary Indicators
Total storage capacity	Total capacity of reservoir estimated to be much larger than the total amount produced from the CO_2 source	Total capacity of reservoir estimated to be similar or less than the total amount produced from the CO_2 source
Depth	1000-2500 m	<800 m or >2500 m
Thickness (net)	>>50 m	<20 m
Porosity	>20%	<10%
Permeability	>300 mD	10-100 mD
Salinity	>100 g/L	<30 g/L
Seal Properties		
Lateral continuity	Un-faulted	Laterally Variable Faults
Thickness	>100 m	<20 m
Capillary entry pressure	Much greater than buoyancy force of maximum produced CO_2 column height	Similar to buoyancy force of maximum produced CO_2 column height

There are many other preliminary factors linked to the storage capacity, injectivity, trapping mechanisms, and containment which should not be neglected during a storage site selection as discussed in Chapter 1. These parameters are reservoir/well types, mineralogy, residual gas saturation, subsurface conditions, rock types, wettability, properties of CO_2, and sealing potential factors, but earlier scholars have not yet been included in any screening criteria, which may bring ambiguity in the preliminary assessment during the initial selection of potential storage media.

Table 2.2 Thresholds used for the pre-screening of CO_2 storages in Netherland (Ramirez et al., 2010)

Parameter	Threshold
Storage capacity	≥4 Mt for gas/oil and ≥2 Mt for aquifer
Thickness reservoir	>10 m
Top depth reservoir	≥800 m
Reservoir porosity	Aquifers: >10%
Reservoir permeability	Aquifers: an expected permeability of 200 mD or more
Thickness of seal	≥10m. Both simple seals as well as complex seal have been taken into account.
Seal composition	Salt, anhydrite, shale or claystones
Reservoir composition	Aquifers: sandstone, hydrocarbon fields: limestone, sandstone, siltstone, carbonates
Initial pressure	Overpressure excluded
Salt domes	Relevant for aquifers. Traps located alongside/ near salt domes/walls have been excluded because there is a high risk of salt cementation

2.3 Preliminary evaluation of injection well

Assessing the potential injection well in depleted petroleum reservoirs is necessary to make for safe CO_2 injection operation as abrupt leakages could occur during and after CO_2 injection through injection or abandoned wells (IPCC, 2005-pp197). Abrupt wellbore leakage/failure is related to time-independent mechanical factors, taking place during drilling, completion, and/or abandonment (Watson and Bachu, 2009; Zhang and Bachu, 2011) which can be reviewed by evaluating the integrity of wellbore and reservoir to avoid leakage.

2.3.1 Integrity of well

Subsurface issues are generally referred to any subsurface failures, such as insufficient performance of barriers, fault reactivation and wellbore leakage which may cause severe loss of money or resources (Cooper, 2009). Wellbore failures, in these cases, may include surface casing vent flow, casing failure, tubing and packer failure, as well as zonal isolation loss. The cement placement also plays a vital role in enhancing the chance of leakage when wells are drilled and completed for injection purposes (Gasda et al., 2004; Bachu and Watson, 2009). In fact, Portland cement which is a conventional type of cement used in oil and gas wells may have leakage pathways due to a poor cement placement (Hawkes et al., 2004) or can be degraded due to exposed to $scCO_2$ (Abid et al., 2015). Several studies have been conducted on

the cement behavior in the presence of $scCO_2$. Most of these studies indicated that the cement cannot withstand the excessive acidic environment created due to CO_2 injection (Zhang and Bachu, 2011; Yamaguchi et al., 2013; Duguid et al., 2014; Abid et al., 2015; Hangx et al., 2015a). Carey et al. (2007) studied on the core samples taken from the interface of casing, cement and shale caprock in a well exposed to CO_2 for almost 30 years. They observed a prominent carbonation in the cement but cement integrity was not completely lost. Watson and Bachu (2008) provided a discussion on the ability of cements with different additives to withstand $scCO_2$ attack. They found that cement additives, such as bentonite (or other gel additives) and gypsum, may have a negative impact on the cement durability. Watson and Bachu (2009) endorsed leakages through the poorly cemented casing/hole annulus and casing failure based on the analysis of 315,000 oil, gas and injection wells drilled in Alberta, Canada. They reported few factors as the indication of potential leakages such as deviation, well type (cased or uncased), abandonment method, quality of cement, non-cemented casing/hole annulus, oil price, regulatory changes, and Surface Casing Vent Flow (SCVF) line through an annulus. No relationship was, however, observed between the leakage and age of wells, operational mode, completion interval, and presence of acid gas (H_2S and CO_2) in the produced fluids. Duguid et al. (2014) reported a similar effect as previously highlighted by Watson and Bachu (2008). They assessed a 68 years old well used for the injection project through logging and laboratory analysis and found a poor isolation and signs of micro-annulus in the cement. Hangx et al. (2015a) stated that chemical induced reactions affect the brittle strength of cements and might be dependent on the exposure time. In fact, potential leakages through abandoned wells are one of the primary risks under these circumstances.

2.3.2 Integrity of reservoir

The hydraulic integrity of the site has also been viewed from different aspects in recent years (Rutqvist et al., 2007; Ferronato et al., 2010; Vidal-Gilbert et al., 2010; Kim and Hosseini, 2014; Tillner et al., 2014; Hangx et al. 2015b). For instance, a high-pressure squeeze or water flooding is the reason of having fractures near the wellbore prior to CO_2 flooding, which can be detected by geomechanical analysis or

reviewing the operation history, cementing and work-over reports (Hawkes et al., 2004). Fracturing during injection can also occur if the injection pressure exceeds the fracture initiation pressure of the reservoir/caprock (Hawkes et al., 2004). Therefore, it is necessary to assess the fracture initiation pressure of the reservoir by considering geomechanical effects associated with pre-production, post-production and future CO_2 injection (Masoudi et al., 2011). This is mainly because mechanical failure of a caprock and/or reservoir in a high injection pressure can cause an excessive fracture propagation in the reservoir which can move towards the caprock if it cannot be controlled (Loizzo et al., 2010). Watson and Bachu (2008) emphasized that hydraulic fractures, perforations, and acidization increase the risk of wellbore leakage due to weakening the cement sheath. In fact, multiple completions or perforated intervals offer a cross flow between zones within the wellbore (Watson and Bachu, 2008). This fracturing can become crucial in terms of subsurface leakage due to chemical reactions induced changes in fracture hydrodynamics (Deng et al., 2013). It happened as a result of time-dependent chemical reactions taken place due to the development of H_2CO_3 (carbonic acid), HCO_3^- (bicarbonate ions) and CO_3^{2-} (carbonate ions) in the formation saline water (Solomon, 2006). These ions affect the strength of the medium and caprock (Espinoza et al., 2011; Erickson et al., 2015). To mitigate leakage from the caprock, monitoring techniques including wellbore integrity tests, fluid sampling, CO_2 gas tracer, electric spontaneous potential measurement, micro-seismic and cross-well seismic data acquisition can be taken into consideration (Zhang et al., 2015a).

To date, none of the studies carried out in the past provided all of essential steps to select a suitable injection well for a storage task. Hence, considering the importance of wellbore leakage and integrity during the well selection, there is a need to propose a guideline based on aforementioned literature to make preliminary evaluation of injection well in depleted petroleum reservoirs that could help to identify a suitable storage site with potential injection wells.

2.4 Preliminary evaluation of injection zone

Assessing the potential injection zone in depleted petroleum reservoirs prior to CO_2 injection can be helpful to achieve favourable CO_2 injectivity. For this, preliminary evaluation (Olierook et al., 2014) and comprehensive evaluation (Jalil et al., 2012) has been carried out. To our best knowledge, there is not any study considering all key factors related to CO_2 injectivity as pointed out in Chapter 1 that is necessary to take into account for preliminary injectivity evaluation. For instance, the good quality lithofacies section (Olierook et al., 2014) as well as the amount of remaining oil in a reservoir significantly affects the relative permeability and injectivity of a depleted site (Kovscek, 2002). These parameters could be utilized along with group of key factors related to injectivity as pointed out in Chapter 1 for making preliminary assessment of injectivity potential that could help to identify a suitable storage site having potential injection zones.

2.5 CO_2 residual trapping

Upon injection, CO_2 residual trapping occurs and results residual CO_2 saturation by capillary forces. The determination of residual trapping exposed the actual residual trapping potential of storage site (Jalil et al., 2012; Saeedi and Rezaee, 2012) that is significant in reservoir characterization for CO_2 storage. Comparatively, it is the most efficient mechanism with a quick trapping capability relative to other trapping mechanisms (Burnside and Naylor, 2014), having considerable impacts on the rate and extent of the plume migration, immobilization and storage security (Krevor et al., 2015).

Residual trapping entraps the injected CO_2 in the same way as it immobilizes the non-wetting phase in oil/water and gas/water systems (Iglauer et al., 2011b). However, there are a number of parameters such as rock-fluid characteristics, geologic settings and injection conditions which are linked to the residual CO_2 trapping, as summarized in Table 2.3 (Raza et al., 2016).

Having known the effect of these parameters on the residual trapping makes it hard to quantify the residual trapping capability of a storage site prior to CO_2 injection.

This might be the reason why there are almost no study on determination of residual trapping in a reservoir scale and most of studies are limited to experimental investigations.

Table 2.3 Effective parameters of CO_2 residual trapping

Reference	Parameter	Approach	Relationship with Residual CO_2 Saturation	Rock type
(Pentland, 2011)	Aspect ratio	Experimental	Direct	Sandstone
(Tanino and Blunt, 2012)	Aspect ratio	Experimental	Direct	Limestone Sandstone
(Almansoori et al., 2009)	Initial oil saturation	Experimental	Direct	Unconsolidated-Sandpacks
(Lamy et al., 2010)	Initial oil saturation	Experimental	Direct	Carbonate
(Krevor et al., 2012)	Initial gas saturation	Experimental	Direct	Sandstone
(Suekane and Nguyen, 2013)	Initial gas saturation	Experimental	Direct	Sandstone
(Bennion and Bachu, 2006)	Interfacial tension (brine-CO_2)	Experimental	Direct	Sandstone
(Jiang and Tsuji, 2015)	Interfacial tension (brine-CO_2)	Numerical	Direct	Sandstone
(Taku Ide et al., 2007)	Gravity number	Simulation	Indirect	Sandstone
(Pentland et al., 2012)	Pore Geometry	Experimental	Direct (Narrow pore throats)	Sandstone & carbonates
(Andrew et al., 2014)	Rock Type	Experimental	Sandstone better than carbonates	Sandstone
(Mansoori et al., 2009)	Porosity	Experimental	Indirect	Sandstone
(Lamy et al., 2010)	Porosity	Experimental	Indirect	Carbonate
(Pentland, 2011)	Pore coordination number	Experimental	Indirect	Sandstone
(Suekane et al., 2010) (Khishvand et al., 2016)	Capillary number	Experimental	Indirect	Sandstone
(Saeedi et al., 2012)	Overburden pressure	Experimental	Direct	Sandstone
	Pore pressure		Indirect	
(Juanes et al., 2006)	Relative permeability hysteresis	Simulation	Have a positive influence	Sandstone
(Iglauer et al., 2011b; Iglauer et al., 2015)	Wettability	Experimental; Review	Have a positive influence (strong water wet)	Sandstone
(Saeedi and Rezaee, 2012)	Residual natural gas	Experimental	No effect	Sandstone
(Tokunaga et al., 2013)	Capillary pressure	Experimental	Direct	Quartz
(Wang and Tokunaga, 2015)	Capillary pressure	Experimental	Direct	Carbonates-Sandstone
(Raza et al., 2016)	Flow rate	Numerical	Direct	Sandstone

2.5.1 CO_2 residual trapping assessment

Residual trapping assessment is essential to predict the potential of residual CO_2 saturation. This assessment is important in reservoir characterization of CO_2 storage to identify potential storage site. CO_2 residual trapping has been estimated in many

studies by using experimental (Iglauer et al., 2010; Saeedi and Rezaee; 2012, Saeedi et al., 2012; Geistlinger and Mohammadian, 2015), numerical (Jalil et al., 2012) and reservoir-scale data analysis (LaForce et al., 2014) based approaches. There are also several trapping models proposed so far, including that of the Land (1968), Killough (1976), Jerauld (1997), and Spiteri and Juanes (2006), to determine the residual gas saturation as a function of initial gas saturation in which the Land trapping model is the most common correlation (Juanes et al., 2006; Iglauer et al., 2011b).

Core flooding without (Saeedi, 2012) or with the elastic waves measurements (Kitamura et al., 2013) are well-known experimental setups for assessments of residual trapping. For instance, Iglauer et al. (2011a) measured the CO_2 residual trapping in sandstones by the computed micro-tomography (m-CT) technique at elevated temperatures and pressures of storage conditions. Saeedi et al. (2012) carried out core flooding to mimic drainage and imbibition phenomenon for quantification of the residual trapping in sandstone samples, where changes in stresses were included in the analysis. Kitamura et al. (2013) utilized elastic wave velocity measurements to calculate CO_2 saturation from shear wave velocity and estimated the irreducible water and residual CO_2 saturations. Myers et al. (2012) stated that a single core sample is only representative of the near wellbore environment rather than the whole reservoir due to abundant heterogeneities. They indicated that prediction of the residual trapping beyond the core scale in a formation can mislead the assessment of the storage site (Myers et al., 2012). Therefore, the impact of heterogeneity and mixed-wet systems on CO_2 immobilization may cause significant uncertainty in estimations (Krevor et al., 2015).

For quantification of long term storage potentials, numerical modeling is often used. For instance, Zhang et al. (2011) introduced a single well injection withdrawal test to estimate the residual CO_2 trapping based on hydraulic tests, temperature data, and partitioning tracer tests. They performed their tests in sequences which could yield CO_2 residual trapping estimations and remove the uncertainty of heterogeneity. Likewise, Myers et al. (2012) introduced an approach for determination of CO_2 residual trapping using reactive ester tracers. They performed a couple of trace

experiments based on a single well-test data and used a numerical simulator of the tracer behavior to estimate the residual saturation by determination of differential breakthrough of the tracers during water production. They highlighted that the subsurface datasets from the reservoir are either missing or not acquired and all the trapping mechanisms cannot be considered simultaneously during numerical modeling. This point was also emphasized by few others (Cinar et al., 2008; Hosseini et al., 2013; Lu et al., 2013).

There are some studies covering the residual trapping capability during CO_2 storage by performing reservoir tests based data analysis (Schlumberger, 2012; LaForce et al., 2014; Myers et al., 2015). For instance, Schlumberger (2012) used a reservoir saturation tool (RST) for estimation of residual CO_2 saturation near injection and observation wells of Frio Research project at Houstan, Texas. They observed a maximum saturation during the injection period, which dropped to less than 20% and stabilised to 15% after a month. LaForce et al. (2014) introduced a sequence of reservoir tests including the dissolution test which could be taken to determine CO_2 residual trapping at OTWAY project. A two-dimensional distribution of residual CO_2 saturation for a full-reservoir model before and after the dissolution test was modelled in this study using downhole pressure data, and surface measurements for the rates of injection and production of water and CO_2. This method was validated successfully against the krypton (Kr) and xenon (Xe) production curves from the reservoir data. Myers et al. (2015) utilized the same OTWAY project reservoir tests data to model the concentration profiles of tracers in production water samples. They developed two consistent residual saturation estimates using different modeling techniques.

Considering the above studies, one may conclude that there is no significant attention given to develop a reservoir scale method for preliminary quantification of CO_2 residual trapping at the depletion stage, which might be due to the variation of CO_2 residual trapping by many effective parameters (Table 2.3). Therefore, there is a need to determine the effective CO_2 residual trapping at the reservoir scale level by developing a reliable approach. This would help to strengthening the existing

screening criteria of the storage sites which is based on a group of key parameters of the reservoir and fluid characteristics, subsurface conditions, properties of CO_2, and sealing potentials (Kovscek, 2002; Chadwick et al., 2008).

2.6 Geomechanical-geochemical effects related to CO_2 injection

Geomechanical and geochemical properties of reservoirs and caprocks have a significant impact on the outcome of projects. CO_2 injection causes geomechanical-geochemical changes in storage site due to pressure build-up and CO_2/brine/rock chemical reactions.

2.6.1 Geomechanical effects

Upon CO_2 injection, there are many geomechanical issues, which can take place because of pressure build-up in depleted hydrocarbon reservoirs and aquifers. This reservoir pressure build-up changes the state of in-situ stresses (Rutqvist et al., 2008; Chiaramonte et al., 2011; Alonso et al., 2012; Kim and Hosseini, 2014), causing an increase in the bulk volume, pore compressibility, pore volume and storage capacity (Vulin et al., 2012).

The geomechanical issues have been covered in numerous studies by (i) predictions of the vertical uplift due to the increase in pore pressure (Shi and Durucan, 2009; Ferronato et al., 2010; Shi et al., 2013; Karimnezhad et al., 2014; Tillner et al., 2014, Zhang et al., 2015b; Zhu et al., 2015); (ii) modeling of fault reactivations due to injection (Rutqvist et al., 2007; Ferronato et al., 2010; Vidal-Gilbert et al., 2010; Olden et al., 2012; Kim and Hosseini, 2014; Tillner et al., 2014; Zhang et al., 2015b); and (iii) analysis of fractures generation within the reservoir and caprock (Rutqvist et al., 2008; Shi and Durucan, 2009; Ferronato et al., 2010; Chiaramonte et al., 2011; Goodarzi et al., 2011; Alonso et al., 2012; Lynch et al., 2013; Kim and Hosseini, 2014). For instance, Rutqvist et al. (2007) proposed a fully coupled numerical analysis to estimate the maximum sustainable injection pressure for the slip tendency of faults in a two-phase system considering continuum stress–strain and discrete fault assessments. The results were compared to a more conventional analytical approach which could only consider a simple reservoir geometry. They concluded that the

maximum sustainable injection pressure obtained from the simplified analytical analysis might be uncertain due to neglecting important geometrical factors associated with the injection pressure and stress. Shi and Durucan (2009) carried out a coupled reservoir-geomechanical modeling at the Aztbach-Schwanenstadt gas reservoir for evaluation of the hydro-mechanical response of the reservoir rocks and potential of shear failure and/or re-activation of pre-existing faults considering depletion and injection scenarios. The simulation results showed that compaction and uplifting during production would be experienced under a reversible stress path if the injection pressure exceeds the reservoir initial pressure. They proposed an analytical approach to estimate the sustainable injection pressure by considering the effect of the in-situ stress and rock mechanical properties under the strike-slip faulting regime. Oruganti et al. (2011) presented an analytical model for estimating the pressure profile as a function of time under the constant and infinite acting boundaries of aquifers to mitigate the risk of fracturing, fault reactivation and leakage from abandoned wells. They indicated that Contour of Over Pressure (COP) is a function of relative permeability together with rock properties and it is time-invariant in a constant pressure boundary. On the other hand, when it comes to the infinite-acting boundary condition, COP can be correlated with the rate of change in the aquifer boundary pressure. Goodarzi et al. (2011) carried out a geomechanical assessment coupled with a flow model for the feasibility analysis of the Nisku aquifer at the Wabamun Area CO_2 Sequestration project (WASP). The results indicated that injection above the injection pressure increases the potential of well injectivity but enhances the possibility of fracturing the caprock. They concluded that thermal effects due to cold CO_2 injection reduce the fracture pressure and increase the horizontal fracture propagation through caprock. Szulczewski et al. (2011) adopted an effective stress principle to predict the pressure, which would cause tensile fractures in the caprock. According to them, the pressure build-up fractures the rock if the pressure becomes equal to the least principal stress. Lynch et al. (2013) examined the stress path hysteresis in a depleted reservoir through a geomechanical-fluid flow modeling for the maximum injection pressure, and concluded that the stress path hysteresis changes during depletion and injection. Kim and Hosseini

(2014) presented an analytical approach to estimate the maximum injection pressure to avoid activation of pre-existing fractures in the normal, reverse, and strike-slip faulting regimes. They concluded that the maximum pressure for normal and reverse regimes depends on the horizontal to vertical stress ratio, Poisson's ratio and the saturated rock density. Table 2.4 summarizes studies carried out in recent years evaluating the geomechanical aspects of depleted reservoirs and saline aquifers chosen for storage purposes.

Table 2.4 Summary of recent studies carried out on geomechanical aspects of storage sites

Reference	Approach	Medium/ Simulation Time	Objective	Conclusions
(Zhang et al., 2015b)	Coupled-geomechanical–fluid flow modeling	Aquifer/20 years	Fault reactivation Ground surface uplifts	No changes in the fracture pressure by the injection rate of 1–5 million tons per year on faults but ground surface uplifts
(Zhu et al., 2015)	Coupled geomechanical–fluid flow modeling	Aquifer/ 10 years	Reservoir stresses	Maximum ground surface uplift of 1.49 mm!
(Kim and Hosseini, 2014)	Analytical	-	Reactivation of pre-existing fractures	New equations were developed for determination of maximum pressure for different stress regimes
(Tillner et al., 2014)	Coupled geomechanical–fluid flow modeling	Aquifer/ 40 years	-Leakage through fault - Reservoir stresses	A large area was affected by ground surface uplift. Neither fault slip nor dilation remained unchanged by CO_2 injection
(Shi et al., 2013)	Coupled geomechanical–fluid flow modeling	Aquifer/5 years	Reservoir stresses	A low vertical surface uplift, accompanied by an enhanced horizontal displacement
(Olden et al., 2012)	Lab/ geomechanical modeling	Aquifer/ 7000 years	Shear failure of interact rock Fault Reactivation	Models were proposed and initially used to determine generic geomechanical property
(Alonso et al., 2012)	Finite element model	Aquifer/ 5.5-22 years	Potential leakage path	Injection exceeds the yield strength of rocks causing deformation in brittle regime and generation of flow paths
(Goodarzi et al., 2011)	Geomechanical modeling	Aquifer/ 50 years	Fracture initiation	The possibility of fracturing caprock increases due to reaching the fracture pressure limits
(Rutqvist et al., 2007)	Coupled-geomechanical–fluid flow modeling	Aquifer/2.5 years	Fault-slip analysis	A fully coupled numerical analysis was provided to estimate the maximum sustainable pressure by considering the structural geometry, fluid pressure and in-situ stress of the field
Lynch et al., 2013)	Coupled geomechanical–fluid flow modeling	Scenario of depleted oil & gas/20 years	Stress path hysteresis	Fractures are key controlling parameters to estimate the `capacity and injectivity of any storage sites
(Chiaramonte et al., 2011)	Stochastic 3D geomechanical modeling	Oil reservoir/6 weeks	Role of minor faults and fault reactivation	No risk of fault reactivation, or losing the caprock integrity by the buoyancy pressure of the maximum CO_2 column height
(Ferronato et al., 2010)	Geomechanical modeling	Gas reservoir/ 22-150 years (Uplift) 140 years (stress)	Reservoir stresses Fault reactivation	Reactivation of faults with generation of preferential leakage pathways, and possible local shear or tensile failures in the caprock with land uplift process
(Shi and Durucan, 2009)	Coupled-geomechanical–fluid flow modeling	Gas reservoir/40 years	Reservoir stresses	Due to variation in stresses, depletion has resulted in formation compaction while injection causes uplift under strike-slip fault stress regime

2.6.2 Geochemical effects

CO_2 injection in subsurface geologic media also results chemical reaction due to generation of carbonic acid that may change porosity and permeability of reservoir and caprock through chemically coupled mechanical mechanisms. This mechanism also induces creep in storage site due to dissolution reactions (Le Guenan and Rohmer, 2011; Tian et al., 2015), enhanced microcracking (Chester et al., 2007; Hangx et al., 2010) and diffusive mass transfer processes (Dewers and Hajash, 1995; Renard et al., 1999), leading to a time-dependent reservoir deformation. Consequently, geomechanical properties, in particular resistance against the pressure build-up, may alter as a result of geochemical reactions (Solomon, 2006; Iglauer et al., 2014). These ions affect the strength of the medium and caprock (Espinoza et al., 2011; Varre et al., 2015; Erickson et al., 2015). A detailed review provided by Shukla et al. (2010) on the storage integrity of geologic media highlighted that changes in the stress together with chemical and physical alterations of the reservoir and caprock caused by the carbonic acid, can lead to strength reduction and failure of the caprock. Although changes due to chemical reactions are faster in carbonates compared to siliciclastic rocks (Bacci et al., 2011), significant impacts of these reactions raise a number of concerns when creep can potentially cause reservoirs compactions and damages to wellbores, caprock or fault/seal systems (Hangx et al., 2013).

2.6.2.1 Geochemical effects in sandstone

Numerical and experimental studies carried out in recent years have shown a link between geochemical reactions and geomechanical characteristics of different storage media including sandstone (Dilmore et al., 2008; Doughty, 2010; Zemke et al., 2010; Fischer et al., 2011; Marbler et al., 2012; Hangx et al., 2013; Fischer et al., 2013). For instance, experimental studies performed on sandstone core samples taken from the Utsira reservoir of the Sleipner reservoir, which was saturated with $scCO_2$, revealed that reactions due to having calcite cements take place primarily during the first 8 days with marginal chemical changes (Rochelle, 2002). Hangx et al. (2010) investigated the effects of injection by performing uniaxial compressive tests on quartz sand taken from the Heksenberg formation in the Netherlands. They found

that injection does not induce any remarkable impacts on geomechanical characteristics of sandstone. An experimental study carried out on sandstones samples obtained from different sites (i.e., Otway/Pinjarra and Harvey) for evaluation of the injection pressure before and after CO_2 flooding revealed that the Pinjarra sandstone is not suffering from chemical reactivity while the Harvey-1 plugs did weaken after flooding but changes were not significant (Evans et al., 2012). Hangx et al. (2013) experimentally simulated depletion and injection conditions to study the mechanical properties of sandstone under a representative reservoir condition. They concluded that the chemical interaction of CO_2 causes a complete dissolution of calcite involved in the sandstone composition without any effects on mechanical properties. This is likely due to quartz cements of grains, which is not impacted by CO_2-rich brine. Kempka et al. (2014) did a numerical simulation by considering a time-depended multi-phase flow for evaluation of the mechanical effects of a pilot site from the Ketzin project. They found that the mechanical stability of the caprock, fault and sandstone reservoirs in a long term is maintained with a negligible effect on rock properties. Recently, Varre et al. (2015) numerically studied the influence of geochemical interactions on the geomechanical responses of an aquifer. They concluded that geochemical interactions change the intergranular texture, pore volume, and permeability of rocks. Another experimental study performed by Campos et al. (2015) reported an obvious alteration in the pore system of the Utrillas sandstone because of injection within two months. Experimental and geomechanical modeling carried out by Huq et al. (2015) suggested that permeability of formations might change due to calcite and anhydrite dissolutions, while calcite dissolution is the major buffering process in the system. Erickson et al. (2015) experimentally studied the geochemical and geomechanical effects of injection on Permotriassic sandstones. They observed changes in mineral surfaces and pore fluid compositions, which affect the deformability and compressive strength of rocks.

2.6.2.2 Geochemical effects in carbonates

There are some other experimental studies discussing the mineral-CO_2-brine chemical reactions into carbonate (Le Guen et al., 2007; Izgec et al., 2008; Noiriel et

al., 2009; Sterpenich et al., 2009; Gharbi et al., 2013; Garcia-Rios et al., 2015; Ott et al., 2015a; Zhang et al., 2016a, 2016b) revealed rock dissolution upon CO_2 injection, changes in rock characteristics, and rock mechanical weakening.

For instance, Le Guen et al. (2007) performed a series of tests by triaxial cells by controlling and monitoring vertical and confining stresses as well as temperature, pressure and composition of the fluid. They indicated the direct effect of high partial pressures of CO_2 (Pco_2) on the kinetic rates of fluid-rock interactions i.e., increase in strain rates of the limestone by a factor of 5. In general, all samples showed a positive correlation between the fluid flow rate and strain rate. They concluded that the effect of compaction and reduction of storage capacity can be potentially balanced by selecting flow rate injections. Izgec et al. (2008) studied permeability and porosity changes during storage of CO_2 in carbonate formations located in South East Turkey by computerized tomography (CT). They found that porosity and permeability would change for different CO_2 injection rates and salt concentrations of formation water. According to them, as the salinity decreases, changes in porosity and the permeability become less pronounced. Noiriel et al. (2009) investigated the impact of CO_2 injection on reactive surface area, permeability and porosity changes on cylindrical limestone samples that were mainly composed of micrite and sparite considering ambient temperatures (T=20 ^oC) and pressures below the supercritical threshold. Micro-computed tomography and chemical analysis of effluent concentrations observed dissolution effect in terms of a non-uniform increase of porosity, connectivity and reactive surface area. Sterpenich et al. (2009) investigated the reactivity of an oolitic limestone in the presence of 1) supercritical CO_2 and pre-equilibrated saline solution, 2) supercritical CO_2 without aqueous solution, and 3) N_2 and pre-equilibrated saline solution. They found minor evidences of transformations in the structure of the samples although dissolution/precipitation patterns were not quite clear in all experiments. Gharbi et al. (2013) investigated pore scale fluid-rock interactions after CO_2 injected into two carbonate samples at a typical storage condition (i.e., 9 MPa and 50 ^oC). Experimental observations at high flow rate confirmed the formation of highly conductive channels, i.e., wormholes and a significant increase in porosity and permeability. Garcia-Rios et al. (2015) followed a

set of percolation experiments for injecting CO_2-rich solutions into fractured limestone cores under the pressure of 15 MPa and the temperature of 60 °C. It was revealed that an increase in the flow rate can lead to an increase in the volume of dissolved limestone per unit of time, and, hence, increase in fracture permeability due to calcite dissolution. Ott et al. (2015a) presented CO_2–brine unsteady-state core flood experiments by means of numerical simulations to characterize CO_2–brine primary displacement in Estaillades limestone. They reported that larger-scale heterogeneity reduces the fluid-phase mobilities. Zhang et al. (2016a) performed experiments under storage conditions to evaluate changes in geomechanical properties of Savonnières limestone before and after injection of supercritical CO_2. They found that the dynamic Young's modulus reduces while permeability and porosity were increased after injection. They concluded that CO_2 injection into limestone weakens the well consolidated areas, but enhances the strength of the weaker areas. In a similar study, Zhang et al. (2016b) conducted high pressure and high temperature core flooding tests on Savonnières limestone plugs before and after exposure to $scCO_2$. They found a significant rock dissolution and mechanical weakening of the rock due to generation of wormholes in the matrix. They concluded that decrease in the geo-mechanical properties of the reservoir may lead to the risk of integrity loss during injection.

Considering the impact of geochemical reactions on petrophysical and geomechanical properties of sandstone and carbonate rocks (i.e., reservoirs and caprock), which may change the fracture pressure variations, it is important to have more clear understanding of changes observed in fracture pressure before and during injection. To date, there have been only few attempts to evaluate the effects of CO_2/brine/rock chemical interactions on geomechanical properties, which can help to understand the rock mechanical response to $scCO_2$ and brine injection under different stress states for addressing the compaction issue.

2.7 Injection rate for CO_2 storage

It is essential to accurately predict the injection rate and pressure for safe and favorable CO_2 injection operation in storage sites (Dempsey et al., 2014). According

to the material balance concept, the total storage volume is a function of the initial reservoir pressure, the fracturing pressure of the formation, fluids (CO_2 and water) compressibility and mobility (Ehlig-Economides and Economides, 2010).There have been studies to predict the trend and safe wellbore injection pressure (i.e. injectivity) trend in aquifers (McMillan et al., 2008; Azizi and Cinar, 2013; Ganesh and Mishra, 2014) and depleted gas reservoirs (Mukhopadhyay et al., 2011) based on geologic media characteristics.

For instance, McMillan et al. (2008) using Darcy's law and the modified form of Buckley-Leverett theory developed a simple model for determination of injectivity into a homogeneous brine reservoir by assuming a constant pressure boundary. They concluded that quantification of the relative permeability is very important in determination of the achievable injection rate. Van der Meer and Egberts (2008) proposed an approach to estimate the Theoretical Maximum Storage Capacity of depleted reservoirs based on maximum pressurization and injectivity. Likewise, McMillan et al. (2008) developed an analytical expression to predict time dependent injectivity in aquifer storage systems that could also estimate of the number of wells required for a target overall injection. Mathias et al. (2011) suggested an explicit approximate solution for assessing pressure buildup and injection capacity during CO_2 injection into closed brine aquifers. Azizi and Cinar (2013) presented new analytical models to estimate the wellbore injection pressure of a vertical carbon dioxide injection well in a radial, homogeneous, horizontal saline formation for closed, constant-pressure, and infinite-acting boundary conditions using the modified form of Buckley-Leverett theory. Ganesh and Mishra (2014) used a set of well-designed full-physics compositional simulations to develop a robust 2D simplified physics model to characterize CO_2 injectivity in semi-confined layered saline aquifer systems as a function of dimensionless variables characterizing rocks and fluid properties based on the results obtained from a sensitivity analysis. Mukhopadhyay et al. (2011) developed an analytical solution for gas reservoirs to predict the transient build-up of pressure resulting from the injection of $scCO_2$ from a partially penetrating well into an infinite cylinder gas reservoir considering formation permeability and anisotropy ratios. No flow conditions were applied at the

top and bottom boundaries, and the constant pressure condition was assumed at radial boundaries.

All of these analytical solutions provided the pressure build-up trend due to injection and can be used as guidelines for selection of the optimum injection rate without exceeding fracture gradient limits, particularly when not much information is available about storage sites. However, these solutions are based on several assumptions and limited to the aquifer system except the one presented by Mukhopadhyay et al. (2011), ignoring the importance of the CO_2-reservoir fluid mixing mechanism which may bring ambiguity to the evaluation of injectivity in petroleum reservoirs. This is mainly because the mixture of $scCO_2$ with the residual hydrocarbon may alter the fluid properties of CO_2 and gas mixture (i.e., density, viscosity, phase behavior together with gas compressibility and solubility) (Oldenburg and Benson, 2001a; Mamora and Seo, 2002; Adisoemarta et al., 2004; Sobers et al., 2004; Al-Hasami et al., 2005; Oldenburg and Doughty, 2011; Xiaoling et al., 2012; Shen et al., 2014). However, mixing of $scCO_2$ with the resident hydrocarbon during displacement relies on reservoir/fluid characteristics and injection conditions (Al-Hasami et al., 2005; Connolly and Johns, 2016). Residual gas saturation and the amount of the remaining oil in reservoir may also affect the efficiency of injectivity (Kovscek, 2002; Oldenburg and Doughty, 2011; Saeedi and Rezaee, 2012). Thus, it would be necessary to evaluate the injectivity aspect of depleted petroleum reservoirs by determination of the optimum injection rate and/or the injection scheme by considering the effect of remaining reservoir fluids and reservoir fracture gradient.

2.8 Summary of chapter

This chapter covers the literature review on different areas related to CO_2 storage reservoir characterization of petroleum reservoirs, which includes preliminary assessment of petroleum reservoir, injection well and injection zone, CO_2 residual trapping assessment method, geomechanical and geochemical interactions impact on reservoir integrity, and need of optimum CO_2 injection rate for CO_2 storage in petroleum reservoirs. From the review on the preliminary assessment of CO_2 storage

sites, it can be concluded that initial evaluation of subsurface geologic site at reservoir scale, injection well and injection zone is first step to mark a suitable storage site for comprehensive reservoir characterization of CO_2 storage. Also, it is understood that CO_2 residual trapping is an efficient trapping mechanisms compared to other trapping phenomenon that is affected by various factors and could be assessed by experimental, numerical and field tests approaches. Many geomechanical-geochemical issues related to CO_2 injection is also reviewed that may have a significant impact on the outcome of projects. Other than that, earlier researchers have also presented different approaches based on different assumptions to govern the injectivity of different storage media by determining the injection rate and injection pressure. The focus of the current studies on the overall reservoir characterization are determined as well and hence the research gaps are addressed accordingly.

2.9 The research gaps

Throughout the review on the existing studies on CO_2 storage reservoir characterization aspects, it can be understood that the focus was on the preliminary assessment of storage site, injection well and injection zone, CO_2 residual trapping assessment method, geomechanical and geochemical interactions impact on reservoir integrity, and selection of CO_2 injection rate for CO_2 storage in petroleum reservoirs. It is important to remark that the reservoir characterization for identifications of suitable storage site is required for a preliminary and comprehensive assessment of key CO_2 storage aspects including storage capacity, injectivity, trapping mechanisms, containment, and geochemical-geomechanical interaction, etc. However, there is no any comprehensive procedure which can be followed for the preliminary evaluation of the storage sites and the current selection criteria would rather bring ambiguity to the overall preliminary assessment of key CO_2 storage aspects. Therefore, a new screening procedure for preliminary assessment of a storage site is highly demanded. There is also a need for a strategy and guideline for injection well and injection zone evaluation. In the context of CO_2 residual trapping, although there have been many studies utilizing experimental and

numerical approaches to evaluate trapping potentials prior to injection, there is not any reservoir scale approaches developed to assess CO_2 residual trapping at the depletion stage of petroleum reservoirs. In the context of injectivity, there have only been few studies carried out to evaluate the geomechanical characteristics of rocks being exposed to chemical interactions induced by CO_2 where the effect of in-situ stress has been ignored. Finally, the selection of injection rate to have an effective CO_2 storage in depleted petroleum reservoirs, where remaining hydrocarbons are left at the depletion stage, have not been fully addressed in the past studies.

CHAPTER 3

PRELIMINARY CHARACTERIZATION FOR CO_2 STORAGE

3.1 Introduction

A preliminary characterization of the subsurface geologic sites is presented in this chapter in order to assess the suitability of reservoir for CO_2 storage. The four perspectives of study that are considered include, i) the proposition of a comprehensive CO_2 storage screening criteria, ii) a preliminary assessment of gas reservoirs, iii) evaluation of injection wells and well selection criteria and iv) preliminary evaluation of CO_2 injectivity based on the current findings in the literature and field data that are available.

3.2 Overview of reservoir development

The undisclosed carbonate Basin, Malaysia is a broad and stable structural block with 200 Miocene carbonate buildups having numerous gas reserves. The carbonates consist of limestone and dolomites with porosities ranging from 0% to 40%. It is a large, asymmetric anticline with spread faulting and folding. It is bounded to the west by the West Bal Line, to the east by the West Bar Line, to the south by compressional structures of the Bal Province, and to the north by the North L Province. Structurally, this basin is characterized by southwest to northeast trending fault-bounded basement highs and elongate troughs. Besides very big gas reservoirs in this basin, this basin has enormous potential for CO_2 storage in aquifer as the gas reservoirs have extensive aquifers with different support level.

The reservoir of this study is one of the major offshore condensate gas reservoirs in carbonate basin, Malaysia starts production in 1983. The reservoir is a build-up of platform type in NNE-SSE orientation with steep flanks covering of approximately 22 km^2 and has a gas bearing zone greater than 1000 ft thick. The geologic succession of the reservoir consists of the transgressive cap phase, intermediate phase, main build-

up phase upper, and main build phase lower which are mainly divided into five zones. The reservoir has two continuous sand horizons located which are separated by the capping shale sequence. After depth > 1850 ft (564 m), an extensive shale sequence of marine origin that extends to approximately 3500 ft (1067 m) SSTVD (980 m below sea floor), underlain by a sand/sandstone sequence approximately 100 m in thickness and the underlying carbonate sequence. The reservoir is capped by a massive shale rock (>500 m) and overlying an extensive aquifer with a limited support. The reservoir has been divided into several reservoir units based on seismic-scale layering. Reservoir units 1-4 occur in the central part of the build-up and are separated by less porous tight layers. Zone 5 is the flank zone that occurs around the margin of the build-up. The flank zone remains an area of high uncertainty in terms of lithofacies and reservoir properties as there is no well-control. Figure 3.1 shows the structure of carbonate condensate gas reservoir. Seismic interpretation shows that the reservoir has a gentle anticline structure with a limited number of faults. The reservoir seems to be appropriate for the structural/stratigraphic trapping of CO_2 because of its dominant anticlinal structure, minor faults, and thick caprock. Periodic downhole testing showed compaction and gas–water contact (GWC) movement in the site. This situation was related to the bottom water encroachment and the preferential flank water influx (Field-Report, 1995). The depth and lithology of the different stratigraphic units are summarized in Table 3.1.

The fluid of the reservoir was characterized as condensate gas, with a low range of salinity (15,000 ppm, 14 g/L). The initial pressure and temperature of the reservoir reported to be 2405 psia (16.5 MPa) and 212 ^{o}F (100 ^{o}C), respectively. The main lithology based on the core description is limestone with less than 10% dolomite, having moldic porosity. A total number of nine lithofacies were then recognized based on petrographic types, gross lithology, porosity and permeability as well as heterogeneity. The results obtained from the Thermal Decay Time (TDT) log revealed that there is 30% residual gas saturation (Sgr) in the reservoir.

Overburden Clastic Caprock

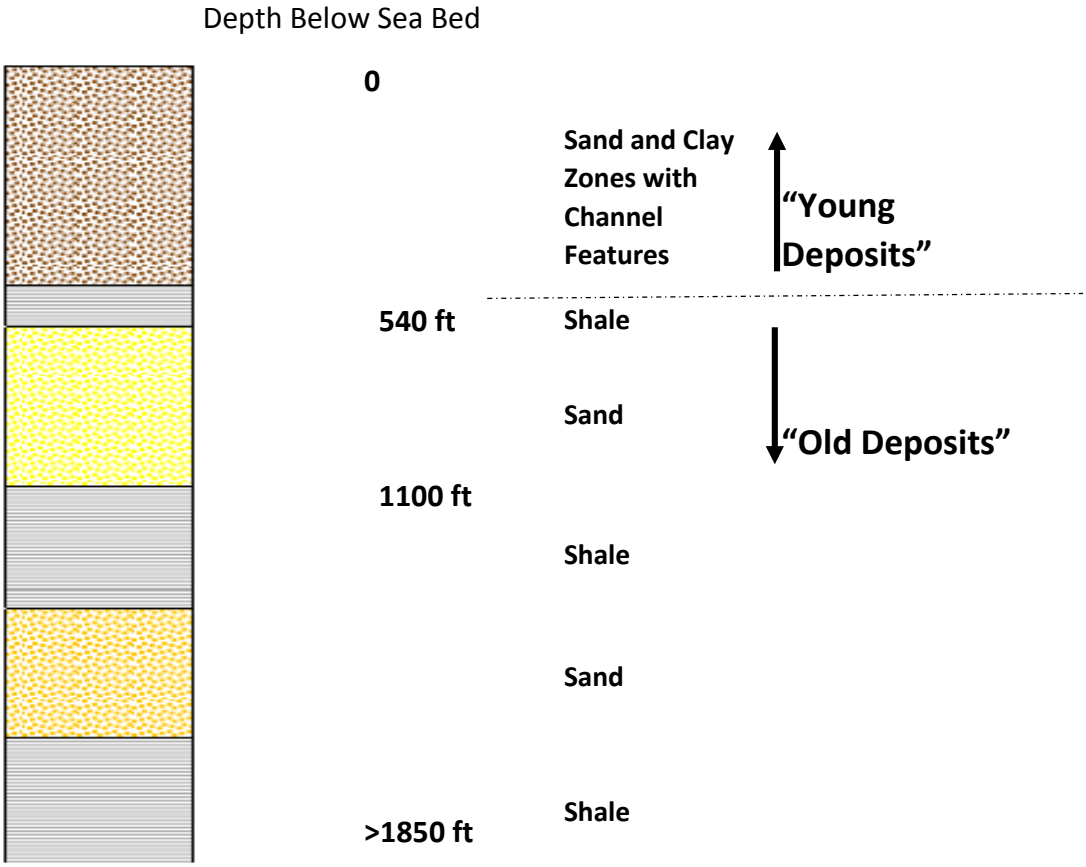

Carbonate Reservoir Cross section

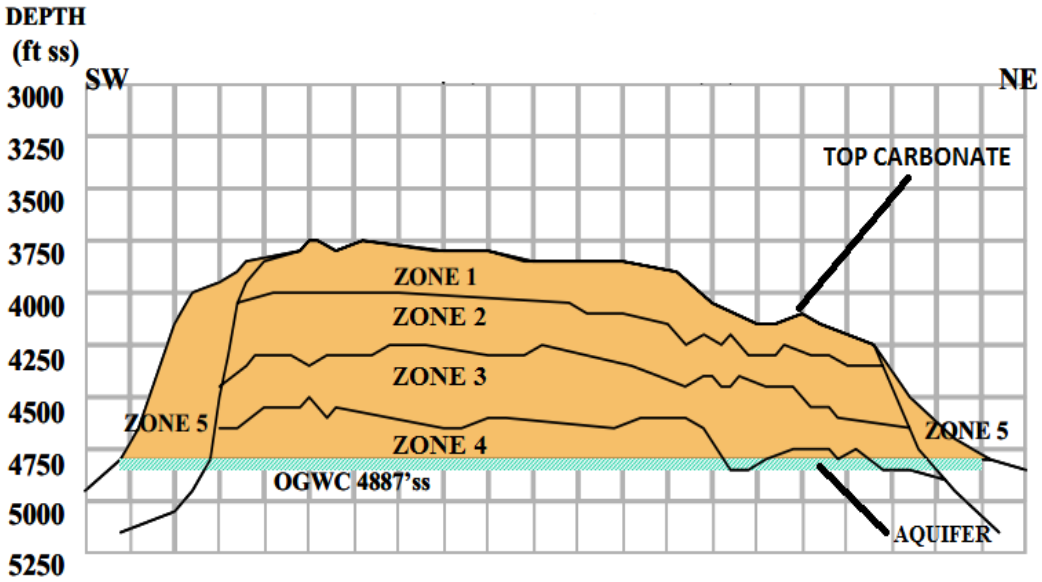

Fig. 3.1 Stratigraphic features above the carbonated reservoir (top) and structure of the reservoir (bottom). The boundaries are laterally extensive tight layers (Field-Report, 1995).

Table 3.1 Geological features of the reservoir

Unit	Environment	Lithology	Formation	Depth (TOP)	Zone
Siliciclastic	Variable shallow-marine origin	Interbedded sand shale sequence	Sand and shale	820 ft	Sand horizons: 1 and 2
	Marine origin	Interbedded sand shale sequence	Sand and shale	1380 ft	
	Variable fluvial-marine origin	Interbedded sand shale sequence	Sand and shale	1650 ft	
	Marine origin	-	Shale	>1850 ft	Caprock
Transgressive cap	Offreef to open-marine origin	Mainly detrital packstone	Carbonate	3830 ft	1
Transitional	Offreef, reefoid and protected	Detrital foraminiferal lime packstones	Carbonate	4090 ft	2
Main build-up (upper)	Protected environment	Moldic lime packstones with two intervals of sucrosic moldic dolomite	Carbonate	4342 ft	3
Main build-up (lower)	Protected environment	Similar to previous one but homogeneous moldic lime packstone	Carbonate	4648 ft	4

3.3 Screening criteria

The criteria/assessment methods described in this section are for the site characterization phase fits into the preliminary stage of geological storage assessment.

3.3.1 Criteria for reservoir scale evaluation

For the purpose of this study, the technical discussion and parameters presented by Chadwick et al. (2008) were combined with other critical factors (discussed in Chapter 1) in order to present a new and more comprehensive screening criteria for depleted gas reservoirs. This criteria for site characterization phase was used to assess the storage suitability of the reservoir by evaluating key CO_2 storage aspects as given in Table 3.2.

This criteria was initially proposed for depleted reservoirs to obtain a comprehensive assessment of the key aspects of CCS, including reservoir and well types, classes of minerals, residual fluid saturation, subsurface conditions, rock types, and wettability, together with the properties of CO_2, sealing potentials, porosity, permeability, and depth. This screening criteria has been divided into four main groups: storage potential (e.g. CO_2 source and total storage capacity, depth, density, and porosity), injectivity (e.g. thickness, permeability, well type, classes of minerals, residual

saturation, and hydraulic integrity of the reservoir), trapping mechanisms (e.g. subsurface conditions, rocks, and fluid properties), and containment (e.g. hydraulic integrity of the seal and reservoir).

Table 3.2 Screening criteria for the evaluation of depleted gas reservoirs worldwide

Sr. No.	Parameters		Positive Indicators	Cautionary Indicators	Indication of Aspect
1	**CO_2 source and total storage capacity**		Total capacity of reservoir estimated to be much larger than the total amount produced from the CO_2 source	Total capacity of reservoir estimated to be similar or less than the total amount produced from the CO_2 source	Storage potential
2	**Depth**		>800 m	800 m >depth>2000 m	Storage capacity
3	**CO_2 density**		high	low	Storage capacity
4	**Porosity**		>20%	<10%	Storage capacity Capillary trapping
5	**Thickness (net)**		>>50 m	<20 m	Storage capacity Injectivity
6	**Permeability (near-wellbore)**		>100 mD	10-100 mD	Injectivity
7	**Well type**		horizontal well with or without hydraulic fracture/vertical well with hydraulic fracture	vertical well without hydraulic fracture	Injectivity
8	**Type of minerals**		Ca-, Mg-, or Fe-rich framework minerals such as (feldspars, clays, micas, and Fe-oxides	fast reacting carbonates minerals	Injectivity/mineral trapping
9	**Residual gas /water saturation**		low	high	Injectivity
10	**Pore throat size distribution**		less heterogeneous	highly heterogeneous	Injectivity and trapping
11	**Salinity**		low	high	Solubility trapping
12	**Temperature**		low temperature gradient	high temperature gradient	Solubility trapping
13	**Pressure**		under pressure	overpressure	Solubility trapping
14	**Gravity number**		low	high	Capillary trapping
15	**Rock type**		quartz rich sandstones and carbonates	highly stress sensitive carbonates	Capillary trapping
16	**Rock wettability**		strong water wet	less water wet or oil-wet	Capillary trapping
17	**Interfacial tension**		high	low	Capillary trapping
18	**Hydraulic integrity**	**Reservoir type**	reservoir without compaction/ aquifer support	reservoir with compaction/aquifer support	Containment
			have not experienced any injection in past	have experienced injection in past	
			low number of faults and fractures	high number of faults and fractures	
		Well location & condition	good completion condition and away from faults & fractures	poor completion and near to faults & fractures	Injectivity
19	**Seal capacity – CO_2 column height**		capillary entry pressure much greater than buoyancy force of maximum produced CO_2 column height	capillary entry pressure similar to buoyancy force of maximum produced CO_2 column height	Containment
20	**Seal geometry - Lateral continuity**		un-faulted	laterally variable faults	Containment
21	**Seal geometry –Thickness**		>100 m	<20 m	Containment
22	**Hydraulic integrity:** Indicates the ability of caprocks or faults against the leakage of the CO_2 plume		presence of mineral and stress characterization data of seal	absence of mineral and stress characterization data of seal	Containment
23	**Distance between CO_2 emissions source and target medium**		<300 km	>300 km	Transportation cost

3.3.2 Criteria for well evaluation

A systematic guideline was proposed for identification of injection wells in depleted reservoirs. The steps involved in this methodology are as follows:

a) Screening the potential wells at the early stages based on the integrity analysis.

i. Mark wells based on their locations to give them priority. Locations of wells on the structure and in the storage site should be studied by looking into the seismic interpretation for selecting those which are away from faults and fractures. These interpretations can mark layers based on density and frequency of fractures. Cold sedimentary basins with no or a limited number of faults and fractures are the best places for a long-term CO_2 storage exercise (IPCC, 2005-pp200). This is mainly because a large increase of the injection pressure during storage may create fractures as well as fault reactivation (Rutqvist, 2012), resulting in potential for CO_2 leakage from the storage site (Watson and Bachu, 2009).

ii. Knowledge of the well status (active, inactive, abandoned), its depth, type (cased or uncased), deviation and completion, as well as the abandonment method is crucial for selections. For instance, analysis of 315,000 oil, gas and injection wells drilled in Alberta, Canada have indicated leakages due to poorly cemented casing/hole annulus and casing failure (Watson and Bachu, 2009). Although, mixing of CO_2 with gas in depleted reservoirs changes the phase behavior of CO_2 and properties of gas (Adisoemarta et al., 2004; Sobers et al., 2004; Xiaoling et al., 2012), depth of selected reservoirs must be greater than 800 m to have supercritical CO_2 in place, which would reduce the buoyancy effect and enhance the storage capacity. This helps to have a better trapping mechanisms, especially residual and solubility trappings which minimize the pressure on the caprock (IPCC, 2005-Sec5.2; Saeedi, 2012). It is generally good to avoid uncased, highly deviated, multiple completion, shallow depth (i.e., less than 800 m) wells, and bridge abandon wells (Watson and Bachu, 2009; Duguid et al., 2014).

iii. Time-independent mechanical factors taking place during drilling, completion, and/or abandonment which are related to wellbore failure and hence abrupt leakage (Watson and Bachu, 2009; Zhang and Bachu, 2011). These wellbore integrities related failures should be avoided by available data. Most importantly, the cement type (Watson and Bachu, 2008) and its placement when wells are drilled and completed for injection purposes (Hawkes et al., 2004; Bachu and Watson, 2009) play important role to remove the likelihood of leakages. In fact, type of cement should be designed such that it can resist against the corrosion in the acidic environment of the storage site (Abid et al., 2015). Thus, integrity of casing, cement and the bond between them should be evaluated through production logs (e.g., time-lapse ultrasonic and cement bond logs) and testing reports.

b) Performing lithofacies and petrophysical data (e.g., logs and core data) analysis to evaluate characteristics of rocks in the near wellbore region in terms of heterogeneity level, porosity and permeability for a favorable injectivity. In the case of stress sensitive formations, a good approach is to review the production data for predicting the injectivity potential.

i. Generally, high quality reservoirs are characterized by high porosity, good permeability and high-quality facies (McGowen and Bloch, 1985; Atkinson et al., 1990; Bloch, 1991). Particularly, permeability along with the thickness of the targeted site are the key parameters for CO_2 injectivity, which ultimately control the cost and efficiency of the injection operation (Cinar et al., 2008; Ghaderi et al., 2009). Generally, a reservoir thickness of larger than 50 m, a porosity of higher than 20% and a near wellbore permeability of greater than 100 mD are recommended for a suitable storage practice (Chadwick et al., 2008). Thus, the observations and measurements of geological and petrophysical parameters should be carried out by using wireline logs data and laboratory measurements to determine porosity, permeability and water distribution, together with petrographical descriptions of sedimentary facies as described by Olierook et al.

(2014) for the GSWA Harvey 1 well in the Western Australia considered for a CO_2 sequestration job (Olierook et al., 2014).

c) Assessing the presence of fractures near the wellbore region prior to CO_2 flooding during production to address the strength of rocks.

i. Mechanical failure of a caprock and/or reservoir in a high injection pressure can cause an excessive fracture propagation in the reservoir which can move towards the caprock if it is not controlled (Loizzo et al., 2010). Therefore, selection of the injection pressure should be determined to keep the injection pressure lower than the original reservoir pressure for a safe storage job (Li et al., 2006). Prediction of the fracture pressure in the production interval using wireline logs is the strategy which can also be taken on these occasions by following the steps provided in literature (e.g., Masoudi et al., 2011; Gholami et al., 2015a, b; 2016). This quantification would help to set a maximum injection pressure without fracturing the caprocks and inducing leakages.

3.3.3 Criteria and integrated approach for injection zone

The properties in Table 3.3 have gained a lot of attention during the preliminary assessment of any geologic sites for a CO_2 injectivity in the past decade (Bachu, 2003; Chadwick et al., 2008; Ukaegbu et al., 2009; Qi et al., 2010; Ramirez et al., 2010; Saeedi and Rezaee, 2012; Saeedi, 2012; Shamshiri and Jafarpour, 2012; Frykman et al., 2013; Ito et al., 2013; Akintunde et al., 2013; Olierook et al., 2014) as grouped together to consider in this study.

An integrated geological approach to evaluate the reservoir for its injectivity based on petrographic, core and well logs data is proposed here. For this purpose, a four steps approach was followed as below:

a) Lithofacies types were identified by the petrographic analysis of core plugs obtained from Well A. The petrographic analysis was supplemented with the corroboration of the pore type and fabric against depth and temporal ranges of facies types.

b) Lab measurements (porosity, permeability, and water saturation) were utilized to calibrate wireline log data which helps to understand the reservoir characteristics and lithofacies types.

c) A composite log analysis, using gamma ray (GR), acoustic transmit-time (DT), neutron (NPHI), and density (RHOB) logs, carried out to evaluate the rock properties of the reservoir. Depth corrections were made to match the core data against the corresponding wireline logs. Log-based estimated properties including porosity, permeability, and water saturation were compared to the measurements made at the lab scale. An analysis was then carried out to recognize lithofacies in non-cored intervals using the log data.

d) Having the petrographic and petrophysical interpretations, the reservoir quality of each zone was determined in terms of its porosity, permeability, thickness, water/residual gas saturation and lithofacies quality.

Table 3.3 The proposed indicators to justify the good zones for favourable CO_2 storage

Parameters	Positive Indicators	Cautionary Indicators	Indication of Aspect
Depth	>800 m	800 m>depth>2000 m	Storage capacity
CO_2 density	high	low	Storage capacity
Porosity	>20%	<10%	Storage capacity
Thickness	>>50 m	<20 m	Injectivity
Permeability (near-wellbore)	>100 mD	10-100 mD	Injectivity
Pore throat size distribution	less heterogeneous	highly heterogeneous	Injectivity
Residual gas /water saturation	low	high	Injectivity
Oil phase saturation	low	high	Injectivity
Lithofacies types	good quality	low quality	Injectivity

3.4 Reservoir scale preliminary assessment

A complete characterization of the reservoir was performed using geological, reservoir, and well data to understand the potential of the reservoir as an effective storage site. This analysis was mainly performed using the screening criteria introduced earlier to cover the key aspects of the reservoir.

3.4.1 Fluid type

Generally, fluids in gas reservoirs are classified into three categories: dry gas, wet gas, and condensate gas (Adisoemarta et al., 2004; Sobers et al., 2004). The reservoir fluid system is condensate fluid if the pressure and temperature are above or below the dew point pressure (McCain Jr, 1994; Terry and Rogers, 2013). Below the dew point pressure, condensate occurs, leading to segregation of the liquid phase in the bottom hole and the reservoir region. It should, however, be noted that the composition of the condensate gas at the depleted stage is different from that of the initial stage (Adisoemarta et al., 2004; Sobers et al., 2004; Abbasov and Fataliyev, 2016; Rahimzadeh et al., 2016). In this study, fluid characterization of the reservoir using compositional analysis, constant volume depletion, and well-stream analysis at the reservoir conditions revealed that condensate gas is the major fluid type with a dew point pressure of 1805 psia (12.4 MPa). The liquid drop-out curve shown in Figure 3.2 indicates a liquid shrinkage behavior in the condensate system during depletion. This condensate gas was estimated to occupy 19% of the pore volume (Field-Report, 1995). There have been many studies in recent years that have pointed out the potential of condensate gas reservoirs as favorable places for successful CO_2 storage practice (Barrufet et al., 2010; Al-Abri, 2011; Jalil et al., 2012; Narinesingh and Alexander, 2014; Shen et al., 2014; Yuan et al., 2015). Considering the above studies, it seems that the reservoir in this study may have significant potential to become a CO_2 storage site based on fluid-type-related analysis.

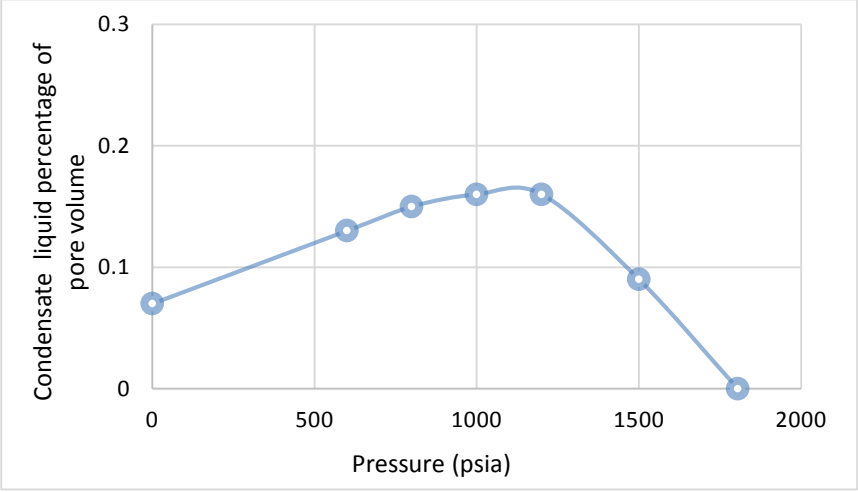

Fig. 3.2 Condensate build-up percentage in the reservoir during depletion

3.4.2 Storage capacity

Injection and storage conditions impact on the thermodynamic properties of CO_2 significantly, which ultimately reflects the fate of storage. In this study, the model developed by Bahadori et al. (2009) was used to estimate the density of CO_2 at the reservoir temperature and pressure (see Table 3.4). The dissolution at the brine–CO_2 interface is another parameter that should be sufficient for good storage capacity, but it is often affected by the injection pressure, reservoir temperature, heterogeneity, and brine salinity (Kovacs et al., 2015). CO_2 solubility under this condition was estimated at the same pressure using the approach presented by Ji and Zhu (2013). It should be noted that this approach is valid for a temperature range from 77 °F (25 °C) to 212 °F (100 °C) and a pressure of up to 5801 psia (40 MPa). The quantity of dissolved CO_2 is very high under the injection reservoir conditions (i.e., 2000 psia (13.8 MPa), 212°F (100°C), and 15, 000 ppm) and thus the dissolution may increase the density of the CO_2 and the pH of the brine significantly.

The interfacial tension (IFT) between the CO_2 and brine is referred to as an imbalance of molecular forces between two phases, and it controls the efficiency of the residual trapping due to the dominant snap-off trapping mechanism (Saeedi and Rezaee, 2012). The interfacial tension was estimated using the methodology presented by Li et al. (2014). It was then found that residual trapping can be achieved at an early stage of the injection if a high IFT (σ) is achieved (Bennion and Bachu, 2006). The results of interfacial tension analysis at the reservoir conditions (i.e., 300-2000 psia, 212°F, and 15, 000 ppm) are reported in Table 3.4.

Table 3.4 The calculated interfacial tension, density, and solubility of CO_2

	Density (g/m^3)	Solubility ($kmol/m^3$)	IFT with brine (gf/cm)
Supercritical CO_2	0.2-0.5	0.002-0.013	0.030-0.041

When examining these results, it seems that the formation temperature and the injection pressure may result in a supercritical density which will reduce the upward flow of CO_2 and the risk of caprock pressurization. Figure 1.3 displays the phase diagram of pure CO_2, indicating the pressure and temperature at which the phase

change may take place in subsurface formations (Saeedi, 2012). The minimum depth at which CO_2 can appear in the supercritical state is about 2625 ft (800 m) if an average hydrostatic pressure gradient of 0.43 psi/ft (9727 Pa/m), an average surface temperature of 59 °F (15 °C), and an average geothermal gradient of 27 °C /km are present (Saeedi, 2012).

Storage capacity is referred to as the effective pore volume of a geological medium fully occupied by CO_2. A number of methods have been recommended to estimate the storage capacity (Bachu et al., 2007; Jalil et al., 2012; Lai et al., 2015). However, for the purpose of this study, the approach presented by Zhou et al. (2013) given in Appendix, developed exclusively for gas reservoirs with the support of an aquifer, was used. The field report revealed an expected volume of gas initially in-place of 4.7 Tscf (0.133 Tscm) and an expected ultimate recovery of 2.8 Tscf (0.079 Tscm), together with a proven and expected ultimate recovery of 18 MSTB and 28 MSTB, respectively. At the recovery factor of 60% for gas and condensate, the estimated CO_2 storage capacity is around 3.16 Tscf (0.09 Tscm) at a pressure of 2000 psia (13.8 MPa) and a temperature of 212 ^{o}F (100 ^{o}C).

3.4.3 Hydraulic integrity

The reservoir is a gentle anticline showing a slope downward to the north-east and upward to the south-west. Seismic lines also revealed a small-scale fault crossing the reservoir, which is a positive sign for reservoir connectivity (Field report, 1995). The reservoir unit is composed of a pile of five zones located between >3000 ft (914.4 m) and 6000 ft (1829 m). The depth of the site plays a vital role in having supercritical CO_2 on site, favoring an efficient utilization of the storage space (Civile et al., 2013). From the depth point of view, shown in Figure 3.1, one may conclude that the reservoir is suitable for having $scCO_2$ in place.

A horizontal permeability of 42 mD, and a vertical permeability of 627 mD, which gives an anisotropy k_v/k_h of 15, were estimated based on the transient pressure (build-up) of the well test analysis. The high value of the vertical anisotropy was due to the presence of vertical fractures in the formation (Well-Report, 2002). For the

interpretation, radial homogeneous analytical models with no flow at the top and bottom boundaries were used to analyze the test data by the operator, while the final build-up test period was used as the basis of interpretation. The sequence of events for the test is given in Table 3.5.

Table 3.5 Sequence of events for the pressure transient well test analysis

Date	Duration (hours)	Event	Average Rate (Mscf/D)
01-xx-yy	7.85	First Flow Period	20
01-xx-yy	7.24	Second Flow Period	40
02-xx-yy	6.50	Third Flow Period	60
02-xx-yy	12.00	Build-up	0.0

For the purpose of storage, reservoirs with no faults or a limited number of faults and fractures are favorable. In fact, large faults in the reservoir can be reactivated due to a significant injection and build-up pressures (IPCC, 2005-pp200). The stability of the basin and small-scale faulting of the reservoir can make it a good candidate for CCS. The presence of the high vertical permeability may result in the upward flow of $scCO_2$ in the absence of any barriers towards the seal at the top. The tight layers may mitigate this concern. In the context of trapping mechanisms, the vertical permeability is favorable for CO_2 dissolution, which can move fast and be replaced by $scCO_2$–undersaturated brine (Solomon, 2006).

According to the screening criteria, the well type and good wellbore conditions have inevitable links with the storage, and a careful selection of the injection well is imperative. Thus, four wells, referred to as wells A, B, C, and D, for which there were full sets of the required data, including core and well log data, depth range, etc, were selected to characterize the reservoir for its storage potential. The experimental and modeling findings suggested that high porosity core samples are highly compressible and show pore collapse behaviors, causing a significant variation in the in-situ stress within the reservoir due to depletion. This is a negative aspect of this reservoir regarding injectivity, residual trapping, and CO_2 leakage. It is, therefore, recommended that a coupled geomechanical–fluid flow analysis be conducted to determine the sustainable injection pressure of the site by considering the rock and caprock compressibility. This modeling helps to evaluate the maximum surface uplift

and other geomechanical aspects of the reservoir, including fault reactivation and changes of the stress state after depletion, which would be beneficial to prevent or at least mitigate the compaction-related issues.

There are other concerns associated with the potential of the reservoir as a suitable place for storage practice, which are linked to the aquifer support at the bottom of the reservoir (Bachu, 2004; Cinar et al., 2008). This aquifer support reduces the storage capacity due to the resistance of brine and significant pressure build-up within the reservoir (Bachu, 2004). However, the Active CO_2 Reservoir Management (ACRM) regulatory rules can be adopted for this reservoir, in which brine production combined with CO_2 injection is considered to relieve the pressure build-up and enhance the trapping mechanism, while the water produced can be disposed of in other zones (Le Guenan and Rohmer, 2011; Buscheck et al., 2012).

3.4.4 Lithological and petrophysical features

The petrophysical analysis of the core samples revealed that carbonates are either pure limestone or partially dolomitized limestone. In this study, lithological features were characterized by the petrographic analysis based on the polarizing microscope (Field of view = 5 mm). All photos were taken under the crossed polarized light (XPL) except the one marked as G and H, which were taken under the plane polarized light (PPL). Thin sections were impregnated with the blue epoxy to have a better insight into the variation of porosity. Dunham's carbonate rock texture classification was used to recognize the depositional texture and fabrics (Dunham, 1962). A total number of nine lithofacies types were then recognized based on petrographic types, gross lithology (limestone/dolostone/dolomite), porosity and permeability as well as heterogeneity. In order to ascertain the occurrence of these lithofacies, modern and ancient techniques were compared. The photomicrographs of textural characteristics of these lithofacies were presented in Figure 3.3.

Considering lithofacies classification in terms of their sediment type, porosity types, and the associated porosity and permeability measured from core samples, it was found that five out of nine lithofacies are good-quality reservoirs. They were then

ranked in a descending order of the reservoir quality as: Peloidal Limestone (LPe), Moldic Limestone (LM), Muddy Moldic Limestone (LMMu), Moldic Dolomitic Limestone (LDM), and Moldic Dolomite (DM). Other four lithofacies types were Tight Limestone (LT), Argillaceous Limestone (ALT), Tight Dolomitic Limestone (LDT), and Tight Dolomite (DT). These four tight and poor lithologies were denoted by the suffix of "T" in their lithofacies codes.

Generally, heterogeneity in the sediment type are beneficial to understand the characteristics of the reservoir within each lithofacies type. This is mainly because of the important role of heterogeneity in the accurate modeling of a CO_2 storage site (Ennis-King et al., 2011). Performing an analysis on the data of the reservoir, it was observed that majority of lithofacies have a good total porosity which can disperse CO_2 and entrap large fraction of the fluid phase (Honari et al., 2015). Table 3.6 summarizes the features of these lithofacies in terms of their sediment type, porosity type, and porosity and permeability measured from core samples. A brief description of each lithofacies is given in the following subsections.

Considering the high dissolution (Espinoza et al., 2011; Farquhar et al., 2015) and precipitation reactions (De Silva et al., 2015) rate in carbonates (Bacci et al., 2011) together with fabric and rock characteristics of this carbonate reservoir, lithofacies may precipitate. This precipitation may bring changes in rock characteristics with more formation damage close to low-permeable areas (Mohamed and Nasr-El-Din, 2013), which would diminish the injectivity during the injection period (Yoo et al., 2013; Andre et al., 2014; Ott et al., 2015b).

3.4.4.1 Peloidal Limestone (LPe)

It is the best reservoir lithofacies with a high porosity and high permeability characteristics. The sediment type is distinctive: a fine-grained, well-sorted, compacted peloidal grainstone with few bioclasts. It is characterized by solution-enhanced moldic porosity, to the point where moulds became interconnected to develop appreciable quantities of intergranular porosity. The image analysis shows

the occurrence of the narrow range of the thin-section-scale macropore sizes while the proportion of macroporosity is equal to or slightly greater than microporosity.

3.4.4.2 Moldic Limestone (LM)

This lithofacies is a good quality reservoir. Heterogeneity has resulted from changes in the sediment fabric and the degree of cementation. The most common sediment type is grainstone, with pack-grainstones and some packstones. Moldic porosity and micro-intragranular porosity are pore types created within bioclasts and grains. Moldic with intercrystalline and stylolite-associated porosity are also present. This lithofacies shows the highest ratio of large pores compared to the number of micropores of all the lithofacies types. A better reservoir quality development in this lithofacies is linked to solution-enhanced pores. A series of image analysis on the core samples shows that microporosity is dominated porosity type in this lithofacies, emphasizing the importance of microporosity to reservoir quality.

3.4.4.3 Muddy Moldic Limestone (LMMu)

This lithofacies is the most common lithofacies present in the core and shows moderate to excellent reservoir characters. It is more heterogeneous than LPe and LM, in original sediment type and in the pore-type development. The petrographic type is predominantly packstones, with pack-wackestones, grainstone and boundstones. This lithofacies is characterized by a high degree of leaching which had resulted in moldic pores (dissolved bioclasts). These pores are connected via matrix intercrystalline or microporosity. The solution-enhanced moldic and intercrystalline porosity are dominated pore-types, with some moldic and intercrystalline porosity. More than half of the total porosity is contributed by microporosity.

3.4.4.4 Moldic Dolomitic Limestone (LDM)

This lithofacies type is characterized by wackestones (green) and pack-wackestones. The heterogeneity is due to different degrees of leaching as well as primary sediment variability. Intercrystalline matrix porosity as a result of dolomitization and solution-enhanced moldic porosity is common. Higher carbonate mud fractions occur in this lithofacies than in LMMu. Some of the pack-wackestones show cemented pores and

some moldic pores are partially reduced by the dolomite cement. The results obtained from the image analysis shows that the contribution made to total porosity by moldic pores in this lithofacies is far less than the DM and LM.

3.4.4.5 Moldic Dolomite (DM)

There is a wide range of porosity and permeability in this poor quality lithofacies. The DM lithofacies has moldic and intercrystalline porosity. More than half of this porosity is contributed by microporosity. The sediment types are wackestones, and packstones. This lithofacies is characterized by intercrystalline porosity along with moldic porosity which was created by the dissolution of less stable bioclasts. There is a wide heterogeneity caused by differences in the proportion of bioclasts in the sediment. These characteristics indicate the porosity enhancement in the marine phreatic zone and cut-off of ambient seawater by the sediment-water interface cement.

3.4.4.6 Tight Limestone (LT)

Lithofacies are predominantly tight packstones, partially cemented by calcite and associated with stylolites. The stylolites are associated with micro-intergranular porosity development.

3.4.4.7 Tight Argillaceous Limestone (ALT)

The ALT is argillaceous mudstone-wackestone having a high argillaceous content which is the major cause of the reservoir quality. It can be identified by high GR readings in the tight reservoir intervals. The micritic fraction of the matrix is not substantially dolomitized. More porous streaks in the ALT are associated with the leaching around stylolites to form zones of moldic, micro-intergranular to intercrystalline porosity in streaks of packstone.

3.4.4.8 Tight Dolomitic Limestone (LDT)

The LDT consists of tight wackestones, in dolomitsed fabrics with intercrystalline porosity. Other pore-types are minor moldic porosity and stylolite-associated porosity. Some moldic pores are occluded by the anhydrite cement.

3.4.4.9 Tight Dolomite (DT)

The DT is a wackestone with a finely distributed porosity with some moulds in the sucrosic dolomite matrix and pore-reducing dolomite cement.

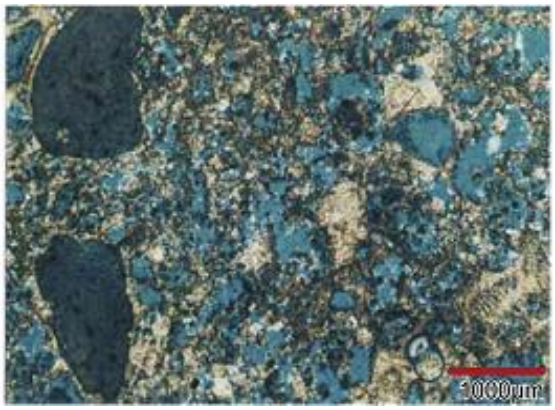

A) Lithofacies:LPe
Thin section 4161 ft, Well A

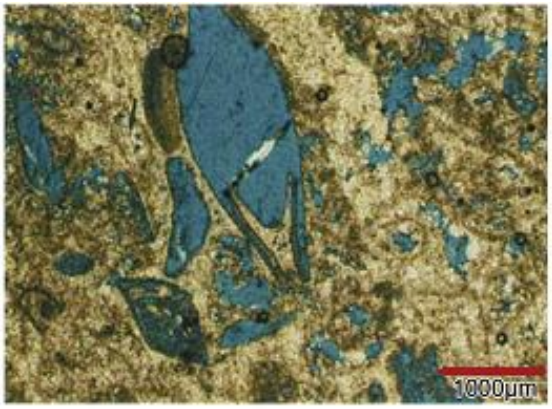

B) Lithofacies:LM
Thin section 4533 ft, Well A

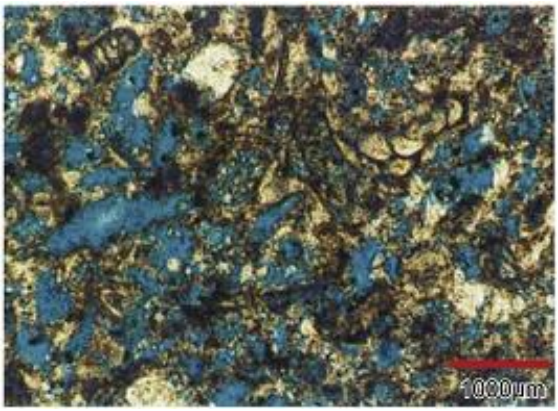

C) Lithofacies:LMMu
Thin section 4384 ft, Well A

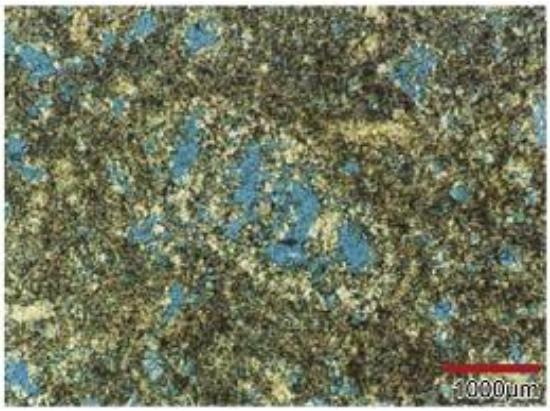

D) Lithofacies:LDM
Thin section 4659 ft, Well A

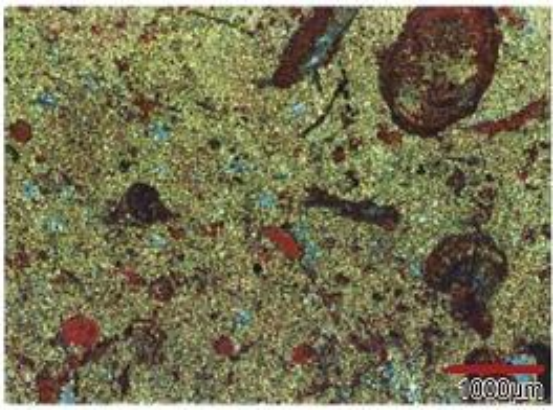

E) Lithofacies:LDM
Thin section 4278 ft, Well A

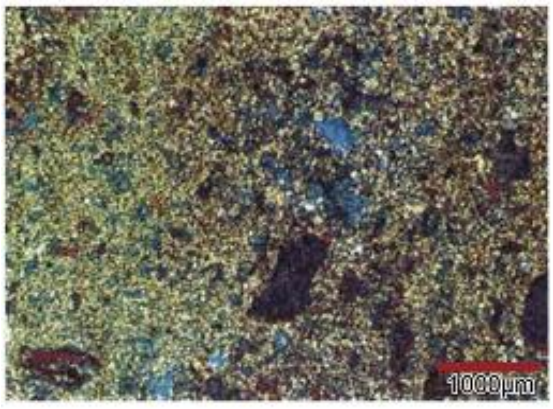

F) Lithofacies:DM
Thin section 4505 ft, Well A

Fig. 3.3 Summary of the most common lithofacies observed in the reservoir's Well A (Scale bar = 1 mm). Blue color depicts porosity.

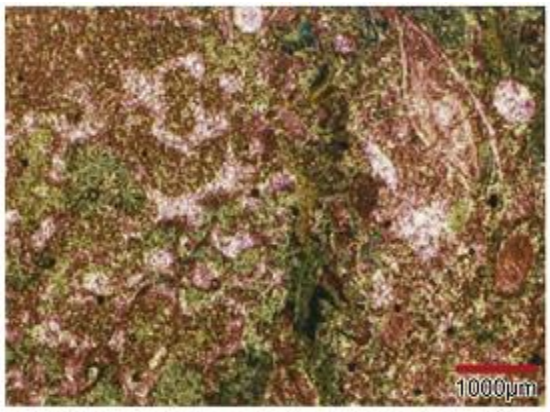

G) Lithofacies:LT
Thin section 4109 ft, Well A

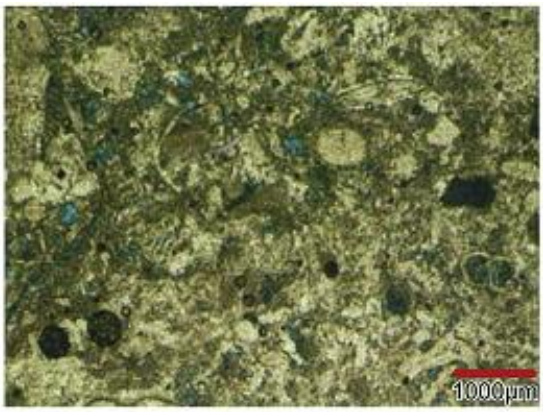

H) Lithofacies:ALT
Thin section 4446 ft, Well A

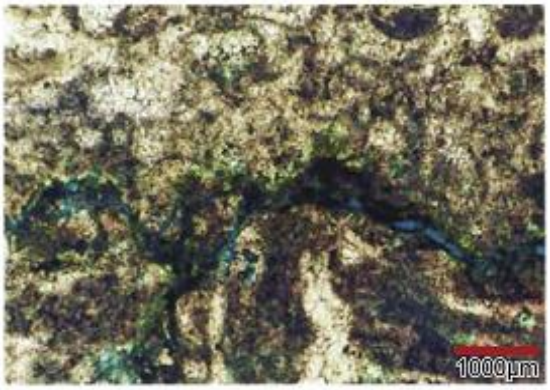

I) Lithofacies: LDT
Thin section 4907 ft, Well A

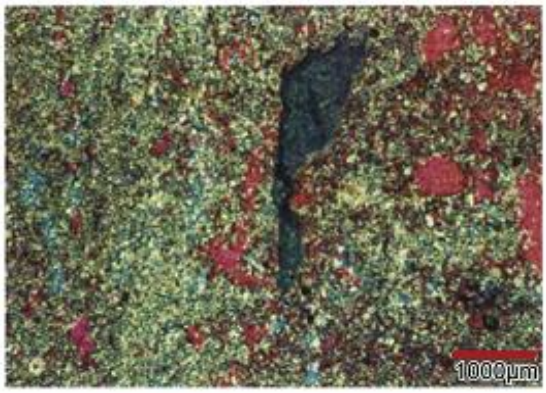

J) Lithofacies:DT
Thin section 4698 ft, Well A

Fig. 3.3 Cont'd Summary of the most common lithofacies observed in the reservoir's Well A (Scale bar = 1 mm). Blue color depicts porosity.

Table 3.6 Lithofacies descriptions of the reservoir in terms of fabric and pore types

ID No	Lithofacies	Depth (ft)	Well	Ø (%)	K (mD)	Fabric	Pore types
A	Peloidal Limestone (LPe)	4161	A	37.5	173	Peloidal grainstone with some bioclasts, originally, but peloids have been dissolved to form moldic porosity (blue)	Solution-enhanced moldic porosity
B	Moldic Limestone (LM)	4533	A	33.5	53	Grainstone (-packstone) (blue)	Solution-enhanced moldic porosity
C	Muddy Moldic Limestone (LMMu)	4384	A	34.7	44	Packstone-grainstone (blue) with some bioclasts	Solution-enhanced moldic and some intercrystalline porosity
D	Moldic Dolomitic Limestone (LDM)	4659	A	33.2	42	Wackestone (green), dolomitised (blue)	Moldic and intercrystalline porosity
E	Moldic Dolomitic Limestone (LDM)	4278	A	20.1	23	Wackestone (green), dolomitised matrix with some bioclasts (red)	Intercrystalline porosity (bioclasts in red color are not dissolved as in A)
F	Moldic Dolomite (DM)	4505	A	26.9	16	Wackestone (green), dolomitised	Moldic and intercrystalline porosity
G	Tight Limestone (LT)	4109	A	4.6	Nil	Grainstone-packstone (some dolomitization) Orange color-packstone	Not seen in photo-styolite associated porosity
H	Tight Argillaceous Limestone (ALT)	4446	A	5.5	3	Fine-grained argillaceous wackestone (light green)	Some intercrystalline porosity and minor primary porosity in small forms
I	Tight Dolomitic Limestone (LDT)	4907.7	A	4.6	Nil	Grainstone-packstone with dolomitized micrite fraction (brown)	Stylolite-associated porosity (blue)
G	Tight Dolomite (DT)	4698	A	17.1	1	Mudstone-wackestone dolomitised with some bioclasts (red)	Fine intercrystalline porosity

Table 3.7 gives a classification based on the grain density which was used in this study to investigate the dependency of petrophysical parameters on lithology.

Table 3.7 Classification of rocks in the reservoir based on their grain density

Grain Density Range (g/cc)	Lithology
2.69 - 2.75	Limestone to dolomitic limestone
2.76 - 2.80	Dolomitic limestone to calcitic dolomite
2.81 – 2.85	Calcitic dolomite to dolomite

When examining this Table 3.7, it is observed that more than 90% of the core data fall within a grain density range of 2.69–2.80 g /cc. This is aligned with the lithological description of the core samples dolomitised by only 10%. Versenate analysis was performed on 20 plugs covering a grain density range of 2.69–2.86 g /cc. The plot of the magnesium/calcium content vs grain density reveals a direct relationship between the magnesium content and the grain density, as shown in Figure 3.4. Dolomite has a higher density than calcite, and thus dolomitization increases the grain density as well as the porosity, which indicates the petrophysical dependence on the lithology.

To further evaluate the heterogeneity level, the capillary pressure was measured for core plugs taken from intervals from 4141 ft (1262 m) to 5038 ft (1535 m) using the porous plate technique, and these revealed a trend of rapid variation in the rock fabric. By normalizing the capillary pressure measurements for differences in the permeability and porosity of samples, as well as differences in the fluids used to measure the capillary pressure, the capillary pressure can be obtained as a function of permeability, porosity, interfacial tension, and wetting angle. This function can be applied to a reservoir with any permeability and porosity ranges or any wetting/non-wetting fluid characteristics. Due to a lack of samples in the grain density range above 2.77 g /cc, it was decided to categories the plugs according to lithology rather than grain density. Seven plugs with a permeability of 0.22 to 111 mD and a porosity of 3% to 34.9%, all described as moldic limestone, from the interval 4624 ft (1409 m) to 5038 ft (1535 m), were selected for averaging purposes. Unfortunately, the attempt

to average the curves of seven core plugs using the J function was not successful because of high tortuosity, as shown in Figure 3.4.

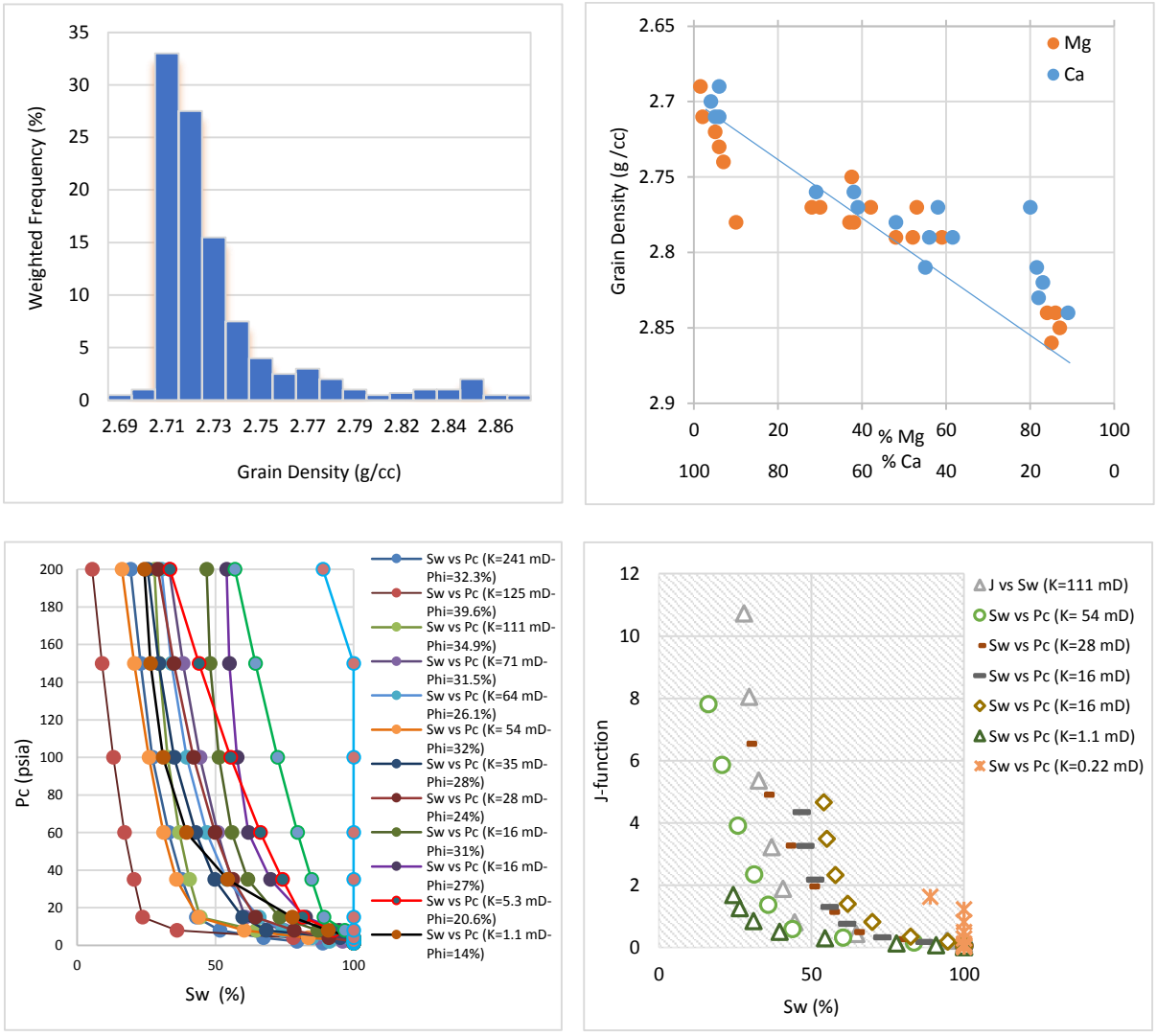

Fig. 3.4 Rock density, chemistry and capillary pressure of the reservoir before CO_2 flooding

The porosity was generally good and could have reached up to 34.9%, which suggests a high storage capacity. On the other hand, the high percentage of water saturation obtained from the capillary pressure data may reduce the storage capacity (Suekane et al., 2008; Pentland et al., 2011). However, the reservoir is favorable for successful injectivity in terms of permeability, as obtained from the core sample analysis, as this parameter is greater than 100 mD (Cooper, 2009). As mentioned earlier, the horizontal permeability is generally low, varying between 42 mD and 50 mD in the reservoir, which would offer a lower injectivity. In total, the core scale properties mark this reservoir as a potential site for storage.

However, the presence of vugs can reduce residual trapping ability and may stop the injection operation if the dissolution or precipitation of carbonates occurs (Civile et al., 2013). As per the screening criteria, highly heterogeneous geologic media have undergone complex diagenesis (IPCC, 2005-pp214) and are not often considered to be suitable sites for CCS applications.

In general, carbonates increase the chance of effective residual trapping if a strong water-wet system prevails (Iglauer et al., 2011a; Pentland, 2011). When it comes to solubility trapping, the temperature, pressure, salinity ranges, and type/composition of the rocks play crucial roles. The increase of CO_2 pressure, on the other hand, increases the CO_2 dissolution and brine density (De Silva et al., 2015). This increase in the density may result in gravitational instabilities in which denser brine moves downward and away from the flowing CO_2 plume, promoting solubility trapping (Ennis-King and Paterson, 2005). According to Chevalier et al. (2010), the CO_2 solubility is favorable in low-temperature and low-saline areas. On the other hand, geochemical reactions result in the dissolution and precipitation of minerals, depending on subsurface thermodynamic conditions, fluid composition, and rock when CO_2 is in contact with brine. It ultimately affects the porosity and permeability of reservoirs (Bacci et al., 2011). Carbonates also offer a relatively high rate of mineral reactions, and may result in large dissolution cavities in the reservoir, developing fast transport paths for CO_2 to flow away from the storage site (Kovacs et al., 2015).

Minerals are generally classified into two types that contribute to the chemical reactions between reservoir rocks and pore fluids:(a) fast-reacting carbonate minerals, and (b) Ca^{-}, Mg^{-}, or Fe-rich framework minerals, which have the capability of slow and long-term mineralization with $scCO_2$ (e.g., feldspars, clays, micas, and Fe oxides) (Hangx et al., 2013; Zheng et al., 2015). This mineral dissolution and precipitation affects storage integrity during and after injection, which may lead to damage to the wellbores, the overlying seal, and any fault/seal systems. Although the mineral composition of the carbonate reservoir may offer a slow and long-term mineralization due to the presence of magnesium (Mg) and calcium (Ca), other concerns related to carbonates include the stress-dependent permeability variation

during storage, which should not be neglected (Zhou et al., 2011). This might be a problem due to the impact of different fabrics and moldic limestones with cement reduced porosity and vugs on the plume migration, injectivity, and hydraulic integrity of the reservoir during the interaction of CO_2 with rocks. Thus, it would be wise to carry out an evaluation of the injectivity and mineral trapping, and the influence of both brine chemistry and CO_2 composition at the experimental level before selecting any carbonate formations as a storage site.

The approach presented by Desbrandeset al. (1990) was applied to determine the wettability using the pressure profile and the rock–fluid data, such as porosity, permeability, fluid densities, and surface tension. The estimated contact angle was 32°, emphasizing the fact that the reservoir is water-wet at a threshold pressure of 36.220 kPa. Using the capillary pressure data, the $J(P_{ct})$ was determined through to be 0.15, and the IFT of the gas and water system was determined to be 0.00005 gf/cm, based on the graphical approach (McCain, 1990). Rock wettability has a highly significant impact on both CO_2 migration and trapping capacities (Iglauer et al., 2015; Al-Khdheeawi et al., 2016). Water-wet reservoirs are preferred, on these occasions, due to their high storage capacity, low structural and solubility trappings and, therefore, high containment security (Al-Khdheeawi et al., 2016).

The well log data were used in the next step to evaluate the porosity, net thickness, permeability, and residual gas saturation of different intervals, as presented in Table 3.8. The conventional well logs were interpreted and the required parameters were estimated, as presented in Figures 3.5–3.8.

Figure 3.5 shows the interpreted well logs acquired for well A. The laboratory results showed that the non-interconnected porosity is minimal, especially for the formations with a porosity of less than 10%. The porosity cut-off was obtained as 10%, and the favorable thickness (net pay) was estimated as 847.75 ft (258 m). Based on the wellbore condition, the GR, resistivity, and porosity responses, the favorable interval for the injection is 3942–5005 ft (1201–1525.5 m). The interpretation of the wireline log data from Well B was conducted in a similar way to that shown in Figure 3.6. The perforated interval of the well was located between 4266 ft (1300 m) and

4848 ft (1478 m). Based on the wellbore condition, the GR, resistivity, and porosity log responses, the interval of 4270–5119 ft (1301–1560 m) seems to be suitable for the injection. The net thickness, gross thickness, and porosity of the reservoir were found to be 655 ft (200 m), 849 ft (259 m), and 22%, respectively. A similar interpretation applies to the logs available for Well C, as displayed in Figure 3.7. The results obtained from such an interpretation indicated that the favorable thickness (net pay), gross thickness, and porosity are 680 ft, 892 ft, and 30.7%, respectively for the reservoir section. The results of the well log interpretation for Well D are shown in Figure 3.8. When examining this figure, it can be seen that the depth interval of 4036–4747 ft (1230–1447 m) has a net thickness of 595 ft (181 m), a gross thickness of 711 ft (217 m), and an average porosity of 20%. The well was perforated over a single interval located between 4047 ft (1233 m) and 4473 ft (1363 m) SSTVD.

The permeability in the wireline log data intervals was estimated using the log-based water saturation and porosity by applying the Timur model (Ahmed, 2001), which provided a better result against the core sample data compared to other correlations, such as the Morris–Biggs and the Schlumberger chart K3 (Schlumberger, 2015). This permeability was, however, only validated with the data from three wells due to the limited available core sample data, as shown in Figures 3.5–3.8. The first indication of there being a carbonate reservoir in the reservoir is perhaps the very low readings of the GR log response. It is generally known that carbonates are less radioactive than shale and sand. The density response decreases because of the low-density fluid (gas), while the neutron log reduces because of the low amount of hydrogen per unit volume. The response of the resistivity logs for Zones 1–4 in all the wells indicates the presence of hydrocarbon. However, the good correlation of the porosity, resistivity, and GR logs for the gas-bearing formation reveals a favorable porosity, permeability, and net thickness, which are essential for good storage capacity and injectivity, as highlighted in the criteria.

Considering the core and reservoir data, the only concern might be the compaction effect of the reservoir, which can be evaluated by performing flooding experiments to determine the injectivity potential.

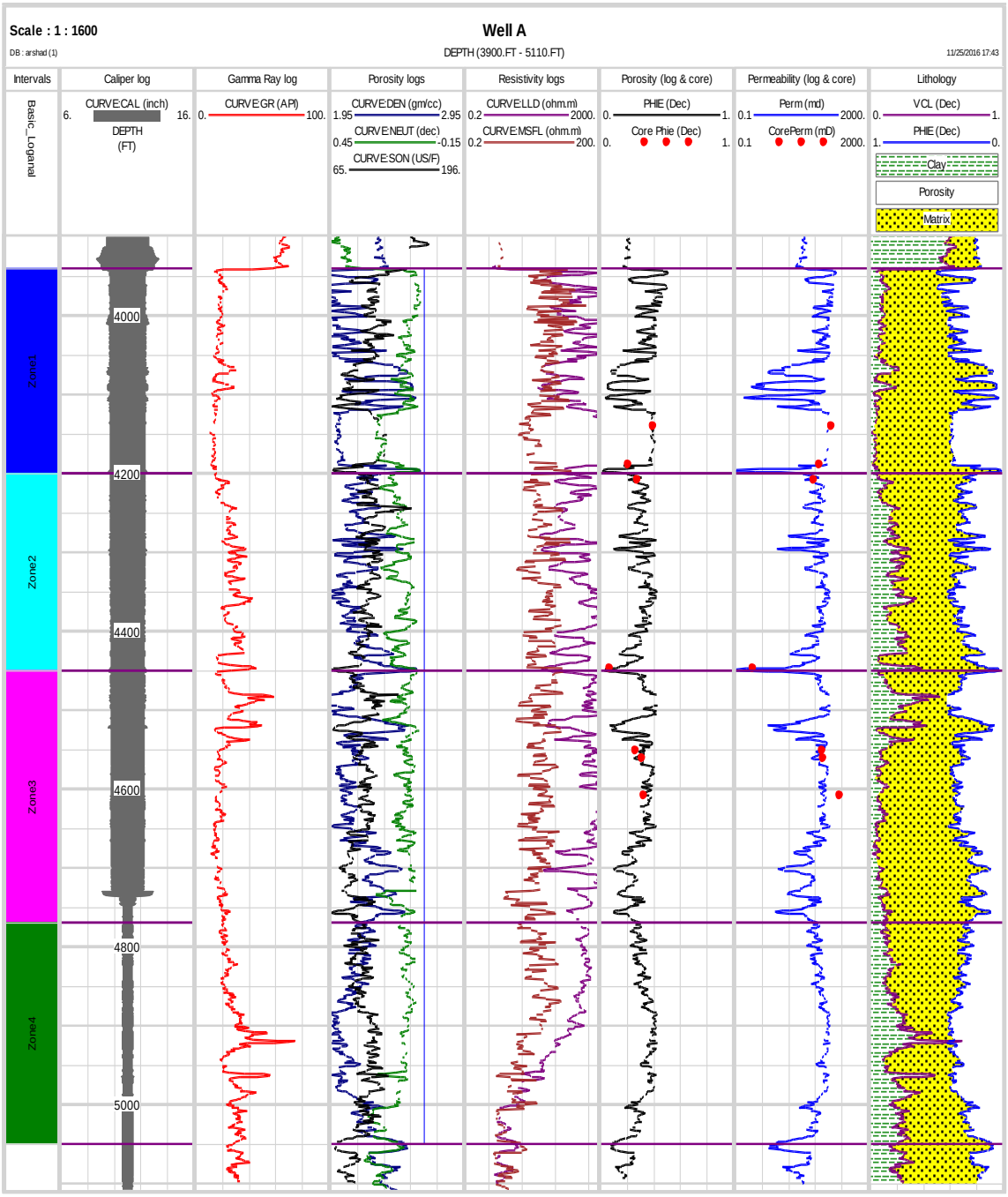

Fig. 3.5 Conventional and estimated logs data for Well A. The first track shows the zone intervals and the second track is the depth and caliper log (Cal). The third to fifth tracks include the gamma ray (GR), combination of density (DEN), neutron (NEU) and sonic (SON) logs, and resistivity logs. The log based total porosity (PHIE) and permeability and core sample data together with lithology are given in the last three tracks

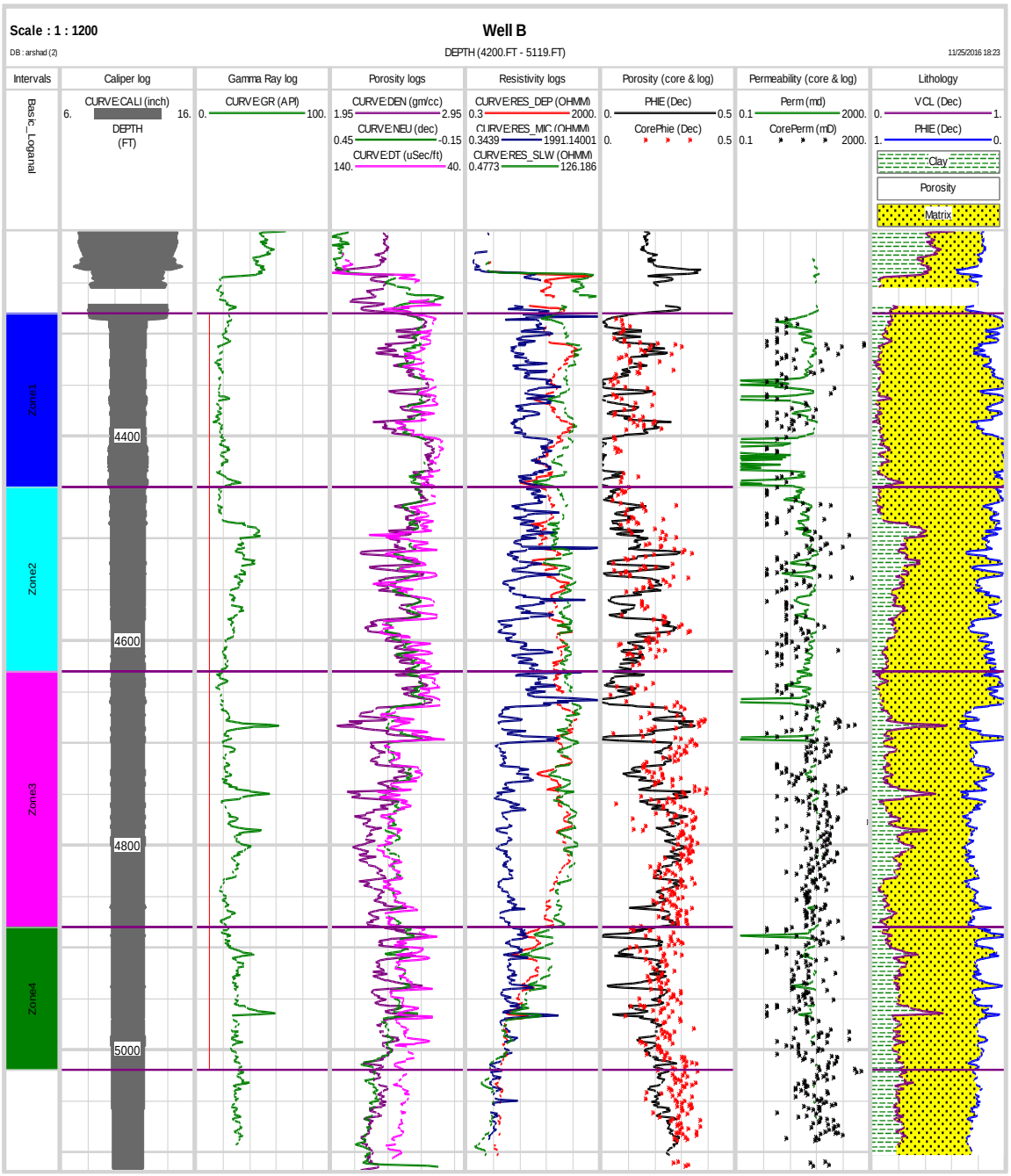

Fig. 3.6 Conventional and estimated logs data for Well B. The first track shows the zone intervals and the second track is the depth and caliper log (Cal). The third to fifth tracks include the gamma ray (GR), combination of density (DEN), neutron (NEU) and sonic (SON) logs, and resistivity logs. The log based total porosity (PHIE) and permeability and core sample data together with lithology are given in the last three tracks

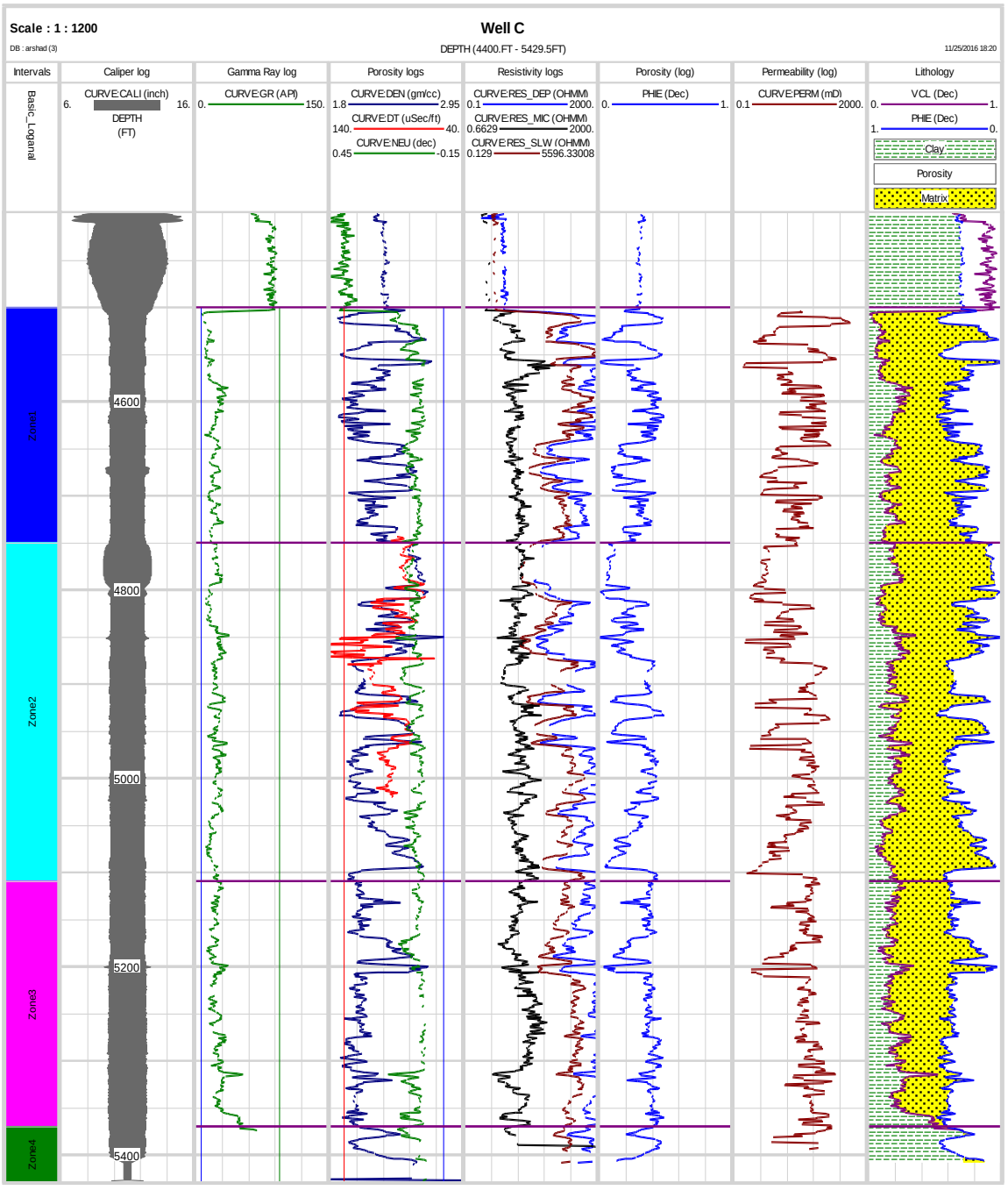

Fig. 3.7 Conventional and estimated logs data for Well C. The first track shows the zone intervals and the second track is the depth and caliper log (Cal). The third to fifth tracks include the gamma ray (GR), combination of density (DEN), neutron (NEU) and sonic (SON) logs, and resistivity logs. The log based total porosity (PHIE) and permeability together with lithology are given in the last three tracks

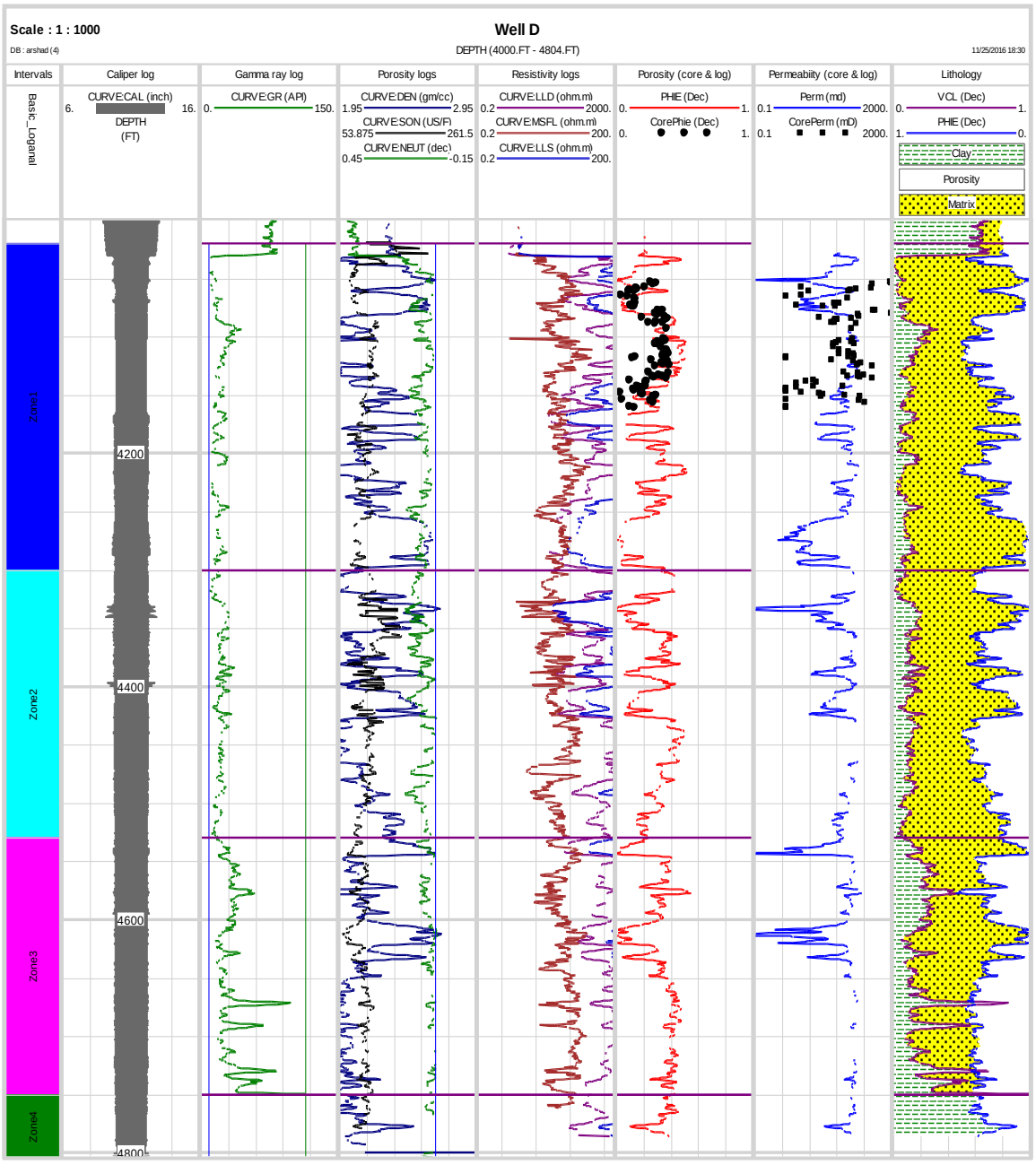

Fig. 3.8 Conventional and estimated logs data for Well D. The first track shows the zone intervals and the second track is the depth and caliper log (Cal). The third to fifth tracks include the gamma ray (GR), combination of density (DEN), neutron (NEU) and sonic (SON) logs, and resistivity logs. The log based total porosity (PHIE) and permeability and core sample data together with lithology are given in the last three tracks

Table 3.8 Porosity and gross and net thickness of the reservoir in different wells

Well ID	Interval of Interest (ft)	Gross Thickness (ft)	Net Thickness (ft)	Actual Perforated Interval (ft)	Porosity (%)
A	3942-5005	1063	847	4218-4278	26
B	4270-5119	849	655	4266-4848	22
C	4503-5395	892	680	4550-5150	30.7
D	4036-4747	711	595	4047-4473	20

The approach developed by Ransom and Holm (1978) was applied to determine the residual gas saturation using the resistivity log, based on the log–injection–log technique. Ransom and Holm (1978) introduced an approach to determine the residual oil saturation based on log–injection–log analysis with the help of the resistivity and thermal decay time logs. This approach can also be applied to estimate the residual gas saturation, where a microspherically focused log is used to measure the resistivity of the flushed zone (R_{xo}), which includes the resistivity of salt water mud-filtrate (R_{mf}) and the residual hydrocarbon saturation (R_h) in the flushed zone (R_{xo}) (Assaad, 2008). In fact, for cases where the log–injection–log technique cannot be applied, a microspherically focused log can be used to measure the flushed zone resistivity R_{xo} in the flushed zone, and hence the residual gas saturation can be obtained via the Archie method, considering the input parameters illustrated in Table 3.9. In this study, the residual gas saturation in the invaded zone was calculated by replacing R_t with R_{xo} and R_w with R_{mf} (the resistivity of the mud filtrate). The formation factor, F, was estimated by considering the cementation factor, m_c and the log-predicted porosity. This estimate offered a reasonable match with the available core measured residual gas saturation. In the next step, the residual gas saturation was estimated using the site resistivity log and the resistivity of the pore volume filled with water. The average residual gas saturation varied from 33% to 50% in four wells, which was similar to the ranges experienced in the Well B core plugs and is near to the measurements plotted in Figure 3.9. In general, it seems that the residual gas saturation must be less that what was estimated to be the case for a good storage site, as highlighted by Oldenburg and Doughty (2011).

Table 3.9 Input parameters for the residual gas saturation in the invaded zone

Well ID	m_c	n	Ø (%)	R_w (ohm·meter)	R_{mf} (ohm·meter)
A	1.9	2	26	0.24	0.20
B	1.9	2	22	0.24	0.241
C	1.9	2	30.7	0.21	0.20
D	1.9	2	20	0.24	0.241

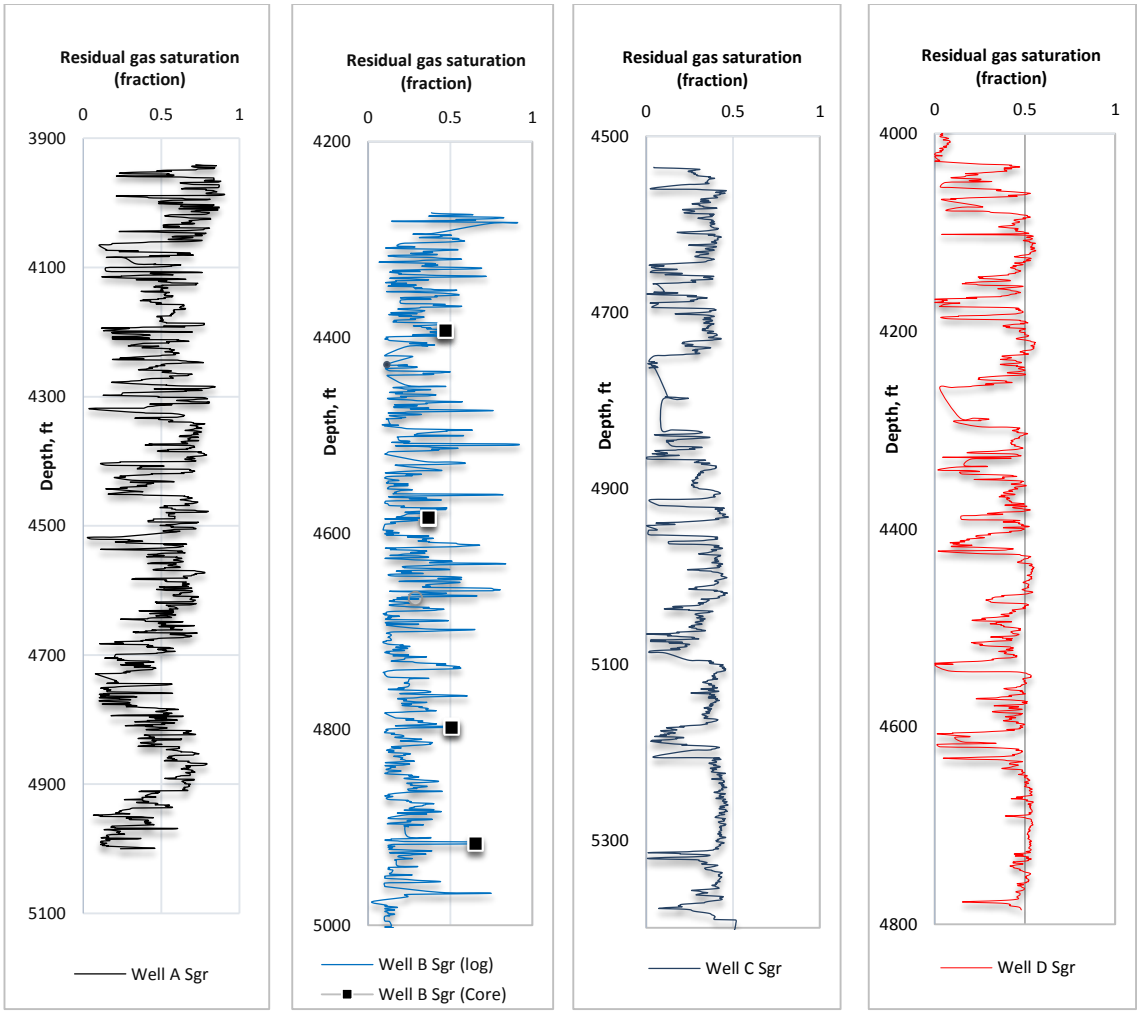

Fig. 3.9 Residual gas saturation estimated using the resistivity log data

3.4.5 Containment

The reservoir has two continuous sand horizons, as indicated earlier, but the risk of breaching them through the injection is very small due to the presence of an extensive shale sequence below them. The shale sequence has a marine origin and a 1650 ft (503 m) thickness extending from 1850 ft (564 m) to 3500 ft (1067 m) SSTVD, underlain by a sand/sandstone sequence. In general, the leak off test (LOT) determines the strength or fracture pressure of the open formations, and it is conducted immediately after drilling below a new casing shoe. During the test, the well is shut-in and the fluid (mud) is pumped into the wellbore to gradually increase the pressure in the annulus space. As the pressure builds up, the fracture initiation pressure will be reached and the fluid will enter or leak-off the formation. The results

of the LOT dictate the maximum pressure that can be applied before the formation fractures at the casing shoe. Thus, to evaluate the formation fracture pressure above the main carbonate formations, a number of LOT's were performed in the wells at different depths, covering the sand horizons and shale caprock intervals (1850 ft to 3500 ft SSTVD). The fluid intake gradient in the caprock section ranged from 0.61 psi/ft (13798 Pa/m) to 0.997 psi/ft (22 553 Pa/m) within the 1233–3693 ft (376–1126 m) interval. The fluid intake gradient obtained from the LOT covering the upper part of the reservoir from 3633 ft (1107 m) to 3798 ft (1158 m) was in the range of 0.87 psi/ft (19 680 Pa/m) to 0.883 psi/ ft (19 974 Pa/ m) (see Figure 3.10). Thus, the seal will be able to bear the pressure build-up as long as the reservoir pressure is less than the seal fracture pressure of 3682 psia (25.3 MPa). However, it will be essential to determine the fracture gradient as the injection begins, because there might be some changes in the fracture pressure due to geochemical reactions between supercritical CO_2 and the caprock. Moreover, characterization of the seal in terms of mineralogy and the state of stress after depletion would be beneficial to predict the actual strength of the seal.

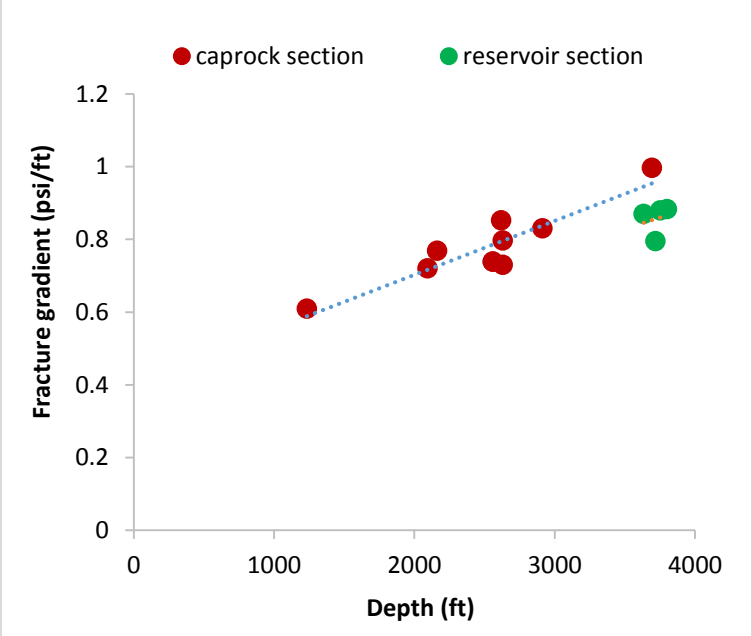

Fig. 3.10 Variations of the fluid intake gradient with depth in the chosen reservoir

3.5 Injection well evaluation

In this section, gas reservoir wells were analyzed to indicate which one of them is the best candidate for the storage practice following the steps mentioned earlier in the injection well selection guideline.

3.5.1 Well integrity

Wells and reservoirs characteristics are linked to each other and a careful selection of injection wells is imperative to have a successful storage practice. However, evaluating different factors related to injection wells depends, to a great extent, on the availability of reservoir and well-data. Table 3.10 summarizes the available data and status of the wells drilled in the reservoir. This 30 years old gas reservoir consists of up to 20 wells, out of which only Well A is vertical and the rest are directional. The majority of wells have been depleted, two were abandoned, and few were drilled for water disposal purposes. Almost all of the wells are deeper than 800 m, which is essential to have $scCO_2$ in place while injecting (Saeedi, 2012). Few wells such as Well J and Well K followed the sidetracks of Well C and Well D. Well D and Well K (s) are observatory wells for periodically monitoring the movement of the transition zone due to a weak aquifer support. An annulus pressure of 1200 psia had been observed in Well C and Well M in the early stage of production. It was stated that poor cement jobs, shallow gas sources, casing communication near the surface might be the possible reasons behind this annulus pressure increase. Well R was a horizontal infill well located at the total depth of 1110 m (3642 ft). Well S was a shallow well to dispose water, which had been replaced by a deeper Well T. Well T was purposely drilled to cover the whole interval of the reservoir for measuring porosity, residual gas saturation, gas saturation in the original aquifer as well as the reservoir pressure. Most of the wells were at a reasonable distance from faults based on the interpretation of seismic data. The preferred completion type in the wells is casings perforated at a single or multistage points. Wellbore conditions prior to CO_2 flooding were investigated by the caliper log, CBL log and the mud density together with fluid losses. However, CBL were not available for any of the wells drilled in this reservoir at this stage except Well B and Well Q. The CBL survey report of Well B indicated that

the amplitude of the signal is relatively high for the interval above 492 m (1615 ft), highlighting the fact that the cement placement in that interval is quite poor. However, the weak amplitude on the VDL suggested a good casing-cement and cement-formation bonds for the intervals deeper than 492 m (1615 ft). The CBL survey in Well Q indicated a generally poor cement bond condition in the intervals deeper than 335 m (1100 ft). Considering the fact that majority of the wells had caliper logs, their evaluation confirms failure observed and the mud weight variation during drilling in different wells. In fact, based on the available information from different reports, it was clear that the mud weight was properly used and no loss was reported in the main interval of 3940 to 5249 ft.

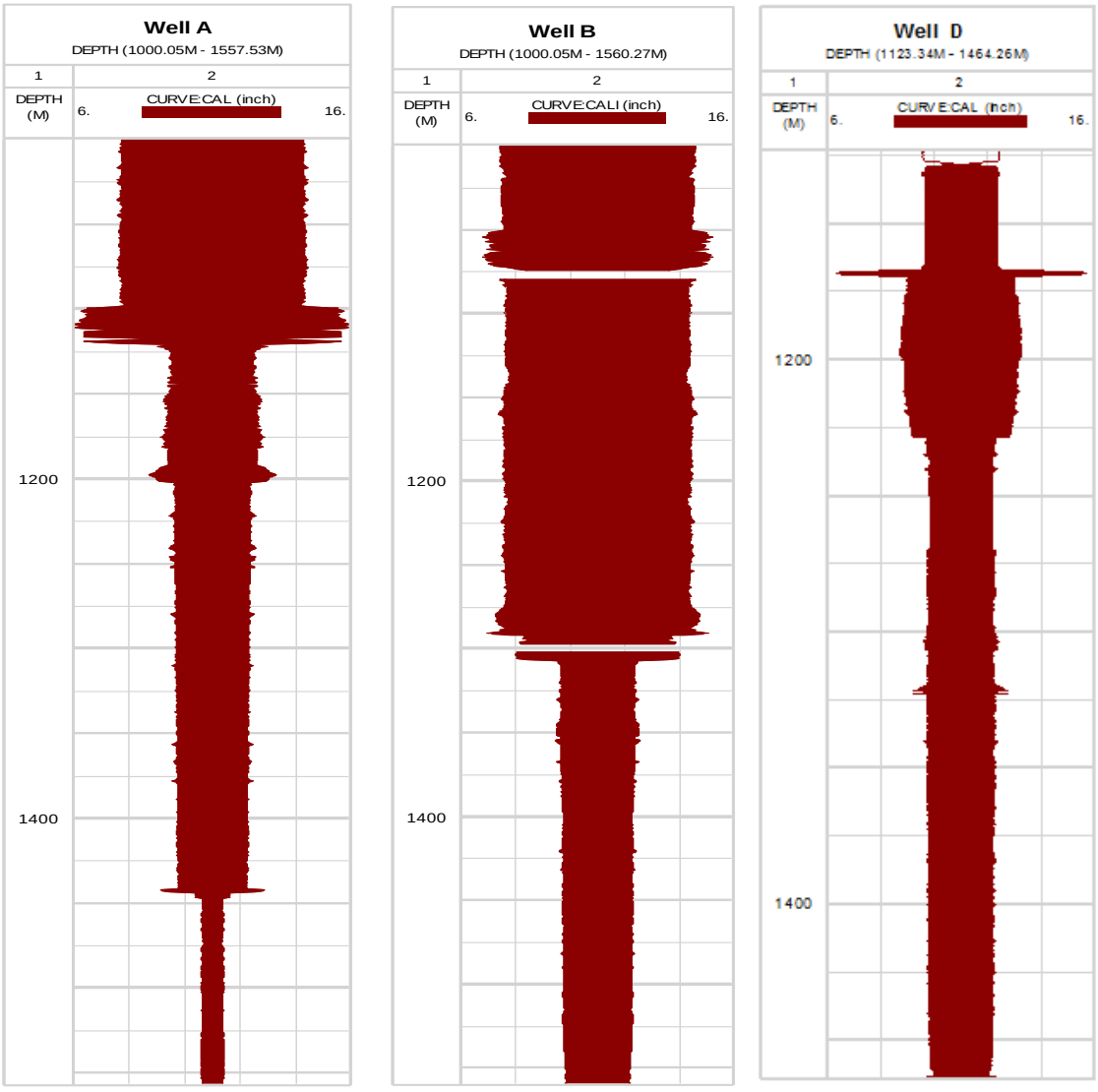

Fig. 3.11 Caliper log responses in Well A,B and D

Having these details in mind, three wells in this reservoir, Well A, B and D, could be considered as part of the analysis due to the availability of a complete set of logs. The results obtained from the caliper log, shown in Figure 3.11, indicated an intermittent breakout/washout at 1100 m (3608 ft) and 1200 m (3937 ft). A minor breakout/washout was also observed between 1300 m (4265 ft) to 1500 m (4921 ft) in Well B and from 1152 m (3779 ft) to 1312 m (4304 ft) in Well D. Portland cement was used in these wells based on the company regulation but it may not be able to survive the CO_2 attack due to the reasons provided earlier.

Finally, considering the availability of petrophysical logs, lithofacies analysis as well as CBL reports, Well B was the only well which could be part of the further assessment based on the methodology presented.

The results of the caliper log (Cal), gamma ray (GR), density (DEN), neutron (NEU), sonic (SON), and resistivity logs were acquired and used for the petrophysical evaluation of Well B in conjunction with the core based porosity and permeability. The results obtained, including porosity, permeability and water saturation determined using conventional approaches (Senergy, 2014), revealed that Well B has crossed the reservoir in a suitable place and injection may not face any difficulties as long as this well is considered. Figure 3.6 shows the estimated parameters obtained from the petrophysical analysis of Well B carried out to evaluate the near wellbore conditions for a favorable injectivity.

The capillary pressure measurements performed by the porous plate technique on the core plugs taken from the intervals of 1409 m (4622 ft) to 1536 m (5039 ft) in Well B suggested a permeability of 0.22 to 111 mD and porosity of 3% to 34.9%. The variation of capillary curves with permeability also revealed a rapid variation in the rock fabrics as displayed in Figure 3.12. These changes might be related to fractures, porosity and consolidation of reservoir rocks. Considering the variation of porosity and permeability obtained from the core data measurements, it seems that the interval between 1409 m (4622 ft) to 1536 m (5039 ft) can be a good choice for a favorable injection due to the net thickness, porosity and near wellbore permeability, as recommended by Chadwick et al. (2008).

Table 3.10 Characteristics of the wells drilled into the carbonate reservoir

Completed Date	Well ID	Well type	Status/ abandonment method	Depth (m) and perforation interval (1 = 3.28ft)	Cement bond log information	Lithofacies analysis	Caliper log	Work Over job	Mud gradient below sand layer, psi/m (1 psi/m = 0.3048psi/ft)	Fluid losses	Availability of all well logs for petrophysical and geomechanical evaluation
1973	Well A	Vertical	Abandoned/no info	1440 -1	Not Available	Available	Available	No	4.95	Only at 1440 m	Yes
1977	Well B	Directional	Abandoned/no info	1560-1	Available	Available	Available	Acidizing	6.46	Not major	Yes
1983	Well C	Directional	Depleted	1083-8	Not Available	Not Available	Available	No	4.66	No	No
1983	Well J (S)	Sidetrack	Depleted	1356-8	Not Available	Not Available	Available	No	4.66	No	No
1983	Well E	Directional	Depleted	1353-7	Not Available	Not Available	Available	No	4.66 and 4.95	Only at 1353 m	Yes
1983	Well F	Directional	Depleted	1338-1	Not Available	Not Available	Available	No	4.40 and 4.66	No	No
1983	Well G	Directional	Depleted	1338-1	Not Available	Not Available	Available	No	4.75	No	No
1983	Well H	Directional	Depleted	1367-8	Not Available	Not Available	Available	No	5.15	Only from 1190 m to 1213 m	No
1983	Well I	Directional	Depleted	1359-6	Not Available	Not Available	Available	No	4.75	No fluid loss	No
1983	Well D	Directional	Observation	1653-1	Not Available	Not Available	Available	No	4.95 and 6.75	Only from 1152 m to 1312 m (partial losses)	Yes
1983	Well K (S)	Sidetrack	Observation	1465-1	Not Available	Not Available	Not Available	No	4.95 and 6.75	No information	No
1983	Well L	Directional	Depleted	1320-1	Not Available	Not Available	Available	No	4.76	No	No
1983	Well M	Directional	Depleted	1371-7	Not Available	Not Available	Not Available	No	4.76	No	No
1983	Well N	Directional	Depleted	1347-6	Not Available	Not Available	Available	No	4.76	Only from 1060 m to 1099 m (partial)	No
1984	Well O	Directional	Depleted	1323-1	Not Available	Not Available	Available	No	4.76	No	No
1984	Well P	Directional	Depleted	1370-7	Not Available	Not Available	Available	No	4.76	No	No
2001	Well Q	Directional	Depleted	1110-nil	Available	Not Available	Not Available	Acidizing	-	No	No
2001	Well R	Directional	Depleted	1110-nil	Not Available	Not Available	Not Available	Acidizing	-	Yes	No
2001	Well S	Directional	Water disposal	597-3	Not Available	Not Available	Available	No	-	yes	No
2013	Well T	Directional	Water disposal	1798-1	Not Available	Not Available	Not Available	No	4.84	Yes and particularly in 1225 m to 1246 m formation section	No

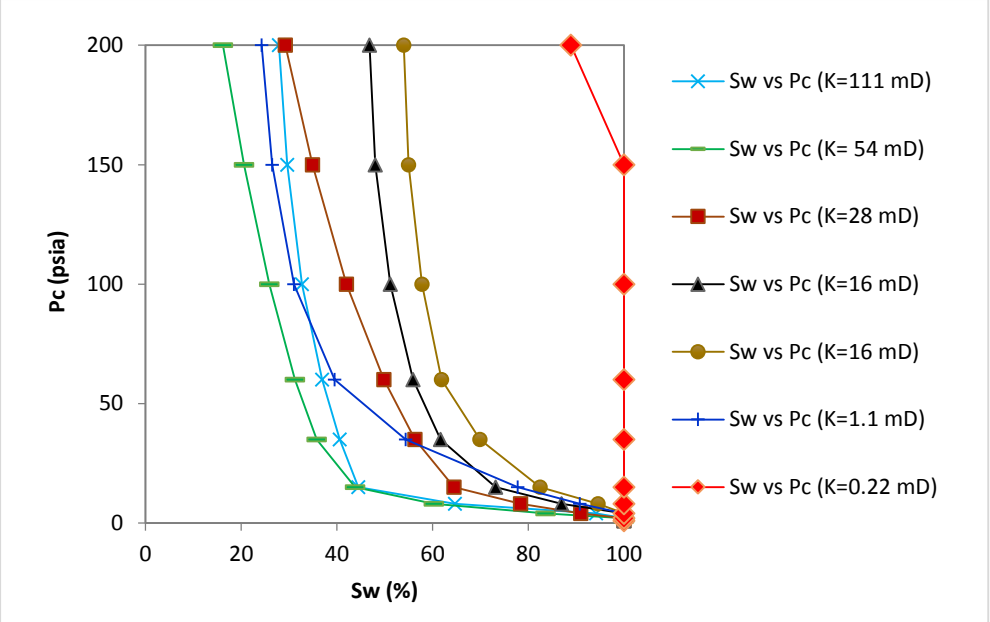

Fig. 3.12 Capillary pressure data obtained from measurements on the core plugs of Well B

A total number of nine lithofacies types were defined during the reservoir characterization based on petrographic types, gross lithology (limestone/dolostone/dolomite), porosity and permeability together with heterogeneity. Two of these lithofacies obtained from the core samples of Well B are shown in Figure 3.13.

Muddy Moldic Limestone (LMMu) lithofacies is the most common lithofacies observed in the core plugs of Well B. The petrographic type is predominantly packstones, with pack-wackestones and some grainstone and boundstones. This lithofacies has a high degree of leaching, which has resulted in moldic pores (dissolved bioclasts). These pores are connected via matrix intercrystalline or microporosity. Moldic Dolomite (DM) is the second lithofacies with a wide range of porosities and permeability. This lithofacies and is characterized by intercrystalline porosity (the mud matrix is dolomitised) along with the moldic porosity created by the dissolution of less stable bioclasts. There is a wide poro-perm heterogeneity, caused by differences in the proportion of bioclasts of solution-enhancement. The last and perhaps the most important step of the well selection is determinations of fracture pressures for seals and caprocks, which is done in the next section.

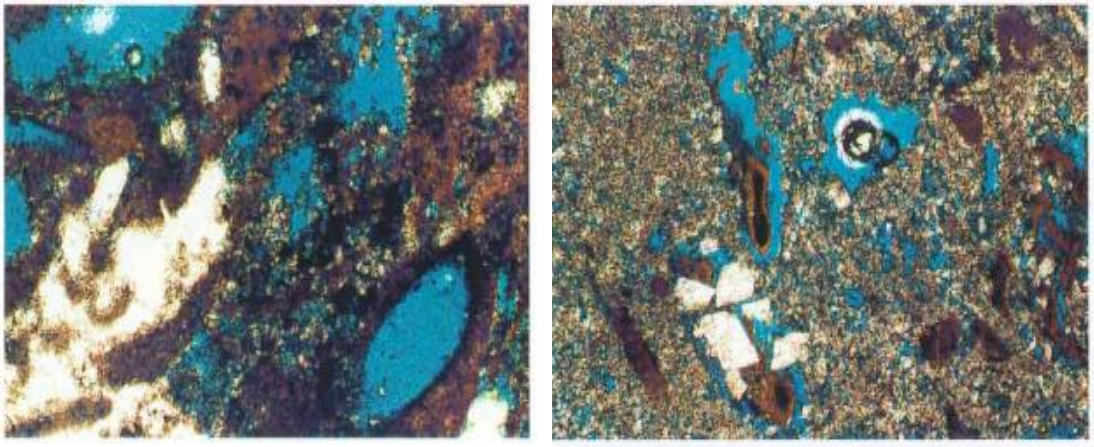

Lithofacies:LMMu
Thin section 4740 ft, Well B
Porosity 26.6%, k-74 mD
Fabric: Packstone
Pore types: Solution enhanced moldic and intercrystalline porosity with larger vuggy pores cemented by calcified anhydrite

Lithofacies:DM
Thin section 4885 ft, Well B
Porosity 27.1%, K-61 mD
Fabric: Wackestone dolomitised
Pore types: Moldic and intercrystalline porosity with some moulds partially cemented by large dolomite rhombs (white)

Fig. 3.13 Summary of the most common lithofacies observed in the core plugs of Well B

3.5.2 Fracture pressure

Fracture initiation during injection may occur if the injection pressure exceeds the fracture pressure of the caprock. As mentioned earlier, the entire set of logs including DSI log (i.e., containing compressional and shear slowness data), were acquired and available for the purpose of this study. However, core samples and MDT data were not available for calibration of geomechanical parameters estimated by the geomechanical analysis. Figure 3.14 shows the logs data used for the purpose of this study.

Dynamic elastic parameters (Young's modulus (E), and Poisson's ratio (υ)) of the formations were analytically determined using the equations provided by Fjær et al. (2008). They were then converted to static parameters using the correlations developed by Wang (2000). This is due to the overestimation of dynamic elastic parameters obtained from the wave velocity data. To estimate the uniaxial compressive strength (UCS) and the friction angle of the rocks, the correlation proposed by Bradford (1998) and Plumb (1994) were used, respectively. Figures 3.15 shows the estimated log-based parameters of Well B.

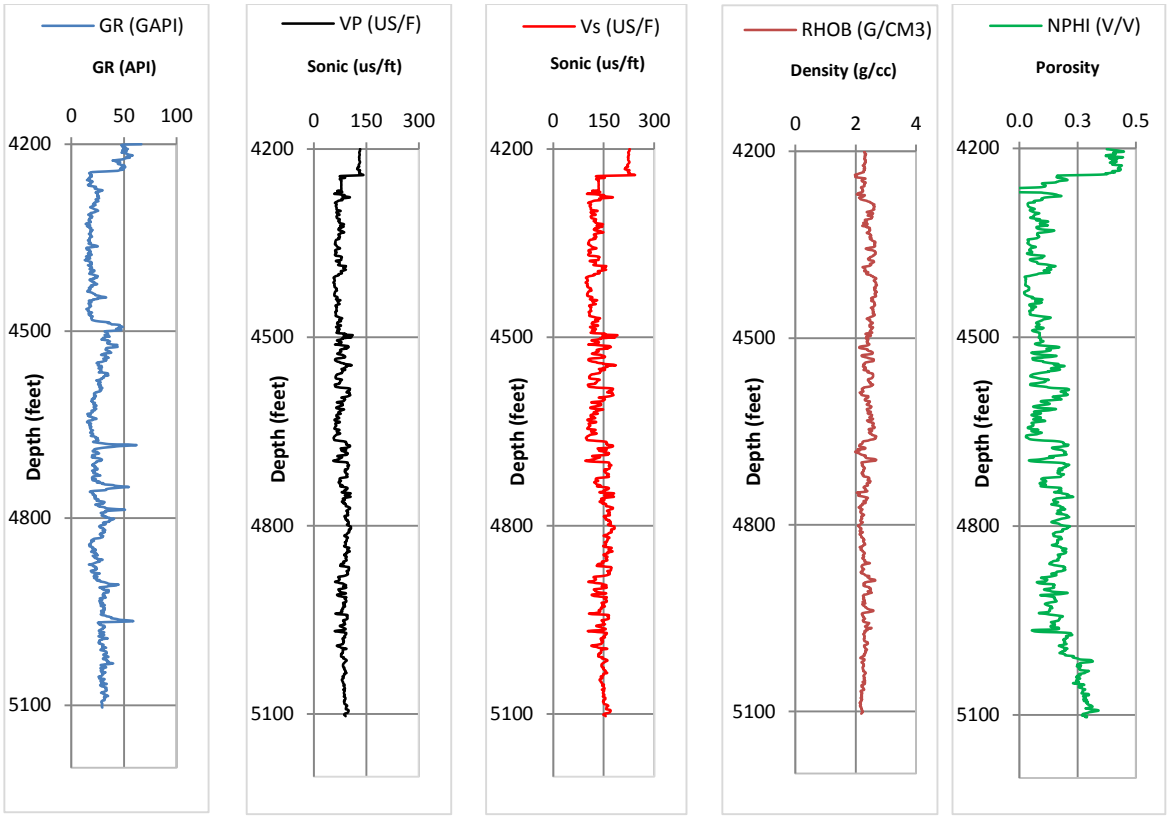

Fig. 3.14 Conventional wireline log data of Well B used for the purpose of this study

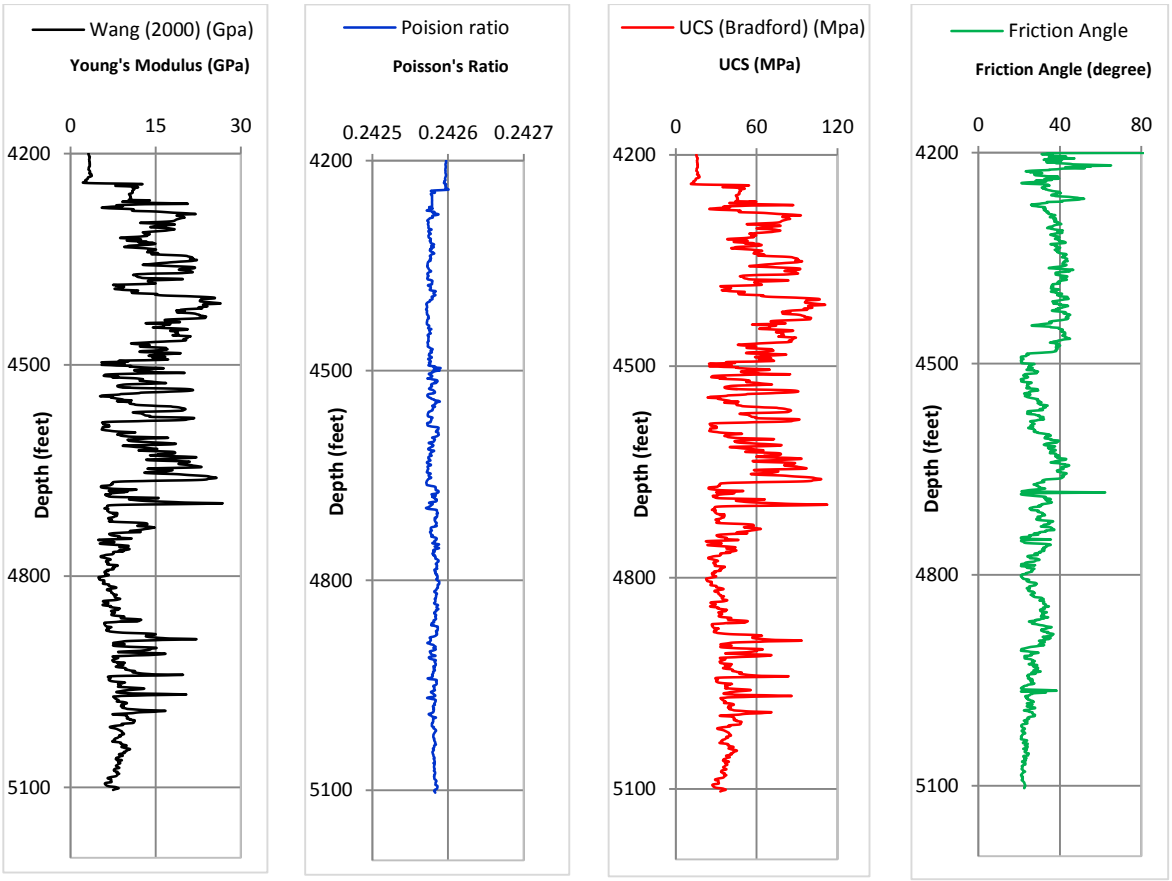

Fig. 3.15 Estimated elastic properties, uniaxial compressive strength and friction angle of Well B

Pore pressure was estimated using the Eaton's equation as it was required to determine the magnitude of effective in-situ stresses (Gholami et al., 2015b; Gholami et al., 2016). Poro-elastic equations were then used for the stress estimation by the help of leak-off tests (LOT) data. The results obtained from the stress analysis highlighted that the dominant stress regime in this reservoir is reverse faulting as the order of the magnitude of in-situ stresses was $\sigma_{Hmax}>\sigma_{hmin}>\sigma_v$.

It is generally known that the pore pressure and other geomechanical parameters must be calibrated using the reservoir and core data. However, those data were not available. Therefore, shear failure observed in the caliper log was used for the calibration purpose. As a result, the breakout pressure estimated using Mohr-Coulomb criteria was used to adjust the geomechanical parameters (elastic and strength parameters together with the pore pressure) linked to the mud weight variation. As a rule of thumb, if a failure criteria can accurately predict the break-out captured by the caliper log, one can safely say that the magnitude of in-situ stresses and other geomechanical parameters are correct. The principle and equations developed for wellbore stability analysis using the Mohr-Coulomb criteria were extensively brought in the literature (Gholami et al., 2015b; Gholami et al., 2016) and interested readers are referred back to those studies. Figure 3.16 shows the stress profiles in the first track, the caliper log and the bit size in the second track and the breakout pressure, mud loss and mud weight in the third track. The last track is the minimum horizontal stress giving the magnitude of the fracture initiation pressure.

Considering the leak of test data (LOT) covering the caprock section and the upper part of the reservoir as discussed earlier, the range of the fracture gradient in the caprock varies from 0.61 psi/ft to 0.997 psi/ft while the fluid intake gradient is within the range of 0.87 psi/ft to 0.88 psi/ft for the interval between 3633 ft to 3798 ft. Figure 3.10 shows the formation intake gradient obtained from the geomechanical analysis. The average and the range of the fracture gradient in Well B obtained from the geomechanical characterization and the average/range of fracture gradient of the caprock obtained from the LOT is given in Table 3.11.

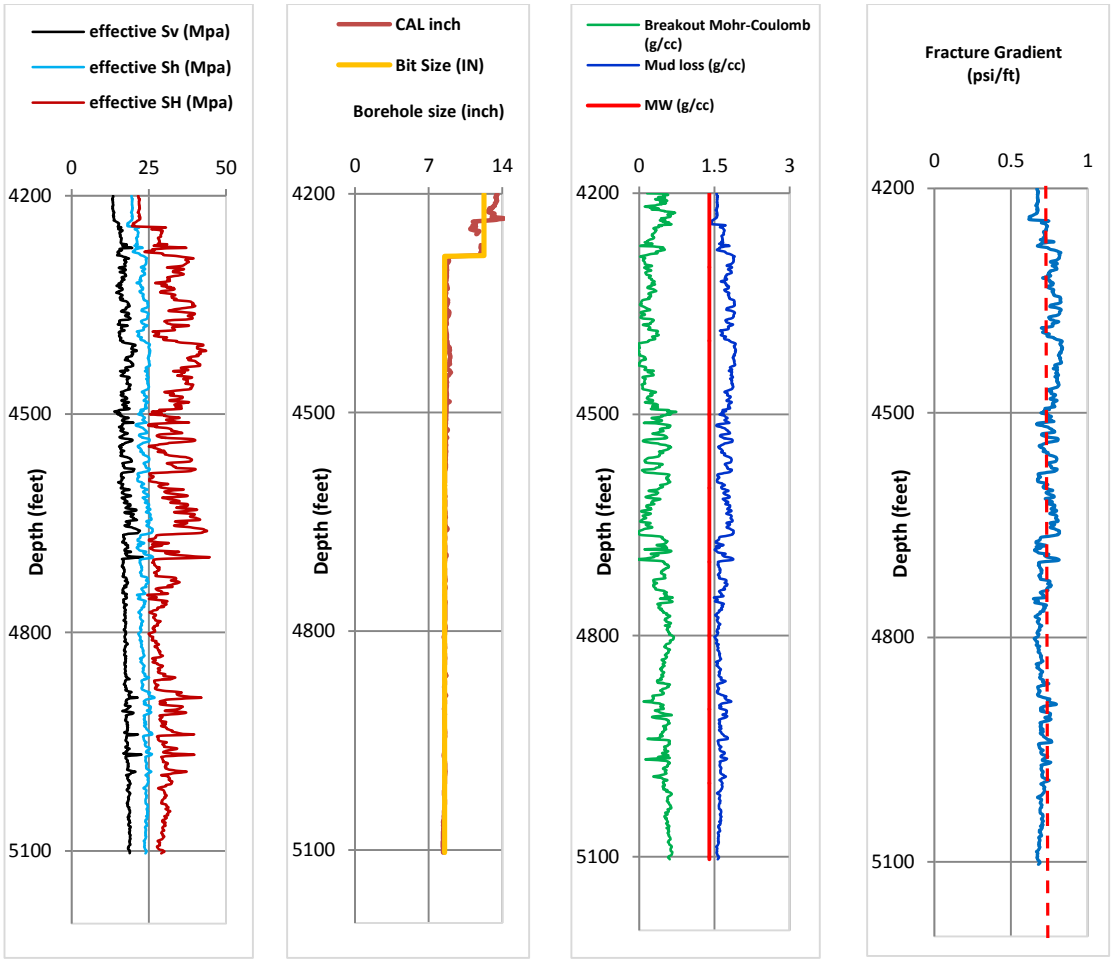

Fig. 3.16 Calibration of the breakout pressure using the caliper log to determine the fracture gradient in Well B

Table 3.11 Thresholds of the seal and reservoir before CO_2 flooding

Sr. No.	Section	Stress Regime	Depth Range (ft)	Fracture Gradient Range (psi/ft)	Average Fracture Gradient Range (psi/ft)
1	Caprock	-	1850-3500	0.61 - 1 (LOT Tests)	0.78
2	Reservoir (Well-B)	Reverse	4200-5101	0.61-0.82 (Log Data Analysis)	0.73

Having the fracture pressure determined, the pressure can build-up and a large volume of $scCO_2$ can be injected in the storage site as longs as the fracture pressure is not exceeded. In fact, knowing the fracture gradient of the caprock and the reservoir would reduce the risk of leakage during the storage operation. However, it would be essential to asses any changes in the magnitude and state of stress during

injection in order to have a clear understanding of the possible reduction taking place in the magnitude of the fracture gradient. Changes in the fracture pressure due to geochemical reactions between $scCO_2$ and caprocks must not also be ignored. This would help to have a safe and secure storage practice.

Having the threshold of the fracture pressure obtained from the geomechanical analysis of wireline logs data and considering favorable rock properties near the wellbore region as well as the lithofacies types, it seems that Well B can be considered as a good conduit for the injection job, however, the location of well on structure could be concern.

3.6 Injection zone evaluation

A well, which is referred to as Well A used for injection zone selection, drilled into this reservoir in late 70s and was perforated over the interval of 4200 ft to 4300 ft. An integrated geological approach was applied on Well A. The results were compared with the proposed indicators (see Table 3.3) to justify the good zones for favourable CO_2 storage.

3.6.1 Petrophysical analysis

Petrophysical analysis performed using wireline logs data is one of the common approaches taken to evaluate different zones in depleted petroleum reservoirs for CO_2 storage (Akintunde et al., 2013; Olierook et al., 2014).

For the purpose of this study, a core sample analysis for determination of petrophysical properties such as porosity, permeability and capillary pressure were done on 16 core plugs taken from different intervals of Well A. All samples were cleaned in hot refluxing methanol before being oven dried at 60 ^{o}C. This was followed by measurements of air permeability and helium porosity on the core plugs taken from 4109 ft to 4698 ft, having a wide range of porosity (4.6 to 39.6%) and permeability (0.38 to 241 mD). The power regression analysis showed a reasonable correlation of 0.651 between the lab measured porosity and permeability as shown in Figure 3.17 (left).

Capillary pressure data obtained was measured on 7 core plugs by humidified air at increasing incremental pressure up to 200 psia until irreducible water saturation was reached. The degree of saturation was then determined gravimetrically after reaching the capillary equilibrium. The results of these measurements are presented in Figure 3.17 (right). The Leverett up-scaling relationship was used to characterize capillary heterogeneity and generate a single reservoir curve, where the relative permeability was assumed uniform (Kuo and Benson, 2015). Attempts were made to average the capillary pressure curves using J-function but it was not successful. It might be due to the effect of heterogeneity and the complex diagenetic phenomenon caused by the presence of many lithofacies types (Ataie-Ashtiani et al., 2002).

There are total of five zones separated by tight layers. Well A is intersecting four of these zones except the flank zone which is on both sides of the reservoir. The well log data of Well A was used in the next step to evaluate the porosity, net thickness, permeability and the residual gas/water saturation as given in Table 3.12.

Table 3.12 Rock characteristics of the reservoir in Well A

Well ID	Interval of Interest (ft)	Gross Thickness (ft)	Net Thickness (ft)	Actual Perforated Interval (ft)	Porosity (%)	Permeability (mD)	Residual Gas/Irreducible Water Saturation (%)
A	3942-5005	1063	847	4218-4278	26	9.13-713	31.25/9

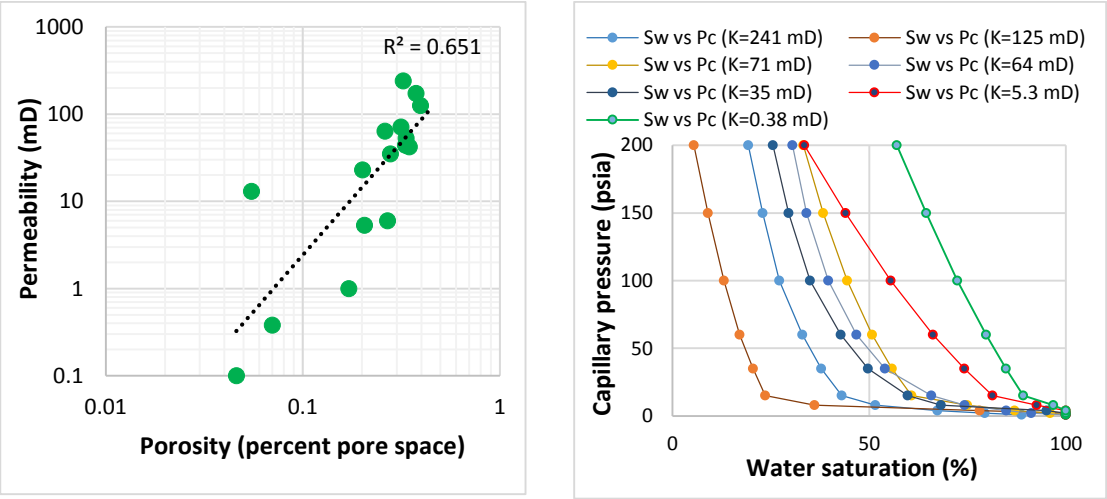

Fig. 3.17 Correlation between core measured porosity and permeability (left) and capillary pressure curves of seven core plugs (right)

Figure 3.18 shows the interpreted logs of Well A for petrophysical evaluation that has been used in this section. For the interpretation purpose, the porosity cut-off was obtained as 10%, and the favourable thickness (net pay) was estimated as 847.75 ft (258 m). Based on the wellbore condition as well as GR, density, porosity, and permeability responses, the favourable interval for the injection was indicated to be 3942-5005 ft (1201-1525.5 m).

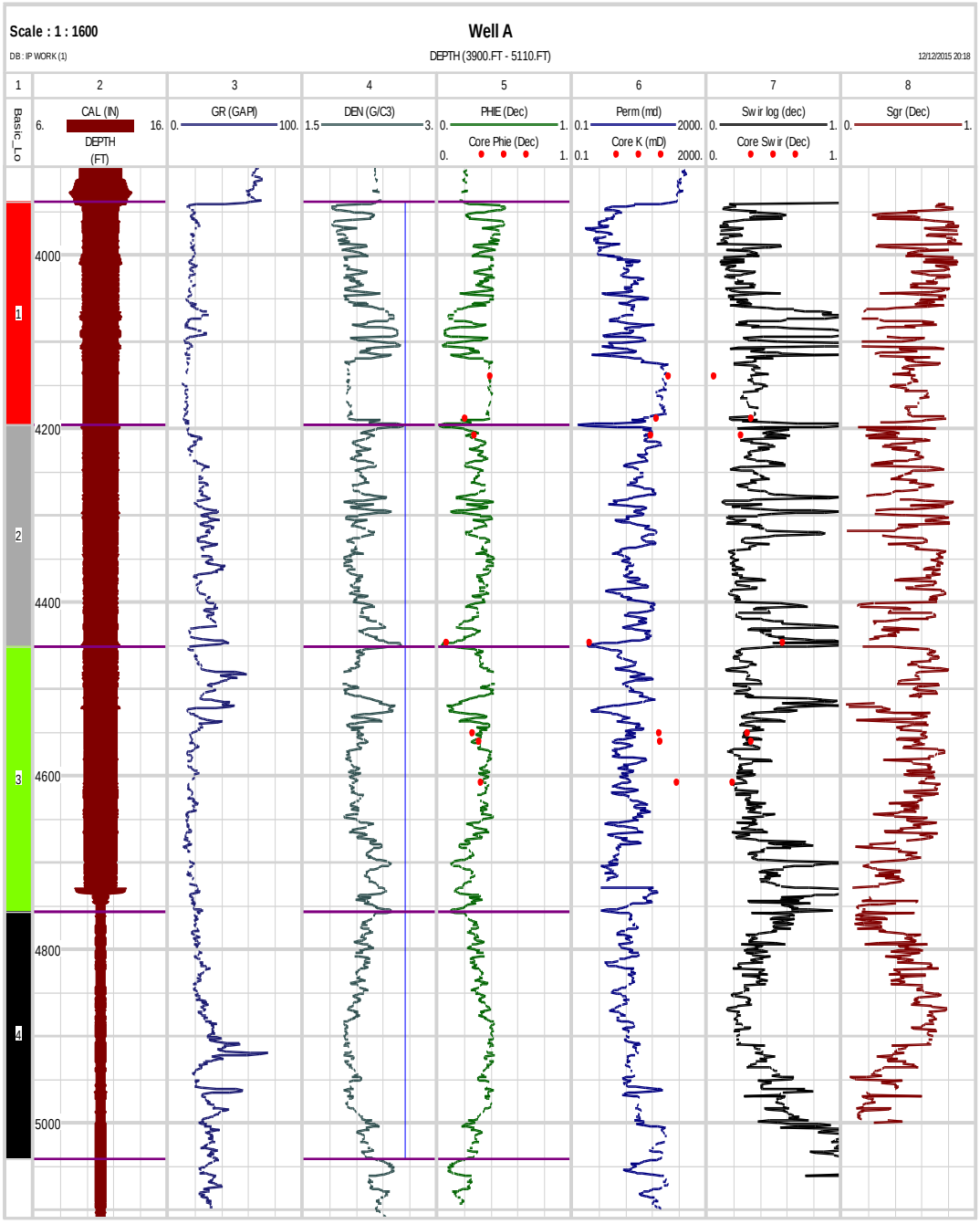

Fig. 3.18 Formation properties in the reservoir interval of Well A

The results obtained also revealed that the effective porosity estimated using the wireline logs has a good match with the lab measured porosity with a correlation of 0.91 (see Figure 3.19). The estimated permeability using the Timur's correlation, however, showed a weak match with the lab measured permeability based on the correlation of 0.44 (see Figure 3.19).

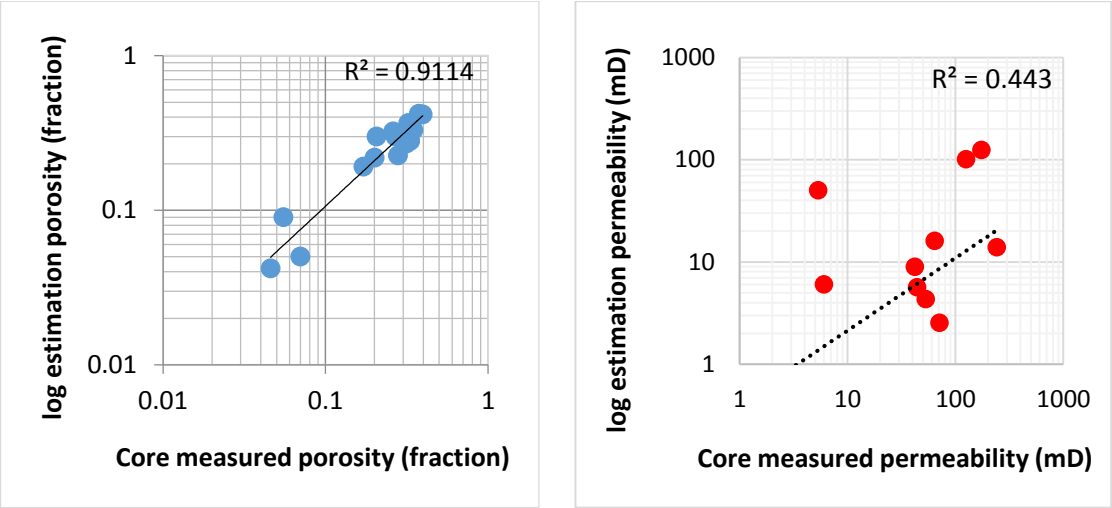

Fig. 3.19 Correlation between laboratory and log measured porosity (left); correlation between laboratory and log measured permeability (right)

It was also found that permeability decreases with depth, from a maximum value of 713 mD at 4141 ft to 9.13 mD at 4698 ft. Porosity and permeability estimated from the logs considering the initial water saturation (Sw_i) were then correlated and gave a good correlation of 0.82 as shown in Figure 3.20.

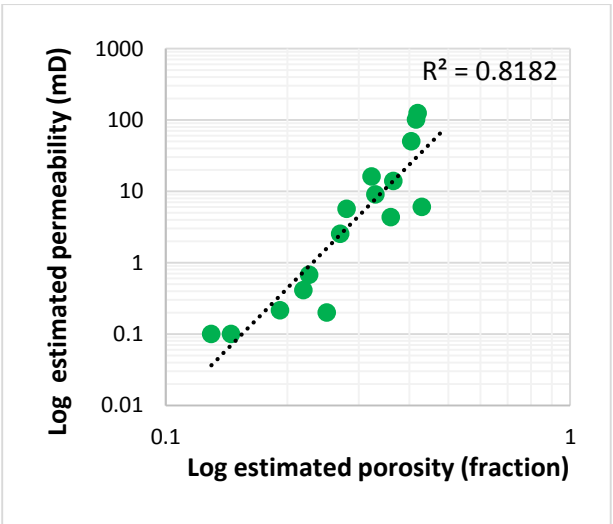

Fig. 3.20 Correlation between log estimated porosity and permeability

It is generally known that recognitions of lithofacies from wireline logs in the non-cored intervals of the well is essential to have an accurate modeling of the storage site. However, due to lateral heterogeneity observed in the analysis, the lithofacies obtained could not be extended for the non-cored intervals using the well log response.

There are several constraints which may affect the injection operation if the chosen reservoir has a remarkable water or gas saturations. As a result, the irreducible water saturation was estimated using porosity and resistivity logs and compared with that of the capillary pressure test data. It was then found that this saturation is quite different in various zones and it has a maximum value in tight formations of the reservoir. This high percentage of water saturation can significantly reduce the chance of having an effective storage capacity (Suekane et al., 2008; Pentland et al., 2011). Residual gas saturation which may also affect the efficiency of injectivity (Oldenburg and Doughty, 2011; Saeedi and Rezaee, 2012) can be estimated using deep and shallow resistivity logs and the approach presented by Ransom and Holm (1978), which is applicable to both oil and gas reservoirs. As discussed earlier that the residual gas saturation is ranging from 33% to 50% within the reservoir and its average value (31.25%) is near to the thermal decay time log (TDT) measurements (30% S_{gr}). The average residual gas saturation within the interval of Zones No. 2 and 3 is less than that of the Zone 1 and Zone 4. Table 3.13 gives the rock/fluid characteristics of different zones observed through the wireline log data. As mentioned earlier, the amount of the remaining oil may also affect the CO_2 relative permeability and, hence, CO_2 injectivity (Kovscek, 2002). At the recovery factor of 60% in carbonate gas reservoir, the remaining condensate could influence injectivity.

Table 3.13 Rock/fluid characteristics of different zones obtained from wireline log data

Parameters	Zone 1	Zone 2	Zone 3	Zone 4
Depth (ft)	3942-4200	4200-4470	4470-4720	4720-5005
Porosity (%)	25.3	26.2	27.5	24.5
Ne thickness (ft)	258	270	250	285
Permeability (near-wellbore) (mD)	81	161.75	172	121.44
Average residual gas /water saturation (%)	36/7	30/9	26/6	33/13

It can be inferred that the interpretation provided based on the wireline log data combined with the results of the core analysis could be useful to highlight the potential zones. Based on the above petrophysics analysis, it can be concluded that the level of heterogeneity as depicted by the capillary pressure and lithofacies analysis could play a crucial role in controlling brine displacement upon CO_2 injection which has a major influence on the plume migration and storage capacity (Honari et al., 2015; Ott et al., 2015a). Having a reasonable match of log estimated porosity, permeability and water saturation with the measured core data, reservoir zones at a suitable depth and pressure-temperature conditions with different rock/fluid characteristics will be selected for having a successful injection operation. Hence, it would be wised to experimentally or numerically evaluate injectivity by considering the residual constraints (fraction of water, remaining gas and condensate (oil phase)) as it varies with the injection rates, salinity of formation water (Izgec et al., 2008), and carbonate mineralization (Yoo et al., 2013).

3.6.2 Reservoir quality and CO_2 injectivity

Petrophysical evaluations of the reservoir alone suggested that it could provide a reasonable injectivity due to its high porosity and permeability, together with high quality facies (McGowen and Bloch, 1985; Atkinson et al., 1990; Bloch, 1991). In this study, the lithofacies analysis indicates that porosity developments are related to the original sediment type and smaller-scale depositional cyclicity. Late-leaching had made a significant positive contribution into the reservoir quality, especially in packstone and grainstone lithofacies. A relationship was found between the lithofacies and original sediment type including peloidal grainstone, packstones, wackestone, and pack-wackestones. The heterogeneities in the sediment type are useful to understand the characteristics of the reservoir within each lithofacies type. The secondary diagenetic pore types developed in these lithofacies are controlled by the primary sediment fabric.

The texture of dolomitized lithofacies was recognized purely fabric-selective to the micritic carbonate mud fraction. Therefore, dolomitic lithofacies (LDM and DM) are

predominantly wackestones or pack-wackestones. The muddy matrix in packstones has undergone dolomitization and caused the development of intercrystalline porosity by the dissolution of bioclasts. Packstones have a higher proportion of grains in the matrix than wackestones, and, thus, the moldic intercrystalline or microporosity porosity dominant. Each lithofacies with microporosity accounts for approximately half of the total porosity of the reservoir lithofacies when it is compared with the visible moldic pores.

The solution-enhancement is common in packstone lithofacies (LMMu) and shows an excellent reservoir character. In grainstone, composed of LM facie, original porosity has been cemented with calcite, and moldic and/or intergranular/micro intergranular porosity developed in bioclasts and peloids. The reservoir quality in this lithofacies has been reduced by moldic porosity which is very well connected. However, late-leaching along with open stylolites is one of the major characteristics of this lithofacies which improves the reservoir quality. LDT lithofacies has a low Stylolite-associated porosity and permeability (Alsharhan, 2000).

Lithofacies such as LPe, LM and LMMu have a solution enhanced moldic porosity and permeability while DM is a low reservoir quality facies. The lithofacies 'T' are characterized by a low porosity and permeability, creating a poor reservoir quality. Moreover, different levels of porosity and permeability observed through the well log data interpretation together with failure to average the capillary pressure data revealed that there is a wide variation of the facies obtained as mentioned and obtained earlier by the petrographic analysis. It is, therefore, concluded that there are four zones with different levels of reservoir quality with lateral heterogeneity.

For a favourable injectivity, the reservoir at the depth of greater than 2625 ft seems to have a good permeability, porosity, and thickness with a low level of water/gas saturation for achieving a maximum storage capacity. The analysis of a wide range of data obtained from well A indicates that Zones No. 2 and 3 are good quality zones with a favourable thickness which can support a high injection rate. According to proposed zone evaluation criteria, the thickness should be greater than 164 ft for a

successful CO_2 injection. Overall, the Zone 3 due to having a good thickness (250 ft), good-quality facies with a favourable porosity and permeability and a small amount of residual gas/water saturation shows a better reservoir quality compared to the Zone 2. Zone 1, on the other hand, should not be selected at all for the injection practice. Zone 4 is a very low-quality interval connected to a wide spread aquifer which should not be chosen as a part of the storage practice. Thus, the intervals from 4200 ft to 4470 ft (i.e., Zone 2) and 4470 ft to 4720 ft (i.e., Zone 3) are the best intervals for the injection. Table 3.14 depicts the characteristics of different zones considered as part of the favourable target selection for a safe storage practice.

Table 3.14 Comparing characteristics of different zones for an optimum injectivity target selection

Parameters	Positive Indicator	Negative Indicator	Zone 1	Zone 2	Zone 3	Zone 4
Depth (ft)	>2625 ft (800 m)	2625 ft (800 m) >depth>6562ft (2000 m)	3942-4200	4200-4470	4470-4720	4720-5005
CO_2 density	high	low	Reservoir pressure and temperature conditions			
Porosity (%)	>20%	<10%	25.3	26.2	27.5	24.5
Thickness (ft)	>>164 ft (50 m)	<66 ft (20 m)	258	270	250	285
Permeability (near-wellbore) (mD)	>100 mD	10-100 mD	81	161.75	172	121.44
Pore throat size distribution	less heterogeneous	highly heterogeneous	High Variation of rock fabrics in 4109ft to 4698ft interval			
Average residual gas /water saturation (%)	low	high	36/7	30/9	26/6	33/13
Oil phase saturation (%)	low	high	Expected 40% Condensate (oil phase) at depleted stage			
Lithofacies types	good quality	low quality	LPe, LT	LMMu, LDM, ALT	LM, LDM, DM, DT	LDT

It is indicated that tight zones can act as barriers to slow down the vertical flow of CO_2 (Frykman et al., 2009; Ukaegbu et al., 2009). According to Frykman et al. (2009), numerical modeling of the Vedsted structure composed of two different facies in Denmark revealed that zones of poor quality facies with intraformational sealing can slow down the vertical flow of CO_2. It seems that having those tight layers (low permeable) in the reservoir can help to achieve a good storage capacity due to the slow vertical movement of CO_2. However, it is worth to evaluate the injectivity through numerical and experimental studies on the zones suggested by this study to ensure that the interval can support a high injection rate. Additionally, an evaluation

on CO_2/brine/rock chemical reactions, and the influence of both brine chemistry and CO_2 composition before selecting any carbonate formations as a storage site would also be useful to make a final decision.

3.7 Summary of chapter

The reservoir that is the subject of this study was evaluated based on proposed screening criteria and consideration of the available data. After assessing every single parameter according to the screening criteria, the reservoir was found to be a suitable place for CO_2 storage. This was confirmed by analysing the depth of the reservoir and its anticline structure, CO_2 properties (density, viscosity, and interfacial tension), porosity, thickness, permeability, well types, well locations/conditions, residual gas/water saturation, salinity, conditions (pressure and temperature), rock types, wettability, and seal geometry (thickness). There are, however, some concerns about the presence of an aquifer support, a compaction issue, and the high heterogeneity level, which may result in poor injectivity. There are a few other parameters, such as the mineralogical interaction of the reservoir and caprock with $scCO_2$, the seal capacity, the seal geometry, and the stress characterization of caprock, which could not be studied due to the absence of the required data.

A long-term and safe CO_2 storage practice depends on the cap rock and well-integrity as well as hydraulic integrity, and trapping mechanisms. According to the proposed methodology, prior to flooding, evaluation of well-integrity, wellbore conditions and hydraulic integrity for the fracture pressure estimation is essential and Well B shows favorable well characteristics to act as injection well.

In this study, an injectivity analysis was also done based on the facies and petrophysical descriptions considering different indicators for target zone selections. The reservoir was found to be highly heterogeneous, undergone through a complex diagenetic phenomenon which controls the brine displacement upon CO_2 injection as well as plume migration and storage capacity. Based on the facies characterization, the reservoir has classified into nine lithofacies where lithofacies marked by A-E show a good quality. Four zones in Well A separated by tight layers were marked based on

the wireline log interpretation at different intervals, having different rock/fluid characteristics. The integrated analysis indicated that Zones No. 2 and 3 are rational choices for injection because of their favourable characteristics.

CHAPTER 4

A NEW CO_2 RESIDUAL TRAPPING METHOD AND ITS IMPLEMENTATION

4.1 Introduction

Considering the importance of field level CO_2 residual trapping for a precise storage site selection, this chapter proposed a method for the residual trapping assessment of CO_2 storage sites by considering related and effective constraints such as residual hydrocarbon saturation, interfacial tension, pore geometry, and wettability. The proposed approach was validated both experimentally and numerically. Data from two wells of the largest gas reservoir in Malaysia were considered as part of this study to show how the proposed method can be executed in the field scale for determination of the residual trapping ability of the petroleum reservoir.

4.2 Theory and calculation

4.2.1 Residual trapping

The residual trapping refers to the immobilization of a fluid due to the capillary force in a snap-off process (Ennis-King and Paterson, 2001; Juanes et al., 2006; Pentland, 2011; Jalil et al., 2012; Zhang and Song, 2014; Raza et al., 2016), even in the presence of a pressure gradient induced by gravity, fluid injection or extraction (Krevor et al., 2011). Pentland et al. (2011) reported two mechanisms in pore scales which are responsible for controlling the amount of residual trappings. The first mechanism is imbibition- a competition between pore and throat filling. At the reservoir scale, this imbibition process is dominant at the tail of the migrating $scCO_2$ plume, while brine as the wetting-phase imbibes behind the migrating non-wetting phase CO_2. When the concentration of $scCO_2$ becomes less than a certain value, it is trapped by the capillary pressure and ceased to flow (Ennis-King and Paterson, 2001; Holtz, 2002). Therefore, at the trail, the immobile $scCO_2$ is left behind the plume as it migrates upward (Juanes et al., 2006). During the Piston-like advance when the

water flow displaces the non-wetting phase from neighboring pore throats, the threshold capillary pressure is expressed as:

$$P_c = \frac{2\sigma \cos\theta}{r} \tag{4.1}$$

In the above equation, P_{ca} (psi), θ (degree), σ (gf/cm), and r (cm) are the capillary pressure, contact angle, interfacial tension and pore throat radius, respectively. To assess the threshold capillary pressure, quantification of these parameters would be essential.

The second mechanism in charge of controlling the residual trapping is the snap-off process, taking place during imbibition process when water preferably refills the smallest pore spaces. The way in which the non-wetting phase gradually occupies small pores and the degree of trapping is controlled by local capillary forces (Pentland, 2011). It is worth to mention that thin films only exist in strongly wetting systems and the snap-off mechanism may be abridged/excluded entirely in intermediate-wet media (Kimbrel et al., 2015). Therefore, strong water and water wet systems are more capable of residual trapping compared to intermediate or oil-wet rocks (Iglauer et al., 2015; Al-Menhali and Krevor, 2015; Al-Menhali and Krevor, 2016). For a throat of square cross-section and inscribed radius, r_t (cm), the threshold capillary pressure, P_c (psi), is obtained by the interfacial tension, σ (gf/cm), and the contact angle, θ (degree), as:

$$P_c = \frac{\sigma(\cos\theta - \sin\theta)}{r_t} \tag{4.2}$$

Basically, the CO_2 residual trapping is the most efficient mechanism contributing into the overall trapping compared to dissolution or mineral trapping mechanisms (Kimbrel et al., 2015), having considerable impacts on the rate and extent of plume migration, immobilization and storage security (Krevor et al., 2015). There are a number of parameters such as rock-fluid characteristics, geologic settings and injection conditions linked to the residual trapping, which many of them are summarized in Table 4.1. Having all of these parameters in mind, quantification of the residual trapping capability of a storage site prior to CO_2 injection seems very

unlikely. This might be the reason why there is almost no study carried out on the determination of the residual trapping in a reservoir scale.

4.2.2 Proposed analytical approach

There are many parameters affecting the CO_2 residual trapping in a depleted reservoir and development of an approach to estimate the residual CO_2 saturation (Sgr_{CO2}) is not an easy and straightforward task. There are studies carried out in the past indicating factors such as capillary forces (Pashin and Dodge, 2010; Iglauer et al., 2011b), interfacial tension (Bennion and Bachu, 2006; Jiang and Tsuji, 2015), wettability (Iglauer et al., 2015), and pore geometry (Pashin and Dodge, 2010; Pentland et al., 2012) as the controlling parameters of the residual trapping. However, there might be few others which have not been recognized yet. In this study, an attempt was made to propose an approach for estimation of the residual CO_2 saturation (residual trapping capability) based on the Laplace model which can be applied at reservoir scales. The Laplace model was used because it is the only theoretical well-established model relating the capillary pressure, P_c (psi), to the contact angle, θ (degree), interfacial tension (capillary force), σ (gf/cm), and pore throat radius, r (cm) (Amyx et al., 1960). It also covers the basic mechanism of the capillary pressure during drainage and imbibition. The capillary pressure by the standard Young-Laplace equation is defined as:

$$P_c = P_{nw} - P_w = \frac{2\sigma\cos\theta}{r} \tag{4.3}$$

Capillary pressure, P_c (psi), in this sense, is referred to as the difference between a non-wetting phase pressure, P_{nw} (psi), and a wetting phase pressure, P_w (psi), arising from the capillary forces. These capillary forces are surface and interfacial tensions. The interfacial tension is the imbalance of molecular forces between two phases (Chalbaud et al., 2009) while wettability of rocks is defined as the ability of one fluid over another to wet the rock's surface (Iglauer et al., 2015). Wettability is determined by the contact angle as the angle created between a fluid and a solid surface. Contact angles for different rock systems is given in Table 4.1.

Table 4.1 Contact angles for different rock systems (modified after Iglauer et al. (2015))

Wettability based on Contact Angle from the Petroleum Engineering Literature		
Wettability	**Treiber and Owens (1972)**	**Dake (1978)**
Water-wet	$0^o \le \theta < 75^o$	$0^o \le \theta < 90^o$
Intermediate-wet	$75^o \le \theta < 105^o$	$\theta = 90^o$
Oil-wet	$105^o \le \theta \le 180^o$	$90^o < \theta \le 180^o$
Wettability Based on Contact Angle for CO_2-Brine-Mineral Systems		
Wettability State	**Water Contact Angle θ °**	
Complete wetting or spreading of water	0	
Strongly water-wet	0-50	
Weakly water-wet	50-70	
Intermediate-wet	70-110	
Weakly CO_2-wet	110-130	
Strongly CO_2-wet	130-180	
Complete non-wetting of water	180	

It is known that CO_2 and hydrocarbons are often form a non-wetting phase and, thus, the Laplace equation (Eq. (4.3)) can be addressed as:

$$Pc_{hyd\text{-}brine} = \frac{2\sigma_{hyd-brine}\cos\theta_{hyd-brine-rock}}{r} \tag{4.4}$$

$$Pc_{CO2\text{-}brine} = \frac{2\sigma_{CO2-brine}\cos\theta_{CO2-brine-rock}}{r} \tag{4.5}$$

In the Eq. (4.4), $Pc_{hyd\text{-}brine}$ (psi) is the capillary pressure between hydrocarbon and brine at a particular hydrocarbon-brine interfacial tension, $\sigma_{hyd\text{-}brine}$ (gf/cm), a rock-fluids contact angle, $\theta_{hyd\text{-}brine\text{-}rock}$ (degree), and pore throat radius, r (cm). In Eq. (4.5), $Pc_{CO2\text{-}brine}$ (psi), $\sigma_{CO2\text{-}brine}$ (gf/cm) and $\theta_{CO2\text{-}brine\text{-}rock}$ (degree) are the CO_2-brine capillary pressure, CO_2-brine interfacial tension, the rock-fluids (CO_2-brine) contact angle, and pore throat radius, r (cm), respectively.

Saeedi and Rezaee (2012) experimentally revealed that the amount of CO_2 trapping in a depleted natural gas system by cycling and brine injection is approximately similar to that of a two-phase system (CO_2/brine) as given in Table 4.2. It should be noted that CO_2 injection in a depleted natural gas system would transform the two-phase system of CH_4-brine into a multiphase system having three phases such as CH_4,

brine, and CO_2. Considering this aspect and dividing Eq. (4.5) by Eq. (4.4), the multiphase storage system (hydrocarbon/brine/CO_2) during CO_2 injection at a particular depth in depleted hydrocarbon system can be written as:

$$\frac{\mathrm{Pc}_{\mathrm{CO2\text{-}brine}}}{\mathrm{Pc}_{\mathrm{hyd\text{-}brine}}} = \frac{\sigma_{CO2-brine}}{\sigma_{hyd-brine}} \times \frac{\cos\theta_{CO2-brine-rock}}{\cos\theta_{hyd-brine-rock}} \tag{4.6}$$

Eq. (4.6) considers the fact that the pore geometry will equally change during depletion and injection. As mentioned earlier, the amount of CO_2 trapping in a depleted natural gas system by cycling CO_2 and brine injection is approximately similar to that of a two-phase system (CO_2-brine). This means that forces trapping natural gases are diminished during the cycling of CO_2, and new forces based on the CO_2-brine interfacial tension develops and traps CO_2. There have been many studies on the relevant factors though indicating that immobilization as the residual CO_2 saturation is taking place in pores due to capillary forces (Ennis-King and Paterson, 2001; IPCC, 2005-pp205; Juanes et al., 2006; Pentland, 2011; Jalil et al., 2012; Cheng, 2012; Zhang and Song, 2014; Burnside and Naylor, 2014; Raza et al., 2016). Considering these studies, it can be claimed that all of the effective and related parameters such as interfacial tension, wettability and pore geometry related to capillary pressure are the major controlling factors of the residual saturation. Thus, Eq. (4.7) was introduced and assumed to be equal to a two non-wetting phase residual CO_2 and hydrocarbon saturations. The parameter α in this equation is an adjusment factor determined by a non-linear regression analysis of $SgrCO_2$. This adjustment factor would consider the impact of other effective parameters such as effective in-situ stress (Saeedi et al., 2012) and the ratio of gravity to viscous forces (Taku Ide et al., 2007) which are related to the residual trapping.

$$\frac{\mathrm{Pc}_{\mathrm{CO2\text{-}brine}}}{\mathrm{Pc}_{\mathrm{hyd\text{-}brine}}} = \frac{\sigma_{CO2-brine}}{\sigma_{hyd-brine}} \times \frac{\cos\theta_{CO2-brine-rock}}{\cos\theta_{hyd-brine-rock}} = \alpha \frac{Sgr_{CO2}}{Sgr_{hyd}} \tag{4.7}$$

or

$$Sgr_{CO2} = \frac{Sgr_{hyd}}{\alpha} \times \frac{\sigma_{CO2-brine}}{\sigma_{hyd-brine}} \times \frac{\cos\theta_{CO2-brine-rock}}{\cos\theta_{hyd-brine-rock}} \tag{4.8}$$

To compute the total residual saturation from the beginning up to the end of injection period at any given pressure, residual saturation is summed up and averaged as expressed in Eq. (4.9).

$$Sgr_{CO2} = \frac{\sum_{i=1}^{N}\left[\frac{Sgr_{hyd}}{\alpha} \times \frac{\sigma_{CO2-brine}}{\sigma_{hyd-brine}} \times \frac{\cos\theta_{CO2-brine-rock}}{\cos\theta_{hyd-brine-rock}}\right]_i}{N} \quad (4.9)$$

In Eqs. (4.7-4.9), α is the adjustment factor, $Pc_{hyd\text{-}brine}$ (psi) is the capillary pressure between hydrocarbon and brine, $\sigma_{hyd\text{-}brine}$, (gf/cm) is the hydrocarbon-brine interfacial tension, $\theta_{hyd\text{-}brine\text{-}rock}$ (degree) is the rock-fluids contact angle, Sgr_{hyd} is the hydrocarbon residual gas saturation. $Pc_{CO2\text{-}brine}$ (psi), $\sigma_{CO2\text{-}brine}$ (gf/cm), $\theta_{CO2\text{-}brine\text{-}rock}$ (degree), and Sgr_{CO2} are the CO_2-brine capillary pressure, CO_2-brine interfacial tension, the rock-fluids (CO_2-brine) contact angle, and residual CO_2 saturation, respectively. Eq. (4.9) can now be used to calcuate the residual CO_2 saturation/residual trapping for different rock types having different wetting characteristics. However, this approach must be validated to ensure its application in different scenarios.

For the purpose of this study, the proposed approach was validated using a strong-water-wet system since this system is capable of providing more residual trapping compared to an intermediate or oil-wet rocks (Iglauer et al., 2015; Al-Menhali and Krevor, 2015; Al-Menhali and Krevor, 2016). A separated numerical modeling was also employed to further verify the developed analtyical model using relative permeability data obtained from the carbonate gas bearing core samples.

4.3 Material and methods

The proposed approach was validated using data obtained from experimental and numerical modelings methods. In this section, these validations were presented and attempts were made to show the application of the approach presented in providing suitable results even in the reservoir scale.

4.3.1 Experimental data

Saeedi and Rezaee (2012) conducted an experimental study to evaluate the effect of residual natural gas saturation on the multiphase flow behavior having CH_4-brine-$scCO_2$ during geo-sequestration in depleted natural gas reservoirs. This is one of the pioneer studies available in the literature which could be utilized to validate the proposed approach. Prior to go through the validation part, a brief summary on the materials, experimental conditions, procedure and the results of the study carried out by Saeedi and Rezaee (2012) is provided.

In total, four types of fluids were used in that study, including dead brine (brine with no dissolved gas content), CO_2-saturated brine (brine saturated with CO_2 (high-purity grade 99.99%) at the in-situ reservoir P–T conditions), water-saturated CO_2 (supercritical CO_2 with water vaporized at the in-situ reservoir P–T conditions) and CH_4 (representing the natural gas) pre-saturated with water vapor. The brine was prepared in the lab using demineralized water and analytical grade (99.95%) sodium chloride (NaCl). Four core samples consisting of three Berea sandstone and a composite sample from the Unit C of the Waarre formation located in the CRC's Naylor reservoir were used for running experiments. The measured porosity and permeability values under in-situ reservoir conditions are given in Table 4.2, covering a wide range of porosity and permeability. Samples were aged in the synthetic formation brine for two weeks to restore their original wettability of strongly water-wet. The core-flooding experiments were carried out using a high pressure-high temperature (HPHT), three-phase steady-state core-flooding apparatus under in-situ reservoir conditions. It should be noted that in these tests, fluids were saturated with each other to avoid dissolution during injection. However, all drainage floods were capillary dominated as predicted based on the capillary numbers and Rapoport scaling coefficients. In total, eight core-flooding experiments were conducted, out of which the first four aimed to investigate the effect of residual CH_4 on the process of CO_2 geo-sequestration, and the rest were taken to establish the base case (pure CO_2-brine injection system) required for evaluating the results obtained from the first four tests.

Table 4.2 summarizes the end-point brine saturations at the end of injection cycles during flooding experiments. To study the effect of the residual natural gas, beyond the primary drainage and imbibition floods, the first four tests were continued with further drainage and imbibition cycles to simulate the CO_2 geosequestration process.

Table 4.2 End-point brine saturations at the end of flooding (Saeedi and Rezaee, 2012)

Test No.	Sample Name	Porosity (%)	Permeability (mD)	End-point brine saturation (%)						
				lst drain.	1st imb.	2nd drain.	2nd imb.	3rd drain.	3rd imb.	4th drain.
1	CO2CRC-2,3-H	17.31	788.3	35.0	71.3	49.5	77.0	49.0	79.8	51.8
2	BS-1-H	17.97	234.6	29.4	68.0	38.0	70.5	40.1	76.5	43.4
3	BS-2-H	18.4	141.13	35	67.6	37.1	73.9	40.6	76.3	43.4
4	BS-3-V	18.64	194.4	29.1	67.6	34.7	72.1	38.5	75.1	43.1
5	CO2CRC-2,3-H	17.31	788.3	50.1	80.4	-	-	-	-	-
6	BS-1-H	17.97	234.6	44.9	78.5	-	-	-	-	-
7	BS-2-H	18.4	141.13	44.8	80.6	-	-	-	-	-
8	BS-3-V	18.64	194.4	45.8	76.5	-	-	-	-	-

4.3.2 Experimental validation

In order to determine the residual saturation of CH_4 and CO_2, the imbibition flooding results with the available interfacial tension (σ) and strongly water-wet rocks (i.e., the contact angle of less than 50°) were considered for both CH_4-brine and CO_2-brine systems (See Table 4.3) together with the modified Laplace model (Eq. (4.9)). It should be noted that the first imbibition flooding data from Table 4.2 was utilized to obtain the residual saturations of non-wetting phases (CH_4 and CO_2). It is clear from Table 4.3 that the residual natural gas is more than the residual CO_2 saturation in similar conditions for all of the core samples. This is because CO_2–brine interfacial tension is less than that of a hydrocarbon–brine and, thus, a lower residual gas saturation is achieved in a CO_2-brine system due to a dominant snap-off trapping mechanism (Saeedi and Rezaee, 2012). Having all of the input data, the residual CO_2 saturation was calculated by considering the adjustment factor, α. Non-linear

regression analysis was done on the residual CO_2 saturation and the value of α was found to be 0.996 with a minimum standard deviation of 8.67. Figure 4.1 compared the estimated and measured values of the residual saturation.

For all samples, the model and experimental data were in a good agreement. However, it is essential to evaluate this approach for low permeable samples to extend its applications. However, the estimation provided by the model was sensitive to the interfacial tension and reliable interfacial tension values were required for the reliable modeling of residual CO_2 saturation. Since a close match could be found between the measured and estimated values if the adjustment factor of 0.996 is used, it is expected to have a same adjustment factor for sandstone samples having similar characteristics and a strongly water-wet system. It is worth mentioning that this comparison is just to validate the proposed approach and can only be used for a strongly water-wet system, although it can be evaluated against any other wetting system (i.e., intermediate or oil-wet systems) and different rock types to tune the adjustment factor (α). As mentioned earlier, the parameter α is determined by a non-linear regression analysis of $SgrCO_2$ which considers the impact of other effective parameters related to the residual trapping such as effective in-situ stress and the ratio of gravity to viscous forces. According to the literature, it might be possible that supercritical CO_2 changes the wettability condition of the rock's surface during flooding (Wang and Tokunaga, 2015; Iglauer et al., 2015) as wettability is a function of pressure, temperature and salinity. It has also been shown that wettability is strongly related to the CO_2-brine interfacial tension as well as changes in density (Arif et al., 2016; Roshan et al., 2016). To avoid these issues, the same core plugs used for two different systems of CH_4-brine-CO_2 and CO_2-brine were employed for validation to mitigate the effect of the above parameters.

The residual CO_2 saturation estimated by taking capillary forces into consideration, wettability and pore geometry at specific reservoir conditions were presented in Figure 4.1. The results shown in this Figure would provide a more in depth understanding of the residual trapping and its major controlling parameters.

Table 4.3 Residual gas saturation in case of CH_4-brine and CO_2-brine systems for a strongly water-wet system

System	Test No.	Sample Name	Experimental Residual Saturation (%) First Cycle Injection (1ST Imbibe)	Interfacial tension between non-wetting phase-brine (gf/cm)
CH_4-H_2O	1	CO2CRC-2,3-H	28.7	0.045
	2	BS-1-H	32	0.045
	3	BS-2-H	32.4	0.045
	4	BS-3-V	33.4	0.045
CO_2-H_2O	5	CO2CRC-2,3-H	19.6	0.030
	6	BS-1-H	21.5	0.030
	7	BS-2-H	19.4	0.030
	8	BS-3-V	23.5	0.030

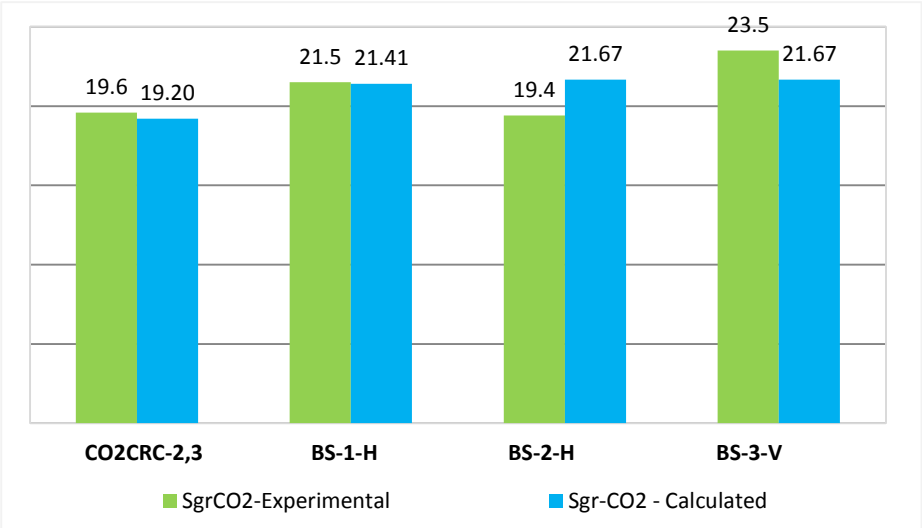

Fig. 4.1 Comparison of calculated (from Eq. 4.9) and measured residual CO_2 saturation by considering the adjustment factor of 0.996

4.3.3 Numerical modeling

4.3.3.1 Modeling background/setup

The CO_2 storage modeling was carried out considering remaining natural methane (CH_4) gas through Eclipse300^{TM}, an industry standard finite difference flow simulator. The GASWAT option in AIM (Adaptive IMplicit) formulation of E300 provides a gas/aqueous phase equilibrium method which was used to run the simulation (Schlumberger, 2014a; Schlumberger, 2014b). The GASWAT option is for a two-phase system only and cannot model the oil phase. This option was used in earlier studies to evaluate the enhanced natural gas recovery by CO_2 storage (Feather and Archer, 2010). The "Egg Model", a synthetic static reservoir model, consisting of an ensemble

of 101 relatively small three-dimensional permeability realizations (Jansen et al., 2013) was used by modifying the grid dimensions. In this study, a 3D Cartesian grid Egg model consisting of 7 zones were considered where each zone had a thickness of 26.25 feet (8 m) with a certain level of heterogeneity (Kuo et al., 2011; Hingerl et al., 2016), time-scale of convective mixing, plume size and degree of CO_2 trapping (Han et al., 2011). To ensure the supercritical state of CO_2, the top depth of first zone was set at 13000 feet. The model has an average porosity and permeability of 20% and 800 mD, respectively. Figure 4.2 displays the permeability distribution in the model in which the X-Y plane has 3600 grid blocks in each direction.

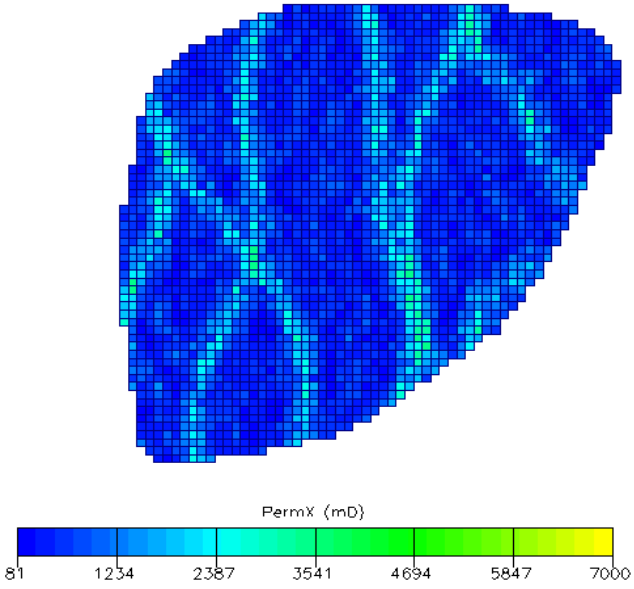

Fig. 4.2 The reservoir model displaying the typical structure of high-permeability meandering channels in a low permeability background

A vertical oriented injection well was placed in the center of the model, perforating the last four zones for up to 105 feet. The reason to select these zones was to take the benefit of the fact that the higher density of CO_2 compared to methane at the reservoir condition causes an undertaking running effect. For the depletion scenario, the initial reservoir pressure was set to be 290 psia. Three components such as CH_4, CO_2 and H_2O were used for the dry gas since CO_2 and H_2O are necessary to take in GASWAT modeling. The total of four salinity conditions (0.085 mol/kg, 0.87 mol/kg, 1.79 mol/kg, and 2.75 mol/kg) and three temperatures (80.6 ^oF, 159.8 ^oF, and 212 ^oF)

were used to run 12 simulation cases. Salinities considering NaCl concentrations were expressed in molal (M) values (mol/kg). The main purpose of considering these salinities and temperatures was to compare the results with those of the experimental values presented by Chalbaud et al. (2009), which could further validate the proposed approach.

Properties of gas, water and carbon dioxide (i.e., critical pressure, critical temperature, acentric factors and binary interaction coefficients) were generated by the PVTi module of the Eclipse. For calculation of PVT properties of methane, the Peng-Robinson equation of state (PR-EOS) was applied as expressed in Eq. (4.10). During simulation, solubilities of CO_2 in water was determined by PR-EOS including Soreide and Whitson modifications (Eqs. (4.11) and Eq. (4.12)) (Soreide and Whitson, 1992), while the solubility of methane was treated by the original Peng Robinson EOS (Eq. (4.10)) (Schlumberger, 2014a).

$$\left[P+\frac{A}{V_M(V_M+B)+B(V_M-B)}\right](V_M-B)=RT \tag{4.10}$$

In the above equation, P is the pressure, V_M is the molar volume, R is the gas constant, T_R is the temperature, A and B are the mixture-specific constants which are a function of temperature and composition. The coefficient A is defined based on the mole fraction, binary interaction coefficients, critical temperature and critical pressure. Soreide and Whitson (1992) proposed two changes for the coefficient A, which could help to have a more accurate result.

1). Modifying the expression $\alpha^{1/2}$ for the water component and expressing it with Eq. (4.11) which is related to salinity (c_s) of brine, expressed as a molality (M) and reduced temperature T_r.

$$\alpha^{\frac{1}{2}}=1+0.4530\left[1-\left(1-0.0103c_s^{1.1}\right)T_r\right]+\left[0.0034(Tr^{-3}-1)\right] \tag{4.11}$$

2). Adding a temperature dependent parameter to the aqueous phase binary interaction coefficients, k_{jw}^{a}, expresed as Eq. (4.12) with default values (bq_i) along with Pitzer acentic factor (w) as given in Table 4.4.

$$k_{jw}^{a} = bq_1 + bq_2 T_{rj} + bq_3 T_{rj}^2 \quad (4.12)$$

Table 4.4 Default values of parameters included in Eq. (4.12) (Soreide and Whitson, 1992)

$bq_1 = A_o(1+S_o c_s)$	$A_o = 1.112 - 1.7369 w_j^{-0.1}$	$S_o = 0.017407$
$bq_2 = A_1(1+S_1 c_s)$	$A_1 = 1.1001 + 0.836 w_j$	$S_1 = 0.033516$
$bq_3 = A_2(1+S_2 c_s)$	$A_2 = -0.15742 - 1.0988 w_j$	$S_o = 0.011478$

The molecular diffusion of gas components is not often included in subsurface simulation models, although it is important in certain reservoirs under flooding conditions. In fact, many studies highlighted the link of diffusion with the matrix-bound oil in fractured reservoirs (Hoteit and Firoozabadi, 2009; Alavian and Whitson, 2010; Yanze and Clemens, 2012). This mixing increases with increasing heterogeneity and reservoir aspect ratios (Connolly and Johns, 2016). In view of this fact, molecular diffusion between gas components was introduced for diffusive flow which is obtained using Eq. (4.14) by defining diffusivity input of Eq. (4.13) (Schlumberger, 2014a).

$$J_i = -x \frac{D_i \partial y_i}{\partial d} \quad (4.13)$$

In Eq. (4.13), x is the total molar concentration (mol m^{-3}), J_i is the flux of component i per unit area (mol m^2 s^{-1}), D_i is the diffusion coefficient of componenti (m^2 s^{-1}), and $\partial y_i/\partial_d$ is the molar concentration gradient of component i in the direction of flow (mole fraction). These diffusion coefficients are used in the simulator module to obtain the gas interblock diffusive flows expresed as Eq. (4.14).

$$F_{ig}^{diff} = (T_D D_{ig})(S_g b_g^m)\Delta y_i \quad (4.14)$$

In the above equation, F_{ig} is the interblock diffusive flow (mol/hour), T_D is the diffusivity (m^2/s), and y_i is the vapor mole fractions, S_g is gas saturation (fraction), and b_p^m is molar density of gas (mol/m^3).

For the multiphase flow in the reservoir without the hysteresis phenomenon, the relative permeability of CH_4-CO_2 and CO_2-brine systems were applied as reported by Seo (2004). Figure 4.3 displays the relative permeability curves of those systems, in which the red line is the relative permeability of CO_2 in the presence of CH_4 (left) and brine (right). It should be noted that the GASWAT option allows only to define CO_2-brine relative permeability drainage/imbibition curves and it is essential to consider the effect of the residual gas during the flow of CO_2 (Schlumberger, 2014b).

The composition flow of gas (remaining hydrocarbon and CO_2) and water phases were governed during simulation using Eq. (4.15).

$$F_{pni}^{c} = T_{ni} y_p^c k_{rp} S_p \frac{b_p^m}{\mu_p} dP_{pni} \tag{4.15}$$

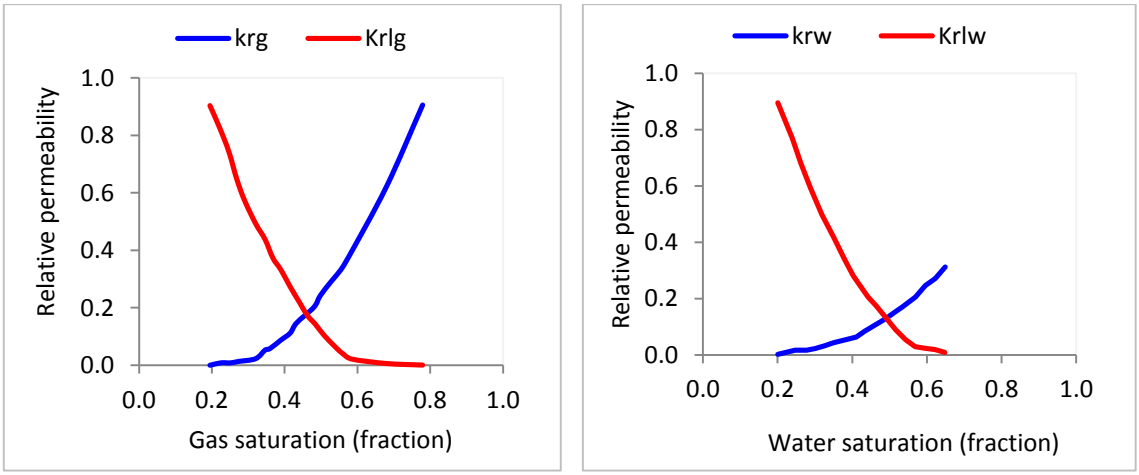

Fig. 4.3 Gas-liquid (CO_2) relative permeability curves (left) and CO_2-brine relative permeability curves (right)

The pure CO_2 was injected into the storage formation with a bottom hole pressure limit of 3800 psia (equal to the capillary entry pressure of the seal) at a low injection rate for 1.2 years without recovering the remaining gas. The GASWAT modeling captures the total molar volume of CO_2 in terms of free (mobile), residual and dissolved components during injection in the depleted gas system. Three models with similar rock and fluid characteristics considering three different temperatures 80.6 ^{o}F, 159.8 ^{o}F, and 212 ^{o}F, respectively were simulated for different salinity of 0.085 mol/kg, 0.87 mol/kg, 1.79 mol/kg, and 2.75 mol/kg till all pore volume were

accumulated and the bottom hole pressure limit was reached. The reservoir and fluid properties are given in Table 4.5.

Table 4.5 Reservoir and fluid properties used in the numerical modeling

Symbol	Variable	Value	Field Units
N	Grid blocks	25200	
h	Grid-block height	26.25	feet
Δx/ Δy	Grid-block length/width	26.25	feet
ϕ	Porosity	20	%
K	Permeability	800	mD
c_r	Rock compressibility	3.402×10^{-7}	1/psia
Sg_i	Initial gas saturation	78	%
S_{wc}	Connate water saturation	20	%
P_R	Reservoir pressure (depleted)	290	psia
Q_g	Gas injection rate	10	Mscf/D
P_{bh}	Bottom hole injection pressure	3800	psia
r_{well}	Well bore radius	0.328	feet
S	Salinity	0.085,0.87,1.79,2.75	mol/kg
Temp	Temperature	80.6, 159.8, 212	°F
Comp	Components	98.5C1, 1H2O and 0.5CO2	%
PV	Initial pore volume	1.17	Bscf
T	Simulation time	1.2	years

Storage was evaluated during injection period for only trapping mechanisms. The results obtained indicated that the CH_4 mixing with $scCO_2$ at a particular temperature would increase the gas mobility and its plume size by decreasing the mixture gas density and viscosity (Oldenburg and Doughty, 2011), which would have a negative impact on the CO_2 storage capacity (ZiabakhshGanji, 2015). After estimating the total molar volume of CO_2 in terms of free, residual and dissolved CO_2, saturations of the injected gas were calculated by dividing the effective pore volume (excluding the trapped gas saturation).

4.3.3.2 Modeling results and discussion

The results of simulations for different temperature and salinity ranges are plotted in Figure 4.4. As it is seen in this figure, it can be concluded that in all cases and at a particular flow rate, the injectivity loss is taking place which was significant at a high temperature and saline level. At 80.6 °F, the residual trapping remains more than the solubility trapping (CO_2 dissolved) up to a certain limit and then solubility trapping overrides the residual trapping. The solubility trapping override starts to decrease with increasing salinity at low temperatures and is completely vanished at the high temperatures of 159. 8 °F and 212 °F. The domination of residual trapping at the initial stage might be due to selection of the injection rate as residual trapping is

significantly affected by the selection of the injection rate (Raza et al., 2016). High interfacial tension values at low pressures offer a maximum residual CO_2 volume compared to free and dissolved CO_2 at the early stage. During injection, it was noted that CO_2 solubility decreases while the amount of free and residual CO_2 increases as salinity and temperature increases. The relationship of salinity and temperature with CO_2 solubility is aligned with the findings of recent studies (Shedid and Salem, 2013; De Silva et al., 2015). These factors are known as the cause of decrease in CO_2 density which diminishes the dissolution phenomenon and increases the buoyancy, forcing CO_2 plume to flow upward as a free gas and trapped by the capillary phenomenon. Moreover, mixing of CH_4 with CO_2 in a particular temperature would increase the gas mobility and its plume size by decreasing the density and viscosity of mixture (Oldenburg and Doughty, 2011). These have a negative impacts on CO_2 storage capacity (ZiabakhshGanji, 2015). The results obtained also indicated that high temperatures and saline reservoirs would not be a good choice for CO_2 storage, as reported in earlier studies (IPCC, 2005-pp214).

The reservoir pressure, as shown in Figure 4.4, generally increases due to increase of the pore fluid pressure by CO_2. Typically, the pressure diffusivity is three to five times larger than the molecular diffusivity, making the reservoir pressurization faster compared to the molecular diffusion (Oldenburg and Benson, 2001b). However, pressure increases by the increase of temperature and salinity. This indicated the fact that any increase in the temperature and salinity may decrease the density of CO_2, which in turn causes the CO_2 plume to flow at a higher rate, making the monitoring far more complicated by enhancing the free gas saturation and over-pressurizing the site.

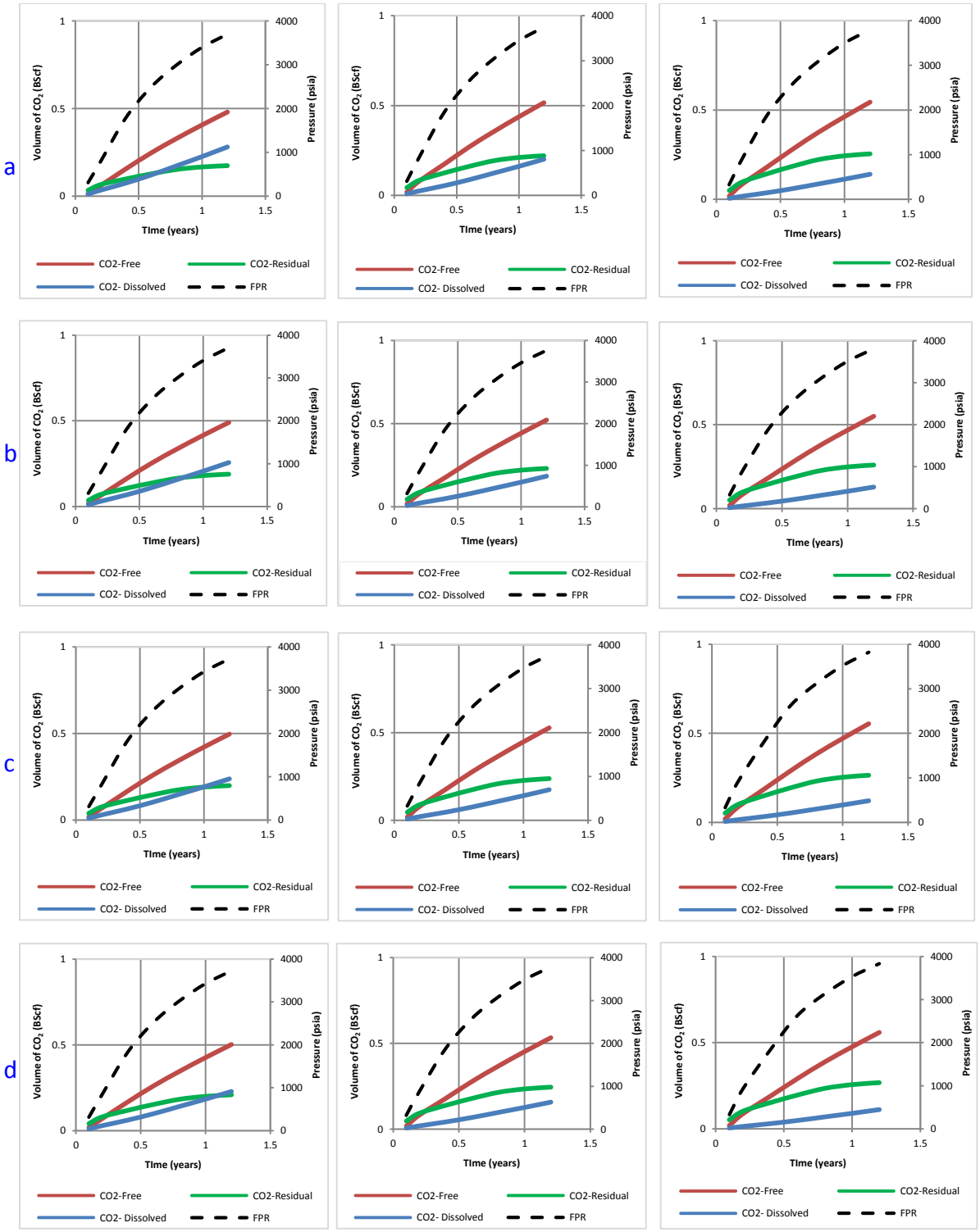

Fig. 4.4 Comparison of simulated CO_2 volume (free, residual and dissolved) and field reservoir pressure (FPR) for cases: 80.6 ^{o}F (Left), 159. 8 ^{o}F (Middle), and 212 ^{o}F) (Right) temperatures with NaCl concentrations (a) 0.085 mol/kg, (b) 0.87 mol/kg, (c) 1.79 mol/kg, and (d) 2.75 mol/kg

4.3.4 Numerical validation

The proposed approach was employed to compute the residual CO_2 saturation. In the first step, the interfacial data of CO_2-brine was obtained under different

pressures (696 psia to 3741 psia), temperatures (80.6 °F, 159.8 °F, and 212 °F), and salinity levels (0.085 mol/kg, 0.87 mol/kg, 1.79 mol/kg, and 2.75 mol/kg) from Chalbaud et al. (2009) as shown in Figures 4.5 and 4.6.

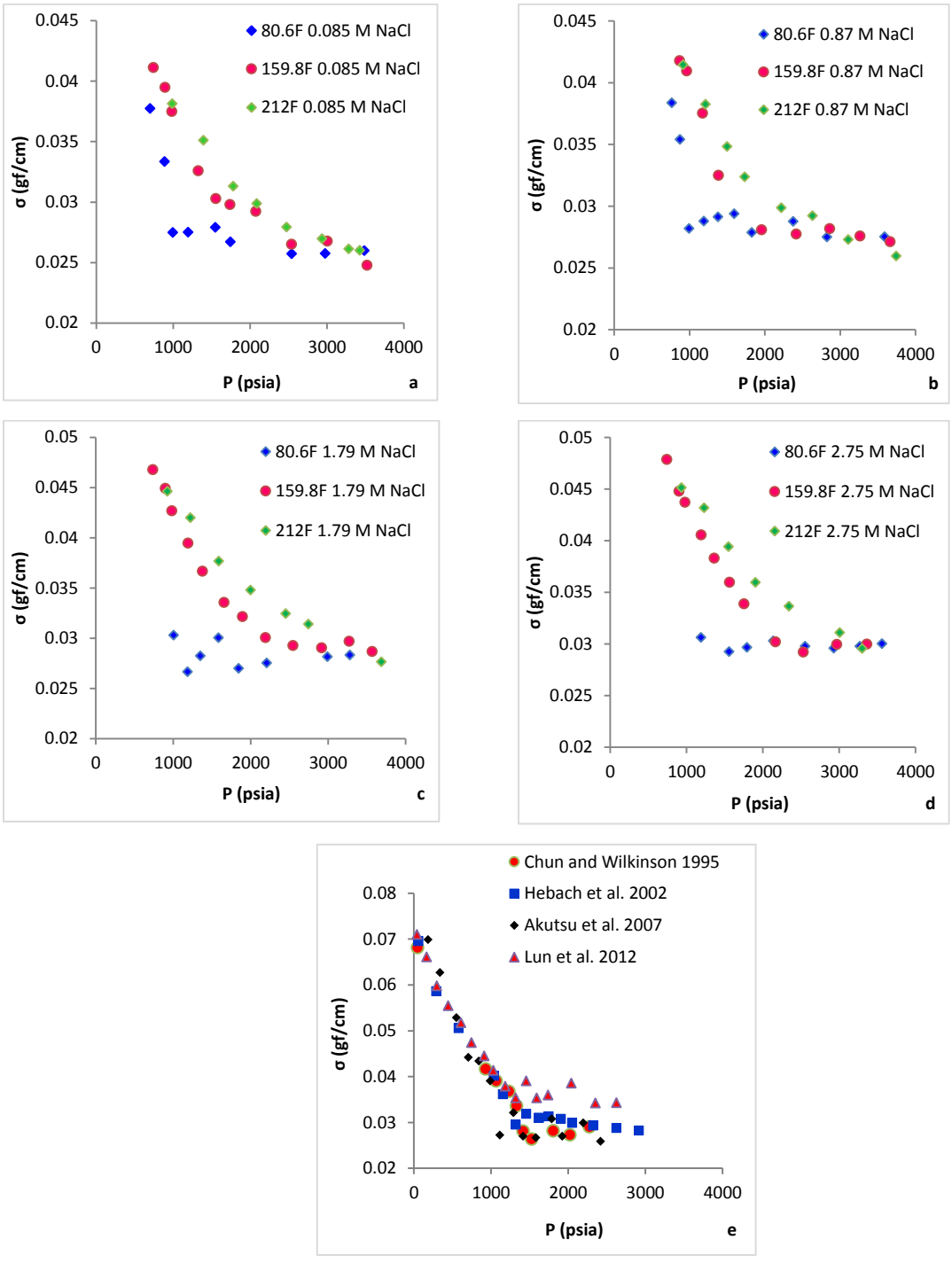

Fig. 4.5 Top a-c: Interfacial tension (σ) of CO_2-brine as a function of pressure (P) for different temperatures and NaCl concentrations (a) 0.085 mol/kg, (b) 0.87 mol/kg, (c) 1.79 mol/kg, and (d) 2.75 mol/kg (Chalbaud et al., 2009); bottom (e): The interfacial tension of the pure water-CO_2 system as a function of pressure at 113 °F reported by different researchers

From Figure 4.5, one can conclude that the evolution of $\sigma_{CO2\text{-}brine}$ with the pressure is aligned with what was reported in the literature (Chun and Wilkinson, 1995; Hebach et al., 2002; Akutsu et al., 2007; Lun et al., 2012). According to Chalbaud et al. (2009), the $\sigma_{CO2\text{-}brine}$ decreases at low pressures while a plateau value of $\sigma_{CO2\text{-}brine}$ is reached for all NaCl concentrations at a high pressure.

Figure 4.6 shows the same experimental results in terms of salinity on the $\sigma_{w\text{-}CO2}$ which are aligned with the results reported in the literature (Lun et al., 2012).

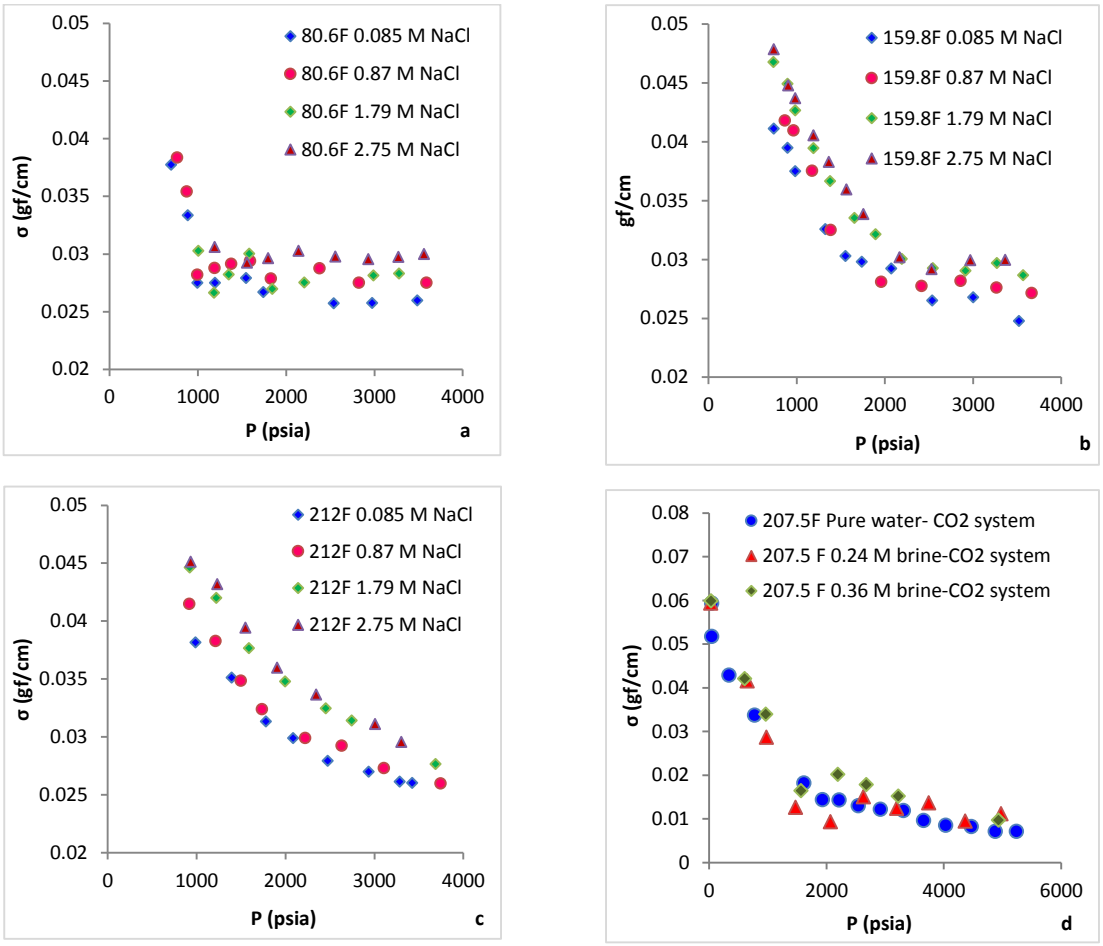

Fig. 4.6 a-c) Interfacial tension (σ) of CO_2-brine as a function of pressure (P) for different NaCl molal concentrations at (a) T=80.6 °F, (b) T=159.8 °F, and (c) T= 212 °F (Chalbaud et al., 2009); d) Measured equilibrium interfacial tension (σ) versus pressure (P) at three systems of pure water-CO_2, 0.24 mol/kg brine-CO_2 and 0.36 mol/kg brine-CO_2 system (Lun et al., 2012)

A linear relationship between the $\sigma_{CO2\text{-}brine}$ and the molal salt concentration was observed which becomes prominent at a high temperature. In a high pressure, CO_2 reaches a constant value by achieving an incompressibility that does not depend on

the pressure nor on the temperature. At lower temperatures, this incompressibility can be reached at a lower pressure. A very similar observation was made by many others (Wiebe, 1941; Malinin and Saveleva, 1972; Malinin and Kurovskaya, 1975).

In the next step, to determine the surface tension of the methane-brine (σ_{hb}), the temperature and salinity levels reported by Chalbaud et al. (2009) were considered to use the approach presented by Sutton (2009). Prior to this, the gas density was calculated by the real gas law. Hydrocarbon gas pseudo-critical properties were predicted by Sutton (2007) and the natural gas compressibility factor, z, were estimated by the method of Dranchuk and Abou-Kassem (1975), which was followed by the adjustment of pseudo critical properties for non-hydrocarbon components as presented by Wichert and Aziz (1972). The pure water density was calculated considering no dissolved gas using the modified method of Rowe and Chou (1970) as reported by Sutton (2009). Theoretically, it is well established that the surface tension of a hydrocarbon-water system is attributed to pure water and hydrocarbon system's density as shown in Eq. (4.16). For dissolved salts in the water, this would be accommodated by using Eq. (4.17). The substitution of these two equations into Eq. (4.18) gives the correct surface tension between hydrocarbon and brine.

$$\sigma_{gw} = \left[\frac{1.53988\left(\rho_{wg/cc} - \rho_{hg/cc}\right) + 2.08339}{\left(\frac{T_{O_R}}{302.881}\right)^{(0.821976 - 1.83785\times10^{-3} T_{o_R} + 1.34016\times10^{-6} T^2{}_{o_R})}} \right]^{3.6667} \tag{4.16}$$

Where, σ_{gw} is the gas-pure water surface tension in gf/cm, T_R is the temperature in Rankine, and $\rho_{wg/cc}$ and $\rho_{hg/cc}$ are water and gas density in g/cm^3. Sutton (2009) proposed the salinity correction for the methane-brine surface tension by comparing the results with those obtained by Standing (1981) as below:

$$\sigma_{cor} = 3.44\times10^{-5} c_s \tag{4.17}$$

$$\sigma_{hb} = \sigma_{gw} + \sigma_{cor} \tag{4.18}$$

In Eqs. (4.17) and (4.18), c_s is the salinity in parts per million, σ_{cor}, σ_{gw}, and σ_{hb} denote the correct, gas-pure water, and hydrocarbon-brine surface tensions in gf/cm, respectively.

Figure 4.7 and Figure 4.8 show the calculated surface tensions at different temperature and salinities. The direct relationship of the gas-brine surface tension with salinity and its inverse correlation with temperature is observed in these figures which are consistent with the findings of Sutton (2009) and Kashefi et al. (2016). This observation might be linked to the increase of salt which elevates the average molecular weight of the aqueous phase, resulting in an overall increase of density and surface tension over the range of the pressures and temperatures considered. These results were part of the validation in the later stages.

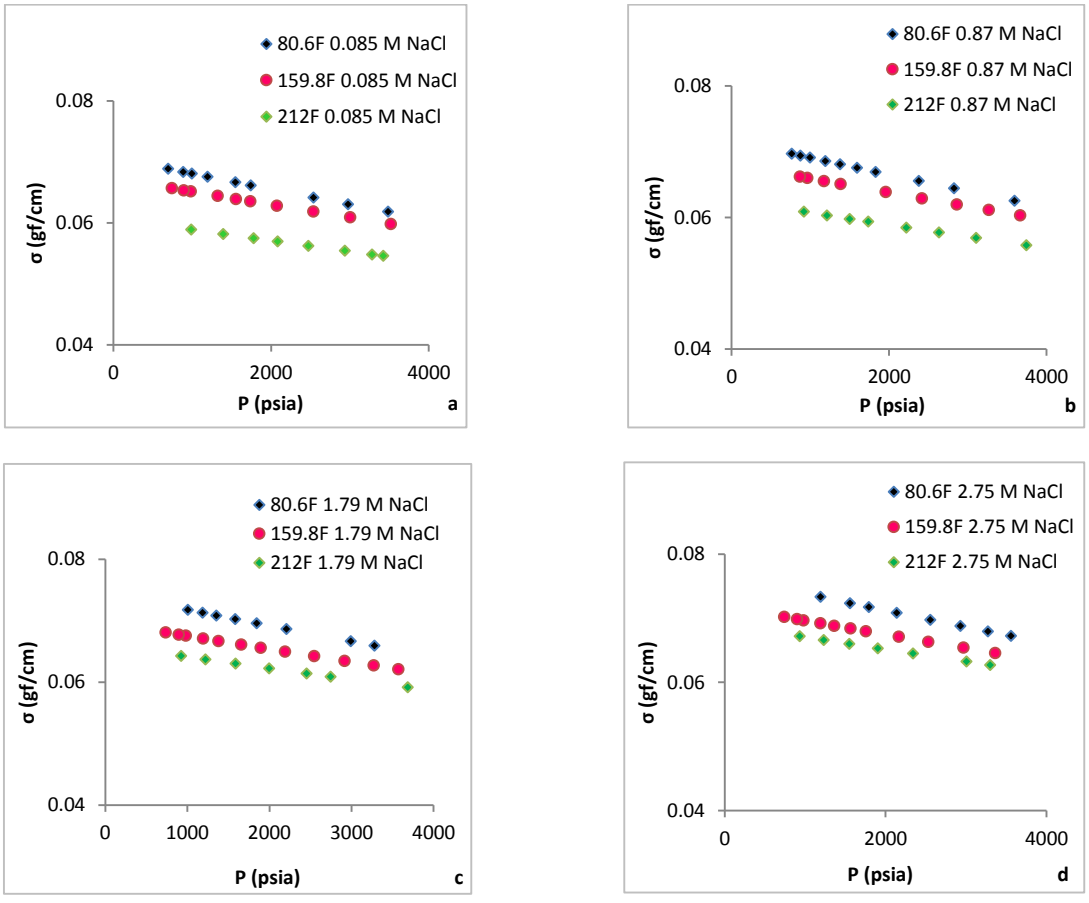

Fig. 4.7 Methane-brine surface tension as a function of pressure for different temperatures and NaCl concentrations (a) 0.085 mol/kg, (b) 0.87 mol/kg, (c) 1.79 mol/kg, and (d) 2.75 mol/kg

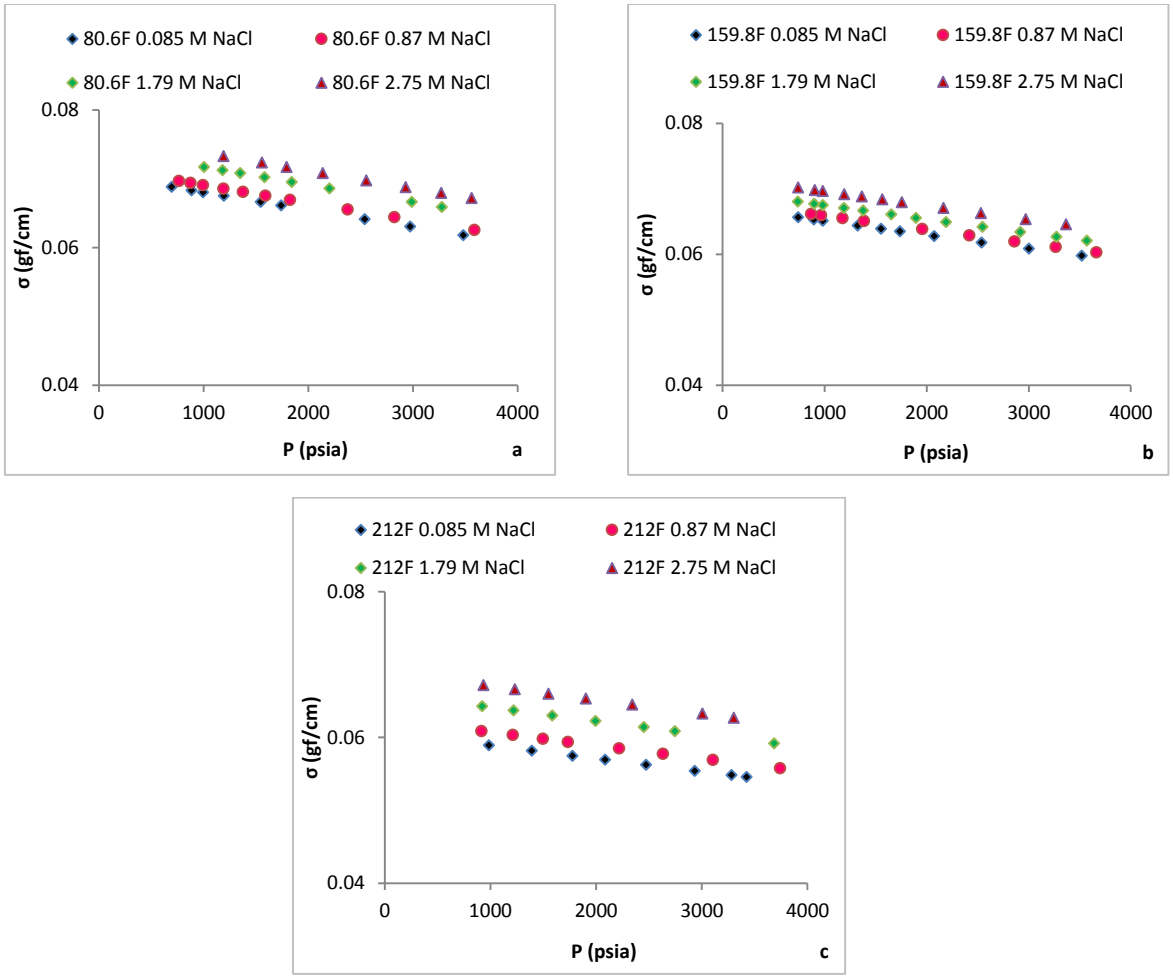

Fig. 4.8 Methane-brine surface tension as a function of pressure for different NaCl concentrations and temperatures (a) 80.6 °F, (b) 159.8 °F, and (c) 212 °F

The computation was begun with the input data of interfacial tensions, and the simulated residual CH_4 saturation. Having the interfacial data at particular temperatures, pressures and salinity levels from Figures (4.5-4.8), Eq. (4.9) were used to predict the residual CO_2 saturations. For all cases, the obtained residual CO_2 saturation was plotted against the pressure as presented in Figure 4.9. To validate the calculated residual CO_2 saturation at different conditions, the simulated residual CO_2 volume obtained from Figure 4.4 was taken into consideration to calculate the cumulative residual CO_2 saturation (total volume of residual CO_2 per effective pore volume) during injection. To calculate the effective pore volume for CO_2 storage, 20% of residual gas (CH_4) saturation was excluded. However, the cumulative residual CO_2 saturation was transformed into individual residual CO_2 saturation by subtracting the previous trapped volume of CO_2. Free and dissolved CO_2 saturations were calculated

in the same manner at each pressure (see Figure 4.4). The simulated saturations were plotted in Figure 4.9 along with the calculated residual saturations.

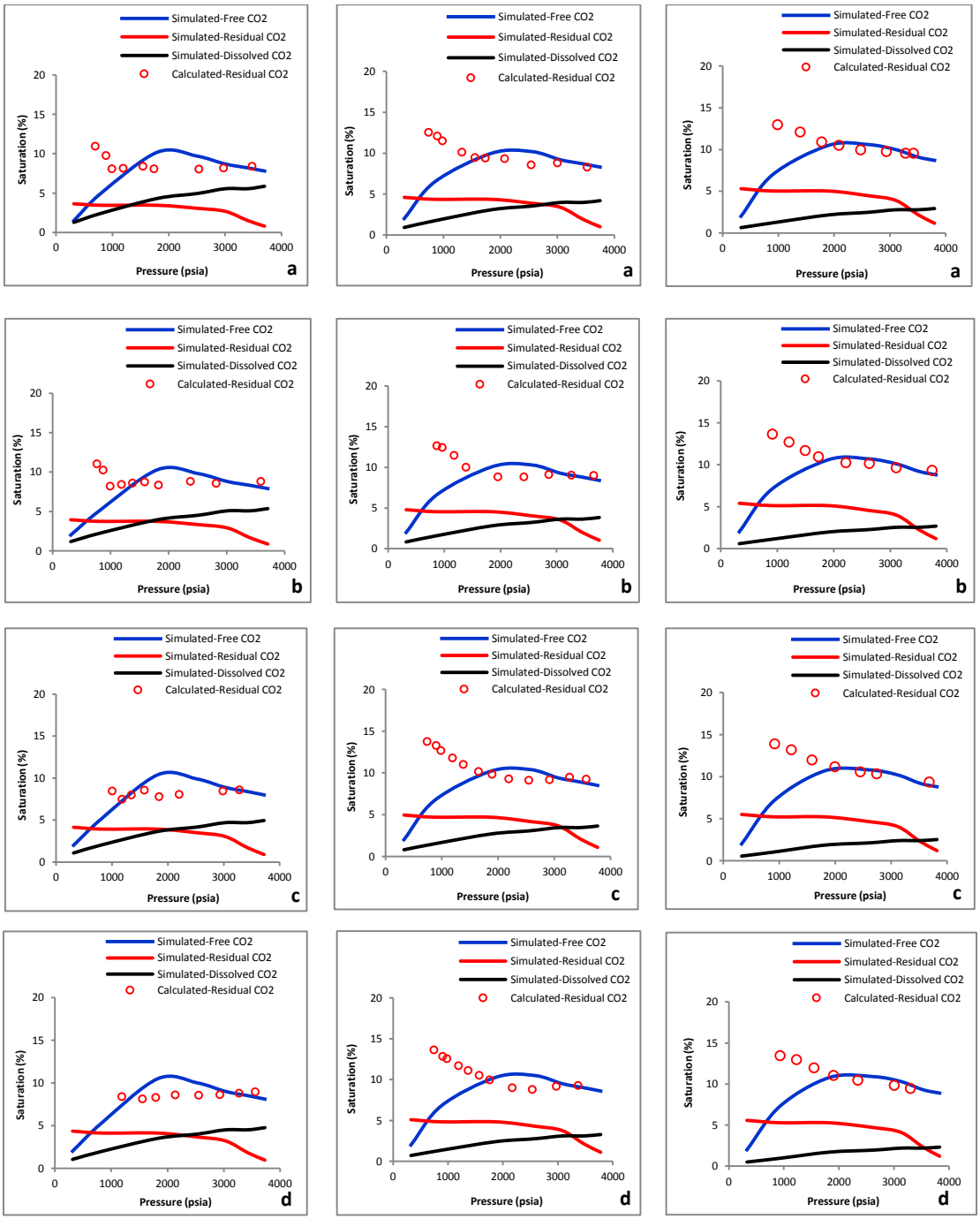

Fig. 4.9 Comparison of simulated saturations (free, residual and dissolved) and calculated saturation (residual) against pressure: 80.6 °F (Left), 159. 6 °F (Middle) and212 °F) (Right) temperatures with NaCl concentrations (a) 0.085 mol/kg, (b) 0.87 mol/kg, (c) 1.79 mol/kg and (d) 2.75 mol/kg

As shown in this figure, one can conclude that the free gas saturation increases up to a particular pressure depending on the temperature and salinity level and then

begins to decline until the effective pore volume is filled by the injected CO_2. This variation might be due to the decrease in the interfacial tension of CO_2-brine system with increasing the pressure, which confirms the validity of the method developed and presented earlier. However, making a comparison between the calculated and simulated residual CO_2 saturations is not possible. The reason behind this mismatch could be the non-uniform variation of capillary forces of CO_2-brine and CH_4-brine systems during the pressure build-up, particularly due to the presence of CH_4 as it drastically reduces the density and viscosity of the gas mixture (Oldenburg and Doughty, 2011; ZiabakhshGanji, 2015).The solubility trapping, at a particular temperature and salinity, increases with the increase of the pressure which is aligned with the finding of De Silva et al. (2015). Since the amount of residual CH_4 saturation is similar in all cases and CO_2 solubility increases in the presence of CH_4 (ZiabakhshGanji, 2015), its qualitative effect on CO_2 solubility at different temperatures and salinity level was not covered here. Table 4.6 shows the cumulative gas saturation at the end of the injection period to highlight the site trapping potentials.

From this table, one can observe the effect of the temperature and salinity on the trapping mechanisms as described earlier. It can be seen that the cumulative residual saturation is less than the cumulative free and dissolved CO_2 at the temperature of 80.6 ^oF, while at both 159. 6 ^oF and 212 ^oF temperatures, it was more than the dissolution cumulative saturation. As stated above, the CO_2 residual trapping contributes more to overall trapping than both solubility and mineral trapping mechanisms (Kimbrel et al., 2015). At a particular salinity level, the temperature and salinity shows a direct relationship with the free and indirect with dissolved CO_2 saturation, which were also endorsed by the earlier studies (Chevalier et al., 2010; Iglauer, 2011). Moreover, the direct effect of salinity and temperature with the residual CO_2 saturation was aligned with the findings of previous studies (Bennion and Bachu, 2006). Considering the free saturation and dissolved CO_2, it is observed that a high temperature and saline reservoir could not be feasible for a storage job as higher brine salinity and temperature leads to an increase in CO_2 mobility by decreasing CO_2 density (IPCC, 2005-pp214; Al-Khdheeawi et al., 2017).

Table 4.6 Cumulative CO_2 saturation in different phases at the end of the injection period

T (°F)	S (mol/kg)	P (psia)	Cumulative CO_2 Saturation (%)		
		upper	Free	Residual	Dissolved
80.6	0.085	3700	51.1	18.58	29.93
80.6	0.87	3705	52.2	20.13	27.35
80.6	1.79	3708	52.8	21.16	25.29
80.6	2.75	3713	53.4	22.19	24.26
159.8	0.085	3720	54.9	23.48	21.42
159.8	0.87	3725	55.5	24.51	19.61
159.8	1.79	3728	56.1	25.29	18.58
159.8	2.75	3733	56.7	26.06	16.77
212	0.085	3738	57.9	27.10	14.97
212	0.87	3743	58.5	27.61	13.68
212	1.79	3747	58.9	28.13	12.90
212	2.75	3753	59.5	28.49	11.87

Although the simulated residual CO_2 saturation against the simulated reservoir pressure doesn't show an acceptable match with the calculated residual CO_2 saturation, the calculated and simulated residual saturation match very well in all cases at the adjustment factor 0.92 under a same pressure range as depicted in Table 4.7. The adjustment factor was determined by a non-linear regression of residual CO_2 saturation against all 12 cases. This average residual saturation is the actual residual trapping ability of the site during the injection period which was used as a benchmark to validate the presented analytical model. Moreover, the applicability of the adjustment factor will be limited to certain conditions such as pressure, temperature and salinity levels.

Table 4.7 Comparison of simulated and calculated average residual CO_2 saturations

T (°F)	Salinity (mol/kg)	Pressure (psia)		Calculated- Sgr_{avgCO2} (%)	Simulated Sgr_{avgCO2} (%)	Standard Deviation
		Upper	Lower			
80.6	0.085	3482	696	9.42	9.60	0.864
80.6	0.87	3590	764	9.73	9.91	0.919
80.6	1.79	3278	1004	8.87	9.13	0.938
80.6	2.75	3561	1189	9.25	9.50	0.975
159.8	0.085	3520	741	10.88	10.95	0.882
159.8	0.87	3664	869	11.02	11.10	0.924
159.8	1.79	3568	735	11.65	11.70	0.969
159.8	2.75	3365	741	11.72	11.77	0.979
212	0.085	3423	986	11.58	11.58	0.867
212	0.87	3742	917	11.98	11.98	0.925
212	1.79	3684	921	12.49	12.46	0.933
212	2.75	3301	933	12.28	12.28	0.968

4.4 Implementation on gas reservoir

In this section, carbonate gas reservoir was introduced and two of its wells were analyzed to evaluate the CO_2 residual trapping potentials. This was done to evaluate the application of the approach presented.

4.4.1 Results and discussion

The wells, which are referred to as Well C and Well D in this study, were drilled into this reservoir at the center of the structure, covering the whole interval of the reservoir. Table 4.8 gives the interval of interest, its thickness, perforated intervals and porosity based on log evaluation reports. To use the proposed approach at the reservoir scale, the available information and analytical correlations were used. For instance, Ransom and Holm (1978) introduced an approach to determine the residual oil saturation based on the log-injection-log analysis by the help of resistivity and thermal decay time logs. This approach can also be applied for estimation of the residual gas saturation using the microspherically focused log as the measure of flushed zone resistivity (R_{xo}), which includes the resistivity of mud filtrate (R_{mf}) and the residual hydrocarbon saturation (R_h) in the flushed zone (R_{xo}) (Assaad, 2008). In fact, for cases where the log-injection-log technique cannot be applied, microspherically focused log can be used to measure the resistivity R_{xo} in the flushed zone, and, hence, residual gas saturation can be obtained from the Archie method, considering the input parameters as illustrated in Table 4.9. In this study, the residual gas saturation in the invaded zone was calculated by replacing R_t with R_{xo} and R_w by R_{mf} (the resistivity of the mud filtrate) in the Archie equation. The formation factor, F, was estimated at the given reservoir level and the log predicted porosity were compared with the core measured porosity. The cementation factor, m_c, and the saturation exponent, n, were also considered to be 1.9 and 2, respectively. In next step, the residual gas saturation was estimated which had a fair match with the available core measured residual gas saturation (Well D). It is worth to mention that the core measured residual gas saturation from Well C was not present and, thus, the estimated residual gas saturation in Well C was calibrated against the wireline logs and reservoir information. However, the estimation of residual hydrocarbon

saturation in the wells might be uncertain if the reservoir section near the wellbore is not ready to have a fluid saturation similar to the bulk of the reservoir (Ransom and Holm, 1978). The average residual gas saturations in Well C and Well D were, then, obtained, respectively, as 33% and 34% which were near to the TDT measurements plotted in Figure 4.10. However, the residual gas saturation can be further reduced in the high heterogeneous area of the reservoir away from the wellbore, which may add some uncertainty to the estimated CO_2 residual trapping ability of the reservoir (Rezaee et al., 2013).

In order to estimate the wettability at the initial and depleted stages, few methods presented based on the pressure profile, porosity, permeability, and interfacial tension data were used (Desbrandes et al., 1990; Desbrandes and Bassiouni, 1990). As calculation made in Chapter 3, the contact angle was then obtained as 32°, emphasizing the fact that the reservoir is water-wet (see Table 4.1).

Table 4.8 Porosity, gross thickness and net thickness of the reservoir in different wells

Well ID	Interval of Interest (ft)	Gross Thickness (ft)	Net Thickness (ft)	Actual Perforated Interval (ft)	Porosity (%)
C	4503-5395	892	680	4550-5150	30.7
D	4036-4747	711	595	4047-4473	20

Table 4.9 Input parameters for the residual gas saturation in the invaded zone

Well ID	m_c	n	ø (%)	R_w, (ohm·meter)	R_{mf}, (ohm·meter)	T_{Rmf} (°F)
C	1.9	2	30.7	0.21	0.20	93
D	1.9	2	20	0.24	0.241	78

For estimation of the interfacial tension of CO_2-H_2O and CH_4-H_2O at representative reservoir conditions from the injection pressure to the final build-up pressure, the experimental approaches (Rushing et al., 2008; Chalbaud et al., 2009; Shariat et al., 2012) and reliable analytical correlations (Chalbaud et al., 2009; Sutton, 2009) can be

used. For instance, the approach presented by Chalbaud et al. (2009) is a well-known method which requires only fluid densities, temperature, pressure together with brine salinity and storage site conditions to determine the interfacial tensions of the CO_2-H_2O system. To estimate the interfacial tension between the CH_4-H_2O system, Sutton's correlation is another approach which can be taken as it has the applicability for the pressure range of 14.7 psia to 43,526 psia and the temperature range of 33 - 500 ^oF with salinity correction to consider the presence of dissolved salts in water (Sutton, 2009). Here, the correlation proposed by Chalbaud et al. (2009) and Sutton (2009) was used to obtain the interfacial tension as given in Table 4.10.

Table 4.10 Associated parameters for calculation of the residual CO_2 saturation

Sr. No	Injection Pressure (psia)	Temperature, (^oF)	$\sigma_{CO2\text{-}brine}$ by Chalbaud correlation (gf/cm)	$\sigma_{gas\text{-}brine}$ by Sutton 2009 correlation (gf/cm)
1	2000	212	0.032	0.0470
2	1800	212	0.034	0.0480
3	1600	212	0.036	0.0490
4	1400	212	0.039	0.0495
5	1200	212	0.042	0.0505
6	1000	212	0.043	0.0515
7	800	212	0.044	0.052
8	600	212	0.045	0.053
9	300	212	0.048	0.054

The residual CO_2 saturation was then calculated by the adjustment factor of 0.996 from 0-2000 psia using the input data of two wells by applying Eq. (4.9). The estimated saturation was averaged for all pressures and plotted against depth as shown in Figure 4.10. Since the estimated saturation of Well D was found to have a good match with the core measured residual gas saturation, it was concluded that the residual natural gas saturation is greater than the residual CO_2 saturation which is probably due to a larger interfacial tension of CH_4-H_2O system compared to CO_2-H_2O system (Saeedi and Rezaee, 2012). This strategy can be helpful to pick the best zones for CO_2 injection. To mark the average site trapping potential near the

wellbore, the average of all saturations against depth were taken for the whole interval which was around 26% and 27% for Well C and Well D, respectively as shown by dashed-dotted black line in the same figure. It seems to be favorable and results are justified as residual CO_2 saturation is less than original residual gas saturation (30% Sgr). Thus, the maximum volume of CO_2 residual trapped could be approximately 0.965 Tscf of the effective pore volume (excluding 30% Sgr), based on the average saturations estimated from the data of Well C and Well D. The residual CO_2 saturation was plotted against the injection pressure from 0 psia to 2000 psia at two starting and ending depths of the porous interval as shown in Figure 4.11.

The average CO_2 saturation at the starting depth was 3% and 12% for Well C and Well D, respectively. These values were 33% and 34% at the ending depth for Well C and Well D, respectively. The results are aligned with the reservoir measurements, where it was revealed that the residual CO_2 saturation increases initially and then decrease to a lower stabilised value (Schlumberger, 2012). This trend was also aligned with the simulation results (see Figure 4.9), where the residual trapping ability is maximum at a low pressure and then begins to decrease with the increase in the pressure in a long term. However, more experimental studies on the core samples taken from the same reservoir are required to validate the results.

The residual wetting ($SgrCO_2$) and original wetting (Sgr) relationships obtained for Well C (left) and Well D (right) were also plotted as shown in Figure 4.12. It should be noted that the estimated average $SgrCO_2$ must be validated against the corresponding core sample measured $SgrCO_2$ at injection conditions before being used for making any judgment.

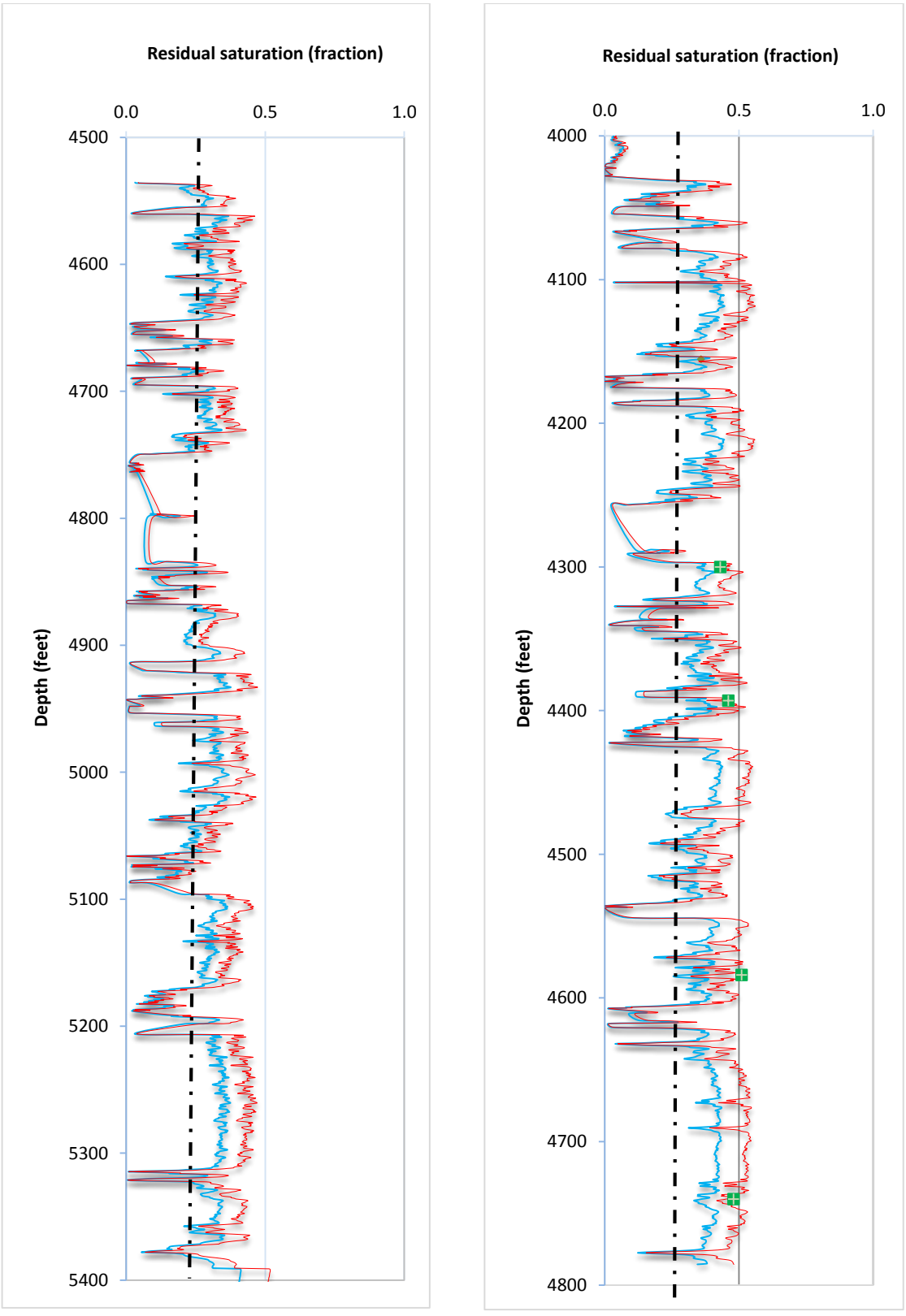

WELL C WELL D

Fig. 4.10 Estimated residual CO_2 saturation (blue line) and residual gas saturation (red line) obtained from the wireline logging data of two wells. Dashed-dotted black line shows the average both saturation. Square green bullets points are showing Sgr near well bore of Well D

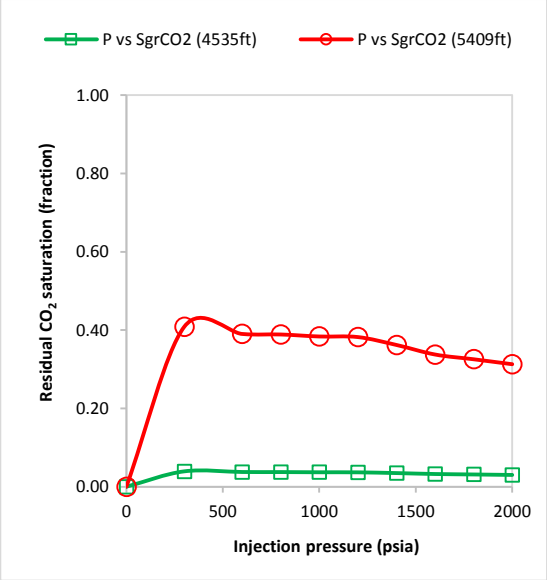

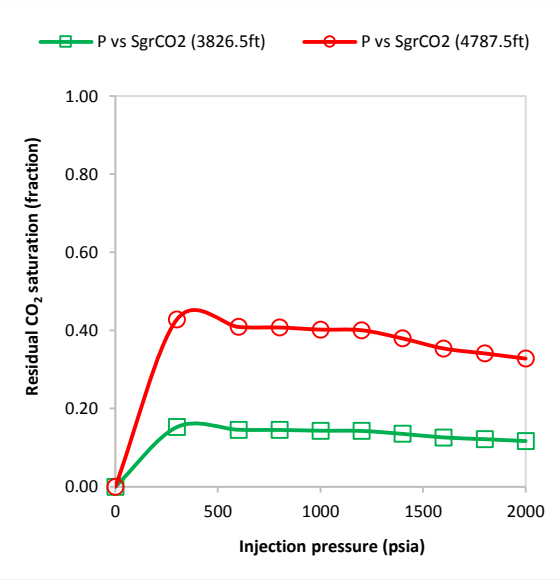

Fig. 4.11 Trends of residual CO_2 saturation against the injection pressure in Well C (left) and Well D (right) at starting and ending depths

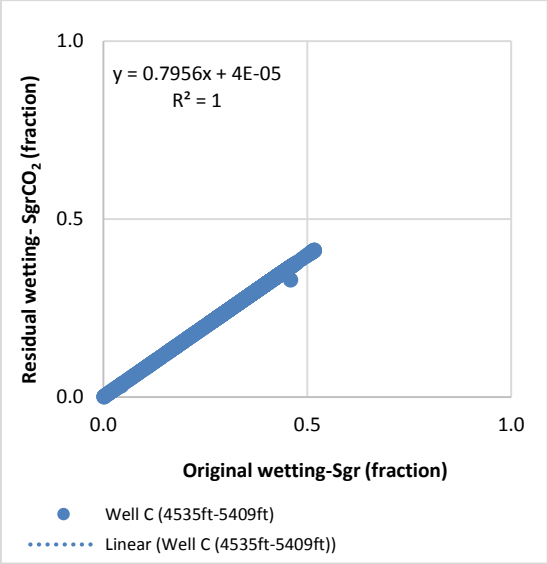

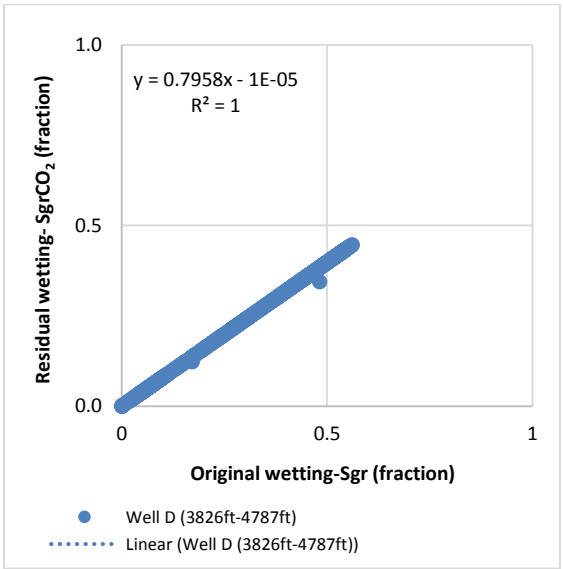

Fig. 4.12 Relationship between the residual wetting and the original wetting saturation before corrections of Well C (left) and Well D (right)

4.5 Summary of chapter

A long-term and safe CO_2 storage practice depends mainly on the efficiency of the trapping mechanisms, especially the residual CO_2 trapping. In this part, an attempt was made to present a new method to estimate the residual CO_2 saturation in depleted petroleum reservoirs. Based on the literature data and a numerical simulation, the method gives reasonable results for a strongly water-wet system.

Although the approach presented provides a good result for a strongly water-wet system, more experimental studies are required to extend its application for other rock wetting characteristics.

The behavior of trapping mechanisms against pressure, temperature and salinity was also simulated where it was found that the amount of free and residual CO_2 increases with the increase in salinity and temperature. It was also revealed that the free gas saturation increases up to a particular pressure depending on the temperature and salinity level and then begins to decline till the effective pore volume is filled by the injected CO_2. The residual CO_2 saturation gradually decreases with the progressive pressure build-up.

Data from two wells of gas reservoir were applied on the proposed method to determine the residual trapping ability. The results obtained indicated that the reservoir has a potential to residually trap CO_2 at the time of injection till the maximum injection pressure. However, the need to numerically evaluate trapping mechanisms including the residual trapping is essential to evaluate the storage potential of the reservoir.

CHAPTER 5

ASSESSMENT OF CO_2 INJECTIVITY AND RESERVOIR INTEGRITY

5.1 Introduction

CO_2 injection in subsurface geologic sites may result in geomechanical issues and $scCO_2$/brine/rock chemical interactions, which could affect the CO_2 injectivity and reservoir/caprock integrity. In this chapter, attempts were made to experimentally evaluate the CO_2 injectivity and effect of $scCO_2$/brine/rock chemical interactions on geomechanical properties of Berea sandstone owing to the absence of carbonate gas reservoir core plugs under different in-situ stress conditions. This would provide more understanding on the behavior of stress sensitive reservoirs under $scCO_2$/brine/rock chemical interactions during CO_2 injection for storage purposes and the results might be useful to understand the integrity of stress sensitive carbonate gas reservoir of Malaysia. A series of measurements (CO_2 flooding, ultrasonic pulse measurements, Hg injection porosimetry, X-ray diffraction (XRD) analysis as well as X-ray fluorescence (XRF) and image analysis using Scanning Electron Microscope (SEM)) were carried out. It is found that injectivity is favourable and complicated CO_2/brine/rock chemical interactions might cause acidification, rock dissolution, and changes in the rock in-situ stress, which in turn may have negative impacts on the elastic and strength parameters of sandstone rock.

5.2 Geomechanical-geochemical interactions

A series of ultrasonic pulse measurements were performed and dynamic elastic parameters were estimated using the velocity of P- and S-waves recorded. This may help to understand how body waves can be used to evaluate changes in the characteristics of reservoirs and seal rocks while flooding is in progress.

5.2.1 Sample characterizations

Berea sandstone is a sedimentary rock have been widely recognized by the petroleum industry as the best rock type for testing and the relatively high porosity and

permeability of Berea sandstone makes it a good reservoir rock (www.bereasandstonecores.com). Berea sandstone was used for the purpose of this study and a series of petrophysical and image analysis was carried out to understand the physical, mineralogical and fabric properties of the sample. The petrophysical tests conducted consisted of: 1) Hg injection porosimetry for pore size distribution estimation, 2) permeability determination using an air permeameter, 3) X-ray diffraction (XRD) analysis and 4) X-ray fluorescence (XRF). The bulk density was measured by determination of the volume of the samples and its dry mass. The saturated density could then be calculated using the sample porosity and the fluid density. The density of the fluid (brine and CO_2) was determined using the NIST Chemistry Web-Book (webbook.nist.gov) under different pressure and temperature conditions.

An image analysis using the Scanning Electron Microscope (SEM) was done in different scales to examine the texture and microstructure of the sample before and after exposure to $scCO_2$. Tables 5.1 and 5.2, respectively, gives the physical properties and distribution of minerals in the sample. Table 5.3 summarizes the results obtained from the XRF analysis. Figures 5.1 and 5.2, respectively, shows the SEM images and the pore throat size of the sample.

Table 5.1 Physical properties of the Berea sample used for the purpose of this study

Samples	Density (g/cm^3)	Porosity (V/V)	Permeability (mD)	Young's Modulus (GPa)	Shear Modulus (GPa)	Poisson's ratio	Compressive Strength (MPa)	Tensile Strength (MPa)
B.1	2.3	0.19	420	25.3	10.2	0.25	53	~5

Table 5.2 Mineral types and distribution in the sample

Samples	Quartz (%)	Microcline (%)	Kaolinte (%)	Chlorite (%)	Albite (%)	Ankerite (%)
B.1	80	6.7	7.3	1.4	2.9	1.7

Table 5.3 Chemical element included in the structure of the sample

Samples	SiO_2 (%)	Al_2O_3 (%)	Fe_2O_3 (%)	FeO (%)	MgO (%)	CaO (%)	Total (%)
B.1	93.13	3.86	0.11	0.54	0.25	0.10	97.99

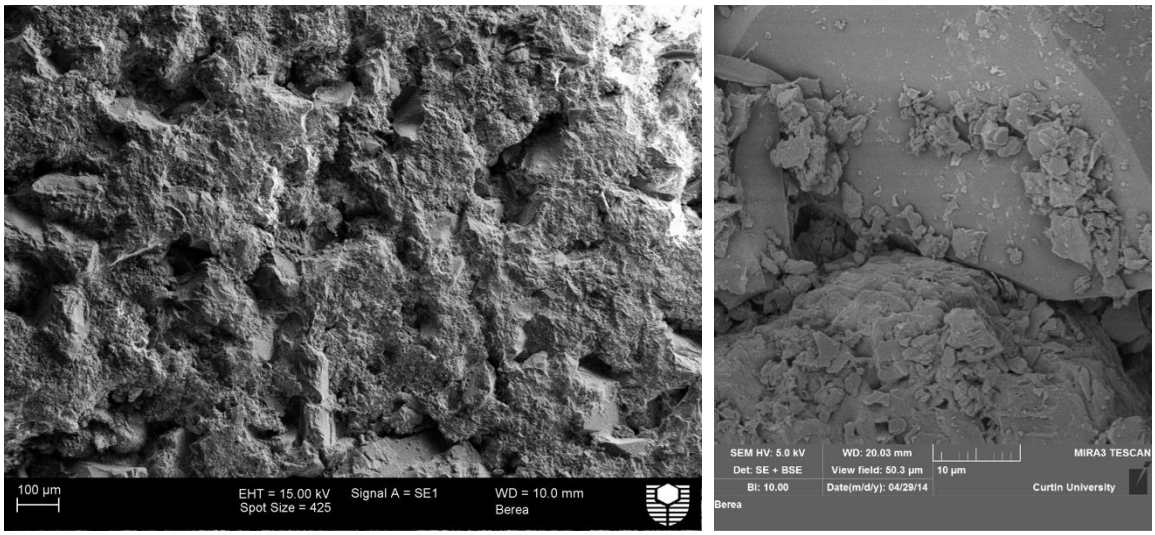

Fig. 5.1 Scanning Electron Microscope (SEM) image of the Berea sandstone. Big grains of quartz and dispersed clays are observed in the sample (right side)

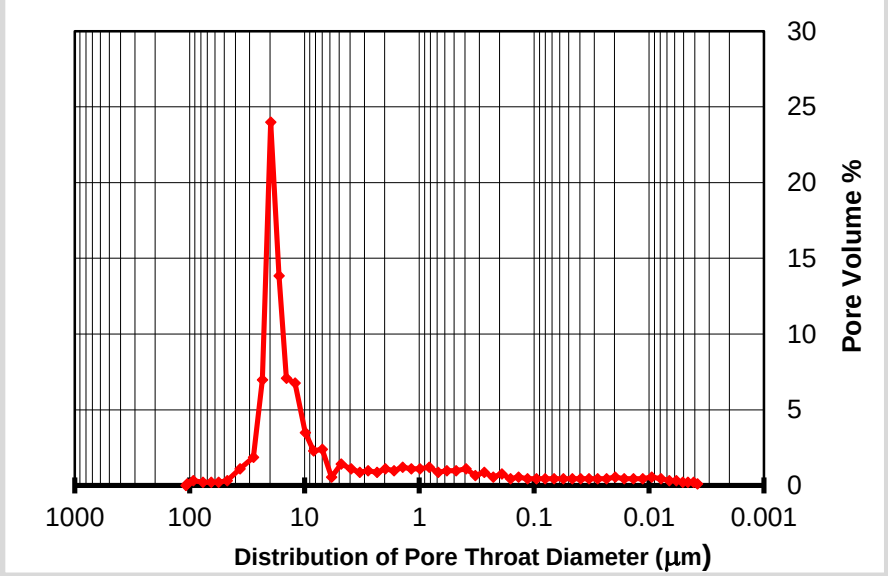

Fig. 5.2 Pore throat size of the sample with an average of 8µm

As it is seen in Table 5.1, the Berea sandstone composed of quartz, feldspars (microcline), kaolinite, chlorite, albite and ankerite (carbonate) with a high permeability and porosity values. Table 5.4 summarizes the chemical reactions observed in sandstone reservoirs having the above minerals.

According to Rathnaweera et al. (2016), calcite dissolution is predominant in a short-term scale compared to other reaction mechanisms involved. The reaction rate on these occasions are directly related to the CO_2 partial pressure and indirectly attributed to the pore fluid pH, and temperature (Rathnaweera et al., 2016). In the

case of siliciclastic sandstones, quartz doesn't make a significant contribution into the geochemical reactions and it is often part of a long-term reaction dominated by the mineral trapping process (De Silva et al., 2015). Aluminosilicates including feldspars, micas, and clays have a slow rate of reaction but it is not as much slow as that of quartz. Feldspars and clay minerals such as anorthite, illite and kaolinite tend to dissolve in a low pH environment created due to generation of the carbonic acid (De Silva et al., 2015). During the dissolution of kaolinite, for instance, the rock mass pore structure is affected by changes of grain-to-grain contacts (Rathnaweera et al., 2016). Considering these rates of reactions for the minerals included in the Berea sandstone, it seems that the dissolution of calcite and dolomite might be the fastest mechanism taking place during and after CO_2 injection in a short-term scale causing geomechanical changes, followed by a slower chemical reaction of aluminosilicats (feldspars and clays).

Table 5.4 Mineral-CO_2-brine interactions taking place in sandstone reservoirs ([1]Espinoza et al., 2011; [2]De Silva et al., 2015)

Primary mineral	Reaction	Reaction Rate[(1)]	Secondary mineral
Dissolution Reactions	$CO_2(g) \rightarrow CO_2(aq)$ $CO_2(g) + H_2O(l) \rightleftharpoons H_2CO_3(aq)$ $H_2CO_3(aq) \rightleftharpoons H^+(aq) + HCO_3^-(aq)$ $HCO_3^-(aq) \rightleftharpoons H^+(aq) + CO_3^{2-}(aq)$		
Silicates[(1)]	$SiO_{2(s)} + 2H_2O \rightleftharpoons H_4SiO_4 \rightleftharpoons H^+ + H_3SiO_4^- \rightleftharpoons H^+ + H_2SiO_4^{2-}$	1.26×10^{-14} mol.m^{-2}s^{-1}	Solubility of quartz does not change with concentration of dissolved CO_2.
Kaolinite[(2)]	$Al_2Si_2O_5(OH)_4(s) + 6H^+(aq) \rightarrow 5H_2O + 2SiO_2(aq) + 2Al^{3+}(aq)$	10^{-14}-to-10^{-15} mol.m^{-2}s^{-1}	Complete Dissolution
Arnorthite[(2)]	$CaAl_2Si_2O_8(s) + CO_2(g) + 2H_2O(l) \rightarrow CaCO_3(s) + Al_2Si_2O_5(OH)_4(s)$	1.2×10^{-5} mol.m^{-2}s^{-1}	Calcite, kaolinite
Illite[(2)]	$Illite + 8H^+(aq) \rightarrow 5H_2O(l) + 0.6K^+(aq) + 0.25Mg^{2+}(aq) + 3.5SiO_2(aq) + 2.3Al^{3+}(aq)$	-	Complete Dissolution
Labradorite[(2)]	$Ca_{0.6}Na_{0.4}Al_{1.6}Si_{2.4}O_8 + 5.4H^+(aq) + CO_2(aq) \rightarrow 0.6Ca^{2+}(aq) + HCO_3^-(aq) + 2.2H_2O(l) + 0.4Na^+(aq) + 1.6Al^{3+} + 2.4SiO_2(aq)$	-	Complete Dissolution
Albite[(2)]	$NaAlSi_3O_8(s) + CO_2(g) + H_2O(l) \rightarrow NaAl(CO_3)(OH)_2(s) + 3SiO_2(s)$	-	Dawsonite, quartz
K-feldspar[(2)]	$KAlSi_3O_8(s) + Na^+(aq) + CO_2(g) + 2H_2O(l) \rightarrow NaAl(CO_3)(OH)_2(s) + 3SiO_2(s) + K^+(aq)$	-	Dawsonite, quartz
Calcite[(2)]	$CaCO_3(s) + H^+(aq) \rightarrow Ca^{2+}(aq) + HCO_3^-(aq)$, *at high PH values only* Complete dissolution	1.6-to-3.2×10^{-5} mol.m^{-2}s^{-1}	Complete Dissolution
Glauconite[(2)]	$Glauconite + 14H^+(aq) \rightarrow 1.5K^+(aq) + 2.5Fe^{3+}(aq) + 0.5Fe^{2+}(aq) + Mg^{2+}(aq) + 1.0Al^{3+}(aq) + 7.5SiO_2(aq) + 9H_2O(l)$		Quartz
Annite[(2)]	$annite + 3CO_2 \rightleftharpoons 3siderite + K\text{-}feldspar$ Siderite, K-feldspar		Siderite, K-feldspar
Chlorite[(2)]	$Chlorite + 20H^+(aq) \rightarrow 5Fe^{2+}(aq) + 5Mg^{2+}(aq) + 4Al(OH)_3(aq) + 6H_4SiO_4(aq)$		Aluminium hydroxide
Dolomite[(2)]	$CaMg(CO_3)_2(s) + 2H^+(aq) + Mg^{2+}(aq) + HCO_3^-(aq)$		Complete Dissolution
Precipitation Reactions[(2)]			
	$Ca^{2+}(aq) + CO_3^{2-}(aq) \rightarrow CaCO_3(s)$		Calcite
	$Fe^{2+}(aq) + CO_3^{2-}(aq) \rightarrow FeCO_3(s)$		Siderite
	$Mg^{2+}(aq) + CO_3^{2-}(aq) \rightarrow MgCO_3(s)$		Magnesite
	$Ca^{2+}(aq) + SO_4^{2-}(aq) \rightarrow CaSO_4(s)$		Anhydrite
	$K^+(aq) + 3Al^{3+}(aq) + 2SO_4^{2-}(aq) + 6H_2O(l) \rightarrow KAl_3(SO_4)_2(OH)_6(s) + 6H^+(aq)$		Alunite
	$Ca^{2+}(aq) + Mg^{2+}(aq) + 2HCO_3^-(aq) \rightarrow CaMg(CO_3)_2(s) + 2H^+(aq)$		Dolomite

5.2.2 Ultrasonic pulse measurement

The ultrasonic pulse measurement system setup used in this study is available in the department of Petroleum Engineering at Curtin University, Australia. The experimental setup consists of a pulse generator unit, transducers, a signal conditioner, and a computer equipped with a high frequency analog to digital (A/D) converter. Measurement were conducted using a triaxial (Hoek) high pressure cell, which allows axial loading of up to 150 MPa, with a confining and pore pressure of 40 MPa and 20 MPa, respectively while temperature could be varied from ambient conditions to up to 80°C. Piezoelectric crystals were used for the pulse transmission and converting electric signals into mechanical vibrations modes of compressional (P) and shear (S). Figure 5.3 shows the location of the Berea sample in the triaxial cell used for the pulse measurements.

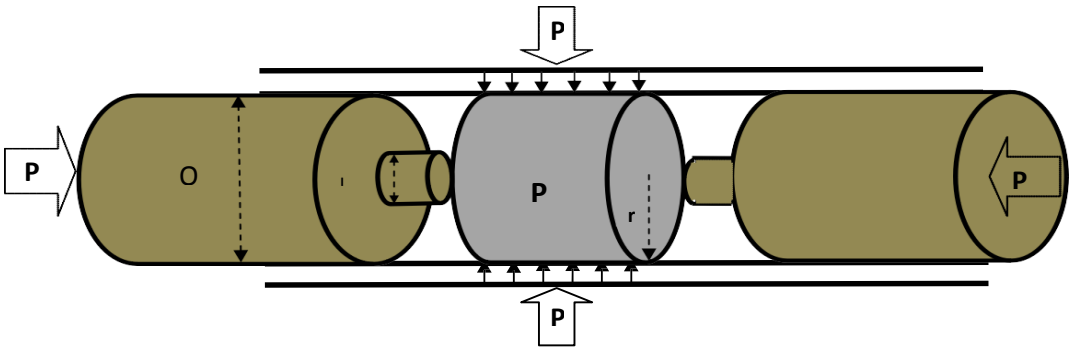

Fig. 5.3 Location of the sample between transducers under the confining pressure (Cp), axial stress (Pa) and pore pressure (Pp)

To accurately measure S-wave velocity which is often tricky to record in traditional experimental setups, due to placing transducers very close to samples, transducers were separated from the sample by 60-mm-long plastic cylinders. This set up decreases wave reverberations inside platens and prevents contamination of the S-wave arrival time because of the proximity of acoustic impedances of the plastic cylinder in the rock sample. Calibration of the system was performed over the whole range of pressures and temperatures using aluminum and stainless-steel samples with the same lengths and diameters as that of the sample. Ultrasonic compressional and shear wave velocities along the symmetry axis of the sample were then measured with a nominal pulse central frequency of 0.5 MHz.

To decrease the random noise, the recorded waveforms were a stack of 100 traces. The experimental errors in determination of P- and S-wave velocities were 1% and 1.5%, respectively induced mainly because of the uncertainty in picking up the arrival time of the waves recorded.

It should be noted that the following nomenclature was used in this study to describe the lab protocol:

i. Confining pressure (Cp): The external (pressure) stress applied to the sample;

ii. Pore pressure (Pp): The internal pressure of the fluid (brine and CO_2) occupying the pore space of the sample;

iii. Differential pressure (Pd): the difference between the confining and pore pressures.

5.2.3 Saturation control

When injection in an aquifer begins, CO_2 dissolves into the brine, which reduces the pH of the system and increases mineral dissolutions and precipitations. This acidification is followed by desiccation in which CO_2 gas bubbles are created around the injection well, pushing the formation water away from the injection site. This leads to formation of a dry zone with a gas saturation degree of almost 1. This dry zone is surrounded by a mixed zone partially saturated by brine and free CO_2. In the more remote parts of the aquifer, however, an aqueous phase fully saturated by brine exist which will be further pushed as injection progresses (Rathnaweera et al., 2015). To simulate this condition, the sandstone sample was gone through the pulse measurement under the following three different conditions:

- **Dry Sample:** The sample was subjected to the ultrasound cleaning in distilled water and then placed in an oven at 105 °C for 24 hours. The dry mass of the specimen was measured after cooling to the room temperature followed by the pulse measurements to record P- and S-waves transit times at different confining pressures ranging from 1 to 30 MPa.

- **Brine Saturated Sample:** A brine solution with the salinity of 1500 ppm containing 5 wt% NaCl and 1 wt% KCl was prepared at this stage. Saturation was initiated by injecting brine into the sample for almost one hour to release all of the gases. Upon full saturation, the outlet valve was closed and the pore pressure was increased to 1.5 MPa. This was followed by conducting the ultrasonic tests under different confining pressures ranging from 0 to ~21 MPa while the maximum pore pressure observed was 18 MPa. Figure 5.4 shows two of the waveforms obtained from these measurements under the pore and confining pressures of 15 MPa.

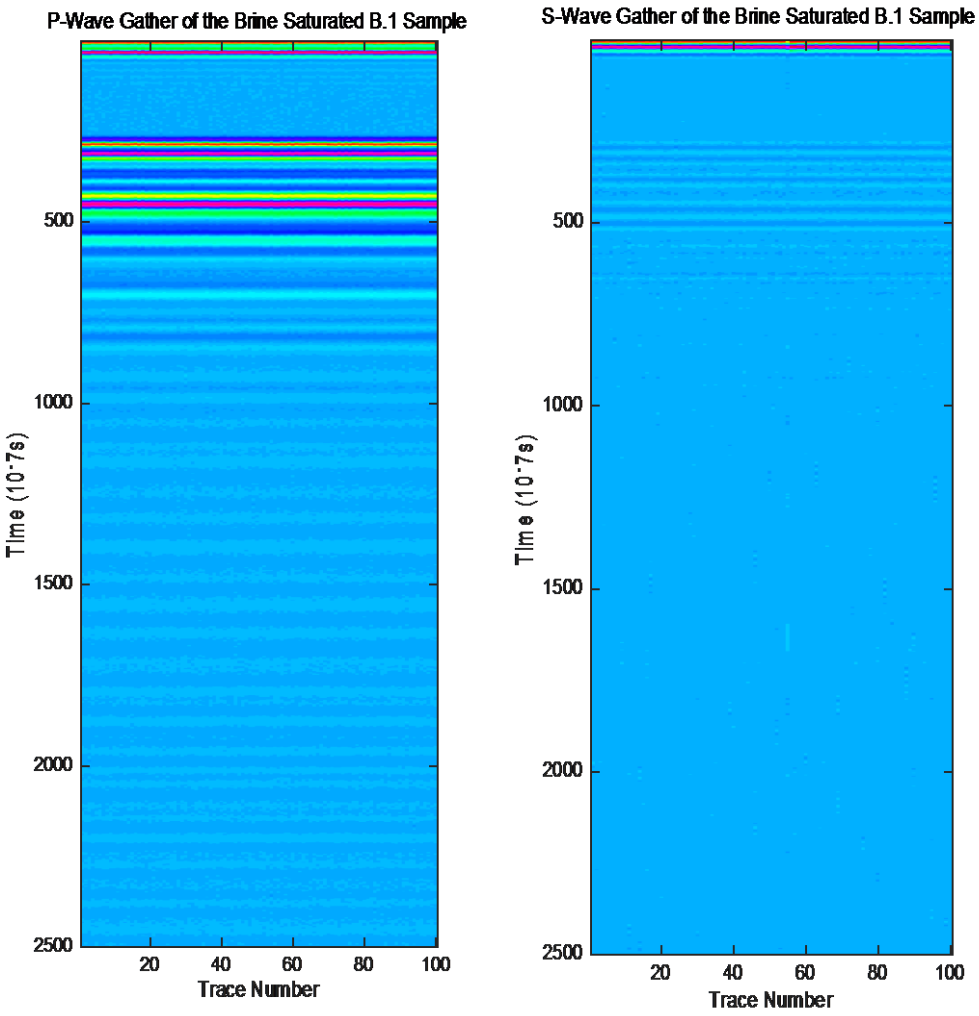

Fig. 5.4 P-wave (left) and S-wave (right) waveforms obtained from the pulse measurements on the brine saturated sample under the pore and confining pressure of 15 MPa. Colors are amplitude variations

- **CO_2 Saturated Sample:** Carbon dioxide in the supercritical phase ($scCO_2$) was injected using the syringe pump into the brine saturated sample. Syringe pump, tubes, and high-pressure cell were heated and maintained at a temperature of 35 °C while the confining pressure was varied from 10 MPa to ~24 MPa to have a fully CO_2 saturated sample. The volume flow rate of CO_2 injected was carefully observed through injection and the volume of brine collected from the sample was used to estimate the average saturation of CO_2 in the sample. Generally, the sample was exposed to CO_2 for five days. Figure 5.5 shows two of the waveforms obtained from these measurements under the pore pressure of 14 MPa and confining pressure of 20 MPa.

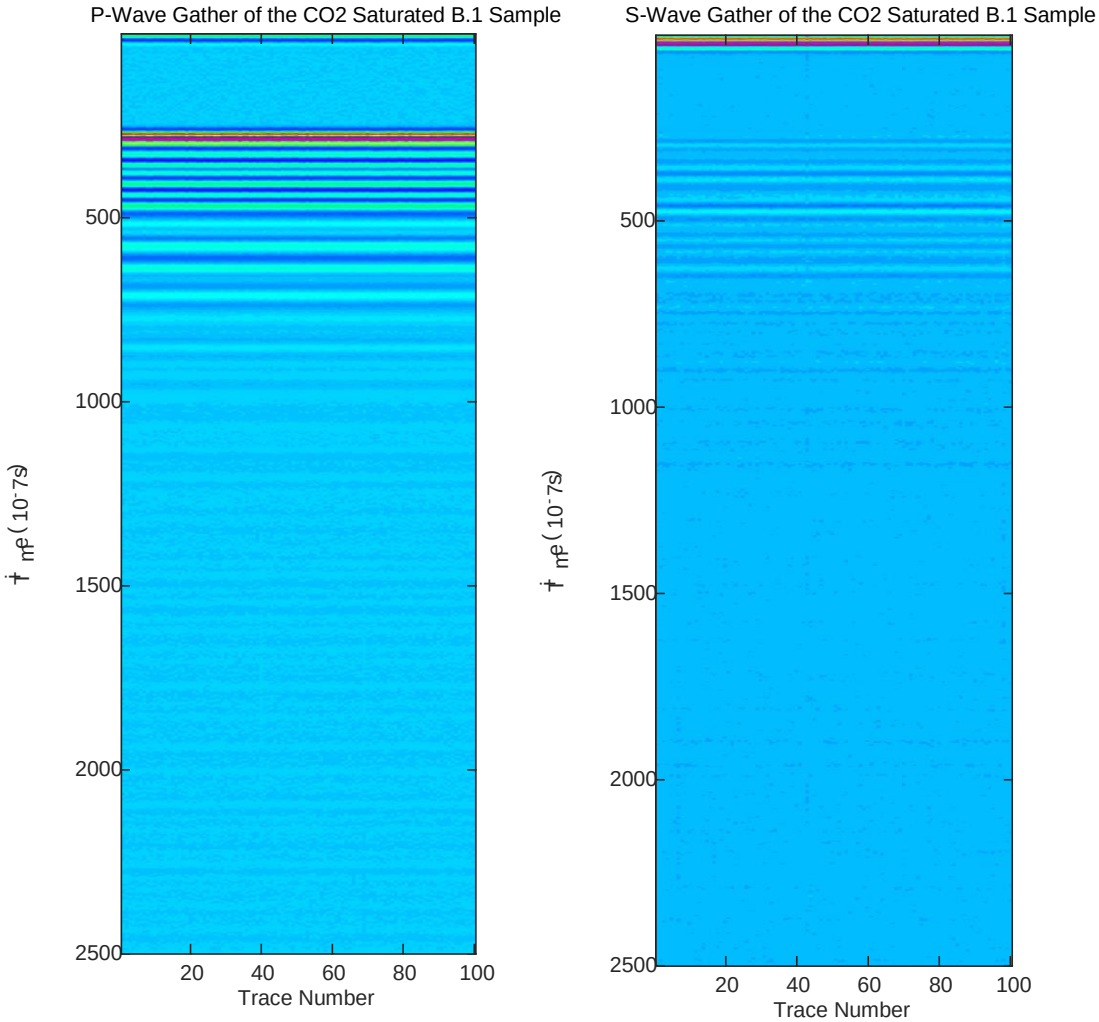

Fig. 5.5 P-wave (left) and S-wave (right) waveforms obtained from the pulse measurements on the CO_2 saturated sample under the pore pressure of 14 MPa and confining pressure of 20 MPa. Colors are amplitude variations

5.2.4 Injection pressure and magnitude of stress

Amplitude is one of the important parameters, carrying a lot of information related to the wave behavior and its attenuation (Alemu et al., 2013). It would, therefore, be a very useful attribute which can be used for characterizations of rocks while being saturated with different kinds of fluids. In this section, attempts were made to evaluate the effect of injection (increases in the pore pressure) and in-situ stress (confining pressure) on the acoustic response of the sample when it is saturated with brine and flooded by $scCO_2$. This helps to understand the possible changes taking place in the elastic and strength parameters of medium during and after injection.

As mentioned earlier, the pulse measurement was done at different confining pressures on the dry sample. Figure 5.6 shows the quality of the P-wave amplitude received under three different confining pressures.

From this Figure 5.6, one may conclude that as the confining pressure increases, the amplitude increases and attenuation decreases under a dry condition. This could be due to the reduction in the matrix anelasticity and closure of pores and cracks in the sample matrix (Thakur and Rajput, 2010). Such stress dependency is typical for sandstones and can be explained theoretically with the dual-porosity model (Shapiro, 2003; Pervukhina et al., 2010).

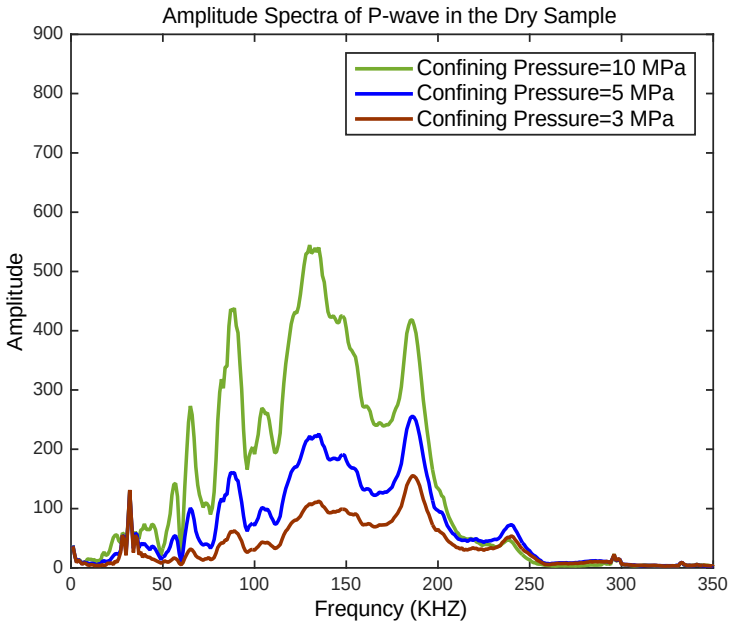

Fig. 5.6 Amplitude spectra of P-wave obtained from the tests on the dry sample

The results obtained from the pulse measurement on the brine saturated sample, in the next stage, indicated that as the confining pressure increases, the amplitude increases due to the closure of the penny shaped pores and thin cracks as well as the compaction of the grains and cement in the sample (Njiekak et al., 2013) (See Figure 5.7). It was also found that increasing the confining pressure increases the density and bulk modulus of the samples because of the compaction effect. This increases in the bulk modulus was more pronounced than the density as the attenuation of the compressional wave was reduced in the brine saturated samples under a high confining pressure.

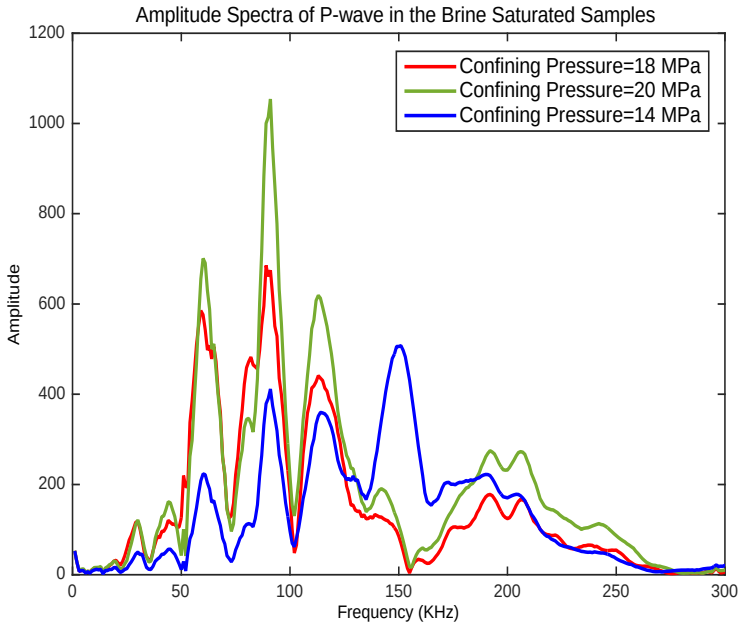

Fig. 5.7 Amplitude spectra of P-wave at as a function of the confining pressure at the pore pressure of 14 MPa in the brine saturated sample

In contrast, the pore pressure revealed that in a same confining pressure, any increases in the pore pressure decreases the amplitude of P-wave going through the brine saturated sample (See Figure 5.8). This is mainly because the pore pressure opens the pores and increases the overall density (Chen et al., 2013). It was then concluded that as the in-situ stress decreases due to the pore pressure increase, stiffness and strength of the medium chosen as the storage site reduces remarkably.

In the next step, the effect of the pore and confining pressure on the acoustic response of the samples being flooded by CO_2 were evaluated. The results obtained indicated that regardless of the confining pressure, the amplitude of P-wave would generally decrease as brine is replaced by CO_2 in the pore spaces. This decreases in the amplitude can be attributed to the reduction of the bulk modulus of the fluids as well as the distribution, extrusion, and movement of CO_2 in the pore space of the sample. Compression and expansion of cracks and pore spaces can be another reason of attenuation which should not be neglected (Njiekak et al., 2013). As a result, the amplitude of the P-wave initially decreases as the injection of CO_2 begins and then rises as the saturation progresses. This amplitude variation and reduction could offer a means to detect CO_2 at the early stage of injection in an aquifer.

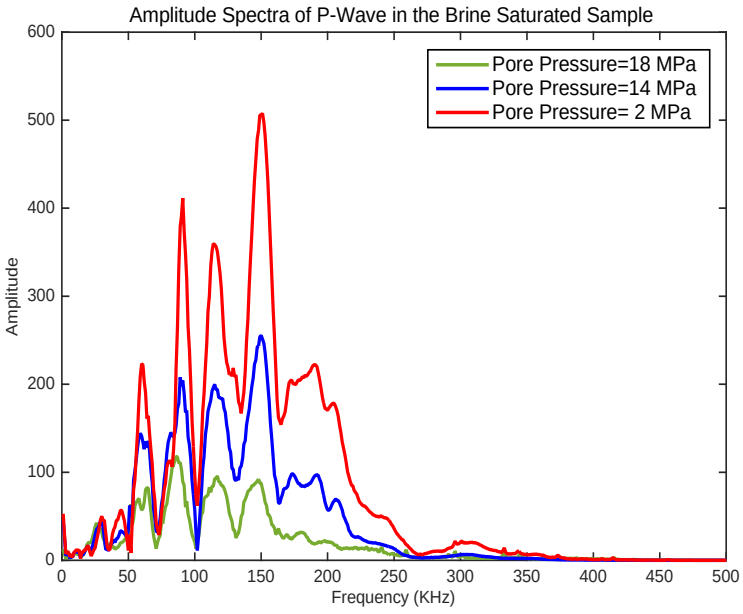

Fig. 5.8 Amplitude spectra of P-wave as a function of the pore pressure in the brine saturated sample under a same confining pressure of 20 MPa

Another observation made during CO_2 injection revealed that as the pore pressure increases, or the confining pressure decreases, the amplitude dispersion increases but this dispersion was more pronounced than that of the brine saturated sample which could be related to the physical properties of CO_2. Figures 5.9 and 5.10 show the amplitude of P-wave obtained during CO_2 injection.

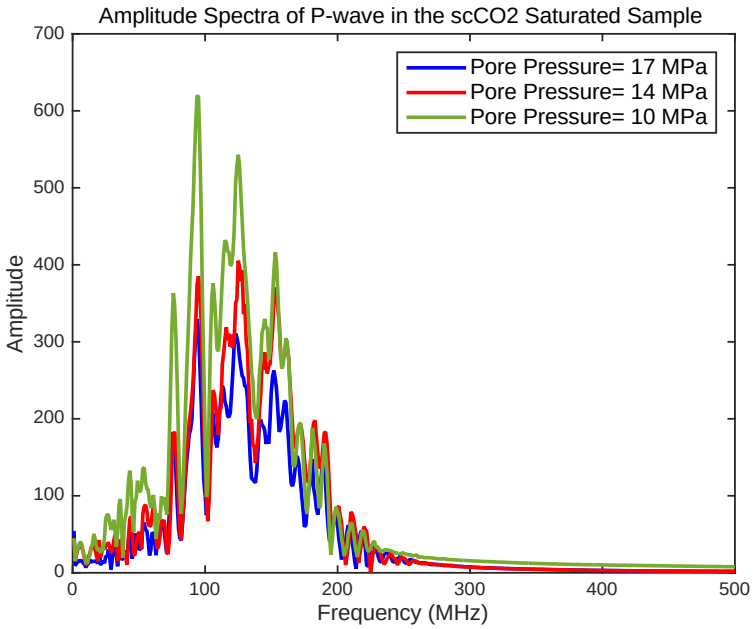

Fig. 5.9 Amplitude spectra of P-wave as a function of the pore pressure during CO_2 injection under the confining pressure of 20 MPa

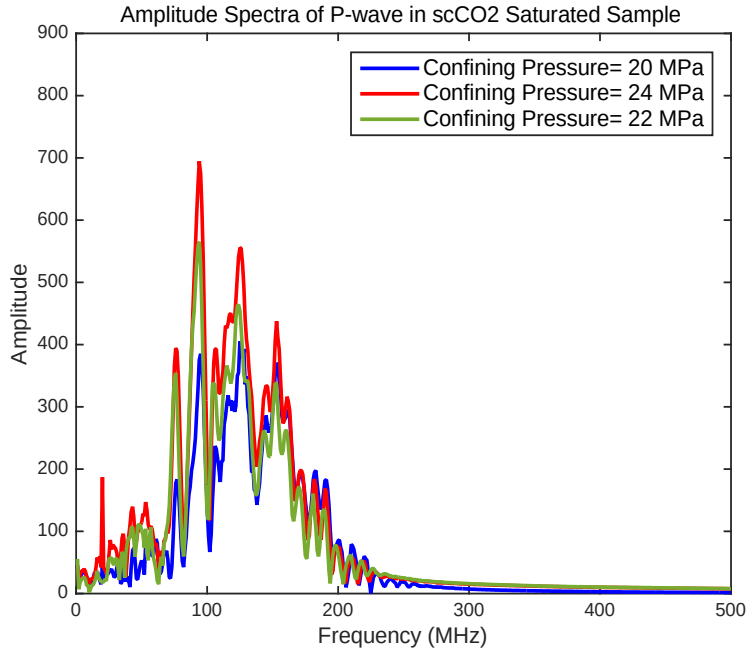

Fig. 5.10 Amplitude spectra of P-wave as a function of the confining pressure during CO_2 injection under the pore pressure of 14 MPa

5.2.5 Elastic parameters

In order to have a good insight into the changes taking place due to the fluid substitution in the sample using the wave velocity, it was crucial to ensure that any

variations in the waveform is due to changes in the pore fluid physical properties and alterations of the sample's solid framework. Thus, a constant differential pressure of 3 MPa was upheld at different stages by assuming that the increase in the confining pressure can cancel the effect of the pore pressure. Figure 5.11 shows the velocity of P- and S-waves obtained from the sample saturated by brine and flooded by $scCO_2$ under the differential pressure of 3 MPa.

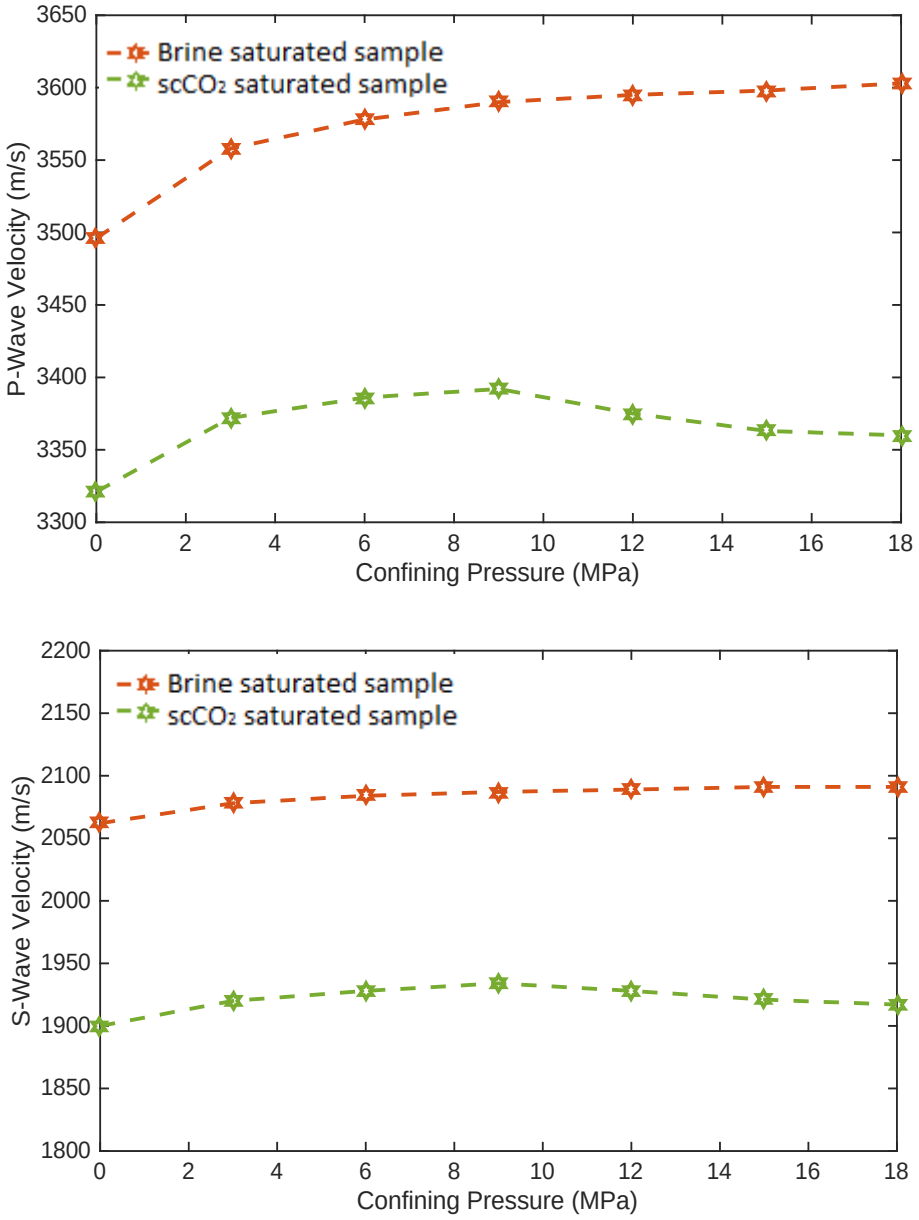

Fig. 5.11 Compressional and shear wave velocities in the CO_2 and brine saturated samples with respect to confining pressure under the differential pressure of 3 MPa

As it is shown in Figure 5.11, the brine-saturated sample gives a higher velocity of P-wave with a value up to 3600 m/s at the confining pressure of 18 MPa (i.e., the pore pressure of 15 MPa and a differential pressure of 3 MPa) while the CO_2-saturated sample shows a lower P-wave velocity which initially increases to 3390 m/s at the confining pressure of 9 MPa and then reduces constantly with a slow rate reaching 3350 m/s. The difference in velocities between the samples is especially manifest at the later stage when the confining and pore pressure increases. The results obtained (see Figure 5.11) from the variation of the shear velocity seems that the shear velocity is sensitive to the fluid types in the pore space, which needs further investigations. The other interesting observation was the reduction of the shear velocity in the CO_2 saturated sample after reaching the confining pressure of 9 MPa, which could be due to increases in the density of samples, alteration of the solid skeleton, or even pore pressure disequilibrium. This can be further evaluated by determination of dynamic shear modulus of the samples with different fluids substitutions.

It has been indicated by many that the strength of a rock can be decreased because of the fluid substitution in the pore space which might be related to mechanical actions of fluids or chemical interactions posed by pore fluids as the surface free energy reduced. However, there are very few studies reporting changes in mechanical responses of CO_2-saturated Berea sandstone. The study performed by Oikawa et al. (2008) and Hangx et al. (2013) suggested that the difference in the strength between the water saturated and the CO_2-saturated sandstone samples are very small. To further evaluate these changes, dynamic elastic parameters including Young's modulus, Poisson's ratio as well as Shear modulus were estimated using the conventional equations provided by Mavko et al. (2009), assuming that the sample is homogenous and isotropic. Figure 5.12 shows the variation of the Young's and Shear moduli obtained from this analysis.

When examining this Figure 5.12, one can conclude that the there is a reduction in the variation of elastic parameters especially the shear modulus. This indicates the fact that the decrease in the shear velocity was not only because of the increases in the density of the sample. It could also be due to mineralogical alterations and

dissolution of calcite and break down of clays in the matrix after exposure to CO_2 (Marbler et al., 2012).

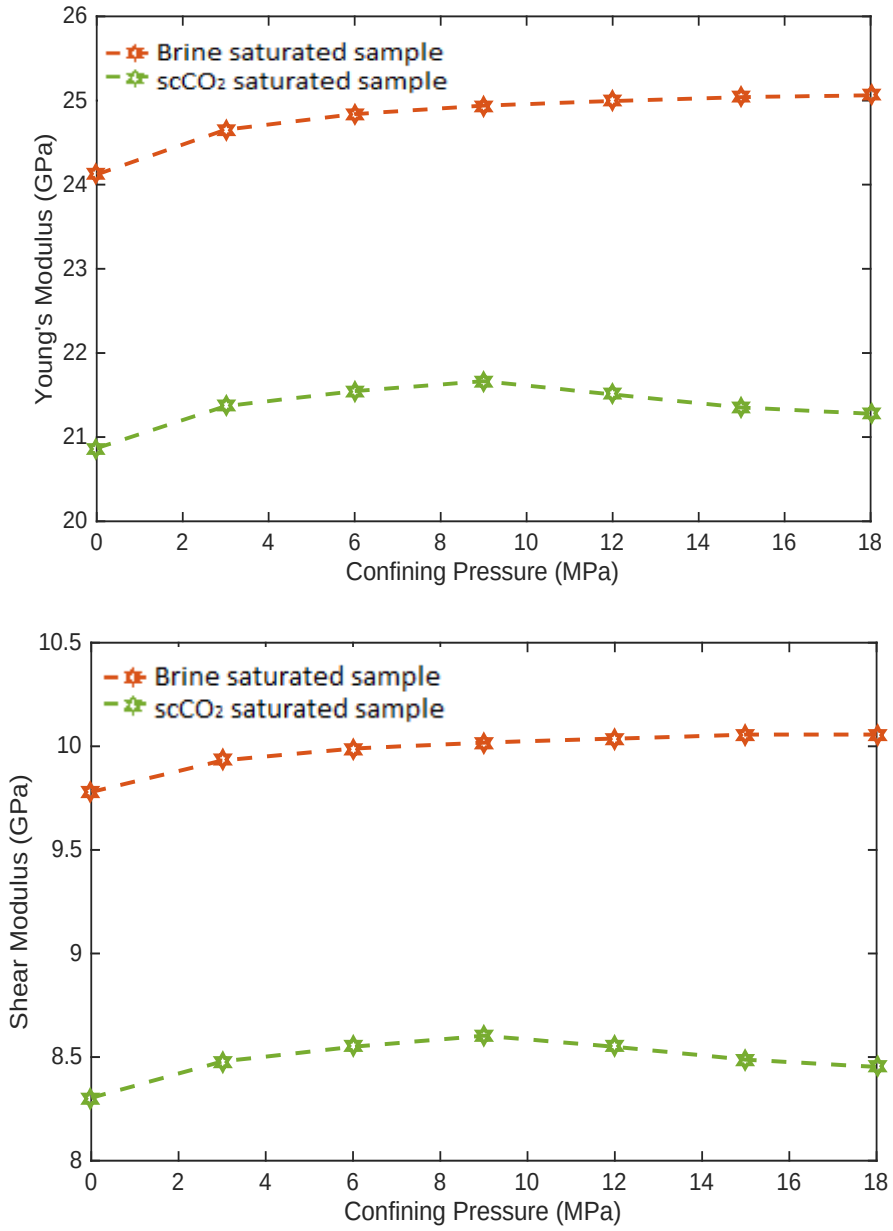

Fig. 5.12 Variations of Young's and Shear's Modulus in the CO_2 and brine saturated samples with respect to confining pressure under the differential pressure of 3 MPa

Generation of carbonic acid may be the other reason leading to the dissolution of carbonates including calcite and a long-term dissolution of feldspars, clay minerals, micas and Fe-oxides during and after injection. According to Marbler et al. (2012), dissolution of CO_2 into brine saturated sandstone samples changes its ability to resist

against differential stresses. Le Guen et al. (2007) observed a clear strength reduction in the wet sandstone due to CO_2 injection.

To further evaluate the alteration of the solid skeleton, the SEM images of the Berea sandstone before and after exposure to CO_2 were studied as shown in Figures 5.13 and 5.14. Tables 5.5 and 5.6 give the element type, their weight concentrations and stoichiometric percentage[1] obtained from the same analysis before and after exposure to CO_2.

The results obtained revealed that the alteration was induced and mineral dissolutions and corrosions were observed, as shown in Figure 5.14. In fact, it seems that the main concerns are corrosion of quartz, K-feldspars and clay minerals (kaolinite) as well as dissolution of carbonates (calcite) (See Table 5.6). Kaolinites often gives marginal mineral dissolution whereas K-feldspar reactions with carbon dioxide in the aqueous solution of aquifer can result in the formation of bicarbonate, silica and kaolinite (Holdren and Berner, 1979).

The surface of the sandstone sample shows a clear alteration of the cement matrix, such as initial dissolution of calcite. This dissolution of the carbonate matrix which was observed after five days of the experiment could also be linked to the formation of HCO_3^- as mentioned earlier. Small grains of secondary carbonate minerals were also observed on the surfaces of quartz in the SEM images (Figure 5.14 right). Some of quartz crystals demonstrate selective surface corrosions which may destabilise the microstructure of the sandstone, due to changes of porosity within the boundary between cement and grains.

When examining this Table 5.6, the concentration and percentage of certain elements may indicate the stage at which the primary minerals dissolve and secondary minerals precipitate in the solution. In this regard, the concentrations of Na, K, Ca, Mg, as well as Si and Al would be particularly important.

[1] - The percentage in which those elements were involved in the reactions taken place due to CO_2 exposure

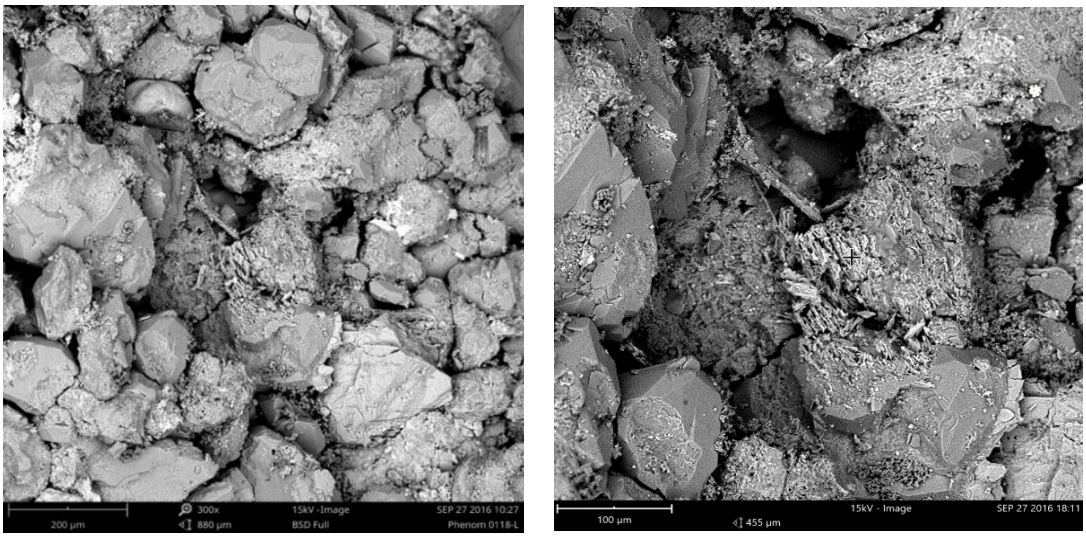

Fig. 5.13 The Berea Sandstone before exposure to $scCO_2$

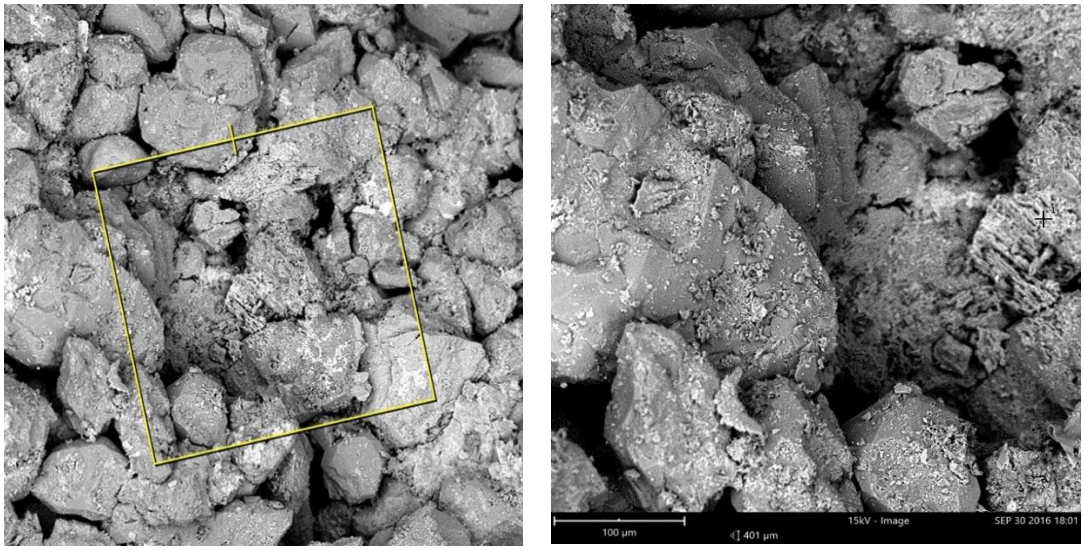

Fig. 5.14 The Berea Sandstone after exposure to $scCO_2$ with signs of changes and alteration in the solid framework

Table 5.5 Element quantification before exposure to $scCO_2$

Element Symbol	Atomic Concentration	Weight Concentration	Stoichiometric Percentage
O	74.81	62.81	
Si	17.74	26.15	70.41
Al	5.42	7.68	21.52
K	1.00	2.05	3.96
Mg	1.03	1.32	4.10

Table 5.6 Element quantification after exposure to $scCO_2$

Element Symbol	Atomic Concentration	Weight Concentration	Stoichiometric Percentage
O	71.61	57.92	
Si	17.95	25.48	63.23
Al	3.83	5.23	13.50
Cl	1.79	3.21	6.32
Ca	1.37	2.78	4.83
Na	1.64	1.91	5.79
Fe	0.60	1.69	2.11
Mg	0.79	0.97	2.77
K	0.41	0.81	1.45

5.3 CO_2 injectivity

Results of CO_2 injectivity (pressure drop) show significant variation in the pressure drop during CO_2 flooding in sandstone. The inlet and outlet pressures of the samples were also monitored during the flooding procedures as the magnitude of the pressure drop across the sample could represent the formation injectivity. During the injection, the pressure drop was measured against time (Figure 5.15), which expressively decreases. Regardless of the presence of two phase flow during CO_2 injection in brine saturated core sample, steady-state condition achieved at 1.5 pore volume (PV) as at this particular PV, the slope of the pressure drop smoothens. Subsequently, the further decrease in pressure difference is indication of complete saturation.

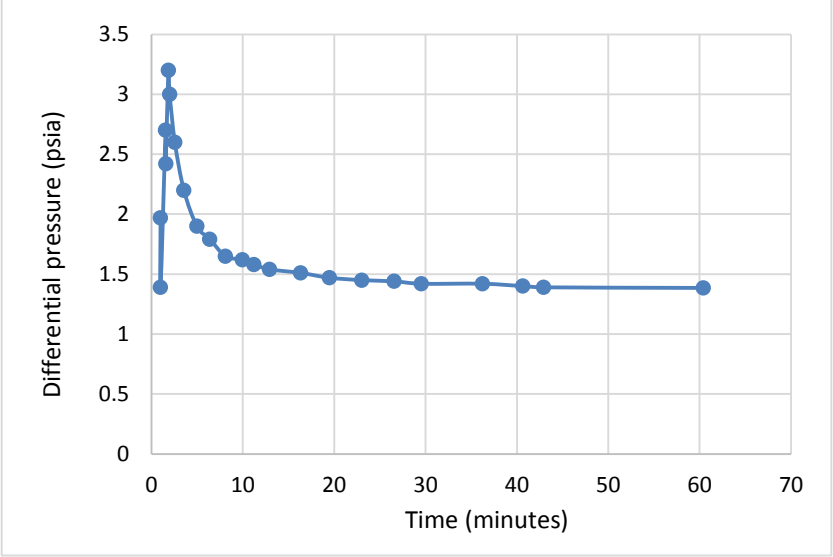

Fig. 5.15 Pressure drop as a function of injected CO_2 in the sample

5.4 Summary of chapter

It is generally known that the long-term storage of CO_2 in a geologic site is affected by complicated chemical interactions causing acidification, mineral dissolution, and changes in the in-situ stress, which in turn may have negative impacts on the elastic and strength parameters of reservoirs and seals. In this work, attempts were made to evaluate the geochemical alteration taking place in rock sample against different in-situ stresses in a short period of time when it is saturated by brine and $scCO_2$. The results obtained indicated that reductions in the shear velocity and modulus which might be attributed to the corrosion of clays and dissolution of calcite in the matrix. This was further evaluated by the SEM image analysis, where clear alteration of the rock sample was observed. In fact, there were signs of carbonate dissolution, kaolinite break-down and even corrosion of quartz which indicates the fact that geomechanical parameters of reservoirs and seals can be affected even in a short-term exposure to $scCO_2$.

CHAPTER 6

CO_2 STORAGE NUMERICAL MODELING

6.1 Introduction

It is essential to accurately predict the injection rate and pressure for a safe and favorable CO_2 injection operation in the storage sites. In this chapter, a scheme for the estimation of the optimum injection rate is presented to achieve favorable injectivity and effective storage potentials within the suitable injection period. The full dataset of a carbonate gas reservoir of Malaysia was utilized to numerically evaluate: 1) storage capacity, and trapping mechanisms, 2) optimum injectivity, and 3) the potential leakage of CO_2 from the reservoir through building a 3D numerical model based on the Peng-Robinson equation of state. It was found that a significant amount of $scCO_2$ can be injected in the reservoir at the optimum injection rate over 20 years with a favorable injectivity.

6.2 Data sources and numerical model setup

Numerical models can be used to assess the storage performance of CO_2 injection. However, these numerical models must be validated against reservoir observations before consideration for reservoir development and designs. Numerical simulations were performed in this study with the Eclipse simulator (E300) which is a flow simulator developed by Schlumberger Limited. It is a major tool used for compositional modeling of enhanced recovery processes and CO_2 storage. A 3D model was established for the carbonate gas reservoir and calibrated through historic data from 1983-2015. The gas reservoir historic data covers monthly gas, condensate and water productions.

A Cartesian model with 70 × 50 × 24 grids was used to model a total reservoir area of 5 km ×4.4 km with a total thickness of 1000 ft. The model has an anticline structure with 4 horizontal zones with different porosity and permeability. These four zones were separated by a tight layer while an aquifer with constant pressure lateral

boundary condition was attached at the bottom of the reservoir as shown in Figure 6.1. In fact, the reservoir has already been divided into four main flow units based on the preliminary assessment obtained from the well log interpretation (see Figure 3.10) of a Well D drilled in the center of the reservoir structure seems as best suitable conduit regarding well location. In an earlier study, wireline log data of the same well (Well D) was analyzed to evaluate the rock characteristics of the different intervals where the depth interval of 4036-4747 ft (1230-1447 m) was indicated to be the reservoir interval with a net and gross thickness of 595 ft (181 m) and 711 ft (217 m), respectively. The porosity and permeability of the reservoir in that was found to be from 4.5–42% and 0.1–2927 mD, respectively which were used for the numerical modeling of this study as shown in Figure 6.2. These details would also help during CO_2 storage modeling to consider the effect of heterogeneity on the multiphase flow behavior (Kuo et al., 2011; Hingerl et al., 2016), time-scale of convective mixing, plume size and degree of CO_2 trapping (Han et al., 2011). Table 6.1 summarizes other reservoir properties used in the numerical model.

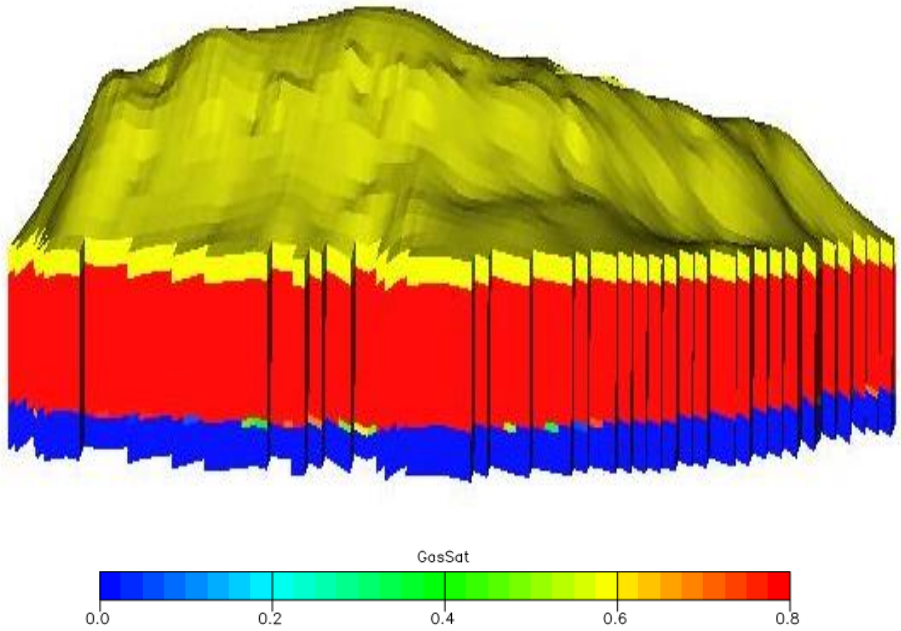

Fig. 6.1 Anticline structure model having carbonate build-up of condensate gas (red) between a thick caprock (yellow) and aquifer (blue)

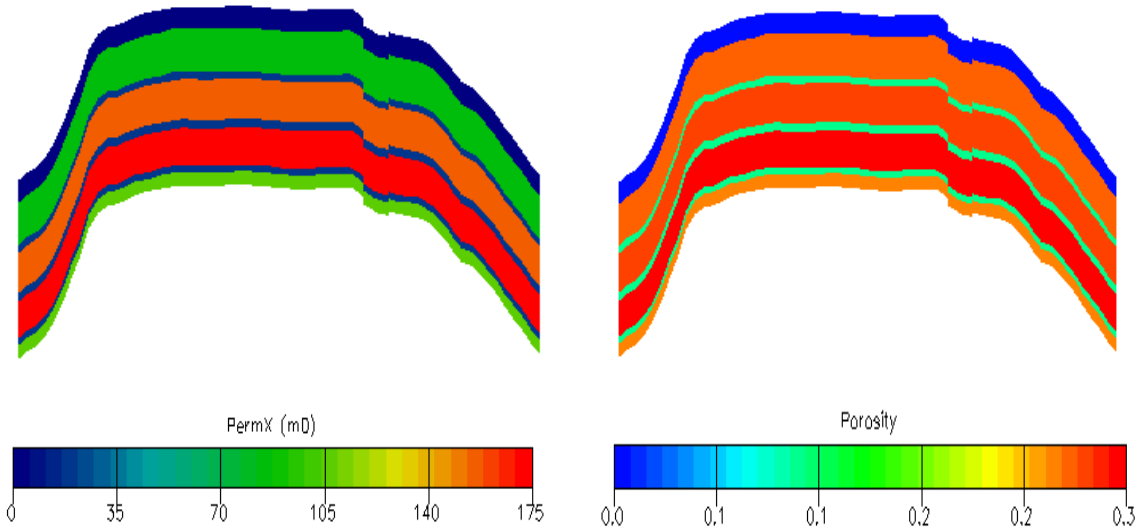

Fig. 6.2 Porosity and permeability distribution maps used in the numerical simulations

Table 6.1 Fluid properties and contacts data used in numerical modeling of the reservoir

Parameter	Value
Molar concentration gradient of component (m^2/sec)	CO_2 $1.72\ 10^{-5}$ C_1 $1.61\ 10^{-5}$ C_2 $4.30\ 10^{-6}$ C_3 $4.30\ 10^{-6}$ C_4 $4.30\ 10^{-6}$ C_5 $4.30\ 10^{-6}$ C_6 $1.20\ 10^{-5}$ C_{7+} $1.40\ 10^{-6}$ Liquid 10^{-10}
Rock compressibility (1/psia)	2×10^{-5}
Connate water saturation (%)	20
Salinity (ppm)	15000
Gas density at standard condition (kg/m^3)	942
Water density (kg/m^3)	1108
Original gas water contact depth (ft)	4887
Dew point pressure (psia)	1805

Table 6.1 summarizes other reservoir properties used in the numerical model. The simulation model is isothermal and uses a single reservoir temperature of 212 ^oF considering the molecular diffusion effect among gas and CO_2 components for values given in Table 6.1 and neglects chemical (dissolution/precipitation) reactions between minerals and fluids due to simulator limitations.

Neglecting these reactions puts some constraints on the analysis of the modeling results as they may affect the injectivity. For instance, dissolution of CO_2 in water results in generation of carbonic acid which decreases the pH of brine and may lead

to potential mineral dissolution and/or precipitation due to the reservoir rock's interactions with the acidic fluid (Ukaegbu et al., 2009; Espinoza et al., 2011).

For PVT properties of condensate gas, the composition provided in Table 6.2 was used. In fact, the black oil PVT analysis with up to seven compositions of the condensate gas mixture along with a constant composition expansion (CCE) and viscosity data were utilized to tune the equation of state (EOS) and Peng-Robinson EOS as given in Figure 6.3. The Black oil model was then converted into the compositional model in which CO_2 and N_2 were kept separated to evaluate individual contributions of a typical flue gas component. Properties of gas, water and carbon dioxide (i.e., critical pressure and temperature, acentric factors and binary interaction coefficients) were generated by the PVTi module of Eclipse at the reservoir condition to history match the static model. These properties are essential as the inputs for the storage modeling governing the fluid properties at the depleted pressure before injection.

Figure 6.4 depicts a phase diagram indicating the fluid type based on the position of the reservoir pressure path, separator conditions and the size of phase diagram (McCain Jr, 1994; Terry and Rogers, 2013).

Table 6.2 Mole composition of typical reservoir fluids

Component	Gas Condensate (mole fraction)
CO_2	2.17
N_2	0.93
C_1	85.88
C_2	3.55
C_3	3.38
iC_4	1.21
nC_4	0.86
iC_5	0.47
nC_5	0.23
C_6	0.32
C7+	1
Total	100
Mol. wt. C7+	111.4

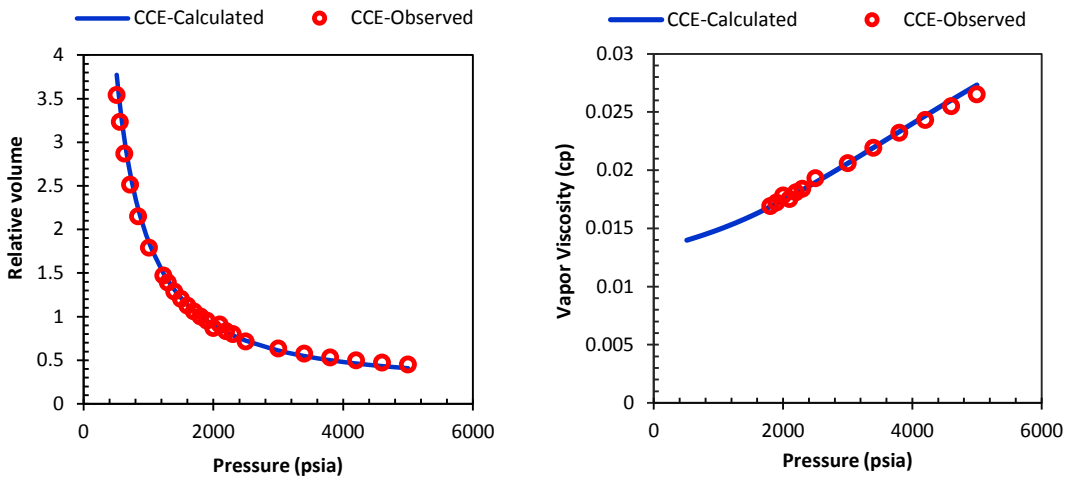

Fig. 6.3 Comparison of experimental and simulating results: (a) relative volume; (b) vapor viscosity

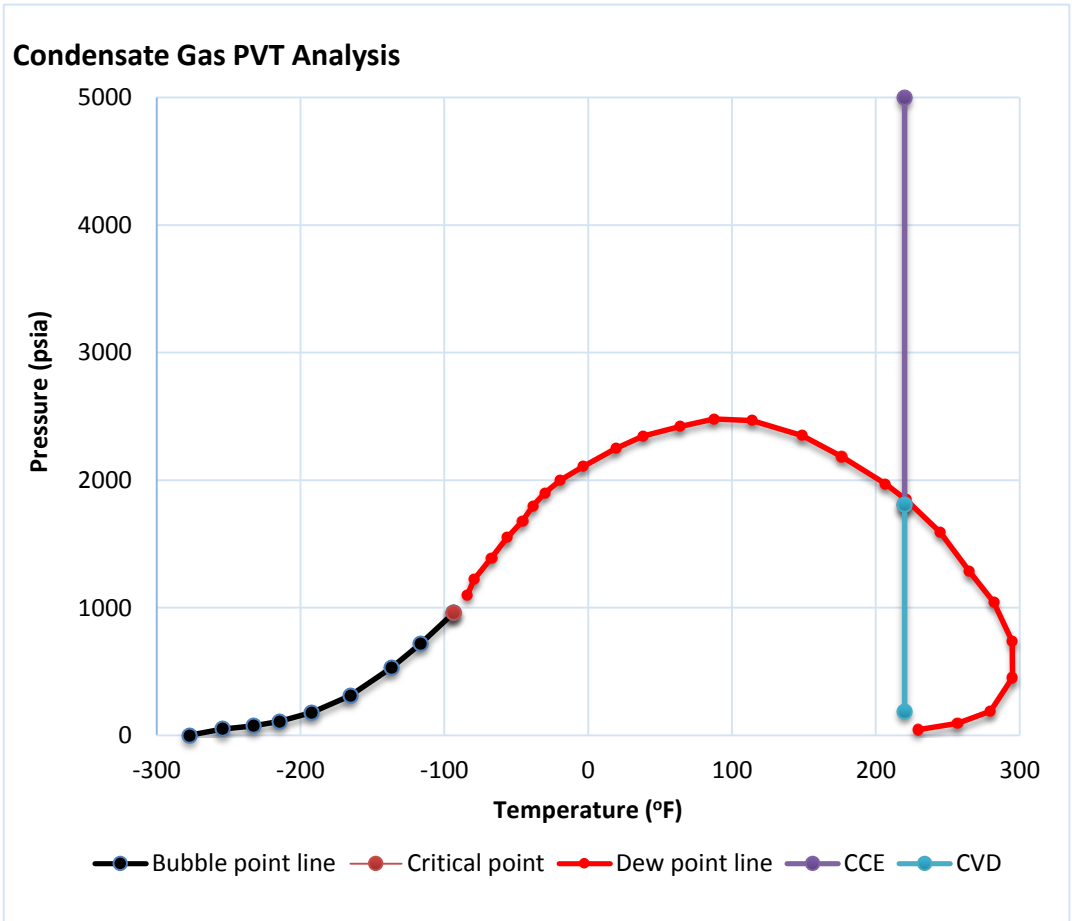

Fig. 6.4 Phase diagram of condensate gas bounded by the bubble point line (black) and the dew point line (red). The vertical line of the reservoir pressure path is crossing the dew point line at 1805psia. Separator conditions are marked by a dark blue lying within the phase envelope

As shown in the phase diagram, below the dew point pressure, condensation occurs leading to segregation of the liquid phase in the near bottom-hole and reservoir region. However, the composition of condensate gas at the depleted stage is different from the composition at the initial stage (Adisoemarta et al., 2004; Sobers et al., 2004; Abbasov and Fataliyev, 2016; Rahimzadeh et al., 2016).

As stated earlier, depleted gas reservoirs have a large amount of remaining gas in place which can only be recovered by employing CO_2 enhanced gas recovery (EGR) (Stevens et al., 1999; Oldenburg and Benson, 2001b; Leeuwenburgh et al., 2014; Shen et al., 2014; Yuan et al., 2015; Patel et al., 2016). Hence, for the purpose of this study, each zone has 30% remaining gas and 40% condensate at the depleted pressure of 500 psia. Water–gas and gas–gas relative permeability data were also used and capillary pressure effects were neglected. Analytical equations are commonly used to estimate the relative permeability for an individual phase in numerical simulations. As a result, the relative permeability was calculated through the analytical expressions given in Table 6.4 using the input parameters given in Table 6.3. Table 6.4 shows the governing equations for the phase flow, fluid properties and relative permeability estimation provided for the reservoir based on the simulation run. The tuned relative permeability curves used in the history matching simulation are shown in Figure 6.5.

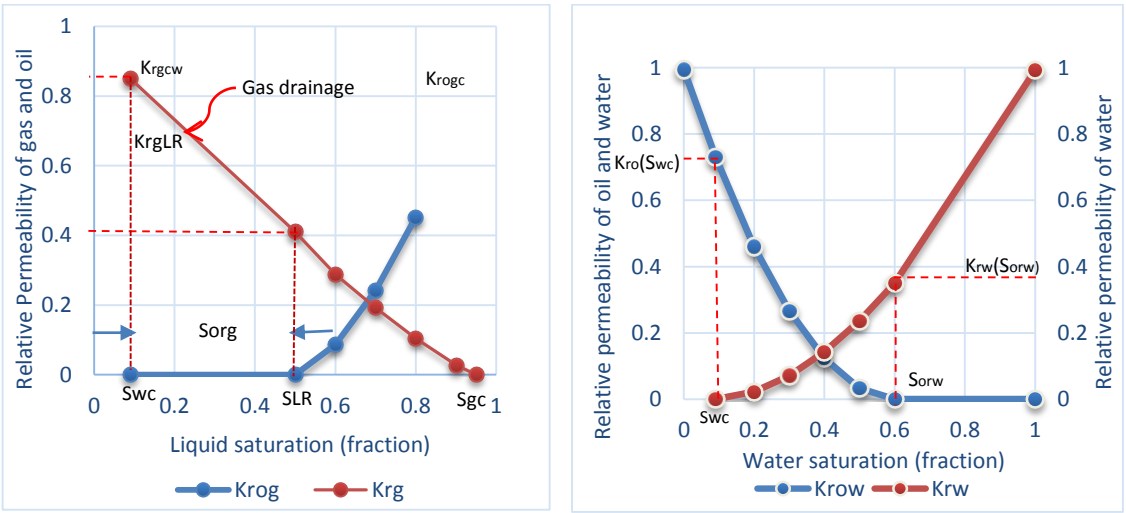

Fig. 6.5 Three phase relative permeability: gas-gas system (left) and water-gas system (right)

Table 6.3 The information on the water-condensate and gas-condensate systems

S_{wc}	S_{orw}	S_{gc}	S_{org}	$(K_{ro})_{Swc}$	$(K_{rw})S_{orw}$	$(K_{ro})_{Sgc}$
9%	40%	5%	40%	0.73	0.39	0.85

Table 6.4 Governing equations for the compositional modeling of the depletion scenario

Mechanism	Model	Governing Equation
Phase (oil, gas, water) flow	Composition flow	$F_{pni}^{c} = T_{ni} x_p^c k_{rp} S_p \frac{b_p^m}{\mu_p} dP_{pni}$
Fluid Properties	Peng-Robinson EOS	$\left[P + \frac{A}{V_M(V_M + B) + b(V_M - B)}\right](V_M - B) = RT$
Molecular Diffusion	Diffusive flow	$J_i = -y\frac{D_i \partial y_i}{\partial d}$, $F_{ig}^{diff} = T_D D_{ig}(S_g b_g^m)\Delta y_i$
Capillary pressure and Relative Permeability	Oil-Water system	$K_{row} = (K_{ro})_{S_{wc}}\left[\frac{1-S_w-S_{orw}}{1-S_{wc}-S_{orw}}\right]^{n_o}$ $K_{rw} = (K_{rw})_{S_{orw}}\left[\frac{S_w-S_{wc}}{1-S_{wc}-S_{orw}}\right]^{n_w}$ $P_{cwo} = (P_c)_{S_{wc}}\left[\frac{1-S_w-S_{orw}}{1-S_{wc}-S_{orw}}\right]^{n_p}$
	Gas-Oil System	$K_{rog} = (K_{ro})_{S_{gc}}\left[\frac{1-S_g-S_{lc}}{1-S_{gc}-S_{ic}}\right]^{n_{go}}$ $K_{rg} = (K_{rg})_{S_{wc}}\left[\frac{S_g-S_{gc}}{1-S_{lc}-S_{gc}}\right]^{ng}$ $P_{cgo} = (P_c)_{S_{lc}}\left[\frac{S_g-S_{gc}}{1-S_{lc}-S_{gc}}\right]^{n_{pg}}$

When it comes to CO_2 storage, residual gas and condensate can be an issue for a favorable injectivity because the amount of remaining gas (Saeedi and Rezaee, 2012; Oldenburg and Doughty, 2011) and oil in reservoirs significantly affects the relative permeability and injectivity of CO_2 (Kovscek, 2002). Thus, it is necessary to consider the residual gas and condensate effect on CO_2 injection to investigate the actual multiphase flow mechanism during storage. For the storage in the reservoir without the hysteresis phenomenon, the relative permeability of the gas-CO_2 and CO_2-brine systems were applied during simulation of storage as reported by Seo (2004). Figure 4.3 (given in Chapter 4) displays the relative permeability curves of those systems, in

which the red line is the relative permeability of CO_2 in the presence of CH_4 (left) and brine (right).

In the numerical model, an active aquifer at the bottom of the reservoir was considered with a water index of 500 STB/day/psia. The approximation of Fetkovich aquifers was used to calculate the water influx from the aquifer. Water can flow from the aquifer into the reservoir and from the reservoir into the aquifer depending on the pressure gradient.

6.2.1 Injection rate estimation

Among the 20 wells drilled in this reservoir, a well was selected for CO_2 injection and storage away from the fault, in the center of the structure, with good wellbore conditions, and favorable rock characteristics. This well has a perforation interval of 4047-4473 ft (426 ft) covering the first two zones with a wellbore radius of 0.8 ft. Permeability and thickness of the zones obtained from the earlier interpretation were used to calculate the injection rate. Geomechanical analysis was carried out based on analytical solutions for the fracture gradient estimation near the wellbore region which is an indicator of the safe injection pressure (Loizzo et al., 2010). This would help to determine when the injection pressure exceeds the fracture initiation pressure of the reservoir/caprock which may results in leakage and seepage of CO_2 to the surface (Burke, 2011).

For the fracture gradient estimation near the wellbore prior to injection, wireline logs data including DSI log (i.e., containing compressional and shear slowness data) were available and used for the purpose of this study. However, core samples and MDT data were not available for calibration of elastic, strength and pore pressure parameters estimated using analytical solutions. Figures 6.6 shows the wireline logs data used for the purpose of this study.

The analysis was initiated by determination of dynamic elastic parameters (Young's modulus (E), and Poisson's ratio (υ)) of the formations using the equations provided by Fjær et al. (2008). The correlation devloped by Wang (2000) was used to convert the dynamic elastic parameters into static ones as the wave velocity data based

elastic parameters are overestimated. To estimate the uniaxial compressive strength (UCS) and the friction angle of rocks, the correlation proposed by Bradford et al. (1998) and Plumb (1994) were employed, respectively. Figure 6.7 shows the estimated log-based parameters of Well D.

For the pore pressure, Eaton's method was utilized which is an essential parameter to determine the magnitude of effective in-situ stresses by poro-elastic equations (Gholami et al., 2015b; Gholami et al., 2016). The results obtained from the stress analysis revealed that the dominant stress regime in this reservoir is reverse faulting as the order of the magnitude of in-situ stresses was $\sigma_{Hmax}>\sigma_{hmin}>\sigma_v$. It is commonly recognized that the pore pressure and other geomechanical parameters must be rectified using the reservoir and core data. Owing to the absence of this data set, shear failure observed in the caliper log was used for the calibration purpose. As a result, the breakout pressure determined by the Mohr-Coulomb criteria was used to regulate the geomechanical parameters (elastic and strength parameters together with the pore pressure) linked to the variation of the mud weight. As a rule of thumb, if a failure criteria can precisely predict the break-out taken by the caliper log, one can safely say that the magnitude of in-situ stresses and other geomechanical parameters are accurate.

Figure 6.8 shows the stress profiles in the first track, the caliper log and the bit size in the second track and the breakout pressure, mud loss and mud weight in the third track. The last track is the minimum horizontal stress representing the magnitude of the fracture initiation pressure. LOT test data in the caprock section of the reservoir at different depth gives the maximum value of 3682 psia for the fracture pressure as discussed in Chapter 3. Results of petrophysical and geomechanical analyses before CO_2 flooding are given in Table 6.5 and Table 6.6 which are used here, respectively.

Considering the effect of CO_2 during and after injection, such as geochemical interactions which may have a huge impact on geo-mechanical characteristics in sandstone and carbonates, the fracture initiation pressure and gradient might be changed. Thus, a safe value of wellbore injection pressure must be selected wisely based on different considerations. In this study, a pressure of 2000 psia, which was

less than the initial reservoir and fracture initiation pressure of the reservoir and caprock, was selected to mitigate the leakage concern (Rutqvist et al., 2007; Dempsey et al., 2014). Since the magnitude of stresses may change during production and injection phases, it would be useful to conduct geomechanical-geochemical studies by following the scheme presented by Masoudi et al. (2011) to assess plasticity, reservoir volume and fracture initiation.

Table 6.5 Thresholds of the caprock and reservoir before CO_2 flooding

Section	Stress Regime	Depth Range (ft)	Fracture Gradient Range (psi/ft)	Average Fracture Gradient Range (psi/ft)
Caprock	-	1850-3501	0.61 – 1 (LOT Tests)	0.78
Reservoir (Well-D)	Reverse	3800-4804	0.65-0.78 (Log Data Analysis)	0.75

Table 6.6 Results of petro-physical and geomechanical analysis

Zone	Interval (ft)	Permeability (mD)	Thickness (ft)	Fracture Gradient (psi/ft)
1	4020-4300	85	280	0.75
2	4300-4530	160	230	0.75
3	4530-4750	175	220	0.75
4	4750-4804	110	54	0.75

Taking into account the maximum injection pressure of 2000 psia and the pore pressure of 500 psia, properties of $scCO_2$ i.e., the formation volume factor and viscosity, were estimated under the reservoir condition using the experimental results presented by Jalil et al. (2012). For the effect of residual gas on $scCO_2$, the relative permeability of CO_2 was considered to be 0.9 at maximum saturation of CO_2 (80%). The effect of condensate on the flow of CO_2 (Kovscek, 2002) was excluded due to absence of relative permeability of CO_2 in the presence of condensate.

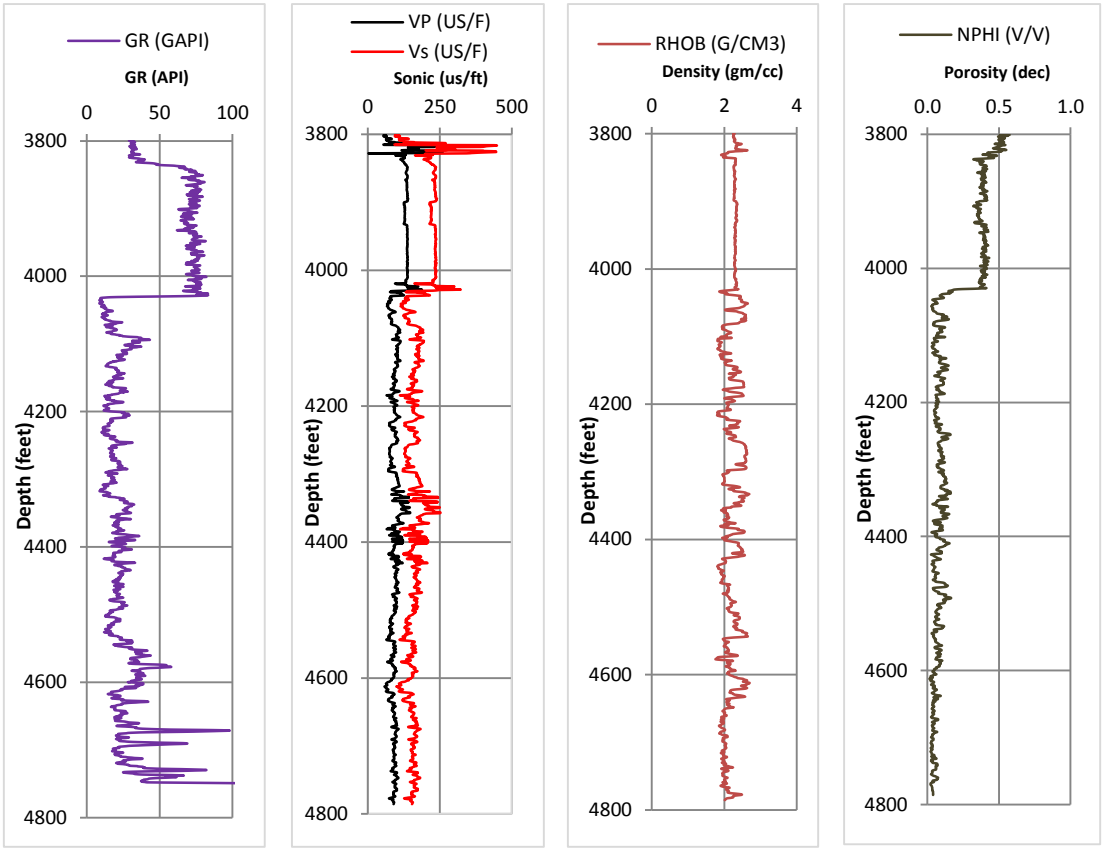

Fig. 6.6 Conventional wireline log data of Well D used for the purpose of this study

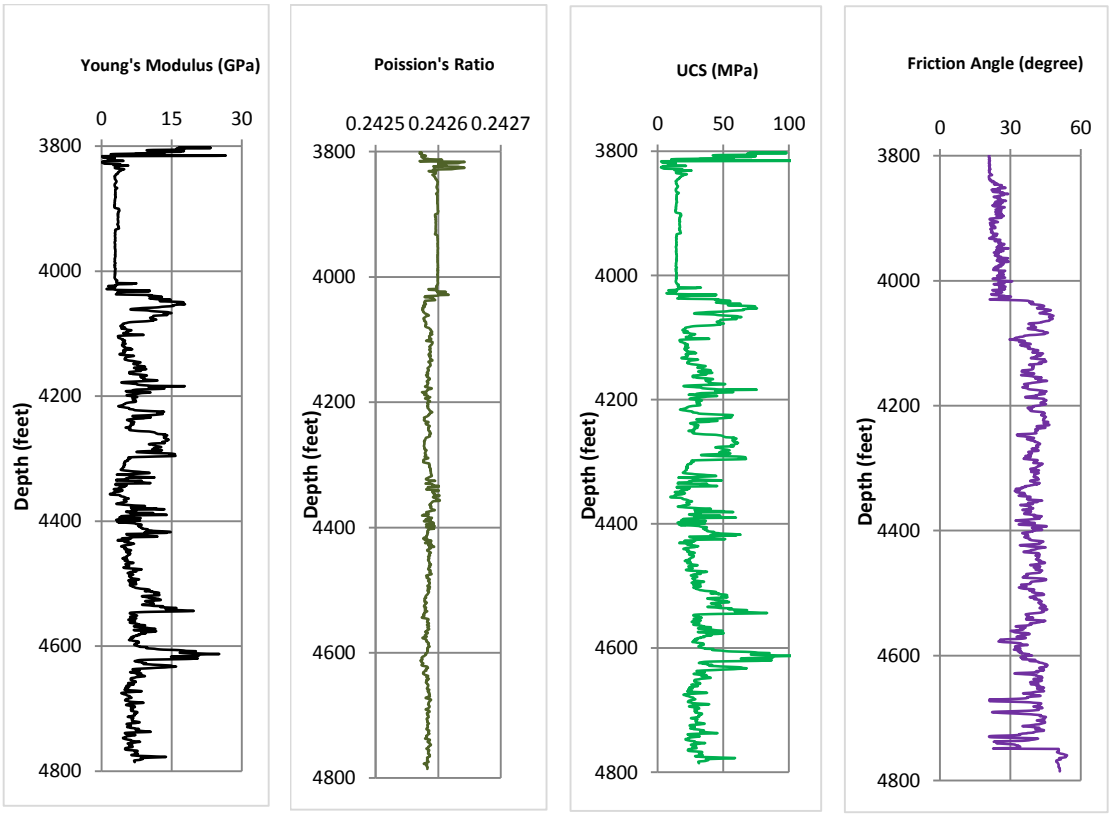

Fig. 6.7 Estimated elastic properties, uniaxial compressive strength and the friction angle of formations in Well D

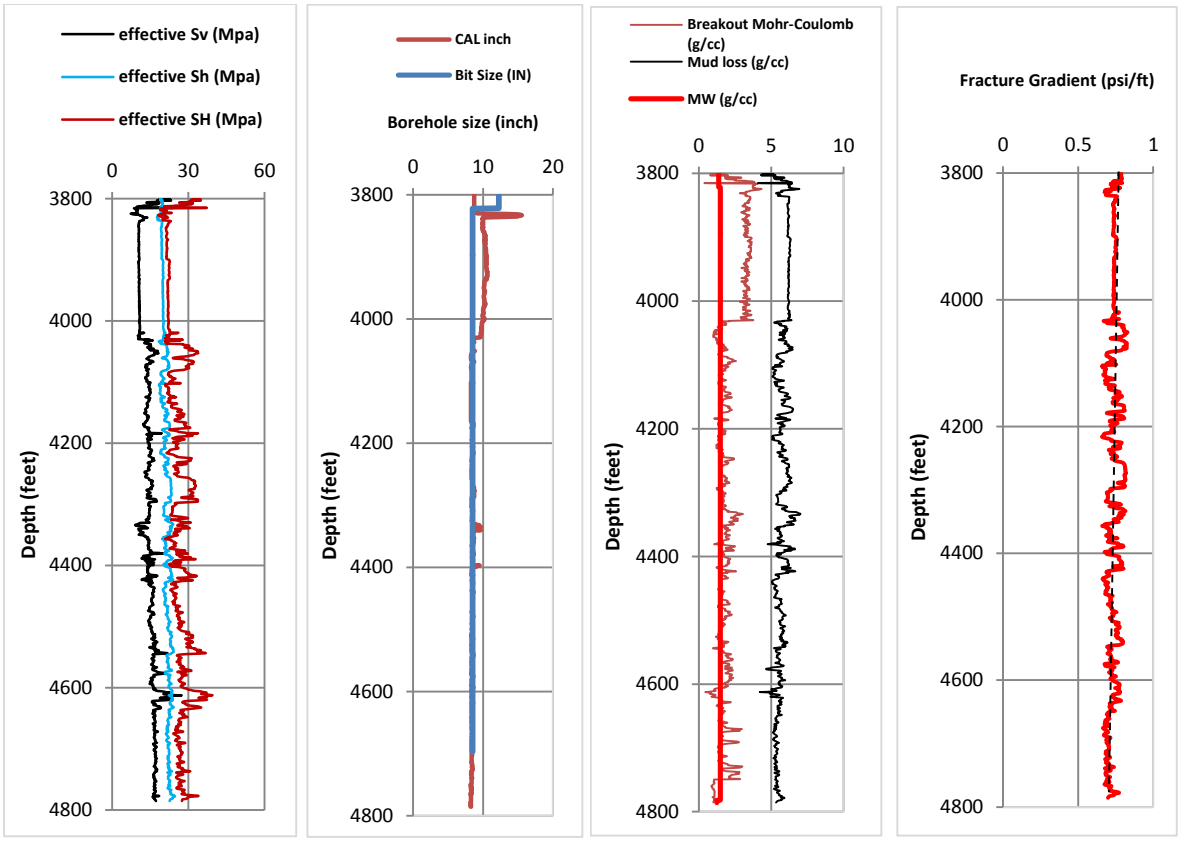

Fig. 6.8 Calibration of the breakout pressure using the caliper log to determine the fracture gradient in Well D

Since selection of the injection rate is related to many parameters considering the scCO$_2$ mixing and residual fluids concerns, the mathematical expression of Eq. (6.1) might be a wise choice to calculate optimum injection rate for CO$_2$ storage under steady-state conditions. This expression is applicable where gas/CO$_2$ is injected through a vertical well located at the center of a brine-filled cylindrical reservoir. In the case of hydraulically fractured vertically wells, horizontal wells, and hydraulically fractured horizontal well, this equation must be modified (Cinar et al., 2008). Moreover, the maximum injection pressure, $P_{w,\,max}$, in Eq. (6.1) can be obtained using analytical approaches and/or through reservoir tests data such as Leak-Off Test (LOT) (Aadnoy and Looyeh, 2011).

$$Qinj_{CO2} = \frac{0.00708(kh)kr_{CO2}(P_{w,\max} - P_e)}{\overline{\mu_{CO2}Bg_{CO2}}\ln\left(\frac{r_e}{r_w}\right)} \tag{6.1}$$

Where $Qinj_{CO2}$ is the CO_2 injection flow rate (Mscf/D), h is the thickness (ft), k is the absolute permeability (mD), Bg_{CO2} is the CO_2 gas formation volume factor (bbl/Mscf), and μ_{CO2} is the viscosity of CO_2 gas (cp). The formation volume factor and gas viscosity are evaluated at the average reservoir pressure where $P_{w,max}$ would be the maximum injection pressure (psia), P_e is the initial reservoir pressure (psia), kr_{CO2} is the CO_2 gas relative permeability, r_e is the external radius of the cylindrical reservoir (ft) and r_w is the internal wellbore radius (ft).

Having all of the required data and considering Eq. (6.1), the injection rate was estimated for the perforated interval (e.g., 4047-4473 ft (426 ft)) as well as the production zones (e.g., 1,2,3 and 4) as given in Table 6.7.

Table 6.7 Reservoir data used to calculate the injection rate

Section	k_{avg} (mD)	h (ft)	k_{rCO2}	$P_{w,max}$ (psia)	P_e (psia)	B_{gCO2} (bbl/Mscf)	μ_{CO2} (cp)	r_e (ft)	r_w, (ft)	$Qinj_{CO2}$ (Mscf/D)
Perforated interval	132	426	0.9	2000	500	3000	0.03	7500	0.6	542
Zone 1	85	280	0.9	2000	500	2500	0.03	7500	0.6	322
Zone 2	160	230	0.9	2000	500	2500	0.03	7500	0.6	497
Zone 3	175	220	0.9	2000	500	2500	0.03	7500	0.6	520
Zone 4	110	54	0.9	2000	500	2500	0.03	7500	0.6	80

When examining this Table 6.7, it is clear that high permeability and large thickness can bear a high injection rate. Although the calculated injection rate may offer a good injectivity, the large volume of $scCO_2$ may require a higher injection rate within the time frame. Thus, it is not possible to select any rates for Zones 1 and 4; hence, the approximate rate of 500 Mscf/D can only be used to evaluate the storage potential for Zone 2, Zone 3 and perforated interval.

6.3 Results and discussion

6.3.1 Depletion and history matching

Before carrying out the injection simulation, the model was calibrated by the history matching of monthly production rates data from 1983 to 2015 to observe reservoir pressures. The Developed PVT model was calibrated for its EoS and then run using Eclipse (E300) for history matching by tuning the relative permeability curves. It is worth noting that historical condensate production rates are difficult to maintain when the reservoir is almost at the residual gas saturation and therefore the simulator brings the bottom-hole pressure down, creating a high gas production rate to compensate this issue. The match between field data and simulated data of water production rate does not look like the best fit that could raise uncertainties in forecast and storage simulations. Historic reservoir data and the simulation match for the reservoir are shown in Figure 6.9.

The history-matched model was then used to forecast the production till 2018. After observing insignificant gas production beyond 2018, the production was stopped and the reservoir model was kept on shut-in for two years, i.e. from 2019-2020, to allow the reservoir pressure to stabilise prior to CO_2 storage.

According to the history match model, the reservoir was estimated to be depleted by 2018 with a maximum forecasted gas recovery based on the sensitivity analysis conducted. The reservoir was predicted to experience approximately 500 psia pressure drop from the initial reservoir pressure of 2405 psia by 2015. However, further reduction of the reservoir pressure was not anticipated because the reservoir is connected to an extensive aquifer with a limited pressure support. This behavior is similar to the carbonate condensate reservoir of Malaysia which has a strong aquifer support and almost similar structure and characteristics (Jalil et al., 2012).

Figure 6.10 displays the distribution of gas, condensate and water phases in the reservoir from 1983 to the end of the reservoir development plan in 2018 where most of the reservoir was invaded by brine.

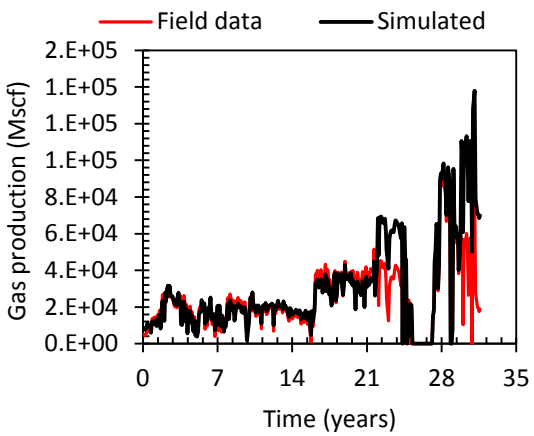

(a) Monthly gas production rate

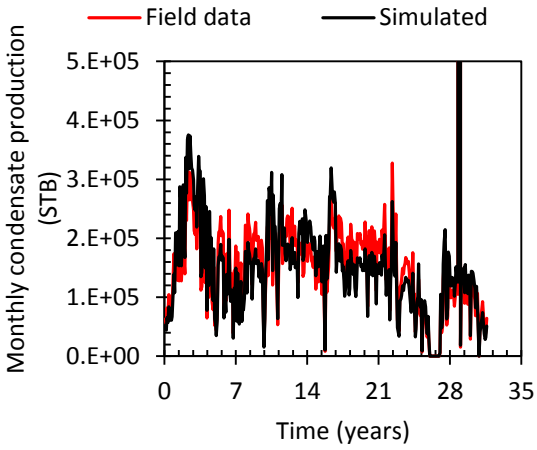

(b) Monthly oil production rate

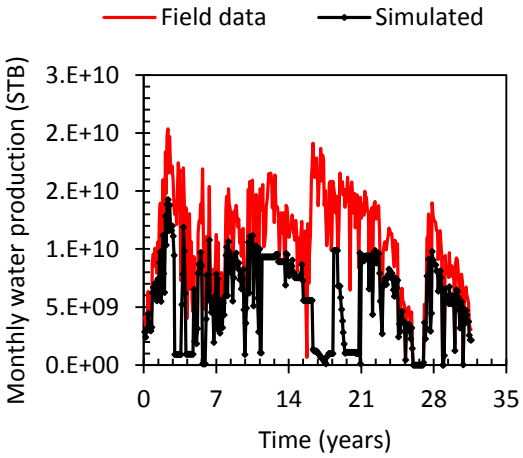

(c) Monthly water production rate

Fig. 6.9 History matching of production data from 1983 to 2015

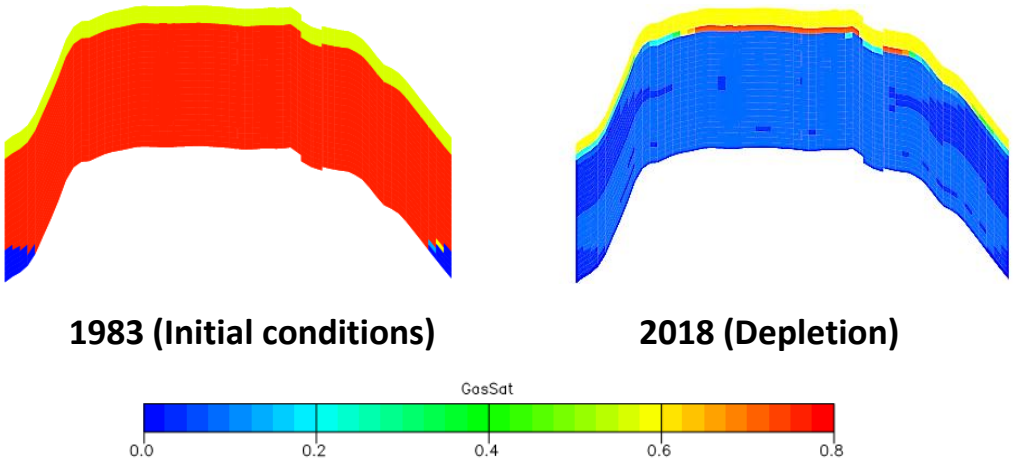

Fig. 6.10 Saturation in the reservoir interval showing a gas saturation of 80% in 1983 (left), which has been swept by water in 2018 (right)

6.3.2 CO_2 storage simulation

The results obtained from the simulation of history matching were used for initialization of the CO_2 storage model. This is different from initializing the entire reservoir model at the residual saturation, allowing to study the performance of CO_2-EOR operations while considering historical production data. In this section, an operation starting from 2021 to 2040 was modelled to initialize the entire reservoir model at the residual saturation.

For CO_2 injection simulations, a comprehensive evaluation was conducted to assess the potential storage capacity of the site. This analysis was carried out for each zone individually considering the bottom-hole injection pressure threshold of 2000 psia. It has been generally implemented in many CO_2 pilot EOR-storage projects where CO_2 was injected in the lower structure of the reservoir (Zhou et al., 2005; Dance, 2013). This is done to have efficient trapping and avoid caprock over-pressurization by the CO_2 mobile phase. Thus, the perforated interval was not considered as it is mainly covering Zone 1 which should not be selected due to the restrict plume movement by the caprock.

In this assessment, an optimum rate of 500 Mscf was used in the storage simulation, instead of choosing different injection rates, to achieve a desired storage potential equal or less than the effective storage potential within 20 years of the injection period. Figure 6.11 plots the trend of FGIR (field gas injection rate) against time at the injection rates of 500 Mscf/D. When examining this figure, it is observed that the injectivity behavior in the four zones is not the same and starts to decline in different zones at different time periods. It is also seen that, unlike Zone 1 and Zone 4, injectivity is sustainable in Zone 2 and Zone 3 for up to 14 and 15 years, respectively. Rock characteristics are affecting the stability of the injection rate and stabilised injection rates are achievable where the reservoir is composed of intervals with high porosity, permeability, and quality lithofacies. Zone 4 is a very low quality interval connected to a wide spread aquifer which should not be chosen as part of the storage operation. Thus, the intervals from 4200 ft to 4470 ft (i.e., Zone 2) and 4470 ft to 4720 ft (i.e., Zone 3) are the best intervals for injection. It would also be possible to

select a low injection rate for Zones 1 and 4, as the injection rate of 500 Mscf/D does not seem to be sustainable after 50% of the injection.

To further evaluate the storage behavior at the injection rate of greater than the estimated rate of 500 Mscf/D, the reservoir model was simulated at 600 Mscf/D. Figure 6.12 shows the injectivity trend at 600 Mscf/D. The high injection rate observed in this figure is causing an earlier decline in the rate of all zones compared to the case where the injection rate of 500 Mscf/D was selected. This confirms that the optimum injection rate initially selected is feasible to for the storage operation.

The storage capacity of a depleted gas reservoir is known to be the effective pore volume available for storage purposes, which can be estimated by using a volumetric method and/or production data. This estimation can then be validated by the compositional modeling, considering reservoir injectivity and injection constraints (Jalil et al., 2012). As mentioned in Chapter 3, estimated storage capacity was up to 3.16 Tscf. The simulation results indicate that the maximum cumulative CO_2 injected through Zones 1 to 4 are around 2.416 Tscf, 2.78 Tscf, 2.88 Tscf, and 2.419 Tscf, respectively at the end of 20 years as shown in Figure 6.13. The cumulative CO_2 injected are almost similar for Zones 1 and 4 a quite different for Zones 2 and 3. This is probably due to the different injectivity behavior of these zones at 500 Mscf/D. The achievable storage volume is maximum in Zone 3 compared to other zones and less than the volumetric estimation of 3.16 Tscf. It is worth mentioning that the injected volume is low in all zones even at 600 Mscf/D compared to the 500 Mscf/D case as shown in Figure 6.14.

It also shows that Zone 3 has the maximum potential to have CO_2 compared to others at 600 Mscf/D. This indicates the fact that even much more CO_2 can be injected in this reservoir but one should assure that the injection pressure would not exceed the fracture pressure of the medium (Rutqvist et al., 2007; Dempsey et al., 2014).

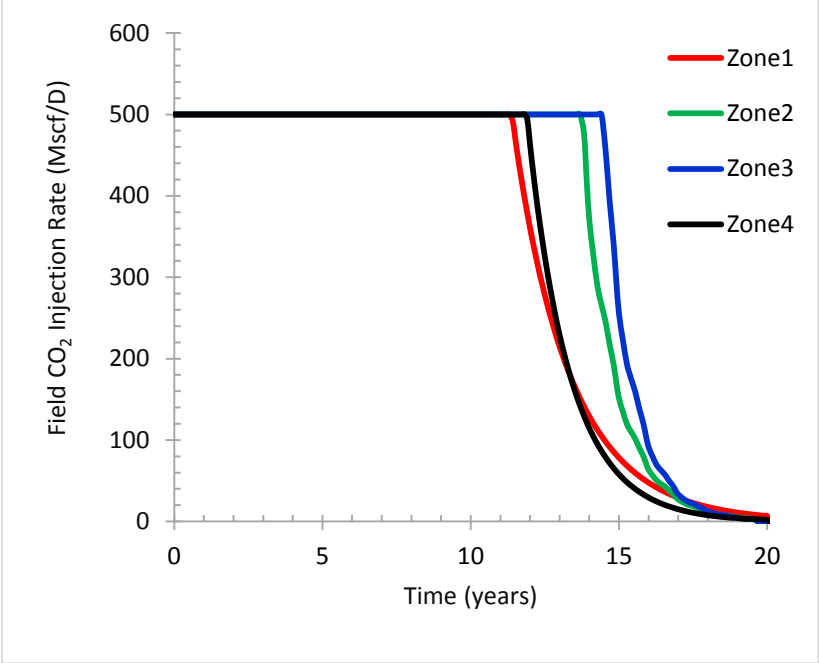

Fig. 6.11 CO_2 Injection rate in different zones for 20 years at 500 Mscf/D

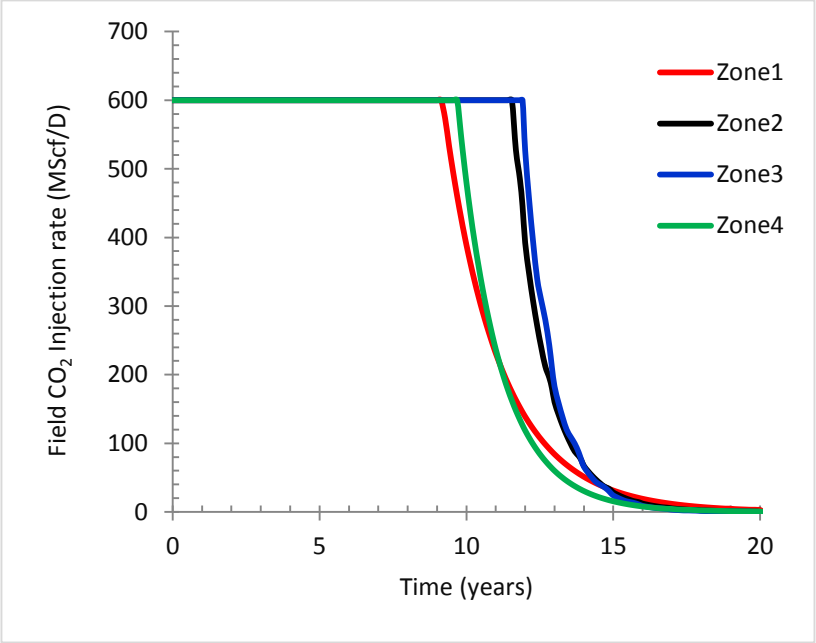

Fig. 6.12 CO_2 Injection rate in different zones for 20 years at 600 Mscf/D

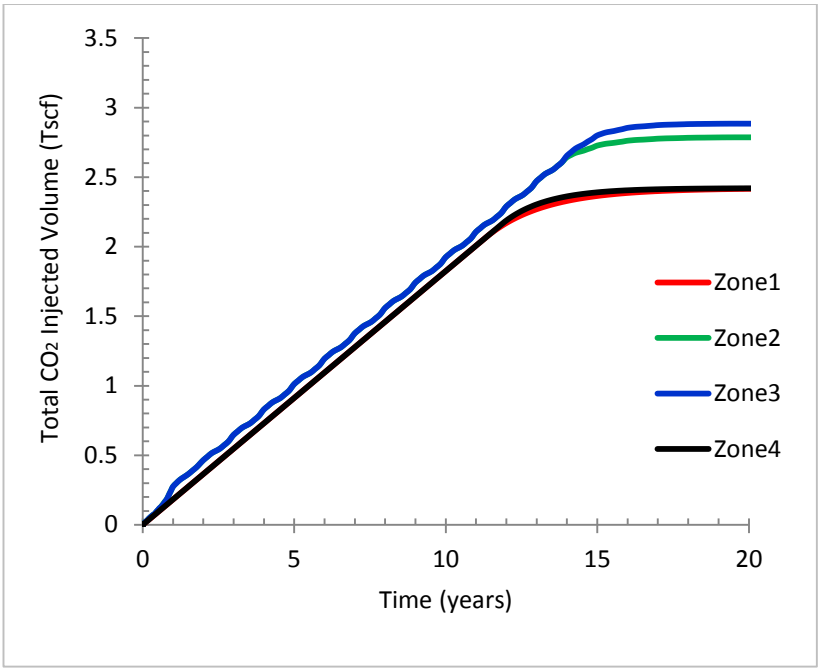

Fig. 6.13 Total CO_2 injection volume in different zones during 20 years injection period at 500 Mscf/D

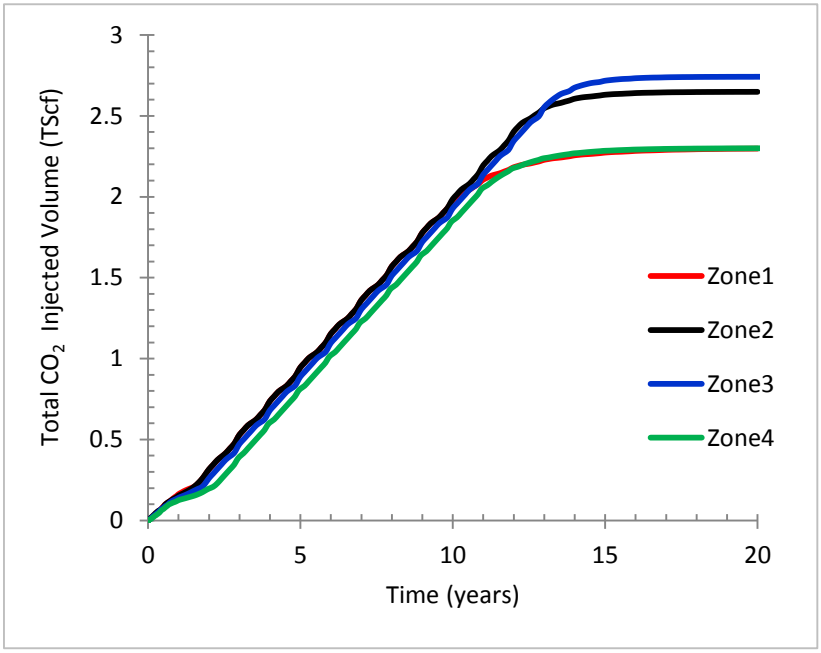

Fig. 6.14 Total CO_2 injection volume in different zones during 20 years injection period at 600 Mscf/D

On the other hand, increasing the injection pressure during the recovery by the condensate re-vaporization (Narinesingh and Alexander, 2014) would be a concern which needs to be addressed when CO_2 injection is taking place in a depleted condensate gas reservoir. It is known that there are four major trapping mechanisms

for CO_2 storage in a gas reservoir. These trapping mechanisms are fully coupled and competitive with each either and, hence, their contribution to CO_2 storage differs with time and space.

Figures 6.15 and 6.16 show the volume and percentage of CO_2 in different phases over time for all zones of gas reservoirs. Within the conditions mentioned in this study, CO_2 is within the supercritical condition and resides mainly in the bulk of the space in the reservoir, while some amount is capillary trapped and dissolved at the early stage of injection. With continuous injection, CO_2 in other phases continues to increase at the end of injection after 20 years, in which CO_2 is trapped under the supercritical phase in different zones within the range of 40% to 48%.

Residual and dissolved trappings are significant and within the range of 14-27% in short-term geological storage. As time passes, the residual phenomenon becomes significant, resulting in the increase of capillary phase while dissolution takes place with a slow rate, enhancing CO_2 residual trapping and dissolution in brine. On the other hand, CO_2 in the supercritical phase is reduced as time passes. At the end of 1000 years, the reservoir shows a good potential for residual trapping and dissolution particularly in Zones No. 2 and 3, where the residual and solubility trapping immobilized more than half of the total CO_2 at the end of 1000 years. It is worth to mention that average CO_2 residual trapping potential of all zones after 20 years and 1000 years is 24% which is approximately near to the estimated residual CO_2 saturation value of 26.5% in reservoir by the proposed method as presented in Chapter 4. Practically, the solubility trapping increases when the capillary trapped CO_2 starts to dissolve into brine (IPCC, 2005-pp208). On these occasions, the dissolution rate is controlled by the rate at which dissolved CO_2 is transported away from the interface of CO_2 and brine, allowing fresh brine to be in close contact with free-phase CO_2 (Emami-Meybodi et al., 2015). The pressure reduction due to CO_2 dissolution enhanced by convective mixing (Mohamed and Nasr-El-Din, 2013), depending on the pressure and temperature condition as well as brine salinity (Saeedi, 2012). It is observed that the percentage of CO_2 in different phases relative to the pore volume is highest in Zone 3 and lowest in the Zone 1 as shown in Figure.

6.16, which might be attributed to the good Injectivity. Zone 4 does not seem to be suitable as it is attached to an aquifer.

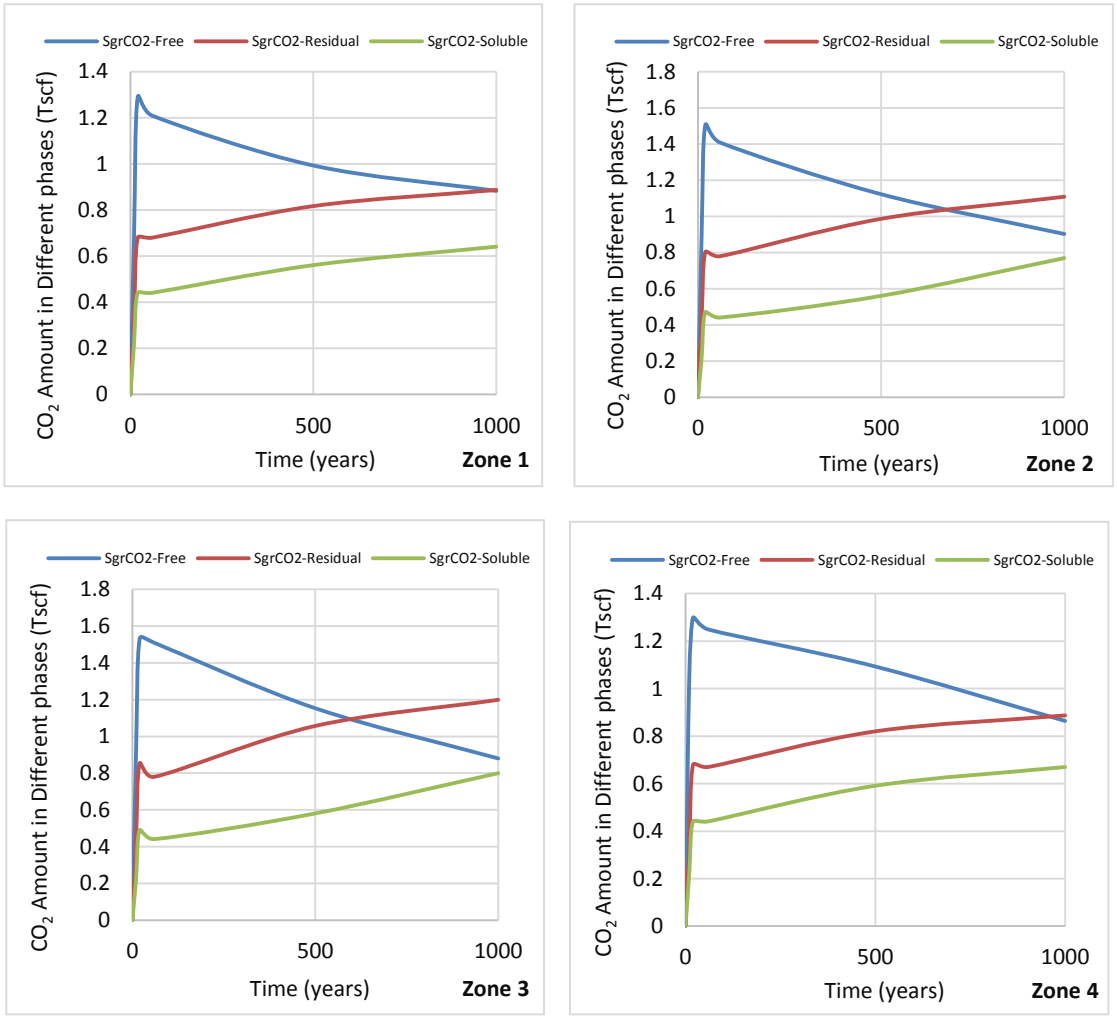

Fig. 6.15 The amount of CO_2 in different phases and its trends in different zones at 500 Mscf/D

6.3.3 CO_2 plume movement

Movements of CO_2 plume during the injection period in the case of 500 Mscf/D injection in Zone 3 is another factor of storage capacity assessment. The reservoir should accept and store CO_2 during the injection period, and provide acceptable containment for the post-injection by trapping the injected CO_2 via different mechanisms such as structural, residual, solubility, and mineral trappings. To evaluate the plume movement for the injection period, the numerical modeling was run for CO_2 storage by overlooking the geochemical reactions. Figure 6.17 shows CO_2 saturation in the reservoir over 20 years of the injection period.

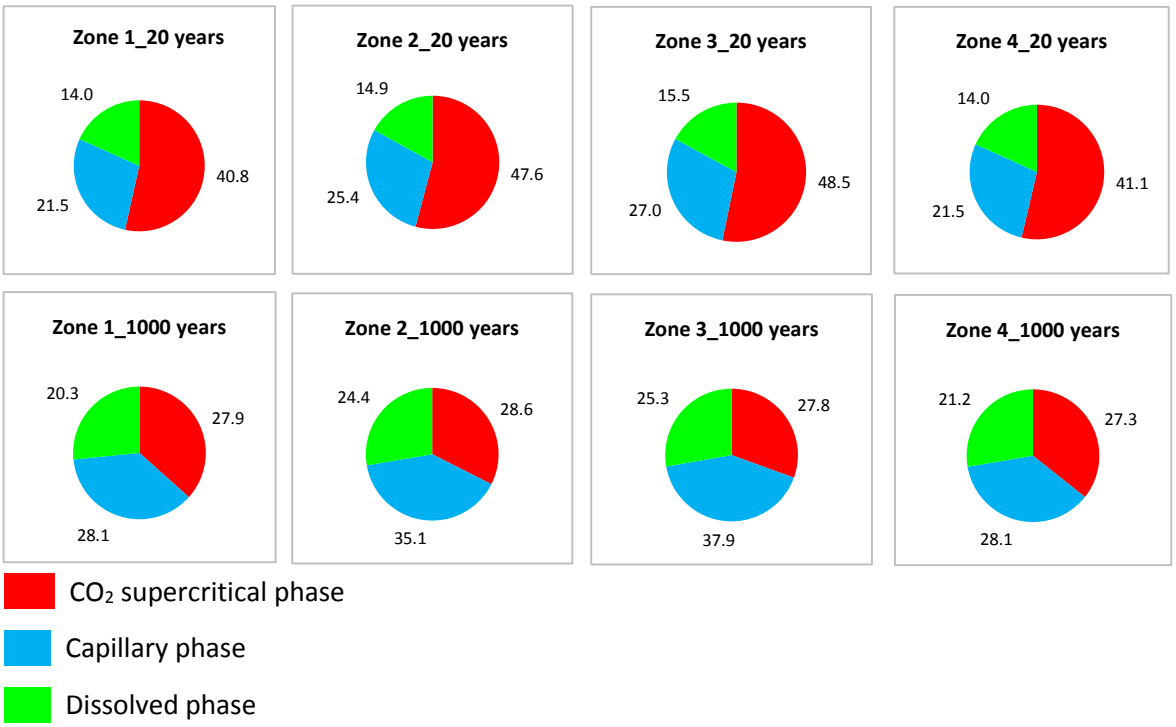

Fig. 6.16 Percentage of CO_2 in different phases after 20 years and 1000 years in different zones at 500 Mscf/D

As it is seen in Figure 6.17, because of gravitational forces and aquifer supported stabilization of the reservoir pressure, CO_2 moves up, towards the center of the anticline, with the plume's areal extension around the model boundaries shrinking. The anticline structure of the reservoir provides a structural trap for CO_2 in supercritical phase. High-permeability channels in the reservoir are the main conduits to move the fluids out of the zone, which could result in free CO_2 migration towards the upper structure and breaching of the caprock. This breaching in long-term could be due to caprock over-pressurization by free CO_2 saturation and thus overcoming the capillary threshold of the caprock. This high vertical fracture reservoir could enhance the risk of leakage in long-term regardless of tight strips among the separated zones. Considering the significant geomechanical-geochemical interactions upon CO_2 injection (Zhang et al. 2016a, b) and its effect on the strength of the reservoir and caprock (Espinoza et al., 2011; Varre et al., 2015; Erickson et al., 2015), it is suggested to conduct extended simulation for long term CO_2 plume movement by including the geochemical reactions.

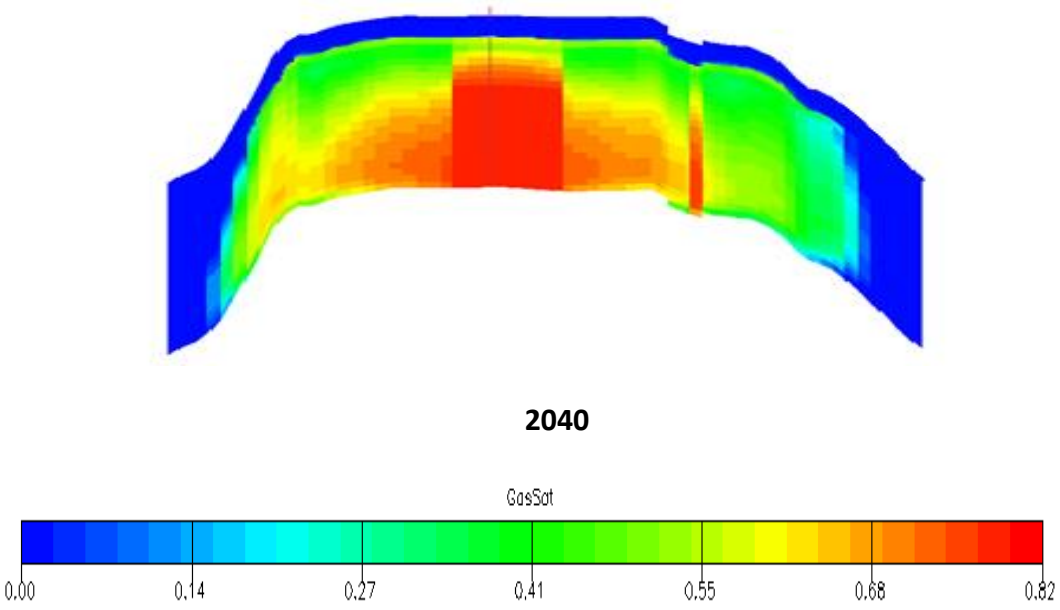

Fig. 6.17 Simulation results indicating that injected CO_2 stays and equilibrates within the site

6.4 Summary of chapter

In this study, a 3-D numerical model of condensate carbonate gas reservoir in a carbonate basin of Malaysia was developed to evaluate key CO_2 storage aspects. The steady-state injection analytical expression was proposed to calculate the optimum injection rate by integrating the effect of remaining hydrocarbons in CO_2 relative permeability. Prediction of the reservoir fluid phase behavior and history matching was carried using reservoir information and 32 years of gas production history data. The history matched-model was employed to quantify the effective CO_2 storage potential of the reservoir.

For the storage, $scCO_2$ was injected for 20 years followed by 1000 years of observation after injection to confirm the safe storage and recognize any potential leakages. The results obtained revealed that the optimum injection rate selected based on reservoir information is a good strategy to evaluate the injectivity of reservoir's zones and effective storage potential. It was also observed that injectivity is reasonable in Zones No. 2 and 3 in which the maximum volume of CO_2 can be

stored. This behavior is in consistent with the preliminary assessment of CO_2 injectivity. In a short or middle term, 40-48% of injected CO_2 can be trapped in the supercritical phase by injection in different zones, while in the long-term (hundreds of years), residual and solubility trappings are dominant. However, the reservoir has a good potential for a CO_2 storage practice, but there might be some difficulties faced in term of geochemical activity and seal pressurization due to the high heterogeneity level, compaction behavior and aquifer supports of the reservoir.

CHAPTER 7

CONCLUSIONS AND RECOMMENDATIONS

7.1 Introduction

This study was carried out to characterize a carbonate gas reservoir located in Malaysia for its CO_2 storage potential and to address different aspects of CO_2 storage and highlight the major steps which must be taken for evaluation of CO_2 storage sites. The main aim was to conduct a preliminary assessment of the storage site, CO_2 residual trapping methods, geomechanical and geochemical interactions, and selection of optimum CO_2 injection rate for CO_2 storage in petroleum reservoirs.

This chapter concludes the key findings of this study, which are worthy of consideration when CO_2 storage reservoir characterizations is done for any gas reservoirs. This last chapter also provides few recommendations for future works in this research area.

7.2 Conclusions

7.2.1. Preliminary characterization for CO_2 storage

Preliminary characterization of the carbonate gas reservoir was carried out based on a newly presented screening criteria and available data. It was found that the new screening criteria is a comprehensive tool at the field scale for a thorough evaluation of petroleum reservoirs and their storage potentials. It was concluded that availability of data from petroleum reservoirs plays a key role to execute the screening tool for a thorough assessment of storage potentials. Although, the screening tool proposed in this study for wellbore and zonal evaluation could not be applied to all wells in the carbonate reservoir due to the absence of data, the result indicates that the chosen reservoir can be a suitable site.

From the preliminary characterization of the gas reservoir, it was found that the reservoir is a suitable place for CO_2 storage based on its geometry, rock

characteristics, and subsurface conditions. The preliminary evaluation of the injection well was also highlighted that the wellbore and hydraulic integrity related analysis of the reservoir/caprock must be done to ensure the potential of the injection wells.

7.2.2. A new method for estimating CO_2 residual trapping

In this study, a new method was developed for determination of residual CO_2 saturation at the reservoir scale, which was validated by numerical and experimental modeling. This method was based on the residual hydrocarbon saturation, interfacial tension, pore geometry, and wettability of reservoir rocks, which were found to be the major factors controlling the residual CO_2 saturation.

Applying this method to the carbonate gas reservoir, the residual trapping potential was determined by wireline logs at the reservoir scale, where it was found that the maximum volume of CO_2 that could be residually trapped in the reservoir is approximately 0.965 Tscf of the effective pore volume. It was also revealed that the residual trapping ability becomes maximum at a low pressure and begins to decrease with the increase of pressure. This is due to the decrease of the interfacial tension with the increase of pressure. Validation of the estimated CO_2 residual saturation, however, was not possible due to the absence of core plugs representing the carbonate gas reservoir.

7.2.3. Injectivity evaluation and reservoir integrity

Significant variation in the pressure drop is initially observed upon $scCO_2$ injection. From ultrasonic pulse measurements, it was highlighted that there is a significant effect of injection (i.e., increases in the pore pressure) and in-situ stress (i.e., confining pressure) on the acoustic response of the sample, when it is saturated with brine and flooded by $scCO_2$. In addition, the increase of the confining pressure was increasing the density and bulk modulus of the samples, which was due to the compaction effect. On the other hand, as the in-situ stress decreased due to the increase of pore pressure, the stiffness and strength of the rock samples reduced remarkably. This helps to have a better understanding of possible changes taking place in the geomechanical parameters of the storage site during and after injection.

Evaluating the texture and microstructure of the sample before and after exposure to $scCO_2$ using imaging analysis in different scales indicated a clear alteration of the sample structure after $scCO_2$ injection due to carbonate dissolution, kaolinite break-down and corrosion of quartz, which resulted in the reduction of the shear modulus.

7.2.4. CO_2 storage numerical modeling

The carbonate gas reservoir was numerically modeled in this study for its CO_2 storage, and the key storage aspects were evaluated at different injection rates. It was then revealed that the optimum injection rate calculated based on the petrophysical and geomechanical analysis is a good strategy to evaluate the storage potential. At this optimum injection rate, the reservoir model shows a favorable storage capacity, injectivity, and trapping mechanisms compared to any other injection rates. It was found that the average CO_2 residual trapping potential of all zones after 20 years and 1000 years is 24% which is approximately near to the estimated residual CO_2 saturation value of 26.5% in reservoir by the proposed CO_2 residual trapping method. The movement of CO_2 plume was also determined in short-term to govern the potential leakage of CO_2, where it was concluded that anticline structure of the reservoir provides a structural trap for CO_2 in supercritical phase. High-permeability channels and geochemical activity in reservoirs/caprock could damage the containment of storage medium and can result the CO_2 leakage.

In general, the results obtained from this research could enable the petroleum industry to characterize reservoirs for CO_2 storage in depleted reservoirs of Malaysia and worldwide.

7.3 Recommendations

Following the course of this study, a few recommendations for future research have been identified.

A frequent feature in the report of this thesis is the lack of CO_2 storage reservoir information and related experimental data/core sample measurements. For instance, a comprehensive screening criteria that has been developed to assess the

suitability of the reservoir requires more real reservoir CO_2 storage data to recheck its validity. Similarly, screening criteria developed for injection well evaluation are valuable tool, but the results of gas reservoir must be further validated by performing numerical simulations of all the existing wells. Although the residual trapping approach provides a good result for a water-wet system, more experimental studies are required to extend its application for other rock wetting characteristics. Moreover, the residual trapping ability of the gas reservoir predicted by the proposed approach could be further validated by a two-phase core flooding experiment if reservoir core plugs are available. Regarding the compaction effect in sandstone, due to absence of core plugs/data of the carbonate gas reservoir, injectivity, three-phase relative permeability and few other parameters such as mineralogical interaction of the reservoir/caprock with $scCO_2$ as well as the seal capacity, seal geometry and stress characterization of the caprock could not be studied. Therefore, it is recommended that a series of experimental and numerical studies on different uncover aspects of carbonate gas reservoir be performed to ensure that CO_2 injectivity does not pose any problems.

Bibliography

AADNOY, B., LOOYEH, R., 2011. Petroleum rock mechanics: drilling operations and well design. Gulf Professional Publishing, 1st Edition, 1-370.

ABBASOV, Z. Y. & FATALIYEV, V. M. 2016. The effect of gas-condensate reservoir depletion stages on gas injection and the importance of the aerosol state of fluids in this process. *Journal of Natural Gas Science and Engineering,* 31, 779-790.

ABID, K., GHOLAMI, R., CHOATE, P. & NAGARATNAM, B. H. 2015. A review on cement degradation under CO_2-rich environment of sequestration projects. *Journal of Natural Gas Science and Engineering, Elsevier,* 27, 1149-1157.

ADISOEMARTA, P. S., FRAILEY, S. M. & LAWAL, A. S. 2004. Measured z-factor of CO_2-dry gas/wet gas/gas condensates for CO_2 storage in depleted gas reservoirs. *SPE/DOE Symposium on Improved Oil Recovery, 17-21 April, Tulsa, Oklahoma.* Society of Petroleum Engineers, 1-11.

AHMED, T. 2001. Reservoir engineering handbook. *Gulf Professional Publishing, Elsevier,* 3rd Edition, 1-1235.

AKINTUNDE, O., KNAPP, C. & KNAPP, J. 2013. Petrophysical characterization of the south georgia rift basin for supercritical CO_2 storage: A Preliminary assessment. *Environmental Earth Sciences,* 70, 2971-2985.

AKUTSU, T., YAMAJI, Y., YAMAGUCHI, H., WATANABE, M., SMITH, R. L. & INOMATA, H. 2007. Interfacial tension between water and high pressure CO_2 in the presence of hydrocarbon surfactants. *Fluid phase equilibria, Elsevier,* 257, 163-168.

AL-ABRI, A. S. 2011. *Enhanced gas condensate recovery by CO_2 injection.* PhD Thesis PhD, Curtin University of Technology. Faculty of Science and Engineering. Department of Petroleum Engineering, 1-100.

AL-HASAMI, A., REN, S. & TOHIDI, B. CO_2 injection for enhanced gas recovery and geo-storage: reservoir simulation and economics. SPE Europec/EAGE Annual Conference, 13-16 June, Madrid, Spain, 2005. Society of Petroleum Engineers, 1-7.

AL-KHDHEEAWI, E. A., VIALLE, S., BARIFCANI, A., SARMADIVALEH, M. & IGLAUER, S. 2017. Effect of brine salinity on CO_2 plume migration and trapping capacity in deep saline aquifers. *The APPEA Journal,* 57, 100-109.

AL-MENHALI, A. & KREVOR, S. Residual trapping of CO_2 in water-wet and mixed-wet carbonates for carbon utilization in mature carbonates oil fields. International Petroleum Technology Conference, 6-9 December, Doha, Qatar, 2015, 1-12.

AL-MENHALI, A. S. & KREVOR, S. 2016. Capillary trapping of CO_2 in oil reservoirs: Observations in a mixed-wet carbonate rock. *Environmental Science & Technology,* 50, 2727-2734.

AL-KHDHEEAWI, E. A., VIALLE, S., BARIFCANI, A., SARMADIVALEH, M. & IGLAUER, S. 2016. Influence of CO_2-wettability on CO_2 migration and trapping capacity in deep saline aquifers. *Greenhouse Gases: Science and Technology*. 7 (2), 328–338.

ALAVIAN, S. A. & WHITSON, C. H. Scale dependence of diffusion in naturally fractured reservoirs for CO_2 injection. SPE Improved Oil Recovery Symposium, 24-28 April, Tulsa, Oklahoma, USA, 2010. Society of Petroleum Engineers, 1-11.

ALEMU, B. L., AKER, E., SOLDAL, M., JOHNSEN, Ø. & AAGAARD, P. 2013. Effect of sub-core scale heterogeneities on acoustic and electrical properties of a reservoir rock: A CO_2 flooding experiment of brine saturated sandstone in a computed tomography scanner. *Geophysical Prospecting,* 61, 235-250.

ALMANSOORI, S. K., PENTLAND, C. H., IGLAUER, S. & BLUNT, M. J. 2009. Three phase measurements of nonwetting phase trapping in unconsolidated sand packs. *SPE Annual Technical Conference and Exhibition, 4-7 October, New Orleans, Louisiana.* Society of Petroleum Engineers, 1-12.

ALONSO, J., NAVARRO, V. & CALVO, B. 2012. Flow path development in different CO_2 storage reservoir scenarios: A critical state approach. *Engineering Geology,* 127, 54-64.

ALSHARHAN, A. S. 2000. Stylolites in lower cretaceous carbonate reservoirs, UAE. *Society of Sedimentary Geology*, 185-209.

AMBROSE, W. A., LAKSHMINARASIMHAN, S., HOLTZ, M. H., NÚÑEZ-LÓPEZ, V., HOVORKA, S. D. & DUNCAN, I. 2008. Geologic factors controlling CO_2 storage capacity and permanence: Case studies based on experience with heterogeneity in oil and gas reservoirs applied to CO_2 storage. *Environmental Geology,* 54, 1619-1633.

AMYX, J. W., BASS, D. M. & WHITING, R. L. 1960. *Petroleum reservoir engineering: Physical properties*, McGraw-Hill College, 133-150.

ANDRÉ, L., PEYSSON, Y. & AZAROUAL, M. 2014. Well injectivity during CO_2 storage operations in deep saline aquifers – Part 2: Numerical simulations of drying, salt deposit mechanisms and role of capillary forces. *International Journal of Greenhouse Gas Control,* 22, 301-312.

ANDREW, M., BIJELJIC, B. & BLUNT, M. J. 2014. Pore-scale imaging of trapped supercritical carbon dioxide in sandstones and carbonates. *International Journal of Greenhouse Gas Control,* 22, 1-14.

ARIF, M., BARIFCANI, A. & IGLAUER, S. 2016. Solid/CO_2 and solid/water interfacial tensions as a function of pressure, temperature, salinity and mineral type: Implications for CO_2-wettability and CO_2 geo-storage. *International Journal of Greenhouse Gas Control,* 53, 263-273.

ASSAAD, F. A. 2008. *Field methods for petroleum geologists: A guide to computerized lithostratigraphic correlation charts case study: Northern Africa*, Springer-Verlag Berlin Heidelberg, 1-112.

ATAIE-ASHTIANI, B., MAJID HASSANIZADEH, S. & CELIA, M. A. 2002. Effects of heterogeneities on capillary pressure–saturation–relative permeability relationships. *Journal of contaminant hydrology,* 56, 175-192.

ATKINSON, G., BLOCH, S. & SCHEIHING, M. 1990. Sedimentology and depositional environments of the Oligo-Miocene gas-bearing succession in the Yacheng 13–1 field, South China Sea, People's Republic of China. *AAPG Bulletin,* 74, 601.

AZIN, R., NASIRI, A. & ENTEZARI, J. 2008. Underground gas storage in a partially depleted gas reservoir. *Oil & Gas Science and Technology-Revue de l'IFP,* 63, 691-703.

AZIZI, E. & CINAR, Y. 2013. Approximate analytical solutions for CO_2 injectivity into saline formations. *SPE Reservoir Evaluation & Engineering*, 1-11.

BACCI, G., KORRE, A. & DURUCAN, S. 2011. An experimental and numerical investigation into the impact of dissolution/precipitation mechanisms on CO_2 injectivity in the wellbore and far field regions. *International Journal of Greenhouse Gas Control,* 5, 579-588.

BACHU, S. 2001. Screening and ranking of hydrocarbon reservoirs for CO_2 storage in the Alberta Basin, Canada. US Department of Energy–National Energy Technology Laboratory, National Conference on Carbon Sequestration, 1-60.

BACHU, S. 2003. Screening and ranking of sedimentary basins for sequestration of CO_2 in geological media in response to climate change. *Environmental Geology,* 44, 277-289.

BACHU, S. 2004. Evaluation of CO_2 sequestration capacity in oil and gas reservoirs in the Western Canada Sedimentary Basin. *Alberta Geological Survey, Alberta Energy and Utilities Board March.* Alberta, Canada. 1-77.

BACHU, S., BONIJOLY, D., BRADSHAW, J., BURRUSS, R., HOLLOWAY, S., CHRISTENSEN, N. P. & MATHIASSEN, O. M. 2007. CO_2 storage capacity estimation: Methodology and gaps. *International Journal of Greenhouse Gas Control,* 1, 430-443.

BACHU, S. & WATSON, T. L. 2009. Review of failures for wells used for CO_2 and acid gas injection in Alberta, Canada. *Energy Procedia,* 1, 3531-3537.

BANDARA, U. C., TARTAKOVSKY, A. M. & PALMER, B. J. 2011. Pore-scale study of capillary trapping mechanism during CO_2 injection in geological formations. *International Journal of Greenhouse Gas Control,* 5, 1566-1577.

BARRUFET, M. A., BACQUET, A. & FALCONE, G. 2010. Analysis of the storage capacity for CO_2 sequestration of a depleted gas condensate reservoir and a saline aquifer. *Journal of Canadian Petroleum Technology,* 49, 23-31.

BEDARD, K., MALO, M., DUCHAINE, Y., KONSTANTIVOVSKAYA, E. & GIROUX, B. Potential CO_2 geological storage sites for carbon capture and storage (CCS) in Québec St. Lawrence Lowlands-A preliminary analysis. AAPG Search and Discovery Article #90172 © CSPG/CSEG/CWLS GeoConvention 2010, Calgary, Alberta, Canada, May 10-14, 2010, 1-4.

BENNACEUR, K., GIELEN, D., KERR, T. & TAM, C. 2008. CO_2 capture and storage: a key carbon abatement option, International energy agency, 1-266.

BENNION, D. B. & BACHU, S. 2006. Dependence on temperature, pressure, and salinity of the IFT and relative permeability displacement characteristics of CO_2 injected in deep saline aquifers. SPE Annual Technical Conference and Exhibition, 24-27 September, San Antonio, Texas, USA: Society of Petroleum Engineers: 1-5.

BLACK, J. R., CARROLL, S. A. & HAESE, R. R. 2015. Rates of mineral dissolution under CO_2 storage conditions. *Chemical Geology,* 399, 134-144.

BLOCH, S. 1991. Empirical prediction of porosity and permeability in sandstones. *AAPG bulletin,* 75, 1145-1160.

BRADFORD, I., FULLER, J., THOMPSON, P. & WALSGROVE, T. Benefits of assessing the solids production risk in a North Sea reservoir using elastoplastic modelling. SPE/ISRM Rock Mechanics in Petroleum Engineering, 8-10 July, Trondheim, Norway, 1998. Society of Petroleum Engineers, 1-9.

BRYANT, E. 1997. *Climate process and change*, School of Geoscience, Cambridge University Press, 1-100.

BURKE, L. 2011. Carbon dioxide fluid-flow modeling and injectivity calculations, p. 16. U.S. Geological Survey Scientific Investigations Report 2011-5083.

BURNSIDE, N. M. & NAYLOR, M. 2014. Review and implications of relative permeability of CO_2/brine systems and residual trapping of CO_2. *International Journal of Greenhouse Gas Control,* 23, 1-11.

BUSCHECK, T. A., FRIEDMANN, S. J., SUN, Y., CHEN, M., HAO, Y., WOLERY, T. J. & AINES, R. D. Active CO_2 reservoir management for CO_2 capture utilization and storage: An approach to improve CO_2 storage capacity and to reduce risk. Carbon Management Technology Conference, 7-9 February, Orlando, Florida, USA, 2012. Carbon Management Technology Conference, 1- 18.

CAMPOS, R., BARRIOS, I. & LILLO, J. 2015. Experimental injection: Study of physical changes in sandstone porous media using Hg porosimetry and 3D pore network models. *Energy Reports,* 1, 71-79.

CAREY, J. W., WIGAND, M., CHIPERA, S. J., WOLDEGABRIEL, G., PAWAR, R., LICHTNER, P. C., WEHNER, S. C., RAINES, M. A. & GUTHRIE, G. D. 2007. Analysis and performance of oil well cement with 30 years of CO_2 exposure from the SACROC Unit, West Texas, USA. *International Journal of Greenhouse Gas Control,* 1, 75-85.

CARNEIRO, J. F. & ALBERTO, M. 2014. Preliminary assessment of CO_2 storage potential in the Rovuma Sedimentary Basin, Mozambique. *Energy Procedia,* 63, 5141-5152.

CHADWICK, A., ARTS, R., BERNSTONE, C., MAY, F., THIBEAU, S. & ZWEIGEL, P. 2008. Best practice for the storage of CO_2 in saline aquifers. *British Geological Survey Occasional Publication,* 14, 267.

CHALBAUD, C., ROBIN, M., LOMBARD, J. M., MARTIN, F., EGERMANN, P. & BERTIN, H. 2009. Interfacial tension measurements and wettability evaluation for geological CO_2 storage. *Advances in Water Resources,* 32, 98-109.

CHALBAUD, C., ROBIN, M., LOMBARD, J.-M., BERTIN, H. & EGERMANN, P. 2010. Brine/CO_2 interfacial properties and effects on CO_2 storage in deep saline aquifers. *Oil & Gas Science and Technology–Revue de l'Institut Français du Pétrole,* 65, 541-555.

CHEN, H., YANG, S., HUAN, K., LI, F., HUANG, W., ZHENG, A. & ZHANG, X. 2013. Experimental study on monitoring CO_2 sequestration by conjoint analysis of the P-wave velocity and amplitude. *Environmental science & technology,* 47, 10071-10077.

CHENG, L. 2012. Advances in multiphase flow and heat transfer. 1 ed. Sharjah: Bentham Science Publishers, Vol. 3, 1-00.

CHESTER, F., CHESTER, J., KRONENBERG, A. & HAJASH, A. 2007. Subcritical creep compaction of quartz sand at diagenetic conditions: Effects of water and grain size. *Journal of Geophysical Research: Solid Earth,* 112, 1-15.

CHEVALIER, G., DIAMOND, L. W. & LEU, W. 2010. Potential for deep geological sequestration of CO_2 in Switzerland: A first appraisal. *Swiss Journal of Geosciences,* 103, 427-455.

CHIARAMONTE, L., ZOBACK, M., FRIEDMANN, J., STAMP, V. & ZAHM, C. 2011. Fracture characterization and fluid flow simulation with geomechanical constraints for a CO_2–EOR and sequestration project Teapot Dome Oil Field, Wyoming, USA. *Energy Procedia,* 4, 3973-3980.

CHUN, B.-S. & WILKINSON, G. T. 1995. Interfacial tension in high-pressure carbon dioxide mixtures. *Industrial & engineering chemistry research,* 34, 4371-4377.

CINAR, Y., BUKHTEEVA, O., NEAL, P. R., ALLINSON, W. G. & PATERSON, L. CO_2 storage in low permeability formations. SPE Symposium on Improved Oil Recovery, 20-23 April, Tulsa, Oklahoma, USA, 2008. Society of Petroleum Engineers, 1-12.

CIVILE, D., ZECCHIN, M., FORLIN, E., DONDA, F., VOLPI, V., MERSON, B. & PERSOGLIA, S. 2013. CO_2 geological storage in the Italian carbonate successions. *International Journal of Greenhouse Gas Control,* 19, 101-116.

CO2CRC. 2015. CO2CRC Limited. Available: http://www.co2crc.com.au/ [Accessed 10/10/2015 2015].

CONNOLLY, M. & JOHNS, R. T. 2016. Scale-dependent mixing for adverse mobility ratio flows in heterogeneous porous media. *Transport in Porous Media,* 113, 29-50.

COOK, P.J. 1999. Sustainability and nonrenewable resources. *Environmental Geosciences*, 6(4), 185–190.

COOPER, C. 2009. A technical basis for carbon dioxide storage. *Energy Procedia,* 1, 1727-1733.

DAKE, L. P. 1978. Fundamentals of reservoir engineering. developments in petroleum science. *Elsevier, Amsterdam*, 1-100.

DANCE, T. 2013. Assessment and geological characterisation of the CO2CRC Otway Project CO_2 storage demonstration site: From prefeasibility to injection. *Marine and Petroleum Geology,* 46, 251-269.

DANIEL, R. & KALDI, J. Evaluating seal capacity of caprocks and intraformational barriers for the geosequestration of CO_2. Eastern Australasian Basins Symposium (3rd: 2008: Sydney, Australia), 2008. Petroleum Exploration Society of Australia, 475-484.

DE SILVA, G. P. D., RANJITH, P. G. & PERERA, M. S. A. 2015. Geochemical aspects of CO_2 sequestration in deep saline aquifers: A review. *Fuel,* 155, 128-143.

DEMPSEY, D., KELKAR, S. & PAWAR, R. 2014. Passive injection: A strategy for mitigating reservoir pressurization, induced seismicity and brine migration in geologic CO_2 storage. *International Journal of Greenhouse Gas Control,* 28, 96-113.

DENG, H., ELLIS, B. R., PETERS, C. A., FITTS, J. P., CRANDALL, D. & BROMHAL, G. S. 2013. Modifications of carbonate fracture hydrodynamic properties by CO_2-acidified brine flow. *Energy & Fuels,* 27, 4221-4231.

DESBRANDES, R., BASSIOUNI, Z. & GUALDRON, J. In-situ formation wettability determination in depleted zones. SSPE Latin America Petroleum Engineering Conference, 14-19 October, Rio de Janeiro, Brazil, 1990. Society of Petroleum Engineers, 1-14.

DESBRANDES, R. & BASSIOUNI, Z. A. In-situ wettability determination in gas reservoirs. 1990/12/1/ 1990. SPE: Society of Petroleum Engineers, 1-6.

DEWERS, T. & HAJASH, A. 1995. Rate laws for water-assisted compaction and stress-induced water-rock interaction in sandstones. *Journal of Geophysical Research: Solid Earth,* 100, 13093-13112.

DILMORE, R. M., ALLEN, D. E., JONES, J. R. M., HEDGES, S. W. & SOONG, Y. 2008. Sequestration of dissolved CO_2 in the Oriskany formation. *Environmental science & technology,* 42, 2760-2766.

DIVKO, L. G., HAMILTON, J. & O'BRIAN, G. 2010. Evaluation of the regional top seal for the purpose of geologic sequestration in the Gippsland Basin, southeastern Australia. *American Association of Petroleum Geologists*, 1-4.

DOUGHTY, C. 2010. Investigation of CO_2 plume behavior for a large-scale pilot test of geologic carbon storage in a saline formation. *Transport in porous media,* 82, 49-76.

DRANCHUK, P. & ABOU-KASSEM, H. 1975. Calculation of z factors for natural gases using equations of state. *Journal of Canadian Petroleum Technology,* 14, 1-4.

DUGUID, A., CAREY, J. W. & BUTSCH, R. 2014. Well integrity assessment of a 68 year old Well at a CO_2 injection project. *Energy Procedia,* 63, 5691-5706.

DUNHAM, R. J. 1962. *Classification of carbonate rocks according to depositional textures,* Classification of Carbonate Rocks--A Symposium, AAPG Special volumes,108-121.

EHLIG-ECONOMIDES, C. & ECONOMIDES, M. J. 2010. Sequestering carbon dioxide in a closed underground volume. *Journal of Petroleum Science and Engineering,* 70, 123-130.

ELENIUS, M. T., VOSKOV, D. V. & TCHELEPI, H. A. 2015. Interactions between gravity currents and convective dissolution. *Advances in Water Resources,* 83, 77-88.

EMAMI-MEYBODI, H., HASSANZADEH, H., GREEN, C. P. & ENNIS-KING, J. 2015. Convective dissolution of CO_2 in saline aquifers: Progress in modeling and experiments. *International Journal of Greenhouse Gas Control,* Special Issue commemorating the 10th year anniversary of the publication of the Intergovernmental Panel on Climate Change Special Report on CO_2 Capture and Storage, 238–266.

ENNIS-KING, J. & PATERSON, L. 2001. Reservoir engineering issues in the geological disposal of carbon dioxide. Fifth International Conference on Greenhouse Gas Control Technologies, Cairns, 290-295.

ENNIS-KING, J. P. & PATERSON, L. Role of convective mixing in the long-term storage of carbon dioxide in deep saline formations. , 2005. Society of Petroleum Engineers,10, 349-356.

ENNIS-KING, J., DANCE, T., XU, J., BOREHAM, C., FREIFELD, B., JENKINS, C., PATERSON, L., SHARMA, S., STALKER, L. & UNDERSCHULTZ, J. 2011. The role of heterogeneity in CO_2 storage in a depleted gas field: History matching of simulation models to field data for the CO2CRC Otway Project, Australia. *Energy Procedia,* 4, 3494-3501.

ERICKSON, K. P., LEMPP, C. & PÖLLMANN, H. 2015. Geochemical and geomechanical effects of $scCO_2$ and associated impurities on physical and petrophysical properties of Permotriassic Sandstones (Germany): an experimental approach. *Environmental Earth Sciences,* 74, 4719-4743.

ESPINOZA, D. N., KIM, S. H. & SANTAMARINA, J. C. 2011. CO_2 geological storage — Geotechnical implications. *KSCE Journal of Civil Engineering,* 15, 707-719.

EVANS, B., SAEEDI, A., RASOULI, V., LIU, K. & LEBEDEV, M. 2012. Predicting CO_2 injectivity properties for application at CCS sites. Report by Curtin University, Australia, 1-100.

FANG, Z. & LI, X. 2011. Preliminary assessment of CO_2 geological storage potential in Chongqing, China. *Procedia Environmental Sciences,* 11, Part C, 1064-1071.

FARQUHAR, S. M., PEARCE, J. K., DAWSON, G. K. W., GOLAB, A., SOMMACAL, S., KIRSTE, D., BIDDLE, D. & GOLDING, S. D. 2015. A fresh approach to investigating CO_2 storage: Experimental CO_2–water–rock interactions in a low-salinity reservoir system. *Chemical Geology,* 399, 98-122.

FEATHER, B. & ARCHER, R. 2010. Enhance natural gas recovery by carbon dioxide injection for storage purposes. In 17th Australia Fluid Mechanics Conference held in Auckland, New Zealand., 1-4.

FERRONATO, M., GAMBOLATI, G., JANNA, C. & TEATINI, P. 2010. Geomechanical issues of anthropogenic CO_2 sequestration in exploited gas fields. *Energy Conversion and Management,* 51, 1918-1928.

FIELD-REPORT 1995. Geocap Reservoir modelling of a carbonate: XYZ FIELD, Malaysia. *Confidental* 1-100.

FISCHER, S., ZEMKE, K., LIEBSCHER, A. & WANDREY, M. 2011. Petrophysical and petrochemical effects of long-term CO_2-exposure experiments on brine-saturated reservoir sandstone. *Energy Procedia,* 4, 4487-4494.

FISCHER, S., LIEBSCHER, A., DE LUCIA, M. & HECHT, L. 2013. Reactivity of sandstone and siltstone samples from the Ketzin pilot CO_2 storage site-Laboratory experiments and reactive geochemical modeling. *Environmental earth sciences,* 70, 3687-3708.

FJÆR, E., HOLT, R., HORSRUD, P., RAAEN, A. & RISNES, R. 2008. Geological aspects of petroleum related rock mechanics. *Developments in Petroleum Science,* 53, 103-133.

FRYKMAN, P., BECH, N., SØRENSEN, A. T., NIELSEN, L. H., NIELSEN, C. M., KRISTENSEN, L. & BIDSTRUP, T. 2009. Geological modeling and dynamic flow analysis as initial site investigation for large-scale CO_2 injection at the Vedsted structure, NW Denmark. *Energy Procedia,* 1, 2975-2982.

FRYKMAN, P., NIELSEN, C. M. & BECH, N. 2013. Trapping effects of small scale sedimentary heterogeneities. *Energy Procedia,* 37, 5352-5359.

GANESH, P. R. & MISHRA, S. 2014. Reduced Physics modeling of CO_2 injectivity. *Energy Procedia,* 63, 3116-3125.

GANESH, P. R., MISHRA, S., MAWALKAR, S., GUPTA, N. & PARDINI, R. 2014. Assessment of CO_2 injectivity and storage capacity in a depleted pinnacle Reef Oil Field in Northern Michigan. *Energy Procedia,* 63, 2969-2976.

GARCIA-RIOS, M., LUQUOT, L., SOLER, J. M. & CAMA, J. 2015. Influence of the flow rate on dissolution and precipitation features during percolation of CO_2-rich sulfate solutions through fractured limestone samples. *Chemical Geology,* 414, 95-108.

GASDA, S. E., BACHU, S. & CELIA, M. A. 2004. Spatial characterization of the location of potentially leaky wells penetrating a deep saline aquifer in a mature sedimentary basin. *Environmental Geology,* 46, 707-720.

GEISTLINGER, H. & MOHAMMADIAN, S. 2015. Capillary trapping mechanism in strongly water wet systems: Comparison between experiment and percolation theory. *Advances in Water Resources,* 79, 35-50.

GHADERI, S. M., KEITH, D. W. & LEONENKO, Y. 2009. Feasibility of injecting large volumes of CO_2 into aquifers. *Energy Procedia,* 1, 3113-3120.

GHARBI, O., BIJELJIC, B., BOEK, E. & BLUNT, M. J. 2013. Changes in pore structure and connectivity induced by CO_2 injection in carbonates: A combined pore-scale approach. *Energy Procedia,* 37, 5367-5378.

GHG, I. 2004. Improvements in Power Generation with Post-combustion Capture of CO_2 report PH4/33, Nov.

GHOLAMI, R., RABIEI, M., RASOULI, V., AADNOY, B. & FAKHARI, N. 2015a. Application of quantitative risk assessment in wellbore stability analysis. *Journal of Petroleum Science and Engineering,* 135, 185-200.

GHOLAMI, R., RASOULI, V., AADNOY, B. & MOHAMMADI, R. 2015b. Application of in situ stress estimation methods in wellbore stability analysis under isotropic and anisotropic conditions. *Journal of Geophysics and Engineering,* 12, 657.

GHOLAMI, R., RASOULI, V., AADNOY, B. & MOHAMMADNEJAD, M. 2016. Geomechanical and numerical studies of casing damages in a reservoir with solid production. *Rock Mechanics and Rock Engineering,* 49, 1441-1460.

GIBSON-POOLE, C., EDWARDS, S., LANGFORD, R. & VAKARELOV, B. Review of geological storage opportunities for carbon capture and storage (CCS). in Victoria. The Cooperative Research Centre for Greenhouse Gas Technologies (CO2CRC), Australian School of Petroleum, 2006. The University of Adelaide, Adelaide. ICTPL Consultancy Report Number. Citeseer, 1-118.

GIORGIS, T., CARPITA, M. & BATTISTELLI, A. 2007. 2D Modeling of salt precipitation during the injection of dry CO_2 in a depleted gas reservoir. *Energy Conversion and Management,* 48, 1816-1826.

GOODARZI, S., SETTARI, A. & KEITH, D. 2011. Geomechanical modeling for CO_2 storage in wabamun lake area of Alberta, Canada. *Energy Procedia,* 4, 3399-3406.

GOODMAN, A., HAKALA, A., BROMHAL, G., DEEL, D., RODOSTA, T., FRAILEY, S., SMALL, M., ALLEN, D., ROMANOV, V., FAZIO, J., HUERTA, N., MCINTYRE, D., KUTCHKO, B. & GUTHRIE, G. 2011. U.S. DOE methodology for the development of geologic storage potential for carbon dioxide at the national and regional scale. *International Journal of Greenhouse Gas Control,* 5, 952-965.

GROBE, M., PASHIN, J. C. & DODGE, R. L. 2009. Carbon dioxide sequestration in geological media—State of the science. *AAPG Studies in Geology 59,* 59.

HAN, W., KIM, K.-Y., ESSER, R., PARK, E. & MCPHERSON, B. 2011. Sensitivity study of simulation parameters controlling CO_2 trapping mechanisms in saline formations. *Transport in Porous Media,* 90, 807-829.

HANGX, S., SPIERS, C. & PEACH, C. 2010. Creep of simulated reservoir sands and coupled chemical-mechanical effects of CO_2 injection. *Journal of Geophysical Research: Solid Earth (1978–2012),* 115, 1-23.

HANGX, S., VAN DER LINDEN, A., MARCELIS, F. & BAUER, A. 2013. The effect of CO_2 on the mechanical properties of the captain sandstone: Geological storage of CO_2 at the Goldeneye Field (UK). *International Journal of Greenhouse Gas Control,* 19, 609-619.

HANGX, S. J., VAN DER LINDEN, A., MARCELIS, F. & LITEANU, E. 2015a. Defining the brittle failure envelopes of individual reaction zones observed in CO_2-exposed wellbore cement. *Environmental science & technology,* 50 (2), 1031–1038.

HANGX, S., BAKKER, E., BERTIER, P., NOVER, G. & BUSCH, A. 2015b. Chemical–mechanical coupling observed for depleted oil reservoirs subjected to long-term CO_2-exposure – A case study of the Werkendam natural CO_2 analogue field. *Earth and Planetary Science Letters,* 428, 230-242.

HAWKES, C., MCLELLAN, P., ZIMMER, U. & BACHU, S. Geomechanical factors affecting geological storage of CO_2 in depleted oil and gas reservoirs: risks and mechanisms. Gulf Rocks 2004 the 6th North America Rock Mechanics Symposium (NARMS), 2004. American Rock Mechanics Association.

HEBACH, A., OBERHOF, A., DAHMEN, N., KÖGEL, A., EDERER, H. & DINJUS, E. 2002. Interfacial tension at elevated pressures measurements and correlations in the water+ carbon dioxide system. *Journal of Chemical & Engineering Data,* 47, 1540-1546.

HERZOG, H., DRAKE, E. & ADAMS, E. 1997. CO_2 capture, reuse, and storage technologies for mitigating global climate change. *A White Paper*, 1-70.

HINGERL, F. F., YANG, F., PINI, R., XIAO, X., TONEY, M. F., LIU, Y. & BENSON, S. M. 2016. Characterization of heterogeneity in the Heletz sandstone from core to pore scale and quantification of its impact on multi-phase flow. *International Journal of Greenhouse Gas Control,* 48, 69-83.

HOLDREN, G. R. & BERNER, R. A. 1979. Mechanism of feldspar weathering—Experimental studies. *Geochimica et Cosmochimica Acta,* 43, 1161-1171.

HOLTZ, M. Residual gas saturation to aquifer influx: A calculation method for 3-D computer reservoir model construction. SPE Gas Technology Symposium held in Calgary, Alberta, Canada, 30 April–2 May 2002, Society of Petroleum Engineers, 1-10.

HONARI, A., BIJELJIC, B., JOHNS, M. L. & MAY, E. F. 2015. Enhanced gas recovery with CO_2 sequestration: The effect of medium heterogeneity on the dispersion of supercritical CO_2–CH_4. *International Journal of Greenhouse Gas Control,* 39, 39-50.

HOSSEINI, S. A., LASHGARI, H., CHOI, J. W., NICOT, J.-P., LU, J. & HOVORKA, S. D. 2013. Static and dynamic reservoir modeling for geological CO_2 sequestration at Cranfield, Mississippi, U.S.A. *International Journal of Greenhouse Gas Control,* 18, 449-462.

HOTEIT, H. & FIROOZABADI, A. 2009. Numerical modeling of diffusion in fractured media for gas-injection and-recycling schemes. *SPE Journal,* 14, 323-337.

HOVORKA, S. D., DOUGHTY, C., BENSON, S. M., PRUESS, K. & KNOX, P. R. 2004. The impact of geological heterogeneity on CO_2 storage in brine formations: A case study from the Texas Gulf Coast. *Geological Society, London, Special Publications,* 233, 147-163.

HUQ, F., HADERLEIN, S. B., CIRPKA, O. A., NOWAK, M., BLUM, P. & GRATHWOHL, P. 2015. Flow-through experiments on water–rock interactions in a sandstone caused by CO_2 injection at pressures and temperatures mimicking reservoir conditions. *Applied Geochemistry,* 58, 136-146.

ICTPL 2005. CO_2 storage prospectivity of selected sedimentary basins in the region of China and South East Asia. *Introduction Assessment of Geologic storage potential of carbon dioxide in the APEC Region-Phase I.* APEC Energy Working Group EWG Project Report. Innovative carbon technologies Pty Ltd, Asia-Pacific Economic Cooperation Secretariat. pp. 57-198.

IEA 2014. CO_2 emissions from fuel combustion-Highlights. *In:* HOEVEN, M. V. D. (ed.) *I E A statistics.* International Energy Agency OECD/IEA statistics report, France (http://www.iea.org).

IEA 2015. Southeast Energy Asia Outlook-World Energy Outlook Special Report. OECD/IEA statistics report, France (http://www.iea.org); : International Energy Agency, OECD/IEA.

IGLAUER, S., LAMY, C., PENTLAND, C., BLUNT, M. & MAITLAND, G. Capillary trapping in carbonate rocks SPE EUROPEC/EAGE Annual Conference and Exhibition, 14-17 June, Barcelona, Spain, 2010. Society of Petroleum Engineers, 1-8.

IGLAUER, S. 2011. *Dissolution trapping of carbon dioxide in reservoir formation brine-A carbon storage mechanism*, In: Mass Transfer (ed.: Nakajima H), ijeka: InTech 2011, 1-50.

IGLAUER, S., PALUSZNY, A., PENTLAND, C. H. & BLUNT, M. J. 2011a. Residual CO_2 imaged with X-ray micro-tomography. *Geophysical Research Letters,* 38, 1-6.

IGLAUER, S., WÜLLING, W., PENTLAND, C. H., AL-MANSOORI, S. K. & BLUNT, M. J. 2011b. Capillary-trapping capacity of sandstones and sandpacks. *SPE Journal,* 6, 1-6.

IGLAUER, S., SARMADIVALEH, M., AL-YASERI, A. & LEBEDEV, M. 2014. Permeability evolution in sandstone due to injection of CO_2-saturated brine or supercritical CO_2 at reservoir conditions. *Energy Procedia,* 63, 3051-3059.

IGLAUER, S., PENTLAND, C. H. & BUSCH, A. 2015. CO_2 wettability of seal and reservoir rocks and the implications for carbon geo-sequestration. *Water Resources Research,* 51, 729-774.

INSTITUTE, G. C. 2016. THE GLOBAL STATUS OF CCS | 2016 SUMMARY REPORT. 9-10.
IPCC 2005. *IPCC special report on carbon dioxide capture and storage. Prepared by Working Group III of the Intergovernmental Panel on Climate Change,* Cambridge, United Kingdom and New York, NY, USA, 1-500.
ITO, D., MATSUURA, T., KAMON, M., KAWADA, K., NISHIMURA, M., TOMITA, S., KATOH, A., AKAKU, K., INAMORI, T., YAMANOUCHI, Y. & MIKAMI, J. 2013. Reservoir evaluation for the moebetsu formation at tomakomai candidate site for CCS demonstration project in Japan. *Energy Procedia,* 37, 4937-4945.
IZGEC, O., DEMIRAL, B., BERTIN, H. & AKIN, S. 2008. CO_2 injection into saline carbonate aquifer formations: laboratory investigation. *Transport in Porous Media,* 72, 1-24.
JALIL, M., MASOUDI, R., DARMAN, N. B. & OTHMAN, M. Study of the CO_2 injection storage and sequestration in depleted M4 carbonate gas condensate reservoir Malaysia. 2012. *Carbon Management Technology Conference*, 1-14.
JANSEN, J. D., FONSECA, R. M., KAHROBAEI, S., SIRAJ, M., VAN ESSEN, G. & VAN DEN HOF, P. 2013. The Egg Model-data files. TU Delft. Dataset. http://dx.doi.org/10.4121/uuid:916c86cd-3558-4672-829a-105c62985ab2.
JERAULD, G. 1997. Prudhoe Bay gas/oil relative permeability. *SPE Reservoir Engineering,* 12, 66-73.
JIANG, F. & TSUJI, T. 2015. Impact of interfacial tension on residual CO_2 clusters in porous sandstone. *Water Resources Research,* 51, 1710-1722.
JIKICH, S. A., SMITH, D. H., SAMS, W. N. & BROMHAL, G. S. Enhanced Gas Recovery (EGR) with carbon dioxide sequestration: A simulation study of effects of injection strategy and operational parameters. SPE Eastern Regional Meeting, 2003. *Society of Petroleum Engineers*. Pittsburgh, Pennsylvania, 2003, pp. 1-9.
JUANES, R., SPITERI, E., ORR, F. & BLUNT, M. 2006. Impact of relative permeability hysteresis on geological CO_2 storage. *Water Resources Research,* 42.
KALDI, J., DANIEL, R., TENTHOREY, E., MICHAEL, K., SCHACHT, U., NICOL, A., UNDERSCHULTZ, J. & BACKE, G. 2013. Containment of CO_2 in CCS: Role of caprocks and faults. *Energy Procedia,* 37, 5403-5410.
KARIMNEZHAD, M., JALALIFAR, H. & KAMARI, M. 2014. Investigation of caprock integrity for CO_2 sequestration in an oil reservoir using a numerical method. *Journal of Natural Gas Science and Engineering,* 21, 1127-1137.
KASHEFI, K., PEREIRA, L. M. C., CHAPOY, A., BURGASS, R. & TOHIDI, B. 2016. Measurement and modelling of interfacial tension in methane/water and methane/brine systems at reservoir conditions. *Fluid Phase Equilibria,* 409, 301-311.
KEMPKA, T., DE LUCIA, M. & KÜHN, M. 2014. Geomechanical integrity verification and mineral trapping quantification for the Ketzin CO_2 storage pilot site by coupled numerical simulations. *Energy Procedia,* 63, 3330-3338.
KETZER, J. M., IGLESIAS, R. & EINLOFT, S. 2012. Reducing greenhouse gas emissions with CO_2 capture and geological storage. *In:* CHEN, W.-Y., SEINER, J., SUZUKI, T. & LACKNER, M. (eds.) *Handbook of Climate Change Mitigation.* Springer US.
KHISHVAND, M., AKBARABADI, M. & PIRI, M. 2016. Micro-scale experimental investigation of the effect of flow rate on trapping in sandstone and carbonate rock samples. *Advances in Water Resources,* 94, 379–399.
KILLOUGH, J. 1976. Reservoir simulation with history-dependent saturation functions. *Society of Petroleum Engineers Journal,* 16, 37-48.
KIM, S. & HOSSEINI, S. A. 2014. Geological CO_2 storage: Incorporation of pore-pressure/stress coupling and thermal effects to determine maximum sustainable pressure limit. *Energy Procedia,* 63, 3339-3346.
KIMBREL, E. H., HERRING, A. L., ARMSTRONG, R. T., LUNATI, I., BAY, B. K. & WILDENSCHILD, D. 2015. Experimental characterization of nonwetting phase trapping and

implications for geologic CO_2 sequestration. *International Journal of Greenhouse Gas Control,* 42, 1-15.

KITAMURA, K., KOGURE, T., NISHIZAWA, O. & XUE, Z. 2013. Experimental and numerical study of residual CO_2 trapping in porous sandstone. *Energy Procedia,* 37, 4093-4098.

KOUKOUZAS, N., ZIOGOU, F. & GEMENI, V. 2009. Preliminary assessment of CO_2 geological storage opportunities in Greece. *International Journal of Greenhouse Gas Control,* 3, 502-513.

KOVACS, T., POULUSSEN, D. F. & DIOSVCIUDEN, C. D. 2015. Strategies for injection of CO_2 into carbonate rocks. *Global Carbon Capture and Storage Institute Ltd*, 1-66.

KOVSCEK, A. R. 2002. Screening criteria for CO_2 storage in oil reservoirs. *Petroleum Science and Technology,* 20, 841-866.

KREVOR, S. C., PINI, R., LI, B. & BENSON, S. M. 2011. Capillary heterogeneity trapping of CO_2 in a sandstone rock at reservoir conditions. *Geophysical Research Letters,* 38, 3-5.

KREVOR, S., PINI, R., ZUO, L. & BENSON, S. M. 2012. Relative permeability and trapping of CO_2 and water in sandstone rocks at reservoir conditions. *Water resources research,* 48, 1-16.

KREVOR, S., BLUNT, M. J., BENSON, S. M., PENTLAND, C. H., REYNOLDS, C., AL-MENHALI, A. & NIU, B. 2015. Capillary trapping for geologic carbon dioxide storage – From pore scale physics to field scale implications. *International Journal of Greenhouse Gas Control,* Special Issue commemorating the 10th year anniversary of the publication of the Intergovernmental Panel on Climate Change Special Report on CO_2 Capture and Storage, 221–237.

KUO, C.-W., PERRIN, J.-C. & BENSON, S. M. 2011. Simulation studies of effect of flow rate and small scale heterogeneity on multiphase flow of CO_2 and brine. *Energy Procedia,* 4, 4516-4523.

KUO, C.-W. & BENSON, S. M. 2015. Numerical and analytical study of effects of small scale heterogeneity on CO_2/brine multiphase flow system in horizontal corefloods. *Advances in Water Resources,* 79, 1-17.

LAFORCE, T., ENNIS-KING, J., BOREHAM, C. & PATERSON, L. 2014. Residual CO_2 saturation estimate using noble gas tracers in a single-well field test: The CO2CRC Otway project. *International Journal of Greenhouse Gas Control,* 26, 9-21.

LAI, N. Y. G., YAP, E. H. & LEE, C. W. 2011. Viability of CCS: A broad-based assessment for Malaysia. *Renewable and Sustainable Energy Reviews,* 15, 3608-3616.

LAI, Y.-T., SHEN, C.-H., TSENG, C.-C., FAN, C.-H. & HSIEH, B.-Z. 2015. Estimation of carbon dioxide storage capacity for depleted gas reservoirs. *Energy Procedia,* 76, 470-476.

LAKE, L. W., JOHNS, R. T., ROSSEN, W. R., & POPE, G. 1986. *Fundamentals of enhanced oil recovery*. *Society of Petroleum Engineers*, 496pp.

LAMY, C. M. M., IGLAUER, S., PENTLAND, C. H., BLUNT, M. J. & MAITLAND, G. C. 2010. Capillary trapping in carbonate rocks. *SPE EUROPEC/EAGE Annual Conference and Exhibition, 14-17 June, Barcelona, Spain.* Society of Petroleum Engineers, 1-8.

LAND, C. S. 1968. Calculation of imbibition relative permeability for two-and three-phase flow from rock properties. *Society of Petroleum Engineers Journal,* 8, 149-156.

LE GUEN, Y., RENARD, F., HELLMANN, R., BROSSE, E., COLLOMBET, M., TISSERAND, D. & GRATIER, J. P. 2007. Enhanced deformation of limestone and sandstone in the presence of high fluids. *Journal of Geophysical Research: Solid Earth (1978–2012),* 112, 1-21.

LE GUENAN, T. & ROHMER, J. 2011. Corrective measures based on pressure control strategies for CO_2 geological storage in deep aquifers. *international journal of Greenhouse Gas Control,* 5, 571-578.

LEEUWENBURGH, O., NEELE, F., HOFSTEE, C., WEIJERMANS, P.-J., DE BOER, H., OOSTHOEK, P., LEFEBVRE, A., GODDERIJ, R. & GUTIERREZ-NERI, M. 2014. Enhanced Gas Recovery – A Potential 'U' for CCUS in The Netherlands. *Energy Procedia,* 63, 7809-7820.

LI, Z., DONG, M., LI, S. & HUANG, S. 2006. CO_2 sequestration in depleted oil and gas reservoirs—caprock characterization and storage capacity. *Energy Conversion and Management,* 47, 1372-1382.

LI, Z., WANG, S., LI, S., LIU, W., LI, B. & LV, Q.-C. 2014. Accurate determination of the CO_2–brine interfacial tension using graphical alternating conditional expectation. *Energy & Fuels,* 28, 624-635.

LOIZZO, M., LECAMPION, B., BÉRARD, T., HARICHANDRAN, A. & JAMMES, L. 2010. Reusing O&G-depleted reservoirs for CO_2 storage: Pros and Cons. *SPE Projects, Facilities & Construction,* 5, 166-172.

LU, C., HAN, W. S., LEE, S.-Y., MCPHERSON, B. J. & LICHTNER, P. C. 2009. Effects of density and mutual solubility of a brine system on storage in geological formations: "Warm" vs. "cold" formations. *Advances in Water Resources,* 32, 1685-1702.

LU, J., KORDI, M., HOVORKA, S. D., MECKEL, T. A. & CHRISTOPHER, C. A. 2013. Reservoir characterization and complications for trapping mechanisms at Cranfield CO_2 injection site. *International Journal of Greenhouse Gas Control,* 18, 361-374.

LUN, Z., FAN, H., WANG, H., LUO, M., PAN, W. & WANG, R. 2012. Interfacial tensions between reservoir brine and CO_2 at high pressures for different salinity. *Energy & Fuels,* 26, 3958-3962.

LYNCH, T., FISHER, Q., ANGUS, D. & LORINCZI, P. 2013. Investigating stress path hysteresis in a CO_2 injection scenario using coupled geomechanical-fluid flow modelling. *Energy Procedia,* 37, 3833-3841.

MALININ, S. & KUROVSKAYA, N. 1975. Solubility of CO_2 in chloride solutions at elevated temperatures and CO_2 pressures. *Geochem. Int,* 12, 199-201.

MALININ, S. & SAVELEVA, N. 1972. Experimental investigations of CO_2 solubility in NaCl and $CaCl_2$ solutions at temperatures of 25, 50 and 75 degrees and elevated CO_2 pressure. *Geokhimiya*, 643.

MAMORA, D. & SEO, J. Enhanced gas recovery by carbon dioxide sequestration in depleted gas reservoirs. SPE Annual Technical Conference and Exhibition, 29 September-2 October, San Antonio, Texas, 2002. *Society of Petroleum Engineers*, 1-9.

MANSOORI, S. A., IGLAUER, S., PENTLAND, C. H., BIJELJIC, B. & BLUNT, M. J. 2009. Measurements of non-wetting phase trapping applied to carbon dioxide storage. *Energy Procedia,* 1, 3173-3180.

MAO, C., YAMADA, Y. & MATSUOKA, T. 2014. A preliminary assessment of geological CO_2 storage in Cambodia. *International Journal of Greenhouse Gas Control,* 30, 19-33.

MARBLER, H., ERICKSON, K. P., SCHMIDT, M., LEMPP, C. & PÖLLMANN, H. 2012. Geomechanical and geochemical effects on sandstones caused by the reaction with supercritical CO_2: An experimental approach to in situ conditions in deep geological reservoirs. *Environmental earth sciences,* 69, 1981-1998.

MASOUDI, R., JALIL, M., PRESS, D. J., LEE, K.-H., PHUAT TAN, C., ANIS, L., DARMAN, N. B. & OTHMAN, M. An integrated reservoir simulation-geomechanical study on feasibility of CO_2 storage in M4 carbonate reservoir, Malaysia. International Petroleum Technology Conference, 2011, 15-17 November, Bangkok, Thailand, 1-18.

MASOUDI, R., JALIL, M. A. A., TAN, C. P., PRESS, D., KELLER, J., ANIS, L., DARMAN, N. & OTHMAN, M. Simulation of chemical interaction of injected CO_2 and carbonic acid based on laboratory tests in 3D coupled geomechanical modeling. IPTC 2013: International Petroleum Technology Conference, 2013, 26-28 March, Beijing, China. 1-18.

MATHIAS, S. A., GONZÁLEZ MARTÍNEZ DE MIGUEL, G. J., THATCHER, K. E. & ZIMMERMAN, R. W. 2011. Pressure buildup during CO_2 injection into a closed brine aquifer. *Transport in Porous Media,* 89, 383-397.

MAVKO, G., MUKERJI, T. & DVORKIN, J. 2009. *The rock physics handbook: Tools for seismic analysis of porous media*, Cambridge university press, 1-525.

MCCAIN, W. D. 1990. *The properties of petroleum fluids,* Penn Well Books, Penn Well Publishing company, TULSA, Oklahoma, USA. pp: 1-500., PennWell Books.

MCCAIN JR, W. D. 1994. *Heavy components control reservoir fluid behavior*, Society of Petroleum Engineers, 1-4.

MCGOWEN, J. & BLOCH, S. 1985. Depositional facies, diagenesis, and reservoir quality of ivishak sandstone (Sadlerochit Group), Prudhoe Bay Field: ABSTRACT. *AAPG Bulletin,* 69, 286-286.

MCMILLAN, B., KUMAR, N. & BRYANT, S. L. 2008. Time-dependent injectivity during CO_2 storage in aquifers. *SPE Symposium on Improved Oil Recovery.* 20-23 April, Tulsa, Oklahoma, USA: Society of Petroleum Engineers, 1-15.

MOHAMED, I. & NASR-EL-DIN, H. A. 2013. Fluid/Rock interactions during CO_2 sequestration in deep saline carbonate aquifers: Laboratory and modeling studies. *SPE Journal,* 18, 468-485.

MUKHOPADHYAY, S., YANG, S.-Y., YEH, H.-D. & BIRKHOLZER, J. 2011. Transient pressure response of a gas reservoir arising from supercritical carbon dioxide injection through a partially-penetrating well: An analytical solution. *Energy Procedia,* 4, 3965-3972.

MYERS, M., STALKER, L., ROSS, A., DYT, C. & HO, K.-B. 2012. Method for the determination of residual carbon dioxide saturation using reactive ester tracers. *Applied Geochemistry,* 27, 2148-2156.

MYERS, M., STALKER, L., LA FORCE, T., PEJCIC, B., DYT, C., HO, K.-B. & ENNIS-KING, J. 2015. Field measurement of residual carbon dioxide saturation using reactive ester tracers. *Chemical Geology,* 399, 20-29.

MAZZOLDI, A., HILL, T. & COLLS, J. J. 2011. Assessing the risk for CO_2 transportation within CCS projects, CFD modelling. *International Journal of Greenhouse Gas Control,* 5, 816-825.

NARINESINGH, J. & ALEXANDER, D. 2014. CO_2 enhanced gas recovery and geologic sequestration in condensate reservoir: A simulation study of the effects of injection pressure on condensate recovery from reservoir and CO_2 storage efficiency. *Energy Procedia,* 63, 3107-3115.

NJIEKAK, G., SCHMITT, D. R., YAM, H. & KOFMAN, R. S. 2013. CO_2 rock physics as part of the Weyburn-Midale geological storage project. *International Journal of Greenhouse Gas Control,* 16, Supplement 1, 118-133.

NOAA. 2013. National oceanic and atmospheric administration, ⟨http://www.esrl. noaa.gov/gmd/ccgg/trends⟩.

NOIRIEL, C., LUQUOT, L., MADÉ, B., RAIMBAULT, L., GOUZE, P. & VAN DER LEE, J. 2009. Changes in reactive surface area during limestone dissolution: An experimental and modelling study. *Chemical Geology,* 265, 160-170.

OH, T. H. 2010. Carbon capture and storage potential in coal-fired plant in Malaysia—A review. *Renewable and Sustainable Energy Reviews,* 14, 2697-2709.

OIKAWA, Y., TAKEHARA, T. & TOSHA, T. Effect of CO_2 injection on mechanical properties of Berea Sandstone. The 42nd US Rock Mechanics Symposium (USRMS), 2008 The 42nd U.S. Rock Mechanics Symposium (USRMS), 29 June-2 July, San Francisco, California. American Rock Mechanics Association, 1-6.

OLDEN, P., PICKUP, G., JIN, M., MACKAY, E., HAMILTON, S., SOMERVILLE, J. & TODD, A. 2012. Use of rock mechanics laboratory data in geomechanical modelling to increase

confidence in CO_2 geological storage. *International Journal of Greenhouse Gas Control,* 11, 304-315.

OLDENBURG, C. M. & BENSON, S. M. 2001a. *CO_2 injection for enhanced gas production and carbon sequestration,* SPE International Petroleum Conference and Exhibition in Mexico held in Villahermosa, Mexico, 10–12 February 2002. Society of Petroleum Engineers Inc, 1-10.

OLDENBURG, C. & BENSON, S. 2001b. Carbon sequestration with enhanced gas recovery: Identifying candidate sites for pilot stud Polaky. *Lawrence Berkeley National Laboratory*, 1-50.

OLDENBURG, C. & DOUGHTY, C. 2011. Injection, flow, and mixing of CO_2 in porous media with residual gas. *Transport in porous media,* 90, 201-218.

OLIEROOK, H. K. H., DELLE PIANE, C., TIMMS, N. E., ESTEBAN, L., REZAEE, R., MORY, A. J. & HANCOCK, L. 2014. Facies-based rock properties characterization for CO_2 sequestration: GSWA Harvey 1 well, Western Australia. *Marine and Petroleum Geology,* 50, 83-102.

ORUGANTI, Y. & BRYANT, S. L. 2009. Pressure build-up during CO_2 storage in partially confined aquifers. *Energy Procedia,* 1, 3315-3322.

ORUGANTI, Y., GUPTA, A. K. & BRYANT, S. L. 2011. Analytical estimation of risk due to pressure buildup during CO_2 injection in deep saline aquifers. *Energy Procedia,* 4, 4140-4147.

OTHMAN, M., ZAKARIA, R. & FERNANDO, W. 2009. Strategic planning on carbon capture from coal fired plants in Malaysia and Indonesia: A review. *Energy Policy,* 37, 1718-1735.

OTT, H., PENTLAND, C. H. & OEDAI, S. 2015a. CO_2–brine displacement in heterogeneous carbonates. *International Journal of Greenhouse Gas Control,* 33, 135-144.

OTT, H., ROELS, S. M. & DE KLOE, K. 2015b. Salt precipitation due to supercritical gas injection: Capillary-driven flow in unimodal sandstone. *International Journal of Greenhouse Gas Control*, 247-255.

OUELLET, A., BÉRARD, T., DESROCHES, J., FRYKMAN, P., WELSH, P., MINTON, J., PAMUKCU, Y., HURTER, S. & SCHMIDT-HATTENBERGER, C. 2011. Reservoir geomechanics for assessing containment in CO_2 storage: a case study at Ketzin, Germany. *Energy Procedia,* 4, 3298-3305.

PASHIN, J. C. & DODGE, R. L. 2010. Carbon dioxide sequestration in geological media—State of the science. *Carbon dioxide sequestration in geological media: State of the Science, AAPG Studies in Geology 59,* 59.

PATEL, M. J., MAY, E. F. & JOHNS, M. L. 2016. High-fidelity reservoir simulations of enhanced gas recovery with supercritical CO_2. *Energy,* 111, 548-559.

PENTLAND, C. H. 2011. *Measurements of non-wetting phase trapping in porous media.* PhD Thesis, Imperial College London: 1-100.

PENTLAND, C. H., EL-MAGHRABY, R., GEORGIADIS, A., IGLAUER, S. & BLUNT, M. J. 2011. Immiscible displacements and capillary trapping in CO_2 storage. *Energy Procedia,* 4, 4969-4976.

PENTLAND, C. H., IGLAUER, S., GHARBI, O., OKADA, K. & SUEKANE, T. 2012. The Influence of pore space geometry on the entrapment of carbon dioxide by capillary forces. Society of Petroleum Engineers, 1-5.

PERVUKHINA, M., GUREVICH, B., DEWHURST, D. N. & SIGGINS, A. F. 2010. Applicability of velocity—stress relationships based on the dual porosity concept to isotropic porous rocks. *Geophysical Journal International,* 181, 1473-1479.

PEYSSON, Y., ANDRÉ, L. & AZAROUAL, M. 2014. Well injectivity during CO_2 storage operations in deep saline aquifers—Part 1: Experimental investigation of drying effects, salt precipitation and capillary forces. *International Journal of Greenhouse Gas Control,* 22, 291-300.

PLUMB, R. Influence of composition and texture on the failure properties of clastic rocks. *Rock Mechanics in Petroleum Engineering*, 1994. Society of Petroleum Engineers, 1-8.

QI, D., ZHANG, S. & SU, K. 2010. Risk Assessment of CO_2 geological storage and the calculation of storage capacity. *Petroleum Science and Technology,* 28, 979-986.

RAHIMZADEH, A., BAZARGAN, M., DARVISHI, R. & MOHAMMADI, A. H. 2016. Condensate blockage study in gas condensate reservoir. *Journal of Natural Gas Science and Engineering,* 33, 634-643.

RAMIREZ, A., HAGEDOORN, S., KRAMERS, L., WILDENBORG, T. & HENDRIKS, C. 2010. Screening CO_2 storage options in the Netherlands. *International Journal of Greenhouse Gas Control,* 4, 367-380.

RANSOM, R. C. & HOLM, L. R. W. 1978. Determining residual oil saturation following flooding. U.S. Patent No. 4,102,396. Washington, DC: U.S. Patent and Trademark Office. 1-4.

RATHNAWEERA, T. D., RANJITH, P. G., PERERA, M. S. A., HAQUE, A., LASHIN, A., AL ARIFI, N., CHANDRASEKHARAM, D., YANG, S. Q., XU, T., WANG, S. H. & YASAR, E. 2015. CO_2-induced mechanical behaviour of Hawkesbury sandstone in the Gosford basin: An experimental study. *Materials Science and Engineering: A,* 641, 123-137.

RATHNAWEERA, T. D., RANJITH, P. G. & PERERA, M. S. A. 2016. Experimental investigation of geochemical and mineralogical effects of CO_2 sequestration on flow characteristics of reservoir rock in deep saline aquifers. *Scientific Reports,* 6, 19362.

RAZA, A., REZAEE, R., BING, C.H., GHOLAMI, R., NAGARAJAN, R. & HAMID, M. 2016, CO_2 storage in heterogeneous aquifer: A study on the effect of injection rate and $CaCO_3$ concentration. IOP Conference Series: Materials Science and Engineering, IOP Publishing, 012023.

RENARD, F., PARK, A., ORTOLEVA, P. & GRATIER, J.-P. 1999. An integrated model for transitional pressure solution in sandstones. *Tectonophysics,* 312, 97-115.

REZAEE, M., ROSTAMI, B. & POURAFSHARY, P. 2013. Heterogeneity effect on non-wetting phase trapping in strong water drive gas reservoirs. *Journal of Natural Gas Science and Engineering,* 14, 185-191.

RIAZ, A. & CINAR, Y. 2014. Carbon dioxide sequestration in saline formations: Part I—Review of the modeling of solubility trapping. *Journal of Petroleum Science and Engineering,* 124, 367-380.

ROCHELLE, C., BATEMAN, K., PEARCE, J., 2002. Geochemical interactions between supercritical CO_2 and the Utsira Formation: An experimental study. *In: British Geological Survey Report CR/02/060: 57.*

ROSHAN, H., AL-YASERI, A., SARMADIVALEH, M. & IGLAUER, S. 2016. On wettability of shale rocks. *Journal of colloid and interface science,* 475, 104-111.

ROWE JR, A. M. & CHOU, J. C. 1970. Pressure-volume-temperature-concentration relation of aqueous sodium chloride solutions. *Journal of Chemical and Engineering Data,* 15, 61-66.

RUSHING, J. A., NEWSHAM, K. E., VAN FRAASSEN, K. C., MEHTA, S. A. & MOORE, G. R. 2008. Laboratory measurements of gas-water interfacial tension at HP/HT reservoir conditions. CIPC/SPE Gas Technology Symposium 2008 Joint Conference, 16-19 June, Calgary, Alberta, Canada: Society of Petroleum Engineers, 1-17.

RUTQVIST, J., BIRKHOLZER, J., CAPPA, F. & TSANG, C. F. 2007. Estimating maximum sustainable injection pressure during geological sequestration of CO_2 using coupled fluid flow and geomechanical fault-slip analysis. *Energy Conversion and Management,* 48, 1798-1807.

RUTQVIST, J., BIRKHOLZER, J. T. & TSANG, C.-F. 2008. Coupled reservoir–geomechanical analysis of the potential for tensile and shear failure associated with CO_2 injection in

multilayered reservoir–caprock systems. *International Journal of Rock Mechanics and Mining Sciences,* 45, 132-143.

RUTQVIST, J. 2012. The geomechanics of CO_2 storage in deep sedimentary formations. *Geotechnical and Geological Engineering,* 30, 525-551.

SAEEDI, A. 2012. *Experimental study of multiphase flow in porous media during CO_2 geo-sequestration processes.* PhD Thesis, Springer Science & Business Media, 1-120.

SAEEDI, A. & REZAEE, R. 2012. Effect of residual natural gas saturation on multiphase flow behaviour during CO_2 geo-sequestration in depleted natural gas reservoirs. *Journal of Petroleum Science and Engineering,* 82–83, 17-26.

SAEEDI, A., REZAEE, R. & EVANS, B. 2012. Experimental study of the effect of variation in in-situ stress on capillary residual trapping during CO_2 geo-sequestration in sandstone reservoirs. *Geofluids,* 12, 228-235.

SARMADIVALEH, M., AL-YASERI, A. Z. & IGLAUER, S. 2015. Influence of temperature and pressure on quartz–water–CO_2 contact angle and CO_2–water interfacial tension. *Journal of Colloid and Interface Science,* 441, 59-64.

SCHLUMBERGER. 2012. *Case study: Measuring residual CO_2 saturation near an injection well* [Online]. [Accessed 29-3-2016 2016].

SCHLUMBERGER 2014a. Reference Manual. 2014.2.

SCHLUMBERGER 2014b. Technical Description 2014.2.

SENERGY 2014. Interactive petrophysics, Senergy Limited- IP Help Manual. *Senergy, Scotland*, 1-1600.

SEO, J. G. 2004. *Experimental and simulation studies of sequestration of supercritical carbon dioxide in depleted gas reservoirs.* PhD Thesis, Texas A&M University, 1-131.

SHAMSHIRI, H. & JAFARPOUR, B. 2012. Controlled CO_2 injection into heterogeneous geologic formations for improved solubility and residual trapping. *Water Resources Research,* 48.

SHAPIRO, S. A. 2003. no. 2 Elastic piezosensitivity porous Fract. rocks Geophys. 68, 482e486.http://dx.doi.org/10.1190/1.1567215.

SHARIAT, A., MOORE, R. G., MEHTA, S. A., VAN FRAASSEN, K. C., NEWSHAM, K. E. & RUSHING, J. A. 2012. Laboratory measurements of CO_2-H_2O interfacial tension at HP/HT conditions: Implications for CO_2 sequestration in deep aquifers. *Carbon Management Technology Conference.* 7-9 February, Orlando, Florida, USA, 1-17.

SHEDID, S. A. & SALEM, A. M. Experimental investigations of CO_2 solubility and variations in petrophysical properties due to CO_2 storage in carbonate reservoir rocks. North Africa Technical Conference and Exhibition, 2013 North Africa Technical Conference and Exhibition, 15-17 April, Cairo, Egypt. Society of Petroleum Engineers, 1-10.

SHEN, C.-H., HSIEH, B.-Z., TSENG, C.-C. & CHEN, T.-L. 2014. Case study of CO_2-IGR and storage in a nearly depleted gas-condensate reservoir in Taiwan. *Energy Procedia,* 63, 7740-7749.

SHI, J.-Q. & DURUCAN, S. 2009. A coupled reservoir-geomechanical simulation study of CO_2 storage in a nearly depleted natural gas reservoir. *Energy Procedia,* 1, 3039-3046.

SHI, J.-Q., SMITH, J., DURUCAN, S. & KORRE, A. 2013. A coupled reservoir simulation-geomechanical modelling study of the CO_2 injection-induced ground surface uplift observed at Krechba, in Salah. *Energy Procedia,* 37, 3719-3726.

SHUKLA, R., RANJITH, P., HAQUE, A. & CHOI, X. 2010. A review of studies on CO_2 sequestration and caprock integrity. *Fuel,* 89, 2651-2664.

SOBERS, L., FRAILEY, S. & LAWAL, A. Geological sequestration of carbon dioxide in depleted gas reservoirs. SPE/DOE Symposium on Improved Oil Recovery, 2004 SPE/DOE, 17-21 April, Tulsa, Oklahoma. Society of Petroleum Engineers, 1-12.

SOLOMON, S. 2006. Criteria for intermediate storage of carbon dioxide in geological formations. *The Bellona Foundation, Oslo*, 1-6.

SOLOMON, S. 2007. Carbon dioxide storage: Geological security and environmental issues–Case study on the Sleipner Gas field in Norway. *Bellona Report, May*.

SOLOMON, S., BUREAU-CAUCHOIS, G., AHMED, N., AARNES, J. & HOLTEDAHL, P. 2014. CO_2 storage capacity assessment of deep saline aquifers in the Mozambique Basin. *Energy Procedia,* 63, 5266-5283.

SOREIDE, I. & WHITSON, C. H. 1992. Peng-Robinson Predictions for Hydrocarbons, CO_2, N_2, and H_2S with pure water and NaCI brine. *Fluid Phase Equilibria,* 77, 217-240.

SPITERI, E. J. & JUANES, R. 2006. Impact of relative permeability hysteresis on the numerical simulation of WAG injection. *Journal of Petroleum Science and Engineering,* 50, 115-139.

STANDING, M. B. 1981. Volumetric and phase behavior of oil field hydrocarbon systems. *9thPrinting, Society of Petroleum Engineers of AIME, Dallas, TX.*, 1-142.

STERPENICH, J., SAUSSE, J., PIRONON, J., GÉHIN, A., HUBERT, G., PERFETTI, E. & GRGIC, D. 2009. Experimental ageing of oolitic limestones under CO_2 storage conditions: Petrographical and chemical evidence. *Chemical Geology,* 265, 99-112.

STEVENS, S., KUUSKRAA, V. & TABER, J. 1999. Sequestration of CO_2 in depleted oil and gas fields: Barriers to overcome in implementation of CO_2 capture and storage (disused oil and gas fields). *Report for the IEA Greenhouse Gas Research and Development Programme (PH3/22),* 87, 81A-81.

SUEKANE, T. & NGUYEN, H. T. 2013. Relation between the initial and residual gas saturations of gases trapped by capillarity in natural sandstones. *Journal of Fluid Science and Technology,* 8, 322-336.

SUEKANE, T., NOBUSO, T., HIRAI, S. & KIYOTA, M. 2008. Geological storage of carbon dioxide by residual gas and solubility trapping. *International Journal of Greenhouse Gas Control,* 2, 58-64.

SUEKANE, T., ZHOU, N., HOSOKAWA, T. & MATSUMOTO, T. 2010. Direct observation of trapped gas bubbles by capillarity in sandy porous media. *Transport in porous media,* 82, 111-122.

SUTTON, R. P. 2007. Fundamental PVT calculations for associated and gas/condensate natural-gas systems. *SPE Reservoir Evaluation & Engineering,* 10, 270-284.

SUTTON, R. P. An improved model for water-hydrocarbon surface tension at reservoir conditions. SPE Annual Technical Conference and Exhibition, Louisiana, 2009. Society of Petroleum Engineers, 1-18.

SUZANNE, K., HAMON, G., BILLIOTTE, J. & TROCME, V. Distribution of trapped gas saturation in heterogeneous sandstone reservoirs. Proceedings of the Annual Symposium of the Society of Core Analysts, 2001. 1-4.

SUZANNE, K. E. D. M. D. P., HAMON, G. T., BILLIOTTE, J. E. D. M. D. P. & TROCME, V. G. 2003. Residual gas saturation of sample originally at residual water saturation in heterogeneous sandstone reservoirs. *Proceedings of the Annual Symposium of the Society of Core Analysts*, 1-4.

SZULCZEWSKI, M., MACMINN, C. & JUANES, R. 2011. How pressure buildup and CO_2 migration can both constrain storage capacity in deep saline aquifers. *Energy Procedia,* 4, 4889-4896.

TAKU IDE, S., JESSEN, K. & ORR JR, F. M. 2007. Storage of CO_2 in saline aquifers: Effects of gravity, viscous, and capillary forces on amount and timing of trapping. *International Journal of Greenhouse Gas Control,* 1, 481-491.

TANINO, Y. & BLUNT, M. J. 2012. Capillary trapping in sandstones and carbonates: Dependence on pore structure. *Water Resources Research,* 48.

TELETZKE, G. F. & LU, P. 2013. Guidelines for reservoir modeling of geologic CO_2 storage. *Energy Procedia,* 37, 3936-3944.

TERRY, R. E. & ROGERS, J. B. 2013. *Applied petroleum reservoir engineering,* Publisher is Pearson hall, Pearson Education.

THAKUR, N. K. & RAJPUT, S. 2010. *Exploration of gas hydrates: geophysical techniques,* Springer-Verlag Berlin Heidelberg, , Springer Science & Business Media, 1-128.

TIAN, H., XU, T., LI, Y., YANG, Z. & WANG, F. 2015. Evolution of sealing efficiency for CO_2 geological storage due to mineral alteration within a hydrogeologically heterogeneous caprock. *Applied Geochemistry,* 63, 380-397.

TILLNER, E., SHI, J.-Q., BACCI, G., NIELSEN, C. M., FRYKMAN, P., DALHOFF, F. & KEMPKA, T. 2014. Coupled dynamic flow and geomechanical simulations for an integrated assessment of CO_2 storage impacts in a saline aquifer. *Energy Procedia,* 63, 2879-2893.

TOKUNAGA, T. K., WAN, J., JUNG, J. W., KIM, T. W., KIM, Y. & DONG, W. 2013. Capillary pressure and saturation relations for supercritical CO_2 and brine in sand: High-pressure Pc (Sw) controller/metre measurements and capillary scaling predictions. *Water Resources Research,* 49, 4566-4579.

TREIBER, L. E. & OWENS, W. W. 1972 A laboratory evaluation of the wettability of fifty oil-producing reservoirs, *Soc. Pet. Eng. J,* 12(6) 531–540.

UKAEGBU, C., GUNDOGAN, O., MACKAY, E., PICKUP, G., TODD, A. & GOZALPOUR, F. 2009. Simulation of CO_2 storage in a heterogeneous aquifer. *Proceedings of the Institution of Mechanical Engineers,* 223, 249-267.

VAN DER MEER, B. 2005. Carbon dioxide storage in natural gas reservoir. *Oil & gas science and technology,* 60, 527-536.

VAN DER MEER, L. & EGBERTS, P. A general method for calculating subsurface CO_2 storage capacity. Offshore Technology Conference, OTC 08-" Waves of Change", 5 May 2008 through 8 May 2008, Houston, TX, 2, 887-895, 2008.

VARRE, S. B. K., SIRIWARDANE, H. J., GONDLE, R. K., BROMHAL, G. S., CHANDRASEKAR, V. & SAMS, N. 2015. Influence of geochemical processes on the geomechanical response of the overburden due to CO_2 storage in saline aquifers. *International Journal of Greenhouse Gas Control,* 42, 138-156.

VIDAL-GILBERT, S., TENTHOREY, E., DEWHURST, D., ENNIS-KING, J., VAN RUTH, P. & HILLIS, R. 2010. Geomechanical analysis of the Naylor Field, Otway Basin, Australia: Implications for CO_2 injection and storage. *International Journal of Greenhouse Gas Control,* 4, 827-839.

VULIN, D., KUREVIJA, T. & KOLENKOVIC, I. 2012. The effect of mechanical rock properties on CO_2 storage capacity. *Energy,* 45, 512-518.

WANG, H. 2000. *Theory of linear poroelasticity with applications to geomechanics and hydrogeology*, Princeton University Press.

WANG, J., RYAN, D., ANTHONY, E. J., WILDGUST, N. & AIKEN, T. 2011. Effects of impurities on CO_2 transport, injection and storage. *Energy Procedia,* 4, 3071-3078.

WANG, S. & TOKUNAGA, T. K. 2015. Capillary pressure–saturation relations for supercritical CO_2 and brine in limestone/dolomite sands: Implications for geologic carbon sequestration in carbonate reservoirs. *Environmental science & technology,* 49, 7208-7217.

WATSON, M. N. & GIBSON-POOLE, C. M. Reservoir selection for optimised geological injection and storage of carbon dioxide: A combined geochemical and stratigraphic perspective. The fourth annual conference on carbon capture and storage. National Energy Technology Laboratory, US Department of Energy, Alexandria, 2005, 1-12.

WATSON, T. L. & BACHU, S. 2008. Identification of wells with high CO_2-leakage potential in mature oil fields developed for CO_2-Enhanced Oil Recovery. SPE Symposium on Improved Oil Recovery, 20-23 April, Tulsa, Oklahoma, USA: Society of Petroleum Engineers, 1-10.

WATSON, T. L. & BACHU, S. 2009. Evaluation of the potential for gas and CO_2 leakage along wellbores. *SPE Drilling & Completion,* 24, 115-126.

WEI, N., GILL, M., CRANDALL, D., MCINTYRE, D., WANG, Y., BRUNER, K., LI, X. & BROMHAL, G. 2014. CO_2 flooding properties of liujiagou sandstone: Influence of sub-core scale structure heterogeneity. *Greenhouse Gases: Science and Technology,* 4, 400-418.

WELL-REPORT 2002. Horizontal well test analysis. Confidental.

WICHERT, E. & AZIZ, K. 1972. Calculate z for sour gases. *Hydrocarbon Processing,* 51, 119.

WIEBE, R. 1941. The binary system carbon dioxide-water under pressure. *Chemical Reviews,* 29, 475-481.

WILDENSCHILD, D., ARMSTRONG, R. T., HERRING, A. L., YOUNG, I. M. & CAREY, J. W. 2011. Exploring capillary trapping efficiency as a function of interfacial tension, viscosity, and flow rate. *Energy Procedia,* 4, 4945-4952.

WRIGHT, I. W. The In Salah gas CO_2 storage project. IPTC 2007: International Petroleum Technology Conference, 2007. 1-10.

XIAOLING, S., FANGUI, Z. & HEJUAN, L. 2012. CO_2-CH_4 system mixing properties and enhanced natural gas recovery. *International Journal of Digital Content Technology & its Applications,* 6, 1-5.

YAMAGUCHI, K., SHIMODA, S., KATO, H., STENHOUSE, M. J., ZHOU, W., PAPAFOTIOU, A., YAMASHITA, Y., MIYASHIRO, K. & SAITO, S. 2013. The long-term corrosion behavior of abandoned wells under CO_2 geological storage conditions: (3) Assessment of long-term (1,000-year) performance of abandoned wells for geological CO_2 storage. *Energy Procedia,* 37, 5804-5815.

YANZE, Y. & CLEMENS, T. 2012. The role of diffusion for nonequilibrium gas injection into a fractured reservoir. *SPE Reservoir Evaluation & Engineering,* 15, 60-71.

YOO, S., MYOJO, T., MATSUOKA, T. & UEDA, A. 2013. Experimental studies of injectivity reduction due to carbonate mineralization. *Procedia Earth and Planetary Science,* 7, 920-923.

YUAN, C., ZHANG, Z. & LIU, K. 2015. Assessment of the recovery and front contrast of CO_2 EOR and sequestration in a new gas condensate reservoir by compositional simulation and seismic modeling. *Fuel,* 142, 81-86.

ZEMKE, K., LIEBSCHER, A. & WANDREY, M. 2010. Petrophysical analysis to investigate the effects of carbon dioxide storage in a subsurface saline aquifer at Ketzin, Germany (CO_2 SINK). *International Journal of Greenhouse Gas Control,* 4, 990-999.

ZHANG, M. & BACHU, S. 2011. Review of integrity of existing wells in relation to CO_2 geological storage: What do we know? *International Journal of Greenhouse Gas Control,* 5, 826-840.

ZHANG, Y., FREIFELD, B., FINSTERLE, S., LEAHY, M., ENNIS-KING, J., PATERSON, L. & DANCE, T. 2011. Estimating CO_2 residual trapping from a single-well test: Experimental design calculations. *Energy Procedia,* 4, 5044-5049.

ZHANG, D. & SONG, J. 2014. Mechanisms for geological carbon sequestration. *Procedia IUTAM,* 10, 319-327.

ZHANG, L., REN, B., HUANG, H., LI, Y., REN, S., CHEN, G. & ZHANG, H. 2015a. CO_2 EOR and storage in Jilin oilfield China: Monitoring program and preliminary results. *Journal of Petroleum Science and Engineering,* 125, 1-12.

ZHANG, Y., LANGHI, L., SCHAUBS, P., DELLE PIANE, C., DEWHURST, D., STALKER, L. & MICHAEL, K. 2015b. Geomechanical stability of CO_2 containment at the South West Hub Western Australia: A coupled geomechanical–fluid flow modelling approach. *International Journal of Greenhouse Gas Control,* 37, 12-23.

ZHANG, Y., LEBEDEV, M., SARMADIVALEH, M., BARIFCANI, A. & IGLAUER, S. Change in geomechanical properties of limestone due to supercritical CO_2 injection. SPE Asia

Pacific Oil & Gas Conference and Exhibition, 2016a. Society of Petroleum Engineers, 1-10.

ZHANG, Y., SARMADIVALEH, M., LEBEDEV, M., BARIFCANI, A., REZAEE, R., TESTAMANTIA, N. & IGLAUER, S. Geo-mechanical weakening of limestone due to supercritical CO_2 Injection. Offshore Technology Conference Asia, 2016b. Offshore Technology Conference.

ZHENG, H., FENG, X.-T. & PAN, P.-Z. 2015. Experimental investigation of sandstone properties under CO_2–NaCl solution-rock interactions. *International Journal of Greenhouse Gas Control,* 37, 451-470.

ZHOU, W., STENHOUSE, M. J., ARTHUR, R., WHITTAKER, S., LAW, D. H. S., CHALATURNYK, R. & JAZRAWI, W. 2005. The IEA Weyburn CO_2 monitoring and storage project — Modeling of the long-term migration of CO_2 from Weyburn. *In:* WILSON, E. S. R. W. K. F. G. T., T. MORRISJ GALEK (ed.) *Greenhouse Gas Control Technologies 7.* Oxford: Elsevier Science Ltd.

ZHOU, D., LI, P., ZHAO, Z., LIAO, J., ZHANG, C., ZHANG, Y., XIE, H., LI, F. & PENG, J. 2013. Feasibility study of CCS-Readiness in Guangdong Province, China (GDCCSR) Final Report: Part 2 "Assessment of CO_2 storage potential for Guangdong Province, China. *Global CCS Institute, South China Sea Institute of Oceanology*, 1-74.

ZHOU, X., ZENG, Z. & LIU, H. Stress-dependent permeability of carbonate rock and its implication to CO_2 sequestration. 45th US Rock Mechanics/Geomechanics Symposium, 2011 San Francisco, California,. American Rock Mechanics Association, 26-29.

ZHU, Q., ZUO, D., ZHANG, S., ZHANG, Y., WANG, Y. & WANG, L. 2015. Simulation of geomechanical responses of reservoirs induced by CO_2 multilayer injection in the Shenhua CCS project, China. *International Journal of Greenhouse Gas Control,* 42, 405-414.

ZIABAKHSHGANJI, Z. 2015. Physical and geochemical impacts of impure CO_2 on storage in depleted hydrocarbon reservoirs and saline aquifers. *Ph.D. Thesis, VU Universiteit Amsterdam,* 1-100.

Appendix

A.1 For calculation of porosity

Density porosity

$$\phi = \left(\frac{Rho_{ma} - Rhob}{Rho_{ma} - Rho_{Fluid}} \right) \quad \text{(A.1)}$$

Sonic porosity

Wyllie's correlation

$$\phi = \left(\frac{DT - DT_{matrix}}{DT_{Fluid} - DT_{matrix}} \right) \times Cp \quad \text{(A.2)}$$

Hunt – Raymer

$$\phi = \frac{(2 \times Vma - Vf) - \sqrt{(2 \times Vma - Vf)^2 - 4 \times Vma \times (Vma - V\log)}}{2 \times Vma} \quad \text{(A.3)}$$

Where,

$$Vma = \frac{1}{Dtma}$$

$$Vf = \frac{1}{Dtfl}$$

$$V\log = \frac{1}{Dt}$$

Neutron porosity

The Neutron input is already in porosity units and routine simply performs lithology transformations. Manually define the input and output lithology along with the type of neutron tool. IP then locates the lithology transform for the tool and outputs the corrected neutron porosity.

A.2 For calculation of water saturation

$$FF = \frac{a}{\phi^m} \quad \text{(A.4)}$$

$$Rwapp = \frac{R_t}{FF} \quad \text{(A.5)}$$

$$Rmfapp = \frac{R_{xo}}{FF} \quad \text{(A.6)}$$

$$Sw = \left(\frac{FF \times Rw}{Rt} \right)^{\frac{1}{n}} \quad \text{(A.7)}$$

$$Sxo = \left(\frac{FF \times Rmf}{Rxo} \right)^{\frac{1}{n}} \quad \text{(A.8)}$$

A.3 For calculation of permeability

Timur's Correlation

$$k = 8.58102\ \frac{\emptyset^{4.4}}{(S_{wir})^2} \tag{A.9}$$

A.4 For calculation of geomechanical parameters

The correlations for Young's modulus (E), and Poisson's ratio (υ) can be applied on compression (V_p), shear (V_s) and density (ρ) logs for elastic properties as presented below:

$$E_{Dyn} = \rho V_s^2 \frac{3\left[\frac{V_p}{V_s}\right]^2 - 4}{\left[\frac{V_p}{V_s}\right]^2 - 1} \tag{A.10}$$

$$\nu_{Dyn} = \frac{1}{2}\frac{\left(V_s/V_p\right)^2 - 2}{\left(V_s/V_p\right)^2 - 1} \tag{A.11}$$

Wang (2000) correlation to relate static (E_{sta}) and dynamic (E_{dyn}) Young's modulus. In this correlation E_{sta} and E_{dyn} are in GPa.

$$E_{sta} = 0.4145E_{dyn} - 1.0593 \tag{A.12}$$

Bradford et al., 1998 proposed the following correlations for UCS as expressed in Eq. (A.13)

$$228 + 4.1089E \tag{A.13}$$

Plumb (1994) correlation used for determination of friction angle using wireline logs measurements of porosity (NPHI) and shale volume (V_{shale})

$$26.5 - 37.4 \times \left(1 - NPHI - V_{shale}\right) + 62.1 \times \left(1 - NPHI - V_{shale}\right)^2 \tag{A.14}$$

V_{shale} is the shale volume obtained through Eq. (A.16) (Li and Wong)

$$GRI = \frac{GR - GR_{\min}}{GR_{\max} - GR_{\min}} \tag{A.15}$$

$$V_{sh} = 0.33(2^{2GRI} - 1) \tag{A.16}$$

Where, Gamma ray index (GRI) is based on GR_{min} 0% shale and GR_{ma}100% shale are for minimum and maximum values of gamma ray log, respectively.

Eaton method (Eq. A.17) is the most common equation to quantify pore pressure through sonic or resistivity logs (Gholami et al., 2015b).

$$P_{pg} = OBG - (OBG - P_{pn})\left[\frac{NCT}{\Delta t}\right]^3 \quad \text{(A.17)}$$

Where, P_{pg} is the pore pressure gradient, OBG is the overburden stress gradient that is calculated using density log. NCT is the normal compacted trend line obtained through fitting a linear or non-linear curve to the compressional wave log data. P_{pn} and Δt are the normal pore pressure and the compressional wave transit time, respectively.

The magnitude of the vertical stress (σ_v), the minimum and maximum horizontal stresses as expressed in Eq. (A-18-A.20) (Fjær et al., 2008). σ_x and σ_y are the tectonic strain in the field.

$$\sigma_v = \rho g h \quad \text{(A.18)}$$

$$\sigma_h = \frac{v}{(1-v)}\left(\sigma_v - \alpha P_p\right) + \alpha P_p + \frac{E_{sta}}{\left(1-v^2\right)}\left(\varepsilon_x + v\varepsilon_y\right) \quad \text{(A.19)}$$

$$\sigma_H = \frac{v}{(1-v)}\left(\sigma_v - \alpha P_p\right) + \alpha P_p + \frac{E_{sta}}{\left(1-v^2\right)}\left(\varepsilon_y + v\varepsilon_x\right) \quad \text{(A.20)}$$

A.5 Density of CO_2 at reservoir conditions

Most successful approach conventionally used for estimation of the density is the one proposed by Bahadori et al. (2009). It should be noted that this approach (Eq. (A.21)) can only be used for the temperature between 293 K to 433 K and the pressure of 25 bar to 700 bar.

$$\rho = \alpha + \beta T + \gamma T^2 + \theta T^3 \quad \text{(A.21)}$$

$$\alpha = (A_1 + B_1 P + C_1 P^2 + D_1 P^3) \quad \text{(A.22)}$$

$$\beta = (A_2 + B_2 P + C_2 P^2 + D_2 P^3) \quad \text{(A.23)}$$

$$\gamma = (A_3 + B_3 P + C_3 P^2 + D_3 P^3) \quad \text{(A.24)}$$

$$\theta = (A_4 + B_4 P + C_4 P^2 + D_4 P^3) \quad \text{(A.25)}$$

In the above equations, P is the pressure in bar, ρ is the density in kg/m^3, T is the temperature in Kelvin, α, β and γ are the temperature coefficients estimated by Eqs. (A.22)–(A.25) and Table A.1.

A.6 Interfacial tension

Chalbaud's approach links the interfacial tension to the differential density and is expressed as:

$$\sigma_{brine-CO_2} = \gamma_{Wplateau} + \lambda^* X_{NaCL} + \left[\frac{P}{M}(\Delta\rho)\right]^{\eta} \times T_R^{\beta} \quad \text{(A.26)}$$

Table A.1: Variations of temperature coefficients included in Eqs. (A.22)–(A.25)

Coefficient	25 bar<P<100 bar	100 bar<P<700 bar
A1	2.09E+05	1.05E+05
B1	-1.46E+04	-9.40E+02
C1	2.89E+02	2.40E+00
D1	-1.60E+00	-1.82E-03
A2	-1.68E+03	-8.25E+02
B2	1.17E+02	7.62E+00
C2	-2.32E+00	-1.96E-02
D2	1.28E-02	1.50E-05
A3	4.45E+00	2.14E+00
B3	-3.10E-01	-2.02E-02
C3	6.16E-03	5.27E-05
D3	-3.42E-05	-4.04E-08
A4	-3.92E-03	-1.83E-03
B4	2.73E-04	1.77E-05
C4	-5.43E-06	-4.65E-08
D4	3.02E-08	3.59E-11

where $\sigma_{brine-CO2}$ is the interfacial tension of CO_2 in gf/cm, T_R is the reservoir temperature in ^oC, P is the pressure in bar, λ, η and β are the regression coefficients obtained from fitting a least-squares curve to experimental data, M is the CO_2 molar mass, $\Delta\rho$ is the differential density of supercritical CO_2 and saline water. The values of λ, η and β coefficients together with P, M and $\gamma_{Wplateau}$ parameters used to estimate the interfacial tension are summarized in Table A.2.

Table A.2: Regression coefficients and parameters used to model the interfacial tension

Regression Coefficients of Eq. (A.26)		Constant Values of Eq. (A.26)	
λ	1.255	P	82
η	4.7180	M (g/mol)	44.01
β	1.0243	$\gamma_{Wplateau}$	26

A.7 Oil and gas capacity estimations

The effective storage capacity of these reservoirs is calculated from the original gas in place using the following equation: (Bachu et al., 2007, Zhou et al., 2013).

$$M_{CO_2} = \rho_{CO2R} \times R_f \times OGIP \times B_g \times C_e \quad \text{(A.27)}$$

Where, M_{CO2} is the storage capacity, OGIP is the volume of original gas in place, R_f is the recovery factor. The subscripts "R" in the above equation indicates the reservoir condition and B_g is the reservoir volume factor. Where, $C_e=C_{eff}.C_{aq}$, where C_{eff} is the effective storage coefficient, representing the CO_2 mobility and density, while C_{aq} represents the reduction in the storage capacity as a result of water invasion during the production.

A.8 Residual gas saturation

Archie equation (Eq. (A.28)) can also be used to determine the water saturation, which in turn gives the hydrocarbon saturation.

$$S_w^{1/n} = (R_o / R_t) \quad \text{(A.28)}$$

$$1 - S_w = S_h \quad \text{(A.29)}$$

$$S_g = S_h - S_o \quad \text{(A.30)}$$

where S_w is the water saturation, R_o is the resistivity of pore volumes filled with water, R_t is the true resistivity, n is the saturation exponent, S_h is the hydrocarbon saturation, S_g is the gas saturation and S_o is the oil saturation.

A.9 Wettability

Having the vertical distance between the free water and movable-fluid levels estimated using the pressure profile, porosity and permeability data can be applied to determine the average wettability through the following equation:

$$J(P_{ct}) = P_{ct}(k/\phi)^{\frac{1}{2}} / \sigma_{nw/w} \cos\theta \quad \text{(A.31)}$$

Where, P_{ct} is the capillary rise or fall expressing as below:

$$P_{ct} = hg(\rho_w - \rho_{nw}) \quad \text{(A.32)}$$

The slopes of the pressure profile curve estimated from moveable hydrocarbon or water levels are used to get the non-wetting and wetting phase's densities in kg/m^3 as formulated below:

$$\rho = \frac{G}{g} \tag{A.33}$$

Where P_{ct} is the minimum threshold pressure when a non-wetting phase (oil or gas) enters into a porous medium.

The $J(P_{ct})$ is often between 0.1 to 0.17 for consolidated formations and varies from 0.35 to 0.447 for unconsolidated intervals. It is estimated using the capillary pressure curve. The contact angle can then be determined using the permeability and porosity data obtained from the wireline logs data analysis while $\sigma_{nw/w}$ is estimated from correlations or fluid sample data analysis.

Statement of Contribution of Candidate

I herby declare the nature and extent of the intellectual input in the papers (Sr No # 1-7) by me and any co-authors.

In the case of this thesis:

Contributor	Sr. No. of Paper	Statement of contribution
Arshad Raza 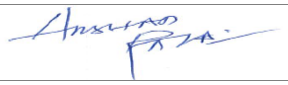 01- 08- 2017	1-7	Developed the problem statement, methodology, data analysis, and wrote the manusript
A/Prof Chua Han Bing  01 – 08 - 2017	1-7	Assisted in writing manusript
Prof. Reza Rezaee	1-7	Assisted in developing problem statement, methodology, data analysis and in writing manusript
A/Prof Ramasamy Nagarajan	1-7	Assisted in writing manusript
Dr. Mohamed Ali Hamid	1-7	Assisted in writing manusript
Dr. Raoof Gholami	1-7	Assisted in data analysis and in writing manusript
Dr. Mohammad Sarmadivaleh	6	Aided experimental design as well as peformed experiment
Nathan Tarom	6	Peformed Experiment
Henry Elochukwu	6	Aided experimental design

Principal Supervisor Confirmation		
I have sighted email from all Co-authors confirming their certifying authorship		
		**01st August 2017**
A/Prof. Chua Han Bing **Name**	_____ **Signautre**	_____ **Date**

Co-authors statement

To Whom It May Concern

I, ARSHAD RAZA, contributed 60% (major) in research and writing phase to the paper/publication will form part of the PhD dissertation as papers entitled:

1. **Raza, A**., Rezaee, R., Gholami, R., Bing, C.H., Nagarajan, R. and Hamid, M.A., 2016. A screening criterion for selection of suitable CO_2 storage sites. Journal of Natural Gas Science and Engineering, Elsevier, 28: 317-327.

2. **Raza, A**., Gholami, R., Rezaee, R., Bing, C.H., Nagarajan, R. and Hamid, M.A., 2017. Preliminary assessments for CO_2 storage in carbonate formations: a case study from Malaysia. Journal of Geophysics and Engineering, IOP, 14: 535–556 (22pp).

3. **Raza, A**., Gholami, R., Rezaee, R., Bing, C.H., Nagarajan, R. and Hamid, M.A., 2017. Well selection in depleted oil and gas fields for a safe CO_2 storage practice: a case study from Malaysia. Petroleum, KeAi, 3/1: 167-177.

4. **Raza, A**., Gholami, R., Rezaee, R., Bing, C.H., Nagarajan, R. and Hamid, M.A., 2017. Preliminary assessment of CO_2 injectivity potential in carbonate storage sites. Petroleum, KeAi, 3/1: 144-154.

5. **Raza, A**., Gholami, R., Rezaee, R., Bing, C.H., Nagarajan, R. and Hamid, M.A., 2017. Assessment of CO_2 residual trapping in depleted reservoirs used for geosequestration. Journal of Natural Gas Science and Engineering, Elsevier, 43C: 137-155.

6. **Raza, A**., Gholami, R., Sarmadivaleh, M., Tarom, N., Rezaee, R., Bing, C.H., Nagarajan, R., Hamid, M.A. and Elochukwu, H., 2016. Integrity analysis of CO_2 storage sites concerning geochemical-geomechanical interactions in saline aquifers. Journal of Natural Gas Science and Engineering, Elsevier, 36PA: pp. 224-240.

7. **Raza et al. 2017**. Numerical modeling to assess CO_2 storage in depleted gas reservoir: A case study from Malaysia. (submitted).

Arshad Raza

I, as a Co-Author, endorse that this level of contribution by the candidate indicated above is appropriate.

(A/Prof Chua Han Bing)[1-7] (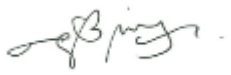)

(Prof. Reza Rezaee) [1-7] ()

(A/Prof Ramasamy Nagarajan) [1-7] (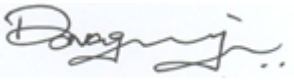)

(Dr. Mohamed Ali Hamid) [1-7] 

(Dr. Raoof Gholami) [1-7] ()

(Dr. Mohammad Sarmadivaleh) [6] ()

(Nathan Tarom) [6] ()

(Henry Elochukwu)[6] (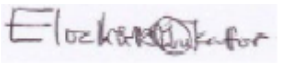)

Permission from the copyright owners

I warrant that I have obtained, where necessary, permission from the copyright owners to use any third-party copyright material reproduced in the thesis (e.g. questionnaires, artwork, unpublished letters), or to use any of my own published work (e.g. journal articles) in which the copyright is held by another party (e.g. publisher, co-author)."

ELSEVIER LICENSE
TERMS AND CONDITIONS

Feb 07, 2017

This Agreement between Arshad Raza ("You") and Elsevier ("Elsevier") consists of your license details and the terms and conditions provided by Elsevier and Copyright Clearance Center.

License Number	4043690074897
License date	Feb 07, 2017
Licensed Content Publisher	Elsevier
Licensed Content Publication	Journal of Natural Gas Science and Engineering
Licensed Content Title	A screening criterion for selection of suitable CO2 storage sites
Licensed Content Author	Arshad Raza,Reza Rezaee,Raoof Gholami,Chua Han Bing,Ramasamy Nagarajan,Mohamed Ali Hamid
Licensed Content Date	January 2016
Licensed Content Volume	28
Licensed Content Issue	n/a
Licensed Content Pages	11
Start Page	317
End Page	327
Type of Use	reuse in a thesis/dissertation
Portion	full article
Format	both print and electronic
Are you the author of this Elsevier article?	Yes
Will you be translating?	No
Order reference number	
Title of your thesis/dissertation	Reservoir Characterization for CO2 Injectivity and Flooding in Petroleum Reservoirs Offshore Malaysia
Expected completion date	Oct 2017
Estimated size (number of pages)	200
Elsevier VAT number	GB 494 6272 12
Requestor Location	Arshad Raza PhD student. GP1 ROOM 5, CURTIN SARAWAK UNIVERSITY, MALAYSIA MIRI, SARAWAK 98009 Malaysia Attn: Arshad Raza
Total	0.00 USD
Terms and Conditions	

Gmail arshad raza <arshadraza212@gmail.com>

Re: Case # 00301964 re-use article (aa5e71) in my PhD thesis

Permissions <permissions@iop.org> Mon, Feb 20, 2017 at 7:45 PM
To: arshadraza212@gmail.com

Dear Arshad,

Thank you for your email and for taking the time to seek this permission.

When you transferred the copyright in your article to us and chose to publish on a subscription basis, we granted back to you certain rights. This included the right to include all or part of the Final Published Version of the article within a thesis or dissertation provided it was not then published commercially. Please note you may need to obtain separate permission for any third party content you included within your article.

We are happy for your thesis or dissertation to be made available via your institution's library and/or your institutional repository.

You may submit your thesis or dissertation (including the article) via ProQuest if that is a requirement of your university. However, we do not then allow the article to be published commercially or made publicly available by ProQuest, so it would need to be removed from your thesis or dissertation prior to publication online or in print. Your institution should be able to withhold the IOP article section of your thesis from the ProQuest version. However, you should still reference the article, include the abstract and provide a DOI link to it on IOPscience so that people know that it has been published.

Any other commercial use of your thesis or dissertation would also require our permission, if it included your IOP article.

Please include citation details, "© Sinopec Geophysical Research Institute. Reproduced with permission. All rights reserved" and for online use, a link to the Version of Record.

Please note, if your article was published on a gold open access basis, then you would be able to publish your article with ProQuest and use it for any other commercial purpose under the terms of the CC BY licence.

In the meantime, I wish you the best of luck with the completion of your dissertation.

Many thanks.

Kind regards,

Kathryn Shaw

Copyright & Permissions Team
Gemma Alaway – Senior Rights & Permissions Adviser
Kathryn Shaw - Rights & Permissions Assistant

Contact Details
E-mail: permissions@iop.org

For further information: http://iopscience.iop.org/page/copyright

Please see our Author Rights Policy http://ioppublishing.org/author-rights/

Please note: We do not provide signed permission forms as a separate attachment. Please print this email and provide it to your institution as proof of permission.

Please note: Any statements made by IOP Publishing to the effect that authors do not need to get permission to use any content where IOP Publishing is not the publisher is not intended to constitute any sort of legal advice. Authors must make their own decisions as to the suitability of the content they are using and whether they require permission for it to be published within their article.

Preliminary assessment of CO2 injectivity in carbonate storage sites Article reference- PETLM118

Well selection in depleted oil and gas fields for a safe CO2 storage practice: a case study from Malaysia Article reference PETLM110

Looking forward to hearing from you.

Warm Regards,

Arshad Raza
PhD Student | Department of Petroleum Engineering
Curtin University, Sarawak Malaysia
Cell No # +60105061628

《Petroleum》编辑部 <petroleum_swpu@163.com> Sun, Feb 12, 2017 at 7:29 AM
To: arshad raza <arshadraza212@gmail.com>

Dear Author
Good day to you. You are permitted to use these two articles. Please cite them in your references.
Thank you for submiting your manuscripts to Petroleum.
Best regards.
Petroleum
[Quoted text hidden]

ELSEVIER LICENSE
TERMS AND CONDITIONS

Apr 13, 2017

This Agreement between Arshad Raza ("You") and Elsevier ("Elsevier") consists of your license details and the terms and conditions provided by Elsevier and Copyright Clearance Center.

License Number	4087240373817
License date	Apr 13, 2017
Licensed Content Publisher	Elsevier
Licensed Content Publication	Journal of Natural Gas Science and Engineering
Licensed Content Title	Assessment of residual trapping in depleted reservoirs used for geosequestration
Licensed Content Author	Arshad Raza,Raoof Gholami,Reza Rezaee,Chua Han Bing,Ramasamy Nagarajan,Mohamed Ali Hamid
Licensed Content Date	July 2017
Licensed Content Volume	43
Licensed Content Issue	n/a
Licensed Content Pages	19
Start Page	137
End Page	155
Type of Use	reuse in a thesis/dissertation
Portion	full article
Format	both print and electronic
Are you the author of this Elsevier article?	Yes
Will you be translating?	No
Order reference number	
Title of your thesis/dissertation	Reservoir Characterization for CO2 Injectivity and Flooding in Petroleum Reservoirs Offshore Malaysia
Expected completion date	Oct 2017
Estimated size (number of pages)	200
Elsevier VAT number	GB 494 6272 12
Requestor Location	Arshad Raza PhD student. GP1 ROOM 5, CURTIN SARAWAK UNIVERSITY, MALAYSIA MIRI, SARAWAK 98009 Malaysia Attn: Arshad Raza
Total	0.00 USD
Terms and Conditions	

ELSEVIER LICENSE
TERMS AND CONDITIONS

Feb 07, 2017

This Agreement between Arshad Raza ("You") and Elsevier ("Elsevier") consists of your license details and the terms and conditions provided by Elsevier and Copyright Clearance Center.

License Number	4043691078547
License date	Feb 07, 2017
Licensed Content Publisher	Elsevier
Licensed Content Publication	Journal of Natural Gas Science and Engineering
Licensed Content Title	Integrity analysis of CO2 storage sites concerning geochemical-geomechanical interactions in saline aquifers
Licensed Content Author	Arshad Raza,Raoof Gholami,Mohammad Sarmadivaleh,Nathan Tarom,Reza Rezaee,Chua Han Bing,Ramasamy Nagarajan,Mohamed Ali Hamid,Henry Elochukwu
Licensed Content Date	November 2016
Licensed Content Volume	36
Licensed Content Issue	n/a
Licensed Content Pages	17
Start Page	224
End Page	240
Type of Use	reuse in a thesis/dissertation
Intended publisher of new work	other
Portion	full article
Format	both print and electronic
Are you the author of this Elsevier article?	Yes
Will you be translating?	No
Order reference number	
Title of your thesis/dissertation	Reservoir Characterization for CO2 Injectivity and Flooding in Petroleum Reservoirs Offshore Malaysia
Expected completion date	Oct 2017
Estimated size (number of pages)	200
Elsevier VAT number	GB 494 6272 12
Requestor Location	Arshad Raza PhD student. GP1 ROOM 5, CURTIN SARAWAK UNIVERSITY, MALAYSIA MIRI, SARAWAK 98009 Malaysia Attn: Arshad Raza
Total	0.00 USD